UNIVERSITÀ DEGLI STUDI DI TRIESTE

XXVIII CICLO DEL DOTTORATO DI RICERCA IN
NANOTECNOLOGIE

MOLECULARLY IMPRINTED POLYMERIC NANOPARTICLES FOR THE THERAPEUTIC DRUG MONITORING OF ANTICANCER DRUGS

CHIM/06

Ph.D. Program Director

Prof. Lucia Pasquato

Ph.D. Student

Elena Pellizzoni

Thesis Supervisor

Dr. Giuseppe Toffoli

Co-Supervisor/Tutor

Dr. Federico Berti

Dr. Flavio Rizzolio

Anno Accademico 2014 / 2015

UNIVERSITÀ DEGLI STUDI DI TRIESTE

XXVIII CICLO DEL DOTTORATO DI RICERCA IN

NANOTECNOLOGIE

MOLECULARLY IMPRINTED POLYMERIC NANOPARTICLES FOR THE THERAPEUTIC DRUG MONITORING OF ANTICANCER DRUGS

CHIM/06

DOTTORANDO
ELENA PELLIZZONI

COORDINATORE
PROF. LUCIA PASQUATO

SUPERVISORE DI TESI
DR. GIUSEPPE TOFFOLI

CO-SUPERVISORE/TUTORE
DR. FEDERICO BERTI

DR. FLAVIO RIZZOLIO

ANNO ACCADEMICO 2014 / 2015

Agli amici

"Chi più in alto sale, più lontano vede.

Chi più lontano vede, più a lungo sogna"[1]

[1] Walter Bonatti

Table of Contents

University of Trieste

PhD School in Nanotechnology

Molecularly Imprinted Polymeric Nanoparticles for the Therapeutic Drug Monitoring of Anticancer Drugs

Ph.D. Thesis

Ph.D. Candidate: *Elena Pellizzoni*

Supervisor: *Dr. Giuseppe Toffoli*

Co-supervisor/Tutor: *Dr. Federico Berti*

Dr. Flavio Rizzolio

Abstract

This thesis is part of a large project granted by the Italian Association for Cancer Research (AIRC) on *"Application of Advanced Nanotechnology in the development of innovative cancer diagnostic tools*". One of the aims of this project, coordinated by the italian cancer institute of Aviano (Centro di Riferimento Oncologico -CRO) is the development of point of care devices for the therapeutic drug monitoring (TDM) of anticancer drugs.

Chemotherapy consists of cancer treatment by administration of a single or a combination of anticancer drugs that are often characterized by a high variability of pharmacokinetic among patients and a high toxicity leading to the appearance of many side effects and decreasing the therapy efficiency. Therefore, the development of point of care devices able to measure directly and rapidly the drug blood levels in small volumes from finger pricks, would be very useful in the development of personalized therapies.

This thesis investigates the potential of soluble imprinted polymeric nanoparticles (MIPs) as sensing elements for the direct detection of the anticancer drugs sunitinib, paclitaxel, SN38 and its produg irinotecan in human plasma. The employment of these soluble MIPs as sensing units in optical devices with fluorimetric or colorimetric detection represents a good chance to obtain simple and cheap point of care devices. To this aim, soluble molecularly imprinted nanoparticles were synthesized by high dilution radical polymerization using different functional monomers. All polymers were characterized by ^{1}H-NMR, Nanosight, and Dynamic Laser Light Scattering. The polymers binding capabilities and selectivity were investigated by rebinding tests using an HPLC method for the quantification of captured drug, while the fluorescence properties of some of these polymers were exploited to study the polymers binding affinities at low

drug concentrations. MIPs containing N-acryloyl-tyrosine methyl ester, N-acryloyl-tryptophan methyl ester, 4-vinyl pyridine or 7-acryloyloxy-coumarin were investigated as possible fluorescent polymers or possible quencher of target fluorescence. A MIP containing 7-acryloyloxy-coumarin as functional monomer and having specific binding sites for sunitinib was used as fluorescence sensor to quantify the drug in plasma samples treated with four volumes of DMSO. The system turned out to be robust and satisfactory as to its precision and accuracy. It was able to quantify sunitinib within 5 $\mu mol \cdot L^{-1}$ - 100 $\mu mol \cdot L^{-1}$ range with a LOD of 400 $nmol \cdot L^{-1}$, using a calibration curve obtained in 4:1 DMSO : water mixture.

Moreover, two fluorescence tests for irinotecan quantification in methanol : plasma mixtures were developed as proof on concept of fluorimetric sensors. The first test is based on the quenching of the intrinsic fluorescence of irinotecan using a MIP containing N-acryloyl-tyrosine methyl ester as functional monomer. The test showed a linear response between 0.5 $\mu mol \cdot L^{-1}$ to 8 $\mu mol \cdot L^{-1}$ drug and turned out to be robust since it had the same behavior also in DMSO : plasma mixture. As second approach a highly fluorescence polymer containing a naphthalimide-based functional monomer was synthesized. Measuring the quenching of MIP fluorescence upon interaction with irinotecan, a calibration curve was obtained with a linear response between 20 $nmol \cdot L^{-1}$ and 100 $nmol \cdot L^{-1}$.

Moreover, a competition technique has been employed to set up a FRET system for paclitaxel quantification. The test is based on the competition between the free paclitaxel and the drug covalently linked to DABCYL dye, for the binding in to an imprinted polymeric nanoparticle containing EDANS fluorescent functional monomer. Since DABCYL is a FRET quencher of EDANS, its binding into the polymer gives a change in the polymer fluorescence. The obtained calibration curve in DMSO has a linear response between 1 $\mu mol \cdot L^{-1}$ and 30 $\mu mol \cdot L^{-1}$.

Finally, a colorimetric test for irinotecan quantification was developed using an imprinted polymer containing 2-acrylamido-2-methylpropane sulfonic acid as functional monomer. The test is based on the binding of aniline yellow dye inside the remaining free binding sites of the polymer after treatment with drug samples. The interaction between the dye and the sulfonic acid in to the polymer gives a change of colour from yellow to red. Using this test irinotecan samples in acetonitrile were quantified from 3.6 $\mu mol \cdot L^{-1}$ to 75 $\mu mol \cdot L^{-1}$. The irinotecan concentrations usually found in patients samples are within the dynamic range of the obtained calibration curve.

Università di Trieste

Scuola di dottorato in nanotecnologie

Nanoparticelle polimeriche ad imprinting molecolare per il therapeutic drug monitoring di farmaci antitumorali

Tesi di dottorato

Dottoranda: *Elena Pellizzoni*

Relatore: *Dr. Giuseppe Toffoli*

Correlatore/Tutor: *Dr. Federico Berti*

Dr. Flavio Rizzolio

Riassunto

Questa tesi prende parte ad un progetto finanziato dall'Associazione italiana per la Ricerca sul cancro (AIRC) intitolato: *"Application of Advanced Nanotechnology in the development of innovative cancer diagnostic tools*". Uno degli obbiettivi di questo progetto, coordinato dal Centro di Riferimento oncologico (CRO) di Aviano, consiste nello sviluppo di dispositivi *point of care* per il Therapeutic Drug Monitoring (TDM) di farmaci antitumorali. La chemoterapia consiste nell'impiego di uno o di una combinazione di farmaci antitumorali per il trattamento del cancro. Tuttavia tali farmaci sono caratterizzati da una famacocinetica molto variabile e da una elevata tossicità che porta alla comparsa di molti effetti indesiderati nei pazienti, diminuendo l'efficienza della terapia. In questo contesto l'impiego del dispositivi *point of care* in grado di misurare direttamente e rapidamente la concentrazione di farmaco in una goccia di sangue risulta particolarmente importante in quanto permette per lo sviluppo di terapie personalizzate per i pazienti aumentando l'efficienza della terapia e la qualità della vita dei pazienti.

Questa tesi ha come obbiettivo lo studio di nanoparticelle polimeriche ad imprinting molecolare (MIP) solubili, come possibili sensori in grado di catturare e quantificare i farmaci antitumorali sunitinib, tassolo, SN38 ed irinotecano nel plasma umano. Tali MIP potrebbero infatti essere impiegati come sensori fluorimetrici o colorimetrici per lo sviluppo di dispositivi *point of care* semplici ed economici. A tale scopo sono state sintetizzate diverse nanoparticelle polimeriche solubili mediante polimerizzazione radicalica ad elevata diluizione utilizzando diversi monomeri funzionali. Tutti i polimeri sono stati caratterizzati mediante ^{1}H-NMR, Nanosigh e Dynamic Laser Ligh Scattering. La capacità di legame e la selettività dei polimeri è stata studiata mediante test di recupero utilizzando un metodo HPLC per la quantificazione del farmaco catturato.

Utilizzando le proprietà fluorescenti di alcuni MIPs sono state studiate le capacità di legame anche a basse concentrazioni di farmaco. Inoltre è stata valutata la possibilità di utilizzare i polimeri contenenti N-acriloil-tirosina metil estere, N-acriloil triptofano metil estere, 4-vinilpiridina e 7-acriloilossicumarina come polimeri fluorescenti o come quencher della fluorescenza della molecola target. In particolare un MIP contenente il monomero funzionale 7-acriloilossicumarina e siti di legame specifici per il sunitinib è stato utilizzato come sensore fluorescente per la quantificazione del farmaco in plasma dopo trattamento con quattro volumi di DMSO. Il sistema ha mostrato una buona robustezza e una precisione e accuratezza soddisfacente. Utilizzando tale sistema è stato possibile quantificare il sunitinib in un intervallo di concentrazioni comprese tra 5 $\mu mol \cdot L^{-1}$ - 100 $\mu mol \cdot L^{-1}$, utilizzando una retta di calibrazione in 4:1 DMSO : acqua. E stato inoltre stimato un LOD pari a 400 $nmol \cdot L^{-1}$.

Inoltre, come esempio di possibili sensori fluorescenti, sono stati sviluppati due diversi test fluorimetrici per la quantificazione dell'irinotecano in metanolo : plasma. Il primo test si basa sul quenching della fluorescenza intrinseca dell'irinotecano utilizzando un MIP contenente N-acriloil-tirosina metil estere come monomero funzionale. Il test ha fornito una risposta lineare a concentrazioni di farmaco comprese tra 0.5 $\mu mol \cdot L^{-1}$ e 8 $\mu mol \cdot L^{-1}$ ed ha dimostrato un comportamento molto simile anche in DMSO : plasma, indicando una buona robustezza.

Invece il secondo approccio si basa sulla sintesi di un MIP fluorescente contenente un monomero funzionale naftalimidico, la cui fluorescenza viene spenta in seguito al legame con l'irinotecano. Utilizzando questo sistema è stata costruita una retta di calibrazione avente una risposta lineare tra 20 $nmol \cdot L^{-1}$ and 100 $nmol \cdot L^{-1}$.

Inoltre unaa tecnica competitivaè stata utilizzata per lo sviluppo di un sistema FRET per la quantificazione del tassolo. Il test si basa sulla competizione tra il farmaco libero ed il farmaco legato covalentemente al DABCYL per il legame ad un polimero ad imprinting molecolare contenente EDANS come monomero funzionale fluorescente. Infatti il DABCYL è un FRET quencher dell'EDANS che, legandosi al polimero, genera una variazione della sua fluorescenza. Utilizzando tale sistema è stata ottenuta una retta di calibrazione tra 1 $\mu mol \cdot L^{-1}$ and 30 $\mu mol \cdot L^{-1}$ in DMSO che rappresenta un punto di partenza per lo sviluppo di un sensore FRET per la quantificazione del tassolo in campioni reali.

Infine è stato sviluppato un test colorimetrico per la quantificazione dell'irinotecano utilizzando un polimero ad imprinting molecolare contenente l'acido 2-acrilamido-2-metil propansolfonico come monomero funzionale. Il test si basa sul legame del colorante giallo anilina nei siti di legame del polimero rimasti liberi dopo interazione con i campioni di farmaco, infatti l'interazione tra il colorante e l'acido solfonico nel polimero genera un viraggio di colore da giallo a rosso. Utilizzando questo test è stato possibile quantificare dei campioni di iriotecano in acetonitrile a concentrazioni comprese tra 3.6 $\mu mol \cdot L^{-1}$ and 75 $\mu mol \cdot L^{-1}$. Le concentrazioni di irinotecano solitamente

riscontrate nei campioni dei pazienti sono all'interno del range dinamico della curva di calibrazione ottenuta.

1.Introduction

1.1 Anticancer Drugs

Sunitinib

Sunitinib (SUTENT, SU11248) is a tyrosine kinases (RTK) inhibitor approved by the Food and Drug Administration for the treatment of gastrointestinal stromal tumors and as first line therapy of metastatic clear cell renal cell carcinoma (ccRCC), a disease that is resistant to traditional chemotherapy and radiotherapy and that has a very poor patient survival rate. [1]

Furthermore sunitinib showed the ability to directly inhibit the survival and proliferation of a wide variety of cancer cells, including small cell lung carcinoma, gastrointestinal stromal tumors, acute myelogenous leukemia and chronic myelogenous monocytic leukemia. Sunitinib is also under investigation as a treatment for several other tumors like breast cancer, colorectal cancer and non-small cell lung cancer.[2]

The high efficiency of sunitinib as anticancer drug could be attributed to its ability to inhibit a wide range of receptors in particular the vascular endothelial grown factors (VEGFR-1, VEGFR-2, VEGFR-3), platelet-derived grown factor receptors (PDGFR-α, PDGFR-β) and fms-related tyrosine kinase 3 (FLT3), cKIT and RET.[3, 4]

The inhibition of tyrosine kinases and in particular of the vascular endothelial growing factor (VEGFR) plays a critical role in cancer therapy as these proteins are involved in the angiogenesis and lymphangiogenesis mechanisms that are among the main causes of tumor growth.[5]

Angiogenesis and lymphangiogenesis are the processes of new blood and lymphatic vessels growth from preexisting vasculature. Both have an essential role in the formation of a new vascular network to supply nutrients, oxygen and immune cells, moreover they are involved in the removal of catabolites. All these process are fundamental for tissue growth, physiological processes, embryonic development, and wound healing, however not only immune cells but also tumor cells can penetrate blood or lymphatic vessels and circulate inside the intravascular stream to reach another site where the tumor can grow (metastasis). Therefore cancer has the ability to spread to adjacent or distant organs by circulating through the vascular network. For these reasons angiogenic and lymphangiogenic factors are two of the main targets for cancer therapy. [6]

Tyrosine Kinases

Kinases are enzymes responsible for the phosphoryl transfer from high-energy donor molecules, for example adenosine triphosphate (ATP), to specific substrates. Kinases

are called also phosphotransferases because they phosphorylate proteins substrates leading to conformational and functional changes in their target proteins.[7]

The human genome encodes 518 protein kinases, 90 of them belong to the group of tyrosine kinases while other groups contains kinases able to phosphorylate first serine and threonine residues. The tyrosine kinases group is further divided in 30 families among which it is possible to distinguish the vascular endothelial grown factors (VEGFR) family, the platelet-derived grown factor receptors (PDGFR) family, the fibroblast growth factor receptor (FGFR) family and the epidermal growth factor receptor (EFGR).[8]

Apart from classification in families, within the group of tyrosine kinases it is also possible to distinguish between 58 receptor tyrosine kinases (RTK) and 32 non-receptor (cytoplasmic) tyrosine kinases.[9] The receptor tyrosine kinases are essential for the transduction of extracellular signals into the cell and therefore for the cellular signaling pathways that are active during embryonic development and adult homeostasis, while non-receptor tyrosine kinases are involved in the intracellular communication.[10]

Receptor tyrosine kinases are multifunctional transmembrane proteins, expressed at the cell surface. These features make them potential multisite targets for cancer therapy using small molecules as cell permeable kinases inhibitors or water soluble macromolecules like antibodies or binding antagonists.

All receptor tyrosine kinases consists of a large glycosylated N-terminal ligand-binding domain, a single transmembrane region and an intracellular portion containing a conserved protein tyrosine kinase domain with catalytic activity, a juxtamembrane region, called also activation loop, and a C-terminal tail.[11]

The kinase domain has a bilobar structure, with an ATP-binding site situated between the N and the C-terminal lobes. The ATP-binding cleft consists into three sub-regions: the adenosine region, the sugar region and the phosphate binding region.[12]

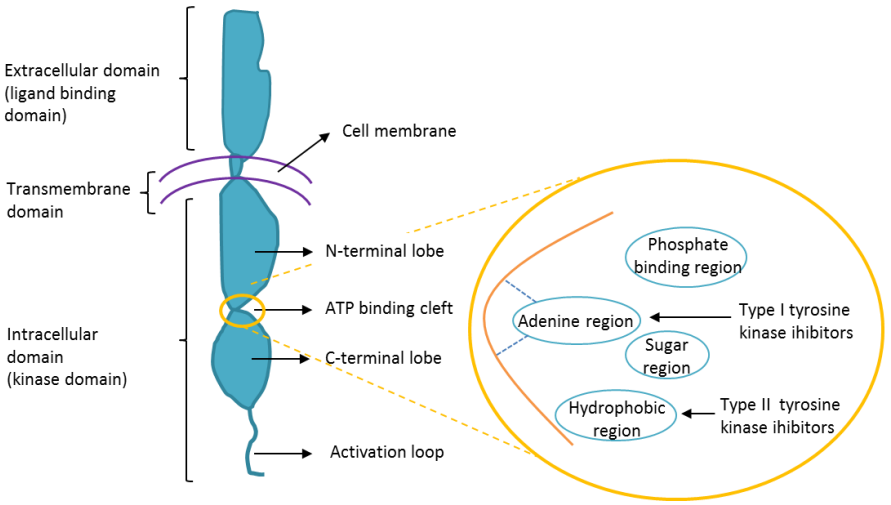

Figure 1.1: structure of a receptor tyrosine kinase (From ref 7)

Receptor tyrosine kinases are generally activated by the ligand binding to its extracellular domain, inducing an oligomerization, typically a dimerization of the receptor. In this phase the two cytoplasmic tyrosine kinase domains of the dimer are juxtaposed, facilitating the auto-phosphorylation in *trans* of tyrosine residues in the kinase activation loop, inducing conformational changes that are necessary for the stabilization of the kinase active state.[13] Moreover, when the receptor tyrosine kinase is activated it could bind some interacting proteins by its auxiliary phosphorylation sites. The subsequent phosphorylation of these interacting proteins lead to signaling proteins that are able to phosphorylate other proteins activating a signaling pathway that will lead to a biological response, like cell activation, proliferation, differentiation, migration, survival and vascular permeability.[14]

Kinase Inhibitors

Human protein kinases present different primary amino acid sequence but they share a great degree of similarity in their 3D structures, in particular in their catalytically active kinase domain where the ATP-binding pocket is located. In fact they are characterized by a β sheet containing an N-terminal lobe, a C-terminal lobe containing mainly α helices, and a connecting hinge region where the ATP-binding site is situated in correspondence of a cleft between the two lobes.[15]
ATP binds in the cleft with the adenine ring forming hydrogen bonds, while the ribose and triphosphate groups of ATP bind in a hydrophilic channel extending to the protein binding site.
Moreover a flexible activation loop, characterized by the conserved specific amino acid sequences DFG at the start of the loop and APE at the ends of the loop, regulate the access to the ATP-binding site by assuming different conformations.[16]
Tyrosine kinases inhibitors could be divided in two categories in base of the binding modes: irreversible and reversible. In the irreversible mode the inhibitor binds covalently to the reactive nucleophilic cysteine residue of the kinase proximal to the ATP-binding site, preventing the access of ATP and leading to an irreversible kinase inhibition. In the reversible mode the binding occurs by weak interactions. In the last case it is possible to distinguish between:

- Type I inhibitors that are ATP-competitive inhibitors able to bind to the active form of kinases by one to three hydrogen bonds, mimiking the interaction between ATP and the residues in the binding site. Moreover, since the kinase is in its active form, the aspartate residue of the DFG sequence in the activating loop is faced towards the active site of the kinase. Type I inhibitors typically consist of a heterocyclic ring system able to interact with the purine binding site, and some side chains that occupy the adjacent hydrophobic region I and II.

- Type II inhibitors, able to bind to specific pockets adjacent to the ATP-binding site when the kinase is in the inactive form. In this case hydrophobic binding pockets are accessible thanks to the rotation of the activating loop when the protein is in the inactive form with the aspartate residue of the DFG sequence protruding outward from the ATP-binding site of the kinase. These inhibitors indirectly compete with ATP by the binding to hydrophobic pocket that is closer to the ATP-binding site.

- Type III inhibitors, binding exclusively allosteric pockets adjacent to the ATP-binding site without making any interaction with it. These inhibitors exhibit the highest degree of kinase selectivity because they exploit binding sites and regulatory mechanisms that are unique to a particular kinase.

- Type IV inhibitors able to bind inside an allosteric pocket away from the ATP-binding site

- type V, bivalent inhibitors because exhibit more than one of the previous described binding modes.[17]

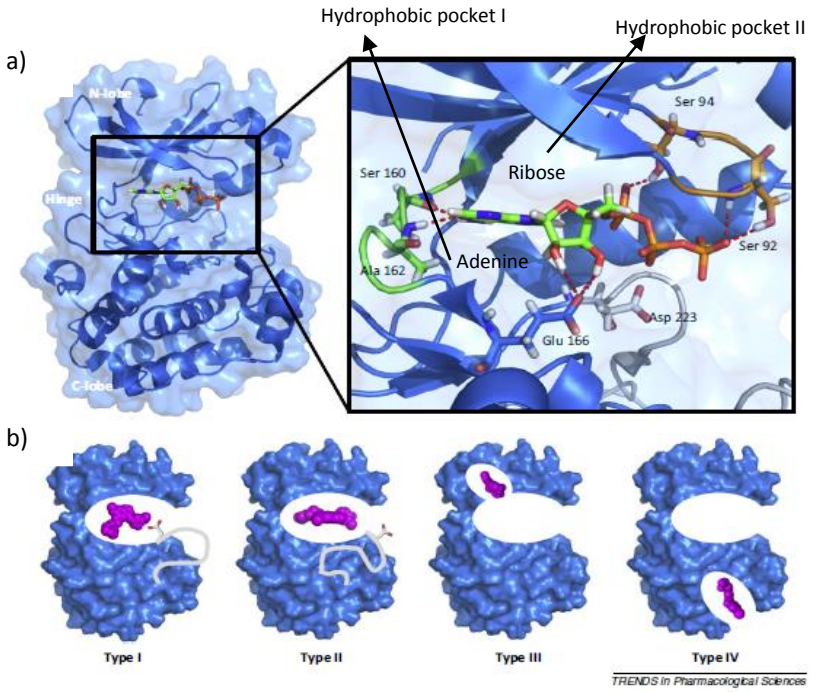

Figure 1.2: a) co-crystal structure of PDK1 with ATP (adenine and ribose in green backbone, phosphate groups in orange). b) Four types of reversible binding mode.(From ref 17)

The presence of a higher conserved region in all tyrosine kinases at the level of the binding site of ATP is due to the necessity of these receptors to bind ATP to perform their activity. Type I kinase inhibitors are not highly selective because are able to bind to ATP-binding sites of a wide number of kinases involved in different signaling processes, while the inhibitors that bind less conserved allosteric pockets or multi domain inhibitors are more selective.[18, 19]

Sunitinib Pharmacology

Sunitinib belongs to the I type inhibitors, it binds the ATP-binding site with the indole moiety making hydrogen bonds with the kinase, while the pyrrole of the side chain is placed inside the hydrophobic pocket I and the fluorine atom inside the hydrophobic pocket II. [16]

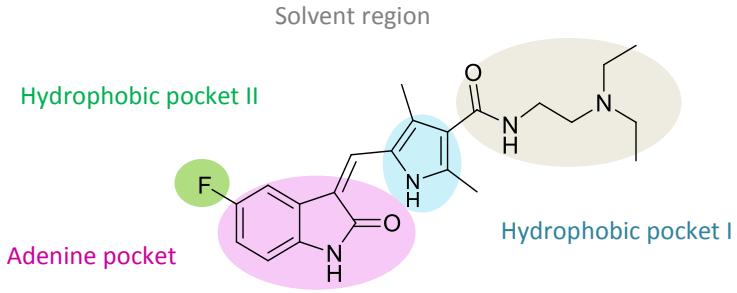

Scheme 1.1: structure of sunitinib and interactions in the binding site of kinases

It is administered orally as the malate salt at a fixed dose once or twice a day because the variability in its pharmacokinetic is not significantly affected by weight.[20] Pharmacokinetic and pharmacodynamic preclinical studies showed that the therapeutic total plasma concentrations of sunitinib and of its primary metabolite (SU12662) are between 50 ng/mL and 100 ng/mL (0.125 µM-0.25 µM). Concentrations lower than 50 ng/mL decrease the therapeutic efficiency while concentrations higher than 100 ng/mL are associated to an increase of the drug toxicity.[21] The common dosage administered to patients is between 25-50 mg to 150 mg of sunitinib malate every day.[22]

Pharmacokinetic studies showed that sunitinib has an half life in plasma of 40-60 h, and is metabolized by the cytochrome P450 enzyme CYP3A4 leading to the primary metabolite. This metabolite has a biochemical activity and potency as anticancer drug similar to sunitinib. Both sunitinib and its active metabolite showed a high tendency to bind serum albumin *in vitro*: 90% for SU12662 and 95% for sunitinib.[23] The active metabolite half life is 80-110 h after that it is further metabolized by CYP3A4 to its secondary inactive metabolite. [24]

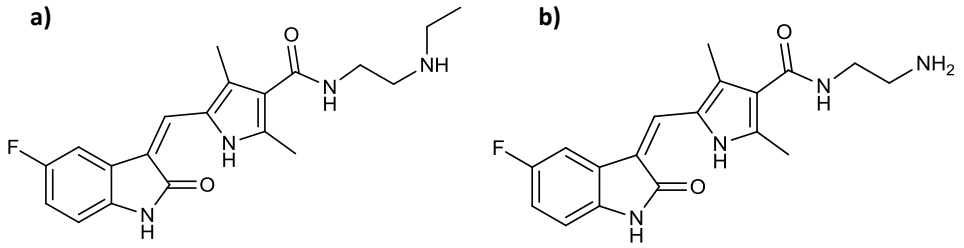

Scheme 1.2: a) active metabolite of sunitinib (SU12662). b) inactive metabolite of sunitinib

Elimination of sunitinib occurs primarily via feces (61%)[25] and in a low amount via urine (16%).[26]
Even if sunitinib has a discrete toxicity profile, the majority of patients showed some side effects, in particular fatigue, gastrointestinal disorders as diarrhea, nausea and stomatisis, nervous system disorders like dysgeusia, and hypertension.[27]

Irinotecan and SN38

Colorectal carcinoma (CRC) is one of the most common types of cancers in Western countries. Usually, patients who develop recurrent or metastatic CRC, undergo surgical resection and start a chemotherapy based on the administration of a combination of oxaliplatin and 5-fluorouracil (5-FU), as first line treatment. If the cancer still advances after this treatment, irinotecan therapy is started as second line chemotherapy. In fact clinical trials showed that irinotecan improves pain-free survival, quality of life, progression-free survival and overall survival in advanced colorectal cancer.[28]
This drug was first discovered and synthesized in Japan by Yakult Honsha Co,Ltd, in 1983.[29]
During the first phase of study, irinotecan was used in combination with 5-Fluorouracil and Leucovorin that, before irinotecan, were the only chemotherapeutic option for the treatment of colorectal cancer.
Further studies approved the administration of irinotecan for the treatment of advanced colorectal cancer either as a first therapy in combination with 5-FU or alone in the treatment of 5-FU refractory cases. [30, 31]

Chemistry

Irinotecan (CPT-11) is a semisynthetic analogue of camptothecin, the quinolone-based alkaloid isolated by Wall and Co-workers in 1966 from the Chinese/Tibetan ornamental

tree *Camptotheca accuminata*.[32] Starting from camptothecin, different analogues, including irinotecan and topotecan, were synthesized to decrease the toxicity and increase the antitumor activity of this drug.[33]

The structure of these alkaloids is characterized by a planar pentacyclic ring with a pyrrolo[3,4-β]-quinolinone moiety (rings A, B and C), a conjugated pyridine moiety (ring D) and an α-hydroxy lactone ring containing a chiral centre at position 20 (ring E) (Scheme 1.3). The planar structure and the presence of the lactone ring are the most important factors in the pharmacological activity of this molecule.[34]

In the case of irinotecan, an ethyl group is linked to the ring B of the camptopthecin, in position 7, while a bipiperidine group is linked in position 10 by a carbamide ester to increase the solubility of the drug. This group is cleaved in vivo by esterase to obtain the active metabolite: 7-ethyl-10-hydroxy campthotecin (SN38).

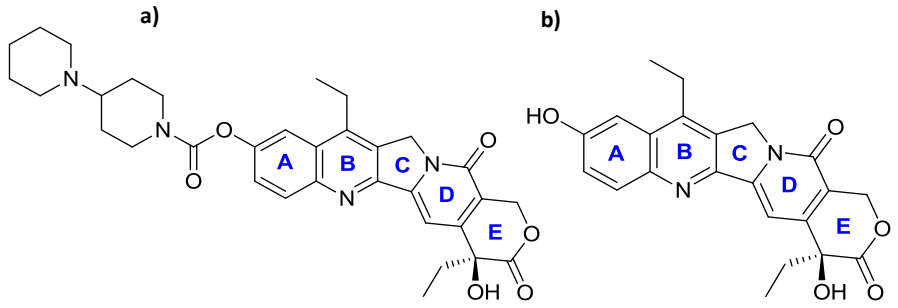

Scheme 1.3: a) structure of irinotecan prodrug. b) structure of SN38 active metabolite

Irinotecan hydrochloride trihydrate is a pale yellow crystalline solid with a solubility greater than 20 mg/mL in water at pH 3-4, thanks to the presence of the basic piperidine group whose pKa is 8.7[35], so the molecule is protonated at both acid and neutral pH.

The α-hydroxy-δ-lactone of irinotecan and of all the camptothecins, undergoes to rapid pH-dependent equilibration with the corresponding open chain carboxylic acid, called irinotecan carboxylate. The lactone form of camptothecins is favoured at pH<5, while the carboxylate form is favoured at pH>8. At pH between 6 and 7 the rates of lactone hydrolysis and formation is similar yielding similar amounts of each species at equilibrium.[36]

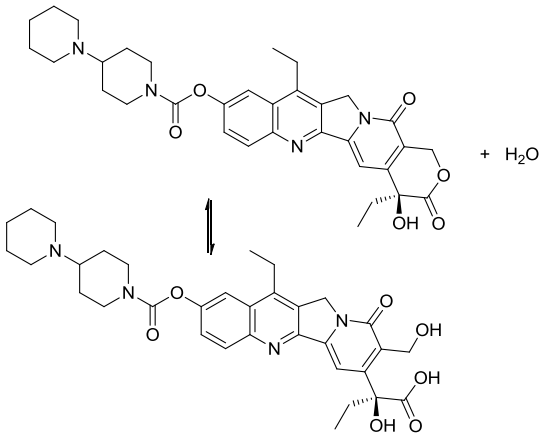

Scheme 1.4: equilibrium between the lactone form and the carboxylate form of irinotecan

SAR

Camptothecins (CPT) are a potent inhibitors of DNA topoisomerase I (TOP I).
Topoisomerases are ubiquitous and essential enzymes that solve the topological problems related to the DNA replication, transcription, chromatin assembly, recombination and chromosome segregation, by introducing transient breaks into the DNA helix. Strand cleavage by all topoisomerases involves nucleophilic attack by a catalytic tyrosine residue on the scissile phosphodiester bound and the formation of a covalent bond between the enzyme and one of the ends of the broken strand. After modification of the DNA topology, the double helix is re-ligated and the enzyme is released. The enzymes that cleave only one strand of DNA are defined as type I and can be further classified as either type IA subfamily if the protein links to the 5' phosphate or type IB if the protein is attached to the 3' phosphate. The topoisomerases able to cleave both strand of DNA are defined as type II.[37]
Human topoisomerase I wraps around DNA and cleaves one single strand through trans-esterification of Tyr723 leading to a 3'-phosphotyrosine intermediate, so the 5'-end is free to rotate, twisting it about the other strand, to release the torsional strain of DNA,

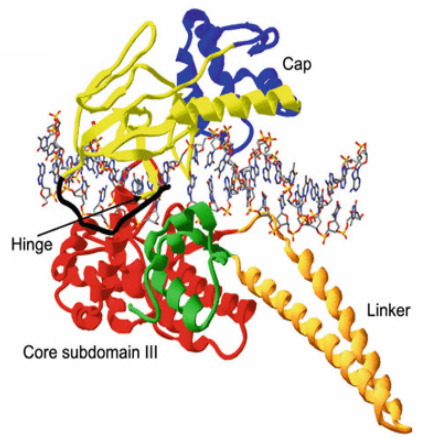

Figure 1.3: The domain structure of human topoisomerase I: co.crystal structure of human topoisomerase I containing a 22 base pair duplex oligonucleotide (pdb entry 1K4T)

that occurs during the synthesis of a new strand of DNA. Finally the broken strands are re-joined by the enzyme.[38] Human topoisomerase I represents an important target in cancer chemotherapy because it is overexpressed in tumour cells and when the enzyme is covalently linked to the DNA, forming the enzyme–DNA complex, it is vulnerable to campthothecins that reversibly trap the complex by intercalating between DNA base pairs at the cleavage site, inhibiting the re-annealing of the parent DNA. This stabilized complex collides with the replication fork of DNA during cell division, leading the DNA break and tumour cell death.[39]

The 3.0 Å X-ray crystal structure of the ternary campthothecin top1-DNA complex reveals that the heterocyclic ring structure of CPT intercalates at the site of DNA cleavage, making π-stacking interactions, while the E-ring of CPT is positioned closely toward the active site of top1 by which it makes H-bonds mainly with three amino acid residues. The C21 lactone oxygen is 4.0 Å away from the bridging phosphodiester oxygen between Tyr723 and thymidine-10, as well as 3.8 Å from the ε nitrogen of Lys532. The pyridone ring oxygen is 4.0 Å from the side chain nitrogen of Asn722. The C20 hydroxyl is 3.4 Å from the Oδ1 side chain atom of Asp533, a residue known to be required for enzyme sensitivity to campthothecin. The closest protein-drug interaction in the CPT ternary complex structure is 2.9 Å from an Nε of Arg364 to a free electron pair of the B-ring N1 of CPT.[40] Also the docking study of the complex SN38-topoisomerase I-DNA reveals an additional H-bounds between Asn352 and the hydroxyl on the A-ring of the drug that increases the inhibitor activity with respect campthothecins.[41]

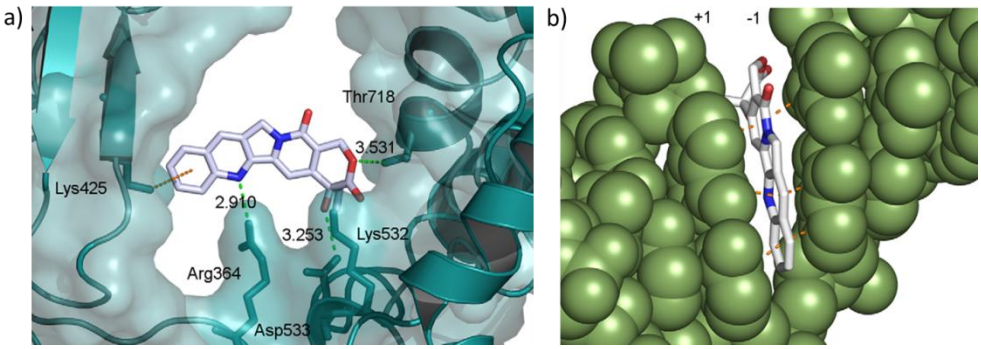

Figure 1.4: a) camptothecin on the Top1 active site viewed down the DNA helix alxis, hydrogen bonds and π-staking ineractions are shown in red and orange respectively. b) camptothecin intercalation with DNA (in green) by π-staking interactions. (From ref 39)

Pharmacology

SN38 and camptothecins can not be administered directly to patients due to their very poor water solubility (2-3 μg/mL for SN38) that makes difficult an intravenous administration.[42]

To overcome the solubility and stability issues associated to camptothecins, various derivatives have been developed.[43] Irinotecan, pro-drug of the active form SN38, was synthesized to improve the solubility by the protonation of the tertiary amino group of the piperidyl ring at low pH. Despite the fact that the efficacy of SN38 to inhibit topoisomerase I is 1000 times higher than that of irinotecan, such pro-drug is sufficiently water soluble to permit a stable aqueous solution and decrease the drug toxicity.

Irinotecan is administered intravenously using a sterile aqueous solution marketed as Camptosar© and containing 20 mg/mL of irinotecan HCl trihydrate, 45 mg/mL of sorbitol and 0.9 mg/mL of lactic acid formulated at pH 3-3.8. This solution has to be diluted until 0.18-2.8 mg/mL in an injection solution containing 5% dextrose or 0.9% sodium chloride, before the injection.[44]

After injection, irinotecan is converted by caboxyesterases to the active form SN38, and it undergoes to a rapid conversion of both irinotecan and SN38 from the lactone to the carboxylate form with a mean half-life of 9.5 min leading to an equilibration *in vivo* between the two forms. Only the closed lactone form is able to inhibit the topoisomerase I.[45]

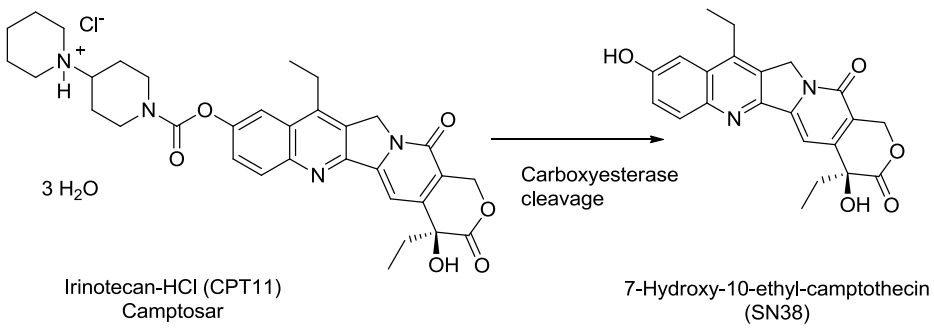

Scheme 1.5: hydrolysis of irinotecan by carboxyesterase to obtain the active drug

Both irinotecan and SN38 are able to bind to plasma proteins, in blood irinotecan is 80% bound to erythrocytes, whereas SN38 is bound for at least 99% mainly to albumin and lymphocytes, but also to erythrocytes and neutrophiles. Binding to albumin increases the stability of the lactone form in SN38. Finally, the active molecule SN38 is converted to the inactive glucuronide derivative (SN38-G) and is excreted into the

intestinal lumen via the bile.[46] The enzyme responsible to the SN38 glucuronidation is uridine diphosphate glucoronosyltransferase 1A1.[47]
The commonly observed plasma concentrations of irinotecan and SN38 are respectively 10 -10000 µg/L (17 nM-17 µM) and 1-500 µg/L (2.5 nM-1.3 µM).
The most frequent irinotecan toxic effects include severe diarrhoea and suppression of the immune system (neutropenia). Other side effects include nausea, hyperbilirubinaemia, fatigue, emesis, fever, weight loss, alopecia, oedema, dyspnoea and thromboembolism.[48]

Paclitaxel

Paclitaxel is one of the most popular anticancer drugs. It was originally extracted from the bark of *Taxum Brevifolia,* but it was also found in leaves, roots and stems of other types of *Taxus*.[49]
Some of *Taxus* properties were known since ancient times when Native Americans used the bark of *Taxum Brevifolia* to treat skin problems, rheumatism and colds,[50] or as disinfectant to treat wounds and as abortifacient.[51] Primary uses of *Taxus Baccata* and *Taxus Brevifolia* were also in North America to treat pulmonary problems and tuberculosis.[52]
Only in 1962 botanists of the United State Department of agriculture created the first collection of *Taxus Brevifolia* for screening purposes and the anticancer activity in its bark was confirmed one year later.[53] In 1966 Wall and Wani extracted paclitaxel from *Taxum Brevifolia* with a very low yield and its chemical structure was identified by NMR and XR-crystallography.[54]
However, the difficulties in understanding the paclitaxel mechanism of action, its low solubility and the low yield of extraction, slowed down the study of this drug. Only in 1979 Susan Horwitz discovered the paclitaxel mechanism increasing the overall interest on this drug that during the 80' started the 1st and 2nd clinical phase.[55] First tests showed some cases of hypersensitivity due to the use of the Cremophor EL surfactant necessary to solubilize the drug. The development of an infusion procedure in continuous mode avoiding the hypersensitivity reactions, allowed Paclitaxel to be approved and commercialized.[56]
Paclitaxel was approved by FDA in 1992 for the treatment of ovarian cancer, breast cancer, non-small-cell lung cancer (NSCLC), esophageal cancer and AIDS-related Kaposi sarcoma. The high popularity of paclitaxel is mainly due to two factors: its efficiency against ovarian and breast cancer[57] and the particularity of its mechanism of action. Paclitaxel stabilizes microtubules inhibiting the cell replication.[58, 59]

Microtubules

Microtubules are non-covalent α- and β- tubulin heterodimers assembled in a filamentous tube-shaped structure. α- and β- tubulin are highly homologous proteins each of ~450 amino acids. Each monomer binds guanosine triphosphate (GTP) which is nonexchangeable in α-tubulin, for this reason the nucleotide binding site of this protein is called N-site, while in β-tubulin the guanine nucleotide is exchangeable and it is called E-site.[60] GTP at the E-site is required for microtubules assembly since the energy provided by its hydrolysis (leading to the GDP) is used for the addition of a new dimer to the microtubule end, upon which it becomes non-exchangeable. The rate of tubulin addition is faster than the rate of GTP hydrolysis during polymerization allowing the creation of the protofilament.[61]

Therefore the polymerization of microtubules occurs by a nucleation-elongation mechanism in which the relatively slow formation of a short microtubule 'nucleus' is followed by rapid elongation of the microtubule at its ends by the reversible, non-covalent addition of tubulin dimers.[62]

In the polymerization stage, the tubulin heterodimers undergo head-to-tail arrangement in which the α-subunit of one dimer is in contact with the β-subunit of the next. The resulting protofilaments comprise the backbone of the hollow, cylindrical microtubule that is approximately 25 nm in diameter. The arrangements of 13 parallel protofilaments in an imperfect helix, lead to a microtubule.[63] The head-to-tail order of the α and β tubulin dimers confers polarity on the microtubule with one end ringed with α-tubulin and the other end ringed with β-tubulin. These are considered the *minus* end and the *plus* end respectively.[64] The microtubules organizing center (MTOC) is a network of microtubules-associated proteins (MAP) to witch the microtubules are attached. In particular the *minus* end of microtubules are attached to the MTOC, while the *plus* ends are distal.

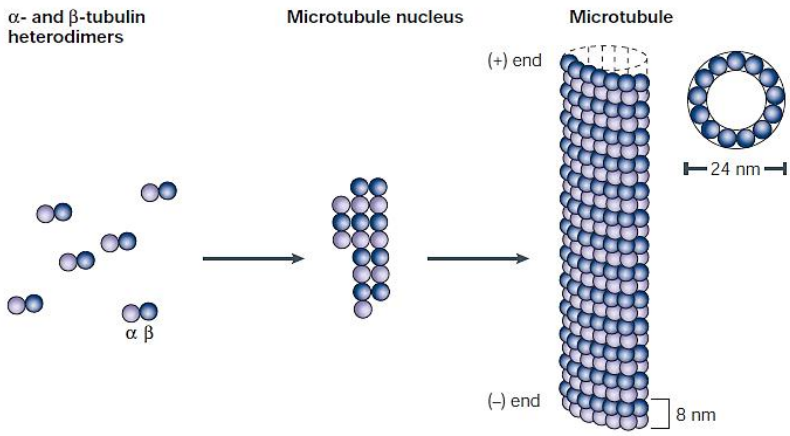

Figure 1.5: microtubule polymerization (from ref. 62)

It is important to emphasize that microtubules are not simple equilibrium polymers.[65] The stability of the microtubules depends on whether the exchangeable site of β-tubulin is occupied by GTP or GDP. A GTP-capped microtubule is stable and will continue to grow, while a microtubule capped with GDP-bound tubulin at the plus end is unstable and will depolymerize rapidly.[66] So the microtubules exhibit two dynamic behaviours: dynamic instability and treadmilling. The dynamic instability is characterized by the switching of microtubules between periods of slow growth, rapid shortening and attenuation, while treadmilling is the net addition of a tubulin subunit to the *plus* end and the corresponding loss at the *minus* end. [67]

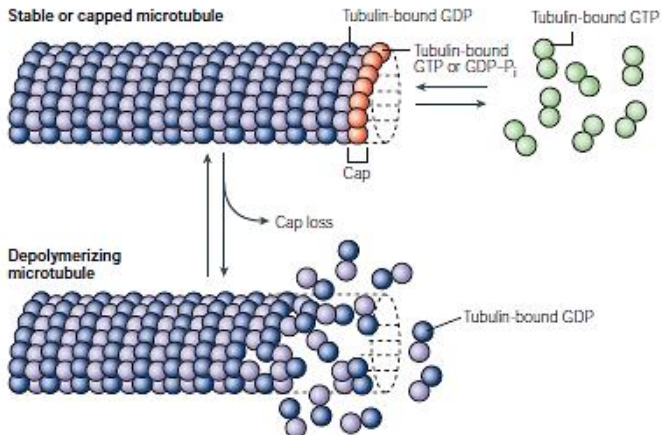

Figure 1.6: microtubules depolymerization (from ref. 62)

Microtubules dynamics are crucial in the mitosis process, particularly for the proper function of the mitotic spindle. During interphase, that is the first stage of cellular cycle, microtubules exchange their tubulin with the soluble tubulin pool in relatively long times, with half-times that range from several minutes to several hours. At the onset of mitosis, the interphase microtubule network disassembles and is replaced by a new population of spindle microtubules that are more dynamic than the microtubules in the interphase cytoskeleton. The spindle microtubules exchange their tubulin in the soluble pool rapidly, with half-times in the order of 10–30 seconds. Mitosis progresses rapidly and the high dynamic spindle microtubules are required for all stages of mitosis in particular to allow the correct attachment of chromosomes to the spindle during prometaphase after nuclear-envelope breakdown; to allow the proper alignment of chromosomes at the metaphase plate, called congression; and for the synchronous separation of chromosomes in anaphase and telophase.[68, 69]

Antimitotic Drugs

Cell proliferation could be inhibited by antimitotic agents that act on the polymerization dynamics of spindle microtubules. The disruption of microtubules dynamic leads to the arrest of the cell cycle in the G_2/M phase, eventually resulting in apoptotic cell death. Antimitotic drugs are usually classified in two main groups: microtubules destabilizing agents and microtubules stabilizing agents. Vinca alkaloids, like vincristine and vinblastine, and other drugs like colchicine, cryptophycins and halicondrins are microtubules destabilizing agents in fact at high concentrations they inhibit microtubule polymerization, depolymerize microtubules and decrease polymer mass.[70]

Instead microtubules stabilizing agents operate by promoting polymerization and increasing the microtubule polymer mass in cells. Taxanes, like paclitaxel and docetaxel, belong to this group of antimitotic drugs.[71, 72] All the antimitotic drugs act also at low concentrations suppressing microtubules dynamics without changing the polymer mass.[73, 74]

SAR

Paclitaxel belongs to the family of taxanes, complex ditherpenes with a tetracyclic core consisting of two cyclohexanes, a cyclooctane and an oxethane. This nucleus, called baccatin core, is the molecule skeleton and is common to all the taxane derivate. The 13th position of paclitaxel is occupied by an ester side chain of phenylisoserine. Also paclitaxel contains 11 stereocenters but only the (-)-paclitaxel is the active stereoisomer.[75]

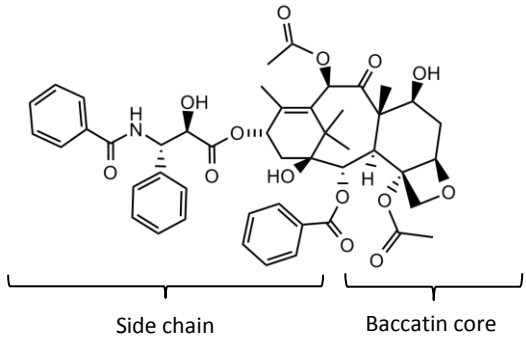

Scheme 1.6: Chemical structure of paclitaxel

Paclitaxel is the first drug able to promote the polymerization of microtubules. After paclitaxel discovery many other derivatives were synthesized in order to maintain the paclitaxel efficiency and decrease the drug toxicity. The structure-activity relationship of paclitaxel showed that removing the C7 or the C10 hydroxyl group the cytotoxicity of paclitaxel remains almost the same[76,77], while on modifying position 4 leading to 4-deacetyltaxol[78] and 4-deacetoxytaxol[79] the drug activity decreases. The presence of a substituent in *ortho* or in *meta* in the 2-benzoyl side chain increases the drug activity while the *para* substituent has the opposite behaviour.[80]

Paclitaxel Interaction with Tubulin

The interaction between paclitaxel and tubulin was widely studied to understand its mechanism of inhibition. Observing the three dimensional map of tubulin complexed with paclitaxel in presence of zinc ions, obtained by electron crystallography, the binding site of drug was founded in the β-subunit in the internal surface of the microtubule.[81] Therefore paclitaxel binds on the other side of the core helix from the GTPase domain on β-tubulin.[82]

Probably paclitaxel axesses to its binding site by diffusing through small breaks in the microtubule or fluctuations of the microtubule lattice. There is one paclitaxel binding site on every tubulin molecule in microtubules. The binding of paclitaxel with free tubulin is difficult due to the different polarity of paclitaxel and the soluble tubulin. However when tubulin is bound into the microtubule, the interaction with paclitaxel increases considerably.

The interaction between the drug and its binding site leads to the stabilization of microtubules and to the increasing of microtubules polymerization probably by inducing a conformational change in the tubulin that increases its affinity for neighbouring tubulin molecules. [654]

Observing the electron crystal structure of tubulin complexed with paclitaxel also the presence of arginine 369, glycine 370 and hystidine 229 was found in the drug binding site.[81] Only after the studies of molecular modelling and NMR NAMFIS of Snyder and co-workers, one of the most probable tubulin conformation, called *T-Taxol conformation* was obtained. They started from the data obtained by electron crystallography to perform some molecular modelling studies and NMR analysis of molecular flexibility in solution, to obtain the *T-Taxol conformation*. In this structures the phenyl groups of the side chain of paclitaxel are arranged perpendicularly to the benzyl group in position 2 leading to a "T" shape. Furthermore in this structure hydrophobic interactions leads hystidine 229 to a particular position, the benzyl group in position 2 and the benzamide group in position 3'. However in this structure one of the main interactions involved in the structure-activity relationship of paclitaxel, that is the hydrogen bound creation between arginine 369 and the hydroxyl group in 2' position of paclitaxel was not found. An interaction between the carbonyl group of the side chain in position 2' and the amide proton of glycine 370 was observed.[83]

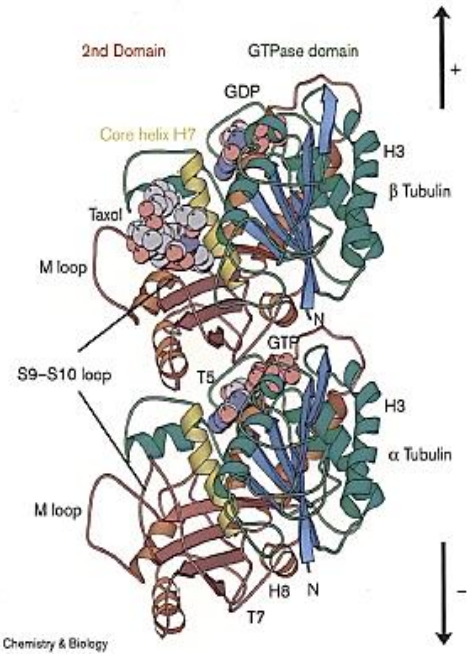

Figure 1.7: the three dimension conformation of cow tubulin dimers, as predicted from 3.7Å resolution map determined by electron crystallography.(From ref 82)

Further studies with rotational echo double resonance (REDOR) NMR a REDOR-taxol structure was identified and accepted as more truthful structure. In fact in this case the interaction between the hydroxyl in 2' position of paclitaxel and hystidine 229 of tubulin was observed and the arrangement of the side chain phenyl of the drug is similar to that described in the *T-Taxol conformation*.[84]

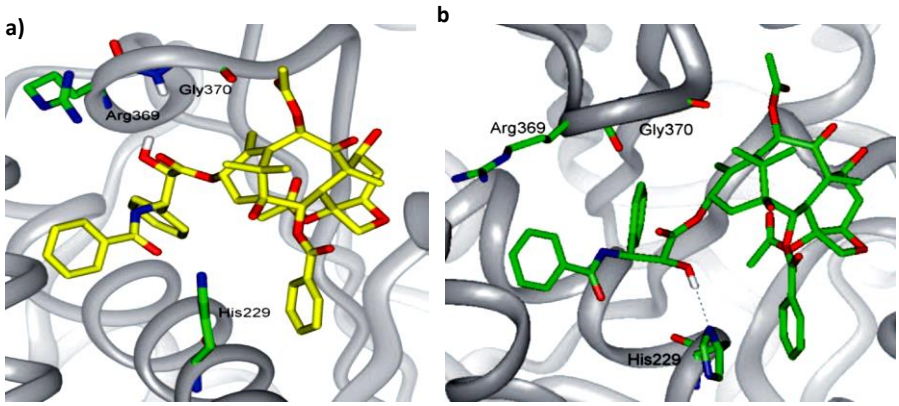

Figure 1.8: a) structure obtained by electrocrystallography and NMR studies: T-taxol conformation. b) structure obtained by REDOR NMR experiments: REDOR-taxol conformation (From ref 83)

Clinical Use of Paclitaxel

Paclitaxel is used for the treatment of ovary, breast cancer, non-small cell lung carcinoma and AIDS-related Kaposi sarcoma. Depending on the State in which it is commercialized, it could be used as mono-therapy or in association with platinum salts, antracycline or trastuzumab. The administration of paclitaxel is intravenous using a mixture of paclitaxel complexed with Cremaphor® EL (polyoxyethylated castor oil) and 49.7% (v/v) of dehydrated alcohol.

In blood 80-90% of paclitaxel is bound to plasmatic proteins showing a high distribution volume of this drug in tissues, while the elimination is hepatic. The paclitaxel plasma concentration is between 1.17 nM and 11.71 µM.

Since paclitaxel administration is associated to many side effects like hypersensibility, alopecia, neutropenia and leukopenia, the determination of personalized dosage among patients becomes very useful to decrease side effects and increase the therapy efficiency. [85]

[1] Motzer R. J., Michaelson M. D., Redman B. G., Hudes G. R., Wilding G., Figlin R. A., Ginsberg M. S., Kim S. T., Baum C. MDePrimo., S. E., Li J. Z., Bello C. L., Theuer C. P., George D. J., Rini B. I. (2006*)* "Activity of SU11248 , a multitargeted inhibitor of vascular endothelial growth factor receptor and platelet-derived growth factor, in patients with metastatic renal cell carcinoma" *J. Clin. Oncol.* 24:16-24

[2] Huang D., Ding Y., Li Y., Luo W., Zhang Z., Snider J., VandenBeldt K., Qian C., The B. T. (2010) "Sunitinib acts primarily on tumor endothelium rather than tumor cells to inhibit the growth of renal cell carcinoma" *Cancer Res.* 70(3):1053-1062

[3] Roskoski Jr. R. (2007) "Sunitinib: a VEGF and PDGF receptor protein kinase and angiogenesis inhibitor" *Biochem. Biophy. Res. Commun.* 356:323-328

[4] Joosten S. C., Hamming L., Soetekouw P. M., Aarts M. J., Veeck J., Van Engeland M., Tjan-Heijnen V. C. (2015) "Resistance to sunitinib in renal cell carcinoma: from molecular mechanisms to predictive markers and future perspectives" *Biochim. Biophy. Acta* 1855:1-16

[5] Kerbel R.S. (2008) "Tumor angiogenesis" *N. Engl. J. Med*. 358: 2039-2049.

[6] Folkman J. (1971) "Tumor angiogenesis: therapeutic implications" *N. Engl. J. Med.* 285: 1182-1186

[7] Gotink K. J., Verheul H. M. W. (2010) "Anti-angiogenic tyrosine kinase inhibitors: what is their mechanism of action?" *Angiogenesis* 13:1-14

[8] Manning G., Whyte D. B., Martinez R., Hunter T., Sudarsanam S. (2002) "The protein kinase complement of the human genome" *Science* 298: 1912-1934.

[9] Robinson D. R., Wu Y. M., Lin S. F. (2000) "The protein tyrosine kinase family of the human genome" *Oncogene* 19:5548-5557

[10] Hubbard S. R., Miller W. T. (2007) "Receptor tyrosine kinases: mechanism of activation and signaling" *Curr. Opini. Cell Biol.* 19:117-123

[11] Bennasroune A., Gardin A., Aunis D., Crémel G., Hubert P. (2004) "Tyrosine kinase receptors as attractive targets of cancer therapy" *Criti. Revi. Oncol./Hematol.* 50:23-38

[12] Liu Y., Gray N. S. (2006) "Rational design of inhibitors that bind to inactive kinase conformations" *Nat. Chem. Biol*. 2: 358-364.

[13] Schlessinger J. (2000) "Cell signaling by receptor tyrosine kinases" *Cell* 103:211-225

[14] Pawson T. (2004) "Specificity in signal transduction: from phos-photyrosine-SH2 domain interactions to complex cellular systems" *Cell* 116:191–203

[15] Knighton D. R. Zheng J. H., Ten Eyck L. F., Ashford V.A., Xuong N. H., Taylor S. S., Sowadski J. M. (1991) " Crystal structure of the catalytic subunit of cyclic adenosine monophosphate-dependent protein kinase" *Science* 253: 407–414

[16] Zhang J., Yang P. L., Gray N. S. (2009) "Targeting cancer with small molecule kinase inhibitors" *Nat. Rev.* 9:28-39

[17] Wu P., Nielsen T. E., Clausen M. H. (2015) "FDA approved small-molecules kinase inhibitors" *Trends Pharmacol. Sci.* 36(7):422-437

[18] Eskens F. A., Verweij J. (2006) "The clinical toxicity profile of vascular endothelial growth factor (VEGF) and endothelial growth factor receptor (VEGFR) targeting angiogenesis inhibitors" *Eur. J. Cancer* 42: 3127-3139.

[19] Klein S., McCormick F., Levitzki A. (2005) "Killing time for cancer cells" *Nat. Rev. Cancer* 5: 573-580.

[20] Houk B. E, Bello C. L., Kang D., Amantea M. (2009) "A population pharmacokinetic meta-analysis of sunitinib malate (SU11248) and its primary metabolite (SU12662) in healthy volunteers and oncology patients" *Clin Cancer Res*. 15:2497–250

[21] Faivre S., Delbaldo C., Vera K., Robert C., Lozahic S., Lassau N., Bello C., Deprimo S., Brega N., Massimini G., Armand J. P., Scigalla P., Raymond E. (2006) "Safety, pharmacokinetic, and antitumor activity of SU11248, a novel oral multitarget tyrosine kinase inhibitor, in patients with cancer" *J. Clini. Oncol.* 24(1): 25-35.

[22] Kollmannsberger C., Bjarnason G., Burnett P., Creel P., Davis M., Dawson N., Feldman D., George S., Hershman J., Lechner T., Potter A., Raymond E., Treister N., Wood L., Wu S., Bukowski R. (2011) "Sunitinib in metastastic renal cell carcinoma: recommendations for management of non-cardiovascular toxicities" *The Oncologist* 16: 543-553.

[23] Bukowski R. M., Figlin R. A., Motzer R. J. (2009) "Renal cancer carcinoma: molecular targets and clinical applications" *Humana Press*, II edition p.152 ISBN 978-1-4939-1622-1

[24] Goodman V. L., Rock E. P., Dagher R., Ramchandani R. P., Abraham S., Gobburu J. V., Booth B. P., Verbois S. L., Morse D. E., Liang C. Y., Chidambaram N., Jiang J. X., Tang S., Mahjoob K., Justice R., Pazdur R. (2007) "Approval summary: sunitinib for the treatment of imatinib refractory or intolerant gastrointestinal stromal tumors and advanced renal cell carcinoma" *Clin. Cancer Res.* 13:1367–1373

[25] Adams V. R., Leggas M. (2007) "Sunitinib malate for the treatment of metastatic renal cell carcinoma and gastrointestinal stromal tumors" *Clin. Ther.* 29:1338–1353

[26] Cavalli F., Kaye S. B., Hansen H. H., Armitage J. O., Piccart-Gebhart M.J. (2009) "Textbook of medical oncology" *Informa Healtcare*, IV edition p.432

[27] Kollmannsberger C., Soulieres D., Wong R., Scalera A., Garpo R., Bjarnason G., "Sunitinib therapy for metastatic renal cell carcinoma: recommendations for management of side effects" *Can. Urol. Assoc. J.* (2007) 1(2):S41-S54

[28] Weekes J., King-Yin Lam A., Sebesan S., Ho J.H. (2009) "Irinotecan therapy and molecular targets in colonrectal cancer: a systemic review" *World J. Gastroenterol* 15(29):3597-3602

[29] Fukuoka M. (2001) "Current status of irinotecan in lung cancer" *Oncol.* 15(suppl 1):6-7

[30] Saltz L. B. (1997) "Clinical use of irinotecan: current status and future considerations" *The Oncologist* 2:402–409

[31] Sawada S., Yokokura T., Miyasaka T. (1995) "Synthesis and antitumor activity of A-ring or E-lactone modified water-soluble prodrugs of 20(S)-camptothecin, including development of irinotecan hydrochloride trihydrate (CPT-11)" *Curr. Pharm. Design*. 1:113–132

[32] Wall M. E., Wani M. C., Cook C. E., Palmer K. H., McPhail A. T., Sim G. A. (1996) "Plant antitumor agents I. The isolation and structure of camptothecin, a novel alkaloidal leukemia and tumor inhibitor from camptotheca acuminate" *.J Am. Chem. Soc.* 88: 3888–90.

[33] Adamovics J. A., Hutchinson C. R. (1979) "Prodrug analogues at the antitumor alkaloid camptothecin" *J. Med. Chem.* 22:3

[34] Lu A., Zhang Z., Zheng M., Zou H., Luo X., Jiang H. (2007) "3D-QSAR study of 20 (S)-camptothecin analogs" *Acta Pharmacol Sin*. 28(2): 307-314

[35] Karadas N., Sanli S., Akmese B., Dogan-Topal B., Can A., Ozkan S. A. (2013) "Analytical application of polymethylene blue-multiwalled carbon nanotubes modified glassy carbon electrode on anticancer drug irinotecan and determination of its ionization constant value" *Talanta* 115: 911-919

[36] Fassberg J., Stella V. J. (1992) "A kinetic and mechanicistic study of hydrolysis of camptothecin and some analogues" *J. Pharm. Sci.* 81:676–684

[37] Champoux J. J. (2001) "DNA TOPOISOMERASES: structure, function, and mechanism" *Annu. Rev. Biochem*. 70:369-413

[38] Stewart L., Redinbo M. R., Qiu X., Hol W. G. J., Champoux J. J. (1998) "A model for the mechanism of human topoisomerase I" *SCIENCE* 279:1534-1541

[39] Drwal M. N., Agama K., Wakelin L. P. G., Pommier Y., Griffith R. (2011) "Exploring DNA topoisomerase I ligand space in search of novel anticancer agents" *PLoS ONE* 6:9

[40] Staker B. L., Feese M. D., Cushman M., Pommier Y., Zembower D., Stewart L., Burgin A. B. (2005) "Structures of three classes of anticancer agents bound to the human topoisomerase I-DNA covalent complex" *J. Med. Chem*. 48:2336-2345

[41] Laco G. S., Collins J. R., Luke B. T., Kroth H., Sayer J. M., Jerina D. M., Pommier Y. (2002) "Human topoisomerase I Inhibition: docking camptothecin and derivatives into a structure-based active site model" *Biochemistry* 41:1428-1435

[42] Xu Y., Villalona-Calero M. A. (2002) "Irinotecan: mechanisms of tumor resistance and novel strategies for modulating its activity" *Annals Oncol.* 13:1841-1851

[43] Venditto V.J., Simanek E.E. (2010) "Cancer therapies utilizing the camptothecins: a review of the *in vivo* literature" *Mol. Pharm.* 2(2): 307-349

[44] Hageman M. J., Morozowich W. (2007) "Case study: Irinotecan (CPT11), a water-soluble prodrug of SN38" *Prodrugs* 5.12: 1269-1279

[45] Rivory LP, Chatelut E, Canal P, Mathieu-Boue A, and Robert J. (1994) "Kinetics of the *In Vivo* interconversion of the carboxylate and lactone forms of irinotecan and of its metabolite SN-38 in patients" *Cancer. Res.* 54:6330–6333

[46] Mathijssen R. H. J., Van Alphen R. J., Jaap V., Loos W. J., Nooter K., Stoter G., Sparreboom A. (2001) "Clinical pharmacokinetics and metabolism of irinotecan (CPT-11)" *Clin. Cancer Res* 7:2182–2194

[47] Glimelius B. (2005) "Benefit-risk assessment of irinotecan in advanced colonrectal cancer" *Drug Saf*. 28:417-433

[48] Cunningham D., Pyrhönen S., James R. D., Punt C. J. A., Hickish T. F., Heikkila R., Johannesen T. B., Starkhammar H., Topham C. A., Awad L., Jacques C., Herait P. (1998) "Randomised trial of irinotecan plus supportive care versus suppoertive care alone after fluorouracil failure for patients with metastatic colonrectal cancer" *Lancet* 352:1413-1418

[49] Manfredi J. J., Parness J., Horwitz S. B. (1982) "Taxol binds to cellular microtubules" *J. Cell Biol.* 94:688-696

[50] Selin H., Moerman D. E. (2008) "Encyclopaedia of the history of science, technology, and medicine in non-western cultures" *Spinger.* p. 323 ISBN 978-1-4020-4960-6

[51] Wang Y., Shi Q.,. Dong M, Kiyota H., Gu Y., Cong B. (2011) "Natural taxanes: developments since 1828" *Chem. Rev*. 111:7652-7709

[52] Lewis W. H. (2003) "Medical botany: plants affecting human health" *Wiley*, 2nd edition, p. 196 ISBN: 978-0-471-62882-8

[53] Kingston D. G. I. (2007) "The shape of things to come: structural and synthetic studies of taxol and related compounds" *Phytochemistry* 68:1844-1854

[54] Wani M. C., Taylor H. L., Wall M. E., Coggon P., McPhail A. T. (1971) "Plant antitumor agents. VI. The isolation and structure of taxol, a novel antileukemic and antitumor agent from Taxus brevifolia" *J. Am. Chem. Soc.* 93(9):2325-7

[55] Shiff P. B., Fant J., Horwitz S. B. (1979) "Promotion of microtubule assembly in vitro by taxol" *Nature* 27:665-667

[56] Rowinksy E. K., Donehower R. C. (1991) "Taxol: twenty years later, the story unfolds" *J. Nat. Cancer Instit.* 83(24):1778-1781

[57] Nabholtz J., Tonkin K., Smylie M., Au H., Lindsay M., Mackey J. (2000) "Chemotherapy of breast cancer: are the taxanes going to change the natural history of breast cancer?" *Exp. Opin. Pharmacother* 1(2).187-206

[58] Patel R. N. (1998) "Tour de paclitaxel: biocatalysis for semisynthesis" *Annu. Rev. Microbiol*. 98:361-95

[59] Orr G. A, Verdier-Pinard P., McDaid H., Horwitz S. B. (2003) "Mechanism of Taxol resistance related to microtubules" *Oncogene* 22:7280-7295

[60] Downing K. H., Nogales E. (1998) "Tubulin and microtubule structure" *Curr. Opin. Cell Biol.* 10:16-22

[61] Perez A. (2009) "Microtubule inhibitors: differentiating tubulin-inhibiting agents based on mechanism of action, clinical activity, and resistance" *Mol. Cancer. Ther.* 8(8):2086-2095

[62] Jordan M. A., Wilson L. (2004) "Microtubules as a target for anticancer drugs" *Nature reviews* 4:253-264

[63] Zhou J., Giannakakou P. (2005) "Targeting microtubules for cancer chemotherapy" *Curr. Med. Chem.-Anti-cancer Agents* 5:65-71

[64] Fan J., Griffiths A. D., Lockhart A., Cross R. A., Amos L. A. (1996) "Microtubule minus ends can be labeled with a phage display antibody specific to alpha-tubulin" *J .Mol. Biol* 259:325-330

[65] Nogales E. (2001) "Structural insights into microtubule function" *Annu. Rev. Biophys. Biomol. Struct*. 30:397-420

[66] Wilson L., Jordan, M. A. (1995) "Microtubule dynamics: taking aim at a moving target" *Chem. Biol*. 2: 569-573

[67] Rodionov V. I., Borisy G. G. (1997) "Microtubule treadmilling in vivo" *Science* 275(5297):215-218

[68] Saxton W. M., Stemple D. L., Leslie R. J., Salmon E. D., Zavortink M., McIntosh J. R. (1984) "Tubulin dynamics in cultured mammalian cells" *J. Cell Biol.* 99:2175-2186

[69] Wadsworth P. (2001) "Cell cycle-dependent changes in microtubule dynamics in living cells expressing green fluorescent protein-α tubulin" *Mol. Bio. Cell.* 12: 971-980

[70] Jordan M. A. (2002) "Mechanism of action of antitumor drugs that interact with microtubules and tubulin" *Curr. Med. Chem. Anticancer agents* 2(1):1-17

[71] Altmann K. H. (2001) "Microtubule-stabilizing agents: a growing class of important anticancer drugs" *Curr. Opin. Chem. Biol.* 5:424-431

[72] Yeung T. K., Germond C., Chen X., Wang Z. (1999) "The mode of action of taxol: apoptosis at low concentration and necrosis at high concentration" *Biochem. Biophysi. Res. Communi.* 263:398-404

[73] Jordan M. A., Toso R. J., Thrower D., Wilson l. (1993) "Mechanism of mitotic block and inhibition of cell proliferation by taxol at low concentrations" *Proc. Natl. Acad. Sci. USA* 90(20):9552-6

[74] Chen J. G., Horwitz S. B. (2002) "Differential mitotic responses to microtubule-stabilizing and-destabilizing drugs" *Cancer Res.* 62:1935-1938

[75] Mastropaolo D., Camerman A., Luo Y., Brayer G. D., Camerman N. (1995) "Crystal and molecular structure of paclitaxel (taxol)" *Proc. Natl. Acad. Sci USA* 92:6920-6924

[76] Chaudhary A. G., Kingston D. G. I. (1993) "Synthesis of 10-deacetoxytaxol and 10-deoxytaxotere" *Tetrahedron Lett*. 34:4921-4924

[77] Chaudhary A. G., Rimoldi J. M., Kingston D. G. I. (1993) "Modified taxols 10. Preparation of 7-deoxytaxol, a highly bioactive taxol derivative, and interconversions of taxol and 7-epi-taxol" *J. Org. Chem*. 58(15):3798-3799

[78] Neidigh K. A., Gharpure M. M., Rimoldi J. M., Kingston D. G. I., Jiang Y. Q., Hamel E. (1994) "Synthesis and biological evaluation of 4-deacetylpaclitaxel" *Tetrahedron Lett*. 35:6839–6842.

[79] Chordia M. D., Chaudhary A. G., Kingston D. G. I., Jiang Y. Q., Hamel E. (1994) "Synthesis and biological evaluation of 4-deacetoxypaclitaxel" *Tetrahedron Lett.* 35:6843–6846

[80] Chaudhary A. G., Gharpure M. M., Rimoldi J. M., Chordia M. D., Gunatilaka A. A. L., Kingston D. G. I., Grover S., Lin C. M., Hamel E. (1994) "Unexpectedly facile hydrolysis of the 2-benzoate group of taxol and synthesis of analogs with increased activities" *J. Am. Chem. Soc.* 116:4097–4098.

[81] Nogales E., Wolf S. G., Downing K. H. (1998) "Structure of the αβ tubulin dimer by electron crystallography" *Nature* 391:199-203

[82] Amos L. A., Löwe J. (1999) "How Taxol stabilizes microtubule structure" *Chem. Biol.* 6(3):R65-R69

[83] Sun L., Simmerling C., Ojima I. (2009) "Recent advances in the study of the bioactive conformation of taxol" *Chem. Med. Chem*. 4:719-731

[84] Alcaraz A. A., Mehta A. K., Johnson S. A., Snyder J. P. (2006) "The T-Taxol conformation" *J. Med. Chem.* 49:2478-2488

[85] Gerritsen-van Schieveen P., Royer B. (2011) "Level of evidence for therapeutic drug monitoring of taxanes" *Fundamen. Clini. Pharmacol.* 25:414-424

1.2 Therapeutic Drug Monitoring (TDM)

Chemotherapeutic agents are commonly administered to patients according to body size measurements ($mg \cdot m^{-2}$ or $mg \cdot kg^{-1}$), however, in spite of this "individualized" dosage, the chemotherapy efficacy and the toxicity vary considerably among patients. Since the toxicity, maybe due to drug overdose, is closely related to the appearance of many side effects, chemotherapy can often lead to a decrease of patient compliance.
The highly inter-individual variability of toxicity and efficacy outcomes of chemotherapy can be in part explained by highly variable pharmacokinetics of anticancer drugs among patients, in terms of variation in rate and extent of absorption, distribution, metabolism and elimination. The variability in pharmacokinetic could be due to genetic factors or physiological status of patients. For example when the same dosage is administered to different patients, the drug plasma concentration may vary over a 10-fold range, due to the inter-patient variability in pharmacokinetics.
In this context therapeutic drug monitoring (TDM) is a valuable tool to maximize the therapeutic outcomes, minimize toxicities and increase the patient compliance. TDM involves the measurements and interpretation of drug concentrations in biological fluids to allow the determination of drug dosage for the individual patient.
TDM is widely used in the clinical care of patients from the early 1960s for the monitoring of a broad range of drugs, as cardiovascular agents, antiepileptics, antibiotics, anti-inflammatory agents, immunosupressants and antidepressants.
However, not all the drugs are suitable for TDM, and they have to fulfill several criteria:

- The drug should have a narrow therapeutic index, for example the exposure needed for a therapeutic outcome is in the same range of that associated with a high risk of toxicity.
- Small changes in drug dosage should lead to large changes in the therapeutic effect.
- The drug pharmacokinetic should be highly variable.
- The drug should have a small intra-individual variability, so the pharmacokinetic is predictable along time within the same patient.
- The drug must be repeatedly administered.
- A sensitive, accurate, precise and reproducible assay must be available for this drug.
- A technically feasible dose-adaptation strategy must be developed and validated for this drug. [1, 2]

Since anticancer drugs fulfill most of these criteria, they could be subjected to TDM.

The main techniques applied for the detection and quantification of sunitinib, irinotecan, SN38 and paclitaxel are based on mass spectrometry, HPLC or fluorescence spectroscopy.

A routine feasible analysis method based on HPLC with an UV detector was developed by Etienne-Grimaldi and co-workers to extract and quantify sunitinib and its main metabolite in plasma. The method showed a recovery of 60% and a LOD of 1.4 ng·mL.[3]

Also Blancket and co-workers developed an HPLC-UV method able to quantify sunitinib in human plasma between 20 ng·mL^{-1} and 200 ng·mL^{-1},[4] while also methods based on HPLC coupled with tandem mass spectrometry were developed at 0.2-50 ng·mL^{-1} with a limit of quantification of 0.2 ng·mL^{-1}.[5, 6]

Finally many LC/MS/MS methods were developed for sunitinib quantification at concentrations between 2 ng·mL^{-1} and 250 ng·mL^{-1},[7] or 20 ng·mL^{-1} and 10 µg·mL^{-1}.[8]

Regarding irinotecan and SN38, Mohammadi and co-workers developed a method based on HPLC using an UV detector able to quantify the drugs in 0.1-10 µg·mL^{-1} range,[9] while the group of Poujol used the HPLC with a fluorescence detector to quantify irinotecan and its metabolites at concentrations between 0.5 and 1000 µg·L^{-1}.[10]

Moreover LC coupled with electrospray mass spectrometry was used to detect irinotecan and SN38[11] with LOD of 2.5 ng·mL^{-1}.[12] Finally, an HPLC-tandem mass spectrometry method was developed by Marangon and co-workers for the simultaneous determination of irinotecan and its metabolites at concentrations of 10-10000 ng·mL^{-1} for irinotecan and 1-500 ng·mL^{-1} for SN38.[13]

Several methods were developed to quantify paclitaxel using liquid chromatography with UV detector [14] or coupled with mass spectrometry.[15] However these methods are characterized on long times for the analisys and large sample volumes (0.5 -1 mL), while the method developed by Gao and co-workers, based on a liquid-liquid extraction and analysis by liquid chromatography coupled with electrospray ionization tandem mass spectrometry was able to quantify paclitaxel from plasma samples at 10-1000 ng/mL concentrations with amount of sample (100 µL) and in a short time (4.5 min).[16]

A nanoparticle-based immunoassay was developed by Cline and co-workers for the paclitaxel quantification. The assay is based on the turbidimetric measurement of the degree of aggregation of paclitaxel monoclonal antibodies-coated nanoparticles and was able to quantify the drug with a limit of detection of 11 ng·mL^{-1} ad a limit of quantification of 19 ng·mL^{-1}.[17]

---

[1] De Jonge M. E., Huitema A. D. R., Schellens J. H. M., Rodenhuis S., Beijnen J. H. (2005) "Individualised cancer chemotherapy: strategies and performance of prospective studies on therapeutic drug monitoring with dose adaptation" *Clin Pharmacokinet* 44 (2): 147-173

[2] Alnaim L. (2007) "Therapeutic drug monitoring of cancer chemotherapy" *J. Oncol. Pharm. Practice* 13:207-221

[3] Etienne-Grimaldi M. C., Renée N., Izzedine H., Gérard Milano G. (2009) "A routine feasible HPLC analysis for the anti-angiogenic tyrosine kinase inhibitor, sunitinib, and its main metabolite, SU12662, in plasma" *J. Chromatogr. B* 877:3757-3761

[4] Blanchet B., Saboureau C., Benichou A. S., Billemont B., Taieb F., Ropert S., Dauphin A., Goldwasser F., Tod M. (2010) "Development and validation of an HPLC-UV-visible method for sunitinib quantification in human plasma" *Clin. Chim. Acta* 404:134-139

[5] De Bruijn P., Sleijfer S., Lam M. H., Mathijssen R. H. J., Wiemer E. A. C., Loos W. J. (2010) "Bioanalytical method for the quantification of sunitinib and its n-desethyl metabolite SU12662 in human plasma by ultra performance liquid chromatography/tandem triple-quadrupole mass spectrometry" *J. Pharm. Biomed. Anal.* 51:934-941

[6] Van Erp N. P., De Wit D., Guchelaar H. J., Gelderblom H., Hessing H. J., Den Hartigh J. (2013) "A validated assay for the simultaneous quantification of six tyrosinekinase inhibitors and two active metabolites in human serum using liquid chromatography coupled with tandem mass spectrometry" *J. Chromatogr. B* 937:33-43

[7] Andriamanana I., Gana I., Duretz B., Hulin A. (2013) "Simultaneous analysis of anticancer agents bortezomib, imatinib, nilotinib, dasatinib, erlotinib, lapatinib, sorafenib, sunitinib and vandetanib in human plasma using LC/MS/MS" *J. Chromotogr. B* 926:83-91

[8] Lankheet N. A. G., Hillebrand M. J. X., Rosing H., Schellens J. H. M., Beijnen J. H.,. Huitema A. D. R. (2013) "Method development and validation for the quantification of dasatinib, erlotinib, gefitinib, imatinib, lapatinib, nilotinib, sorafenib and sunitinib in human plasma by liquid chromatography coupled with tandem mass spectrometry" *Biomed. Chromatogr*. 27:466-476

[9] Mohammadi A., Esmaeili F., Dinarvand R., Atyabi F., Walker R. B. (2010) "Simultaneous determination of irinotecan hydrochloride and its related compounds by high performance liquid chromatography using ultraviolet detection" *Asian J. Chem.* 22(5):3966-3972

[10] Poujol S., Pinguet F., Malosse F., Astre C., Ychou M., Culine S., Bressolle F. (2003) "Sensitive HPLC-fluorescence method for irinotecan and four major metabolites in human plasma and saliva: application to pharmacokinetic studies" *Clin. Chem*. 49(11):1900-1908

[11] Nussbaumer S., Fleury-Souverain S., Antinori P., Sadeghipour F., Hochstrasser D. F., Bonnabry P., Veuthey J. L., Geiser L. (2010) "Simultaneous quantification of ten cytotoxic drugs by a validated LC–ESI–MS/MS method" *Anal. Bioanal. Chem.* 398:3033–3042

[12] Ragot S., Marquet P., Lachâtre F, Rousseau A., Lacassie E., Gauliera J. M., Dupuya J. L., Lachâtre G. (1999) "Sensitive determination of irinotecan (CPT-11) and its active metabolite SN-38 in human serum using liquid chromatography–electrospray mass spectrometry" *J. Chromotogr. B* 736:175-184

[13] Marangon E., Posocco B., Mazzega E., Toffoli G. (2015) "Development and validation of a High-Performance Liquid Chromatography–Tandem Mass Spectrometry method for the simultaneous determination of irinotecan and its main metabolites in human plasma and its application in a clinical pharmacokinetic study" *PLOS ONE* DOI:10.1371

[14] Andersen A, Warren D. J., Brunsvig P. F. (2006) "High sensitivity assays for docetaxel and paclitaxel in plasma using solid-phase extraction and high-performance liquid chromatography with UV detection" *BMC Clin. Pharmacol*. 6:2.

[15] Basileo G., Breda M., Fonte G., Pisano R., James C. A. (2003) "Quantitative determination of paclitaxel in human plasma using semi-automated liquid-liquid extraction in conjunction with liquid chromatography/tandem mass spectrometry"*J. Pharm. Biomed. Anal*. 32:591–600.

[16] Gao S., Zhou J., Zhang F., Miao H., Yun Y., Feng J., Tao X., Chen W. (2013) "Rapid and sensitive liquid chromatography coupled with electrospray ionization tandem mass spectrometry method for the analysis of paclitaxel, docetaxel, vinblastine, and vinorelbine in human plasma" *The Drug Monit*. 0:1-7

[17] Cline J. D., Hongxia Zhang H., Lundell D. G., Harney L. R., Riaz H. K., Jarrah J., Li Y., Miyazaki M., Courtney J. B., Baburina I., Salamone S. J. (2013) "Development and evaluation of a nanoparticle-based immunoassay for determining paclitaxel concentrations on routine clinical analyzers" *Ther. Drug. Monit*. 35(6):809-815

1.3 Point of Care Devices

In addition to the TDM as a useful technique to monitor the drug concentrations in blood samples during chemotherapy, the application of point of care devices represents a crucial step to improve the patient quality of life.

During the past 40 years, the number of available point of care devices is considerably increased, aimed at making the healthcare more centered around patient, thanks also to the development of highly sensitive and miniaturized technologies that found many applications in sensor technique.

Within the point of care devices market, those for glucose monitoring and for pregnancy test are the most popular ones, while other devices including critical care, infectious disease, cardiac markers, diabetes, lipids coagulation and haematology are mainly used by clinicians.[1]

Point of care devices are small and portable systems based on sensors able to provide a rapid response of the sample with no human intervention besides adding the sample and collecting the data. The main required features of a point of care device are the simplicity to use, the use of cheap and stable reagents. They should be robust in storage and usage, and the results should be concordant with an established laboratory method. The overall device with associated reagents and consumables must be safe to use.[2]

Two different types of point of care devices can be distinguished: small handheld ones including qualitative and quantitative strips that are the most popular, and those which are larger benchtop devices with more complex built-in fluidics, often variants to that used in conventional laboratories. Test strips are based on dipsticks, lateral flow assays (LFAs) and microfluidic paper-based devices (μPADs).[3] Dipsticks, such as pH test strips and urine test strips are simple to design and easy to manufacture and to use. These tests, usually based on a colorimetric reaction, give a qualitative or semi-quantitative response. A qualitative strip test is able to discriminate “plus” and “minus” results by a simple visualization or by optical detection using a simple readout device, where the observed optical signal can be produced by a chemical indicator reaction or by an immunological reaction. The strips are made of a porous matrix, usually a cellulose filter paper or chromatography paper, mixed with dried reagents onto a carried element. The sample, urine or blood, is settled onto the matrix and, after soaking the strip, penetrates inside the matrix and reacts with other components leading to a coloured response. Using this method different point of care devices were obtained for pregnancy testing, detection of blood in stool,

Figure1.9: example of glucometer, from ref 4

detection of infectious agents in swab materials and detection of analytes in urine.[4]
Lateral flow assays strips are typically composed of a nitrocellulose membrane, sample pad, conjugated pad, wicking or absorbent pad and backing pad. The recognition element is placed on the nitrocellulose support to form test and control lines, and after placing a small amount of sample in the sample pad, it migrates along the strip and reaches the recognition elements giving a qualitative and quantitative response.[5] In the μPAD technique, 2D or 3D microfluidic channels are created on paper which are able to transport liquids in the predesigned pathways on paper where the analyte detection and semi-quantification occurs.[6]
The simplest method to obtain a quantitative device is that applied for glucose quantification in blood. The test is based on a biosensor incorporating an enzyme containing redox groups that change redox state during the biochemical reaction. Enzymes of this type are glucose oxidase and glucose dehydrogenase. The detection occurs by potentiometric or electrochemical measurement, where the latter is usually preferred since the it gives a device less subjected to interferences, more compact and able to produce a rapid response analyzing small sample amounts.[7]
Finally integrated cartridges were applied as point of care devices for the rapid measurement of sodium, potassium, chloride, urea, nitrogen, glucose and hematocrit. The system is composed of a portable hand-held analyzer and a disposable cartridge where the sample analysis takes place. The analyzer consists of a mechanical system that controls the flow of calibrator and sample within the cartridges, an electrical connector to receive signal from the cartridge, an electronic system that measures and monitors signals from the biosensors in the cartridges and a liquid crystal screen that displays the results. The cartridge contains a calibrator solution, a sample-handing system, conductivity pads that make electrical contact with the analyzer and a series of biosensors. Different analytes are quantified by different mechanisms: sodium potassium and chloride are measured by direct ion-selective electrode potentiometry, urea is hydrolyzed by urease and the ammonium ions are measured by ion selective electrode, while glucose is measured amperometrically via the hydrogen peroxide product of glucose oxidase reaction. Finally, hematrocrit is determined by conductivity.[8]
Despite the widespread application of point of care devices in clinical diagnostic, these systems are not commercialized yet in the therapeutic drug monitoring field.[9]

Figure 1.10: example of disposable cartridge, from ref 5

[1] St John A., Price C. P. (2014) "Existing and emerging technologies for point of care testing" *Clin. Biochem. Rev*. 35(3):155-67

[2] Piletsky S. A., Turner N. W., Laitenberger P. (2006) "Molecularly imprinted polymers in clinical diagnostics—Future potential and existing problems" *Med. Eng. And Physics* 28 (2006) 971–977

[3] Hart R. W., Mauk M. G., Liu X., Qiu X., Thompson J. A., Chen D., Malamud D., W. R. Abrams, Bau H. H. (2011) "Point-of-care oral-based diagnostics" *Oral Diseases* 17:745-752

[4] Luppa P. B., Müller C., Schlichtiger A., Schlebusch H. (2011) "Point-of-care testing (POCT): current techniques and future perspectives" *Trends Anal. Chem*. 30(6):889-898

[5] Hu J., Wang S. Q., Wang L., Li F., Pingguan-Murphy B., Lu T. J., Xu F. (2014) "Advances in paper-based point-of –care diagnostics" *Bios. Bioelectr*. 54:585-597

[6] Li X., Ballerini D. R., Shen W. (2012) "A perspective on paper-based microfluidics: current status and future trends" *Biomicrofluidics*. 6(1):011301-1 – 011301-13

[7] Newman J. D., Turner A. P. F. (2005) "Home blood glucose biosensors: a commercial perspective" *Bios. Bioelectr.* 20:2435-2453

[8] Erickson K. A., Wilding P. (1993) "Evaluation of a novel point-of-care system, the i-STAT portable clinical analyzer" *Clin. Chem*. 39(2):283-287

[9] Sanavio B., Krol S. (2015) "On the slow diffusion of point-of-care systems in therapeutic drug monitoring" Front. *Bioeng. Biotechnol*. 3:20.

1.4 Sensors, Point of Care Devices and Imprinted Polymers

Sensors

A sensor is a device able to detect and quantify with high specificity and selectivity the target molecule. The core of the sensor is a recognition element, a receptor able to bind selectively the target molecule. The chemical signal generated by the recognition process is used by the transducer to produce an electrochemical, optical, mass or thermal signal that could be finally amplified by a computer.[1, 2]

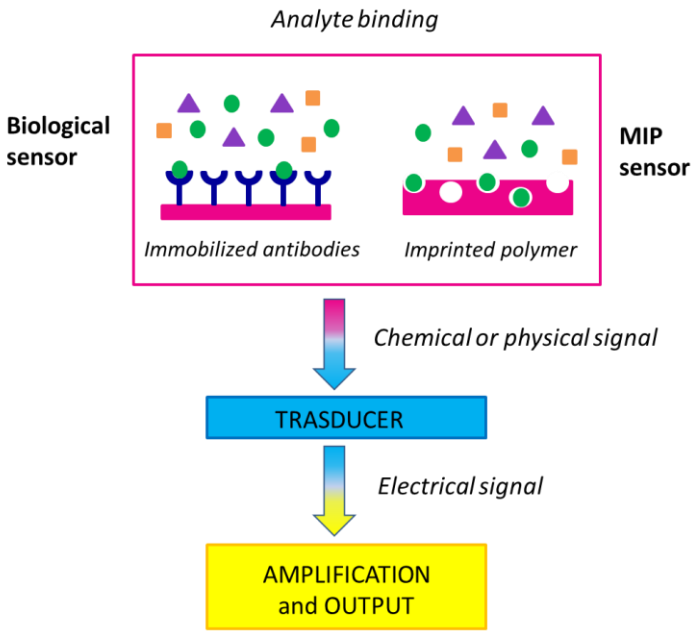

Figure 1.11: general structure of a sensor

Over the past few decades, chemical and (bio)sensors have attracted considerable attention within the field of analytical chemistry, in particular food[3,4,5] and environmental analysis[6], production monitoring as well as detection of illicit drugs[7,8] and clinical diagnostic.[9,10] These sensors, could be used for the development of new devices that are less expensive, simpler to construct and operate, reliable and able to

quantify the analyte with an adequate detection limit and a good selectivity and accuracy.

A biosensor is a sensor containing a biological component such as an antibody, enzyme, nucleic acid, proteins or whole cells as recognition elements. Initially these bio-elements were isolated from living systems, while with the development of recombinant antibodies and phage display antibody libraries, biosensors could be obtained now also for analytes for which a natural receptor does not exist.[11]

The choice of antibodies as recognition elements is very convenient thanks to their high specificity, but the main problems are related to the cost of antibodies production and to their stability.[12,13] Numerous attempts were done to obtain smaller and more stable receptors, like bio-engineered antibodies fragments and affibodies, single domain proteins obtained by phage display and characterized by affinity and specificity to any given protein target. Other types of artificial receptors are nucleic acids and small peptides. However the majority of these biomolecules showed a poor chemical and physical stability preventing their application under harsh conditions.[14]

To overcome this problem, artificial receptors could be obtained by rational design and chemically synthetized, however this approach is more appropriate for targeting small molecules, such as inorganic ions and it is usually requires many synthetic steps.[15] This approach may proves difficult if the analyte is a large molecule; in this case the molecularly imprinting of synthetic polymers becomes one of the most preferred techniques. In fact the binding sites generated during the imprinting process have affinities and selectivities similar to those of antibody-antigen systems, but due to their highly crosslinked polymeric matrix, the imprinted polymers are more stable and robust than natural antibodies.[16] For these reasons they could be easily applied as artificial receptors in sensor development able to work also in extreme environments such as the presence of acids or bases, inorganic solvents, of high pressures and temperatures. Moreover these polymers are cheap and fast to produce and they could be stored in the dry state at room temperature for long time.[17]

Molecular Imprinting Technology

In the molecular imprinting process, functional monomers and a crosslinker are co-polymerized in the presence of the target molecule that acts as a template. The functional monomers are molecules containing particular functional groups able to interact with the target molecule, and the presence of a polymerizable acryloyl or vinyl group allow their incorporation in the polymeric matrix during the synthesis.

In the non-covalent approach, a complex between the functional monomer and the template is created before polymerization, and during the synthesis the functional groups involved in the interaction are held in position by the highly crosslinked polymeric matrix that surrounds the complex. Subsequent removal of the template molecule reveals binding sites that complement in shape, structure and functional groups, the analyte. In that way, a molecular memory is introduced inside the polymer, which is now capable to rebind the target molecule with high specificity.[18]

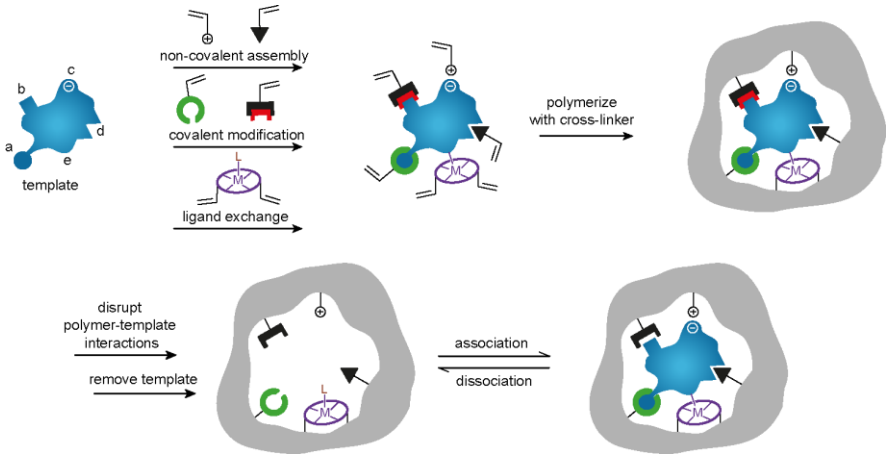

Figure 1.12: imprinting process

In this first approach a pre-polymerization complex is created between the functional monomer and the template by weak interactions (self assembly) like hydrogen-bonds, ion pair interactions, Van der Waals forces, ion pair interactions and dipole-dipole bonds. In this process, originally developed by Mosbach,[19] functional monomers are positioned in a particular orientation with respect the template prior to polymerization. The number of non-covalent interaction must be sufficient to allow the organization of the binding pocket during polymerization. Also the use of a cross linking functional monomer during polymerization allows to create a three dimensional rigid structure around the template molecule and produces stable binding cavities. The non-covalent process is the most used imprinting technique due to the large availability of functional monomers and the possibility to use the imprinting process with a large number of target molecules. This technique is not particularly successful for templates lacking appropriate functional groups able to create many strong non-covalent interaction with the functional monomers.[20, 21]

To overcome this limitation Wulff et al. introduced the covalent approach that is based on the creation of reversible covalent interactions between the target molecule and the functional monomer before polymerization. The covalent bonds are cleaved after polymerization to release the template, while the active functional groups are renewed to allow them to make the same covalent interactions with the target molecule in the obtained binding cavities of the polymer.[22]

Despite the high specificity of binding sites created by the covalent approach, it is limited by the rather small number of useful reversible covalent interactions that can be used. Therefore both the template and functional monomers must possess appropriate functional groups able to create a covalent bond. The most common functionalities involved in this process are boronic acid, aldehyde, diol or amine groups.[23, 24, 25]

Composition and Synthesis of Imprinted Polymers

The choice of functional monomers and crosslinker is an important step in the synthesis of molecularly imprinted polymers because the functional monomer allow to create characteristic interaction with the template molecule, while the co-monomer and the crosslinker give to the polymer the necessary stability and rigidity to maintain a memory for the template molecule. Moreover, the crosslinker is important in controlling the morphology of the polymeric matrix, whether it be gel-type, macroporous or a microgel powder, and it imparts the mechanical stability to the polymer. [26]

The majority of imprinted polymers are based on polystyrene or polyacrylamide. The attractiveness of vinyl and acrylic polymers arises for the large availability in commerce of these types of functional monomers. Moreover these molecules can be positively or negatively charged, hydrogen bonding, hydrophobic or metal coordinating, allowing the interaction with the template molecule.[27]

The imprinting technique was also applied to obtain inorganic materials like xerogels using tetraalkoxysilanes as precursors.[28]

The most important synthetic method to obtain organic imprinted polymers is the free radical polymerization, a widely exploited technique in industry field for the production, on a multi-tone scale, of numerous commercially important plastics. Radical polymerization can be performed under mild reaction conditions, like room temperature and atmospheric pressure, in bulk or in solution, with a wide range of low cost functional monomers like styrene, ethylene, methyl methacrylate which are of particular industrial importance. Since this technique is simple, cheap and very tolerant of functional groups in the monomers and impurities in the system (eg. water), it represents a good choice for the synthesis of molecularly imprinted polymers.

In radical polymerization, (Scheme 1.7) a reactive species, produced from the initiator, adds to the π-bond of the functional monomer to form a new radical that reacts with

another monomer molecule to propagate the reactive center increasing the chain length. Polymer growth terminates by destruction of the reactive center, leading to a polymer that could be linear or cross-linked depending on the properties of the functional monomers used.[29]

Three main steps could be distinguish in the radical polymerization process: *initiation*, *propagation* and *termination*. The initiation step involves two reactions: the production of free radicals by homolytic dissociation of the initiator giving a pair of radicals, and the addition of one of ex radicals to the first monomer molecule, by reaction on the π-bond, to produce the chain initiating radical.

The second step, called propagation, consist of the growth of the chain initiating radical by the successive addition of large numbers of monomer molecules in sequence, where each addition creates a new radical that has the same identity as the one previously, except that it is larger by one monomer unit. The propagation step occurs very rapidly with a rate constant of 10^2-10^4 $Lmol^{-1}s^{-1}$ for most monomers.

Finally, the polymer stops growing and the polymerization terminates. The termination process consist at the annihilation of the radical centers by bimolecular reaction between two radicals that could occurs by *combination* (*coupling*) or, more rarely by *disproportionation*. In the combination process a covalent bond is created between two radical chains or molecules, leading to a single macromolecule. Instead, in disproportionation, a hydrogen that is *beta* to one radical center is transferred to another radical center giving two polymer molecules, one saturated and one unsaturated. Typical termination rate constants are in the range of 10^6-10^8 $Lmol^{-1}s^{-1}$.

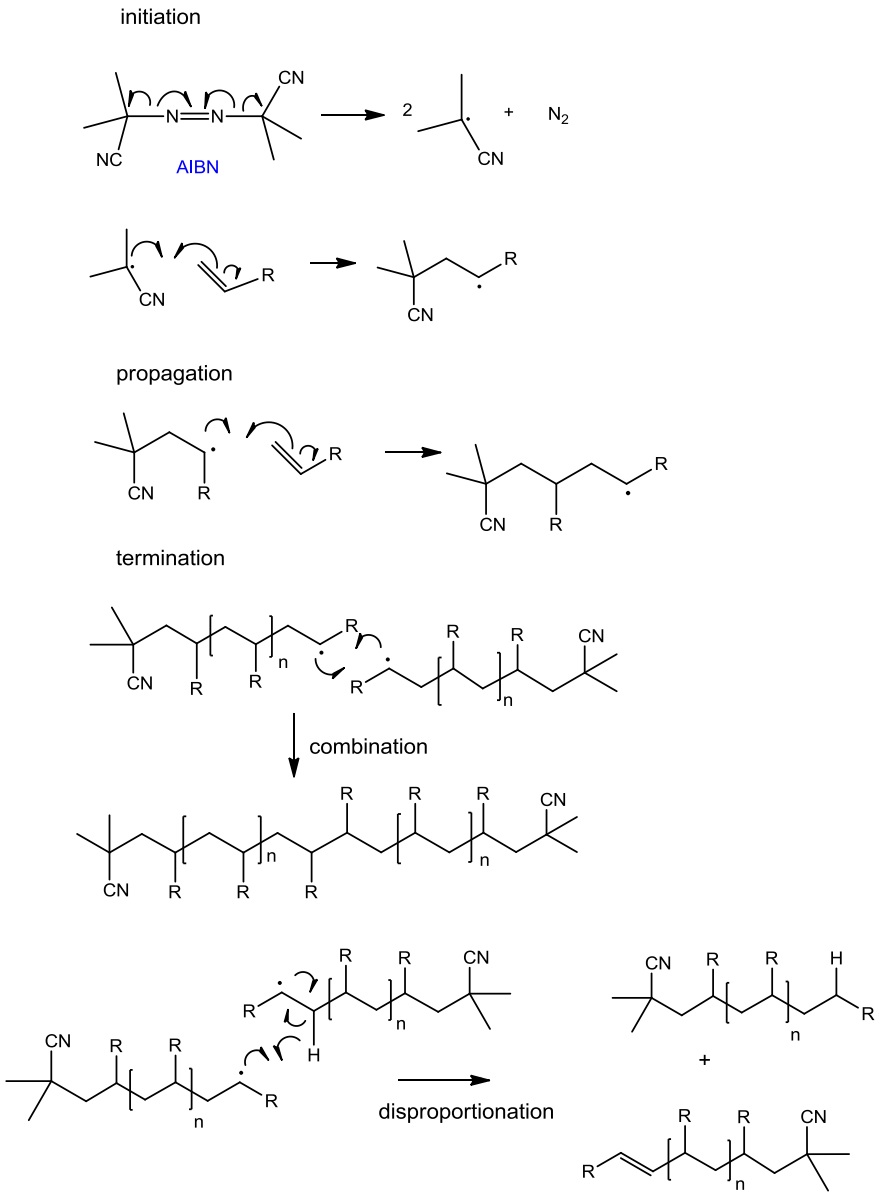

Scheme 1.7: radical polymerization

The structural arrangements of monomer units during the polymer synthesis is influenced by the presence of substituents (R) on the double bond of the monomer. The propagating radical could be on carbon 1:

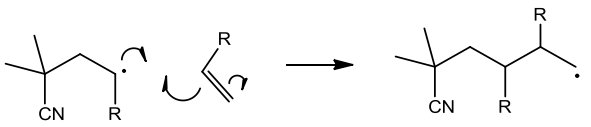

Equation 1

Or on carbon 2:

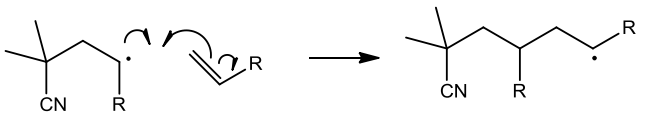

Equation 2

If during the propagation step the subsequent addition of monomers occurs always in the same manner, the final product will have an arrangement of monomer units in which the substituents are on alternate carbon atoms leading to the *head-to-tail* arrangement. On the other hand, if the monomer additions occurs alternatively by equations 1 and 2, the *head-to-head* placement is obtained.

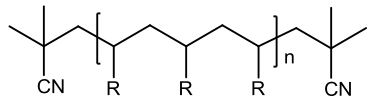

Head-to-tail placement

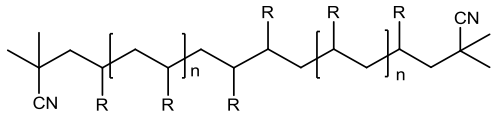

Head-to-head placement

Scheme 1.8: monomers arrangements in the obtained polymeric chain

The *head-to-tail* propagation is the most common process because the propagating radical obtained by the addition on carbon 2 of the monomer unit is more stable than that generated by the reaction on carbon 1 of the monomer. Stabilization is due to both a resonance effect of the substituents, and a steric effect, since the approach of a propagating radical at the unsubstituted carbon of a monomer molecule is much less sterically hindered compared to the approach at the substituted carbon.

The propagation process characterized of only head-to-tail placement is regioselective and lead to polymer structures called *isoregic*, while it is called *syndioregic* if the resulting polymer structure contains alternated regions of *head-to-tail* and *head-to-head* arrangements, finally if there are random arrangements of *head-to-head* and *head-to-tail* the resulting structure is called *aergic*. [30]

Structure of the Polymers

Different structures can be obtained during polymerization depending on the way of synthesis and on the types of functional monomers used. Functional monomers containing only one polymerizable double bound could lead to only linear polymers by a radical polymerization. In the presence of both functional monomers and crosslinker (a molecule containing two or more double bonds) linear chains are chemically linked each other to obtain reticulated co-polymers. Depending on the extent of crosslinking, branched macromolecules or crosslinked polymers are created.

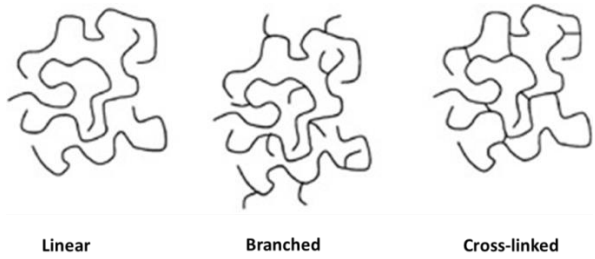

Figure 1.13: polymer structure

Branched Macromolecules

Branched macromolecules are polymers containing side chains that could be placed at irregular intervals along the polymer backbone or could be arranged into layers extending from the center of the polymer to obtain a regular structure called dendrimer. The possibility to obtain monodisperse dendrimers with a known number of end groups, due to their ordered structure, makes dendrimers attractive candidates for the development of drug delivery systems, gene-delivery or of supports for catalysis. For example the group of Zimmerman developed a molecularly imprinted polymer based on dendrimer technique and containing only one binding site. The porphirin target molecule was covalently linked to eight dendrons to obtain a dendrimer whose termini were after polymerized. The target molecule was removed by hydrolysis to obtain the imprinted dendrimer. This technique is advantageous because of a good efficiency of the imprinting process, an easy removal of the template and good solubility properties of the imprinted dendrimer in organic solvents. [31]
Since the dendrimer synthesis requires multiple reaction-purification steps with a difficulty to obtain large amounts of polymers, this technique is not appropriate for large scale applications. Moreover, this synthetic approach is incompatible with the majority of target molecules. [32]

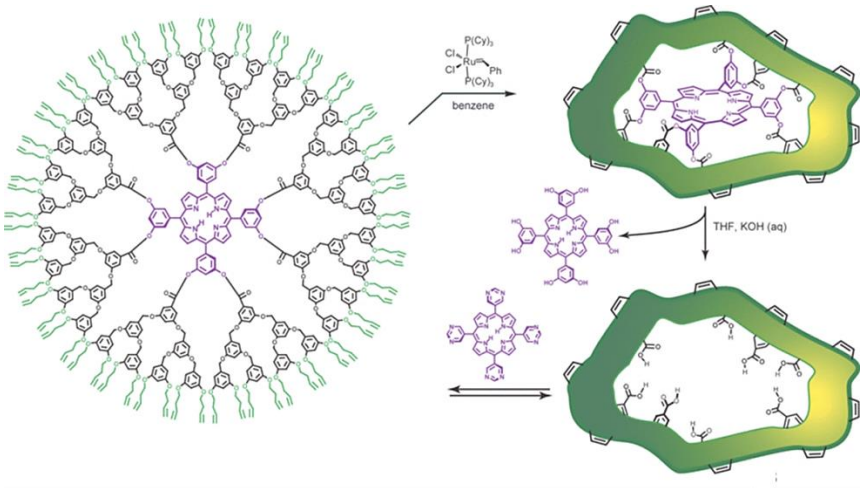

Figure 1.14: example of a molecularly imprinted dendrimer (from ref 31)

Crosslinked Polymers

If the branches of a polymeric backbone are covalently linked to other polymer chains, a polymeric network is created to obtain a crosslinked polymer. Since this is a simple, fast and cheap reaction, it is particularly useful for large scale applications.

In a co-polymerization process involving functional monomers and a crosslinker, the physical nature of the product is mainly dependent on the nominal crosslinking ratio, defined as the percentage of cross-linker with respect to the total number of moles of monomer, and the volume and the nature of the solvent in which the polymerization is carry out. If the polymerization occurs with a high ratio of crosslinker and high concentration of monomers, macroporous polymers are obtained by precipitation from the polymerization mixture. These polymers are characterized by a permanently porous structure even in the dry state, that leads to an high specific surface area and allow the access to the pores also with thermodynamically non-compatible solvents. These features added to a high mechanical robustness of the polymer due to the high percentage of crosslinker used, make the macroporous polymers very attractive for the development of molecularly imprinted polymers.[33, 34]

This technique is widely used to obtain molecularly imprinted resins for affinity chromatography, HPLC and solid-phase extraction (SPE) to extract and quantify a wide range of analytes from biological samples.[35, 36, 37, 38, 39,40]

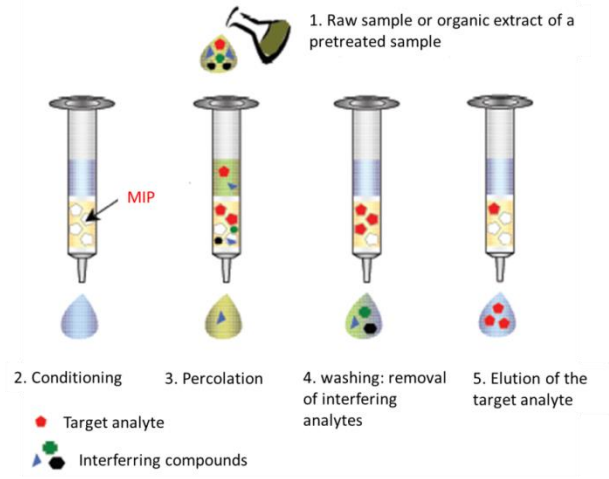

Figure 1.15: example of solid phase extraction, from ref[41]

When the volume of solvent in the polymerization mixture is higher than that normally used for the synthesis of macroporous polymers, small particles are synthetized of micro or nano scale and their aggregation during the synthesis is prevented by the high dilution conditions.[42]

In recent times, this technique was widely applied for the synthesis of molecularly imprinted micro or nano-particles, characterized by an high surface-volume ratio and an easy accessibility to a high number of binding sites. Thank to these properties, MIPs have found application in the drug delivery field for the controlled release of drugs, as recognition elements for the development of specific sensors, or as artificial enzymes in catalysis.[43]

Changing the polymerization conditions, also core-shell nanoparticles could be obtained. The group of Perez, for example, synthesized core-shell nanoparticles containing specific binding sites for cholesterol by emulsion polymerization. The process consists of a preliminary synthesis of 30-40 nm non-imprinted nanoparticles followed by polymerization of the same functional monomers in the presence of the nanoparticles and the template to obtain a thin layer of imprinted polymer around the non-imprinted particle.[44] Since they used a covalent approach for the imprinting process, the removal of template was achieved by hydrolysis, however other examples are reported in literature of synthesis of imprinted core-shell nanoparticles for caffeine, atrazine and propranolol by a non-covalent approach. [45, 46, 47]

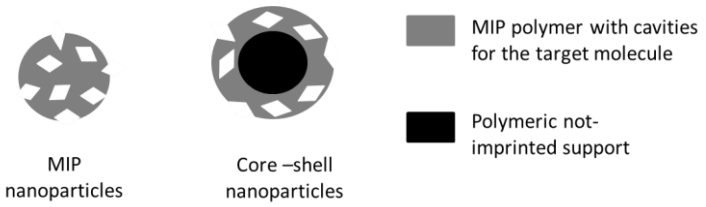

Figure 1.16: examples of MIP nanoparticles and MIP-core-shell nanoparticles.

To increase the surface area available in the imprinted polymer and to facilitate the removal of template, other polymeric structures were exploited. Nanowires and nanotubes were synthetized with the imprinting technique. The group of Xie synthetized nanowires containing binding sites for 2,4,6-trinitrotoluene (TNT) on the surface. During the synthesis, a modified alumina membrane was used to bind the template that interacts also with the functional monomers. The following polymerization and removal of the membrane and the template, gives the imprinted nanowire.[48]

To increase the surface to volume ratio, nanotubes were synthesized and applied in particular to develop specific sensors for β-estradiol detection.[49]

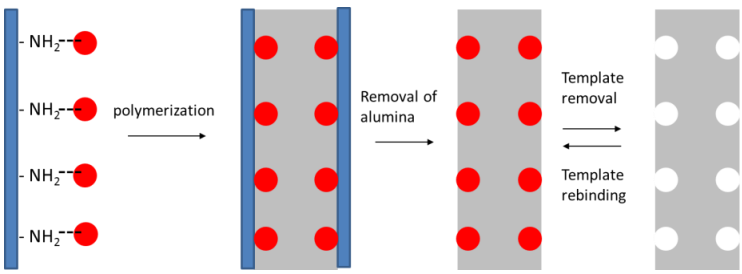

Figure 1.17: example of molecularly imprinted nanowire
(in red: target molecule, in grey: MIP matrix, in blue: alumina support), (From ref 48)

Sensors Based on Molecularly Imprinted Polymers

The high stability, the simple and low cost synthesis and the binding affinities and selectivities similar to those of antibodies, enzymes or hormones receptors, make molecularly imprinted polymers very useful for the development of sensors.
In this field the imprinted polymer could be used as the recognition element of the sensor where the polymer is immobilized on a transducer able to convert the chemical signal generated from the binding process, to a quantifiable output signal, usually an electrical signal.
Alternatively, the imprinted polymer could be a sensor itself if some reporter groups are incorporated in to the polymeric matrix giving characteristic properties to the polymer, like fluorescence or colour, that could change upon binding with the target molecule. [50]

MIP Immobilized on the Transducer

The general structure of a MIP-based sensor consists of the recognition element, that is the imprinted polymer, immobilized on a transducer able to create quantifiable signal that is after amplified and analyzed by a computer. The first sensor developed with MIP was a capacitance sensor based on a MIP membrane imprinted with phenylalanine anilide placed on a field-effect capacitor.[51] The binding of the analyte leads to a change in capacity that is detected, however this sensor is only qualitative, while later, the same transducer method was applied to set up a quantitative sensor containing electropolymerized polyphenols layers on gold electrodes to quantify phenyalanine.[52]
Subsequently, different electrochemical sensors were synthesized.[53, 54] Mass-sensitive acoustic transducers such as the quarz crystal microbalance (QCM) have found large application in MIP sensor field. A sensor for glucose was set up by electropolymerization of a poly(*o*-phenylenediamine) template with the target molecule, directly on the transducer surface. The sensor was able to detect glucose with a good selectivity against ascorbic acid, paracetamol, cysteine and fructose, but the limit of detection was high and only millimolar concentrations could be measured.[55]
To improve the limit of detection, conductometric sensors were developed. In this case two electrodes are separated by an imprinted polymer, usually in a membrane form. The binding of the analyte to the polymer changes its conductivity, which is translated into an electrical signal. Using this method a sensing device to quantify atrazine was obtained. The sensor is based on atrazine imprinted acrylic polymer membrane whose flexibility and stability was regulated changing the kind and molar ratio of crosslinker and the amount of porogenic solvent in the imprinting mixture. The conductometric response seems to be dependent on the ability of the polymer to change its

conformation upon analyte binding. For these reason the membrane flexibility is an important factor in this type of sensor. This sensor showed an excellent low detection limit of 5 nmol·L^{-1}, rapid measurement times between 6-10 min and high selectivity for atrazine over structurally related triazine herbicides.[56]
Recently, also the cyclic voltammetry technique was applied to develop a MIP-based sensor to quantify atrazine with high sensitivity between 5 nmol·L^{-1} and 140 nmol·L^{-1} with a limit of detection of 1 nmol·L^{-1}.[57]
Also optical techniques could be used, in particular surface plasmon resonance (SPR) was widely applied. Thin films of electropolymerized imprinted polymer for theophylline detection were synthesized on gold coated glass slides to obtain a SPR sensor, able to capture the target molecule in a 10-50 µmol·L^{-1} range and a limit of detection of 3.36 µmol·L^{-1}.[58] Thermal and radical polymerization methods were developed by Xu and co-workers to cover a gold chip with a molecularly imprinted polymer for Sudan I dye. The radical initiator was covalently linked to 1-dodecanethiol that is immobilized on the gold chip. After thermal radical polymerization or photo-initiated polymerization of methyl methacrylate and ethylene glycol dimethacrylate in the presence of Sudan I dye, a thin layer of imprinted polymer was obtained on the gold surface. The resulting SPR sensor exhibited high sensitivity with a limit of detection of 30 ng*mL^{-1} and a good selectivity. [59]
During the recent years many efforts were spent to miniaturize these sensors. In this context Surface Enhanced Raman Spectroscopy (SERS) becomes a useful analytical technique to detect, quantify and in some cases identify the target molecule. In fact micro-Raman spectroscopy was used to develop MIP nanosensors for propranolol, however the first sensor was characterized by low sensitivity and reproducibility.[60] To overcome these problem, the recognition properties of MIP were combined with noble metal nanocomposities for signal amplification and optical readout to obtain a single particle nanosensor. The obtained Au-MIP core-shell nanoparticle is a single particle nanosensor for SERS measurements, able to detect propranolol at concentrations as low as 10^{-7} mol·L^{-1}.[61] Core-shell Au nanoparticles containing an imprinted shell based on triethoxysilane (AuNPs) were also synthesized to detect bisphenol A by SERS technique with a limit of detection of 0.52 µmol·L^{-1}.[62]

MIPs-embedded Sensors

Fluorescent Molecularly Imprinted Polymers

Fluorescence spectroscopy represent a valid technique in MIP sensors mainly due to its high sensitivity in comparison to other spectroscopic techniques, allowing the detection and quantification of low analyte concentrations. If the analyte is not a fluorescent

molecule, these sensors can be based on two different detection schemes: a fluorescent imprinted polymer can be obtained incorporating a fluorescent functional monomer into the polymeric matrix. These functional monomers are placed inside the binding sites of the polymer and are able to interact with the target molecule leading to a change of the emission intensity, lifetime or emission wavelength of the resulting MIP upon analyte binding. Using this technique the imprinted polymer is a sensor itself because an intrinsic property of the MIP is used as the transducing system. Otherwise if both the analyte and the polymer are not fluorescent, a competitive or displacement assay can be set up synthesizing a fluorescent analogue that can compete with the analyte for the polymer binding sites.[63]

Following the first approach a fluorescent chemosensor was developed for the aqueous detection of cAMP. The MIP was synthesized by a radical polymerization of 2-hydroxyethyl methacrylate (HEMA) and trans-4-[p-(N,N-dimethylamino)styryl]-N-vinylbenzylpyridinium chloride, a fluorescence functional monomer able to bind cAMP by electrostatic interactions, π-stacking and hydrogen bonds, leading to a quenching of its fluorescence. Therefore observing the fluorescence quenching of the obtained bulk MIP, aqueous cAMP could be quantified using this sensor in a micromolar range.[64]

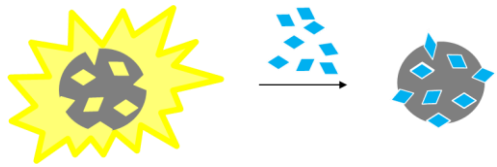

Figure1.18: quenching of MIP fluorescence due to the analyte binding

A fluorescent sensor based on molecularly imprinted polymer was also developed to detect highly explosive compound such as TNT. In this case, MIP micro-particles based on acrylic acid and ethylene glycol dimethacrylate (EGDMA) were covalently linked to fluorescence CdSe quantum dots by a coupling reaction between the carboxylic acid of the MIP and the amine-functionalized surface of the quantum dots. The resulting sensor exhibits a quenching of fluorescence upon the binding of TNT, allowing the analyte quantification with a detection limit of 40.7 $\mu mol \cdot L^{-1}$.[65]

The interactions between the fluorescence functionality into the MIP and the target analyte could lead also to an increase of the fluorescence emission. Using this approach a molecularly imprinted polymer was synthetized with 2-acrylamidoquinoline fluorescent monomer to detect cyclobarbital, where the fluorescence enhancement was generated by the hydrogen bonds created between amino and carbonyl groups of both the analyte and the quinoline mojety. The MIP was able to detect cyclobarbital in a 0.1 - 2 $mmol \cdot L^{-1}$ range.[66]

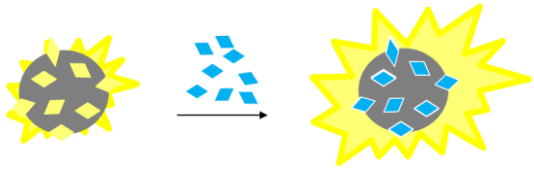

Figure 1.19: fluorescence enhancement due to target binding to MIP

The same approach was also used to synthetize a fluorescent imprinted polymer for (D)-fructose using an antracene-boronic acid conjugate with a methacrylate molecule as functional monomer. The interaction between the analyte and the fluorescent functionality in the polymer gives a fluorescence enhancement that is proportional to the amount of analyte bound. Using this fluorescent polymer, D-fructose was quantified at concentrations between 1 mmol·L^{-1} and 100 mmol·L^{-1}.[67]

A fluorescence-based optical fiber sensor was constructed to detect cocaine using molecularly imprinted polymer containing acrylamidofluorescein (AAF) as functional monomer, EDGMA as crosslinker and acrylamide as co-monomer. The carboxylate group of AAF can be deprotonated by cocaine that acts as a base in the ion pair complex leading to an increase of fluorescence, since the deprotonated form of fluoresceine is much more fluorescent than the protonated one. The imprinted polymer was covalently attached to an optical fiber to obtain a portable system able to detect cocaine at concentrations between 2 µmol·L^{-1} and 500 µmol·L^{-1} in aqueous acetonitrile mixtures with good reproducibility over one month.[68]

In order to improve the sensitivity, gold nanoparticles could be embedded in the polymeric matrix. In particular MIP-based fiber optic sensors were developed by Ton and co-workers, using 4-vinyl pyridine and a piperazinyl naphtalimide derivate fluorescent molecule as functional monomers and EDGMA as cross-liker. The presence of gold nanoparticles allow to increase the sensitivity lowering the LOD, using this technique the herbicide 2,4-dichlorophenoxyacetic acid was detected at 250 pmol·L^{-1} concentration, LOD comparable to LC/MS technique.[69]

An alternative approach to obtain fluorescent sensors to detect non-fluorescent analytes, is the development of a competitive binding assay using a fluorescent tracer. For example a competitive flow-through assay for chloramphenicol was developed by Suàrez-Rodrìguez and co-workers based on the competition between the analyte and 2-amino-1-(4-nitrophenyl)-1,3-propanediol, a fluorescent molecule characterized by a similar structure of chloramphenicol. The analyte was detected in a 8 µg·mL^{-1}-100 µg·mL^{-1} (25 µmol·L^{-1}-310 µmol·L^{-1}) range.[70]

An automated flow-through assay based on the dye displacement technique was also developed for zearalenone mycotoxin sensing using a molecularly imprinted polymer containing 1-allyl piperazine as functional monomer, trimethylolpropane

trimethacrylate as crosslinker, AIBN as initiator and a zearalenone mimic: cyclododecyl 2,4-dihydroxybenzoate as template. Measuring the fluorescence emission of 2,4-dihydroxybenzoic acid 2-[(pyrene-l-carbonyl)amino] ethyl ester (PARA), displaced from the MIP binding sites upon addition of the analyte, a calibration curve for zearalenone in acetonitrile was obtained with a dynamic range between 50 $\mu mol \cdot L^{-1}$ and 500 $\mu mol \cdot L^{-1}$and a limit of detection of 25 $\mu mol \cdot L^{-1}$.[71]

An automated molecularly imprinted sorbent assay for the rapid and sensitive analysis of penicillin-type β-lactam antibiotics in human urine was developed by Urraca and co-workers. The assay was obtained using a bulk MIP containing ethyleneglicol dimethacrylate as crosslinker, methacrylamide as co-monomer and N-[3,5-bis-(trifluoromethyl)phenyl]-N'-(4-vinylphenyl)urea as functional monomer and imprinted with penicillin G procaine salt. The concentration of penicillin G was calculated measuring the emission signal of the highly fluorescent competitor pyrenemethylacetamido penicillanic acid (PAAP) displaced by the target molecule from the polymer binding sites. The sensor showed a dynamic range from $6.80 \cdot 10^{-7}$ $mol \cdot L^{-1}$ to $7.21 \cdot 10^{-6}$ $mol \cdot L^{-1}$ and a detection limit of $1.97 \cdot 10^{-7}$ $mol \cdot L^{-1}$.[72]

Colored Molecularly Imprinted Polymers

Optical sensing represent in principle a valuable technique in the development of simple and portable sensors. For these reasons the molecularly imprinted technology was applied in the construction of colored optical sensors. To these aim, many articles reported dye displacement methods based on the competition between the free analyte and a modified dye, for the binding into the polymer, leading to a change in the polymer color (Figure 1.20).

Using this technique, Levi and co-workers synthesized a molecularly imprinted polymer for chloramphenicol by radical polymerization of the functional monomer (diethylamino)-ethylmethacrylate and the crosslinker EDGMA. The MIP was first saturated with chloramphenicol covalently linked to methyl red dye. Free chloramphenicol displaces the modified drug from the binding sites of the polymer due to the better affinity of the MIP for the free analyte with respect to the modified dye. The release of methyl red modified-chloramphenicol upon addition of chloramphenicol was monitored by an HPLC method. This system allowed to discriminate well between the analyte and other similar molecules and was able to detect chloramphenicol within a range of 3 and 1000 $\mu g \cdot mL^{-1}$ (9.3 $\mu mol \cdot L^{-1}$-3.1 $mmol \cdot L^{-1}$).[73]

Greene and Shimizu developed a colorimetric sensor array based on dye displacement strategy and composed of seven molecularly imprinted polymers able to capture seven different aromatic amines.

The imprinted polymers containing methacrylic acid and EDGMA, were first saturated with a benzofurazan dye giving a strong yellow color to the polymer. In this case the dye was used directly, without further modification. Benzofurazan is a small molecule with shape and functionalities similar to the target molecules, so it can easily interact with the functional monomers into the binding site of the polymer. After addition of the analyte, the dye was displaced and the intensity of the polymer color decreases.

One of the main advantages of this strategy is the possibility to develop a colorimetric test to detect analytes that do not possess a colour itself. Also the use of imprinted polymers without colored functional monomers makes the synthesis cheaper, for the test it is only required an appropriate dye able to bind into the MIP and to be displaced by the analyte.[74]

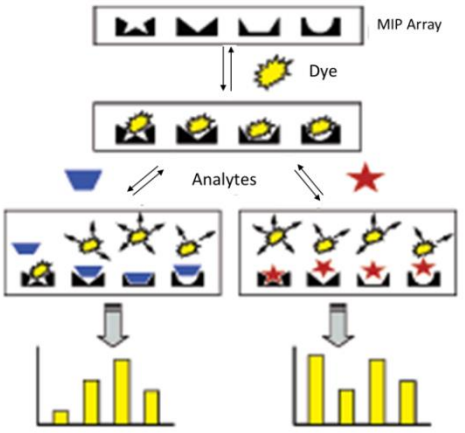

Figure 1.20: MIP sensor array using dye displacement (from ref 74)

Analyte Generating Signal

In some cases the target molecule possesses some properties like fluorescence or color that could be exploited as the signal in the sensor.

A flow injection system based on a molecularly imprinted polymer was developed for the selective and sensitive monitoring of carbaryl in water samples by measuring its fluorescence emission. The system has demonstrated an high specificity for the target molecule against other methyl-carbamate pesticides and a limit of detection of 0.27 µg/mL.[75]

A flow-through optosensing device based on the fluorescence of a flavonol target molecule was set up containing a molecularly imprinted polymer synthetized with methacrylic acid and EDGMA by a non-covalent approach. This system was able to detect flavonol in oily matrix and in general it could be an useful tool for the determination of analytes in hydrophobic samples without a separation step.[76]

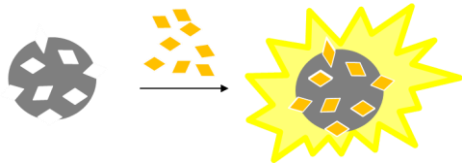

Figure 1.21: binding of fluorescent molecules

Finally, the group of Rachkov developed a fluorescent sensing system to quantify β-estradiol using a molecularly imprinted polymer as recognition element and exploiting both the intrinsic fluorescence of the target molecule as sensing element and the fluorescence led by a fluorescent dye that could bind to the polymer by a competitive mode.[77]

A fiber optic sensor based on MIP was also developed to capture the basic red 9 dye. The polymer was based on EDGMA and the functional monomer 2-acrylamido-2-methyl-1-propane sulfonic acid. The absorbance of the captured dye was detected with a fiber-coupled spectrometer until μM concentrations.[78]

Molecularly Imprinted Polymers for Taxoids and Camptothecins

Recently some molecularly imprinted polymers were synthesized to capture campthotecins, like irinotecan, and taxanes, as paclitaxel, while MIP specific for sunitinib are not developed yet.

A molecularly imprinted sorbent resin was synthesized for the simultaneous enrichment and separation of four taxoids: 10-deacetylbaccatin III, baccatin III, cephalomannine and paclitaxel, from the twigs of *T. x media*. The resin is based on Fe_3O_4 particles coated with silica and functionalized with vinyl groups that were after used to create a molecularly imprinted polymeric matrix containing both the metal nanoparticles and specific binding sites for taxoids. In this case, since the polymer has to capture different molecules having a very similar structure, and cephalomannine was selected as template molecule. Using the MIP resin 74% of 10-deacetylbaccatin III, 52% of baccatin III, 84% of cephalomannine and 60% of paclitaxel were recovered from the initial extracts. Moreover the highest recovery of cephalomannine with respect other taxoids verified the selectivity of the MIP for this molecule, since it was the template molecule.[79]

Silica nanoparticles coated with molecularly imprinted polymer layers were also synthesized by Li and co-workers to capture paclitaxel. The imprinted polymer was

synthesized at the surface of uniform silica nanoparticles using tetraetoxysilane (TEOS) and aminopropyltriethoxysilane (APTES) as functional monomers and paclitaxel as template. The Scatchard analysis obtained by rebinding tests in 0.005-0.2 $mg \cdot mL^{-1}$ (8-340 $\mu mol \cdot L^{-1}$) paclitaxel concentration range, showed the presence of two types of binding sites with different affinities for the target molecule. The association constants (K_D) obtained were 0.0094 $g \cdot L^{-1}$ for high affinities binding sites and 0.0509 $g \cdot L^{-1}$ for low affinities binding sites.[80]

Recently a MIP to detect campthotecin was also synthesized for purification and extraction purposes. A solid phase extraction method based on carbon nanotube supports coated with molecularly imprinted polymers, was developed to detect and extract campthotecin in *Camptotheca acuminate* fruit, bark and leaf. The imprinted polymer was synthesized with EDGMA and methacrylic acid using camptothecin as template molecule, while the extraction method based on MIP was coupled with high performance liquid chromatography for the quantification of the analyte. The method showed a good linearity of camptothecin in the range of 1-200 $\mu g \cdot mL^{-1}$ (2.9-574.2 $\mu mol \cdot L^{-1}$) and a limit of detection of 0.13 $\mu g \cdot mL^{-1}$ (0.4 $\mu mol \cdot L^{-1}$).[81]

A MIP for the selective solid phase extraction of irinotecan from human serum samples was synthesized. The polymerization was performed in dichloroethane with methacrylic acid and 4-vinyl pyridine as functional monomers, EDGMA as crossliker and irinotecan free base as template molecule. The obtained bulk polymer was grounded until 25-36 µm and packed into a cartridge. The drug detection was performed by LC-PDA showing an extraction recovery of 88% for human serum spiked with 10 $\mu g \cdot mL^{-1}$ (17 $\mu mol \cdot L^{-1}$). [82]

MIPs and Plasma

The behavior of soluble imprinted polymers in plasma has never been investigated in a systematic way, usually bulk imprinted polymers were applied as recognition elements of electrochemical, quantum dots or fiber optic based sensors for the drug quantification in plasma. Concerning anticancer drugs, a silica-molecularly imprinted polymer composite fiber using carboxylated multi-wallet carbon nanotubes was synthesized as electrochemical sensor able to quantify uracil and 5-fluorouracil in aqueous and blood plasma samples with an LOD of 1.3 $ng \cdot mL^{-1}$ for 5-fluorouracil and 0.56 $ng \cdot mL^{-1}$ for uracil.[83] Another electrochemical sensor for these drugs was developed by Prasad and co-workers using a drop coating method to coat a hanging mercury drop electrode with a specific MIP. Using this system uracil and 5-fluorouracil were quantified with an LOD of 3 $nmol \cdot L^{-1}$ and 2 $nmol \cdot L^{-1}$ respectively.[84] While an electrochemical sensor based on carbon-nanotubes-modified pencil graphite electrode coated with a bulk MIP was synthesized for the quantification of 1,4-dihidroxyanthraquinone, a molecule having the basic structure of anthraquinone-based

anticancer drugs like AQ4N and doxorubicin, in aqueous and blood samples. Using this system the analyte was quantified within 10 $nmol \cdot L^{-1}$ and 100 $\mu mol \cdot L^{-1}$ with an LOD of 4 $nmol \cdot L^{-1}$.[85]

Conversely, the quantification of other drugs in blood or plasma by sensors with MIP immobilized on metal nanoparticles or fibers was also reported. For example non soluble $CdTe@SiO_2$ quantum dots coated with a MIP were used as fluorescent sensor for recognition of norepinephrine between 0.04 $\mu mol \cdot L^{-1}$ and 10 $\mu mol \cdot L^{-1}$ (LOD 8 $nmol \cdot L^{-1}$) in water and in rat plasma.[86] Moreover a fiber optic array based on a competition test, was developed by Carrasco and co-workers to quantify enrofloxacin in sheep serum. The fiber was chemically etched to create microwells where the bulk MIP was deposited. The analyte displace a modified fluorescent molecule from the polymer binding sites leading a change of fluorescence intensity. Using this system enrofloxacin was quantify from 0.29 $\mu mol \cdot L^{-1}$ to 21.54 $\mu mol \cdot L^{-1}$, with an LOD of 0.04 $\mu mol \cdot L^{-1}$.[87]

---

[1] Eggins B. R. (2003) "Chemical sensors and biosensors" *Wiley* p.4 ISBN: 978-0-471-89914-3

[2] Kriz D., Ramström O., Mosbach K. (1997) "Molecularly imprinting: new possibilities for sensor technology" Anal. *Chem. News Feat.* 345A-349A

[3] Pittner F. (2009) "Sensor devices and biosensors in food analysis" *Monatsh. Chem.* 140:859-860

[4] Saini S. S., Kaur A. (2013) "Molecularly imprintes polymers for the detection of food toxins: a minireview" *Adv. Nanopart.* 2:60-65

[5] Garcia R., Cabrita M. J., Freitas A. M. C. (2011) "Application of molecularly imprinted polymers for the analysis of pesticide residues in food-a high selective and innovative approach" *Am. J. Anal. Chem.* 2:16-25

[6] Niessner R. (1991) "Chemical sensor for environmental analysis" *Trac-Trends Anal. Chem.* 10(10):310-316

[7] Baker B. R., Lai R. Y., Wood M. S., Coctor E- H., Heeger A. J., Plaxco K. W. (2006) "An electronic, aptamer-based small-molecule sensor for rapid, lebel-free detection of cocaine in adulterated samples in biological fluids" *J. Am. Chem. Soc.* 128(10):3138-3139

[8] Zurutuza A., Bayoudh S., Cormack P. A. G., Dambies L., Bischoff R., Sherrington D. C. (2005) "Molecularly imprinted solid-phase extraction of cocaine metabolites from aqueous samples" *Anal. Chim. Acta* 542(1):14-19

[9] Jain K.K. (2005) "Nanotechnology in clinical laboratory diagnostic" *Clin. Chim. Acta* 358(1-2):37-54

[10] Allender C. J., Richardson C., Woodhouse B., Heard C. M. Brain K. R. (2000) "Pharmaceutical applications for molecularly imprinted polymers" *Int. J. Pharm.* 195:39-43

[11] Turner A. P. F. (2013) "Biosensors: sense and sensibility" *Chem. Soc. Rev*. 42:3184-3196

[12] Holford T. R. J., Davis F., Higson S. P. J. (2012) "Recent trends in antibody based sensors" *Biosens. Bioelectr.* 34(1):12-24

[13] Byrne B., Stack E., Gilmartin N., O'Kennedy R. (2009) "Antibody-based sensors: principles, problems and potential for detection of pathogens and associated toxins" *Sensors* 9:4407-4445

[14] Pavan S., Berti F. (2012) "Short peptides as biosensor transducers" *Anal. Bioanal Chem.* 402(10):3055-3070

[15] Hof F., Craig S. L., Nuckolls C., Rebek J.J. (2002) "Molecular encapsulation" *Angew. Chem. Int. Ed. Engl*. 41(9):1488-1508

[16] Vlatakis G., Andersson L. I., Müller R., Mosbach K. (1993) "Drug assay using antibody mimics made by molecular imprinting" *Nature* 361:645-647

[17] Haupt K., Mosbach K. (2000) "Molecularly imprinted polymers and their use in biomimetic sensors" *Chem Rev.* 100:2495-2504

[18] Vasapollo G., Del Sole R., Mergola L., Lazzoi M. R., Scardino A., Scorrano S., Mele G. (2011) "Molecularly imprinted polymers: present and future prospective" *Int. J. Mol. Sci*. 12:5908:5945

[19] Mosbach K. (1994) "Molecular imprinting" *Trends Biochem Sci*. 19(1):9-14

[20] Holthoff E. L., Brigh V. F. (2007) "molecularly template materials in chemical sensing" *Anal. Chim. Acta* 594:147-161

[21] Zang H., Ye L., Mosbach K. (2006) "Non-covalent molecular imprinting with emphasis on its application in separation and drug development" *J. Mol. Recognit*. 19:248-259

[22] Wulff G., Vesper W., Grobe-Einsler R., Sarhan A. (1977) "Enzyme-analogue built polymers" *Makromol. Chem.* 178:2799-2816

[23] Spivak D. A. (2005) "Optimization, evaluation, and characterization of molecularly imprinted polymers" *Adv. Drug Deliv. Rev.* 57:1779-1794

[24] Khasawneh M. A., Vallano P. T. , Remcho V. T. (2001) "Affinity screening by packed capillary high performance liquid chromatography using molecular imprinted sorbents II. Covalent imprinted polymers" *J. Chromatogr. A* 922:87-97

[25] Tang Y., Fang G., Wang S. (2011) "Covalent imprinted polymer for selective and rapid enrichment of ractopamine by a non covalent approach" *Anal. Bioanal. Chem*. 401:2275-2282

[26] Yan H., Row K. H.(2006) "Characteristic and synthetic approach of molecularly imprinted polymers" *Int. J. Mol. Sci.* 7:155-178

[27] Haupt K. (2003) "Imprinted polymers: the next generation" *Anal. Chem.* 377A-383A

[28] Holthoff E. L., Stratis-Cullum D. N., Hankus M. E. (2010) "Xerogel-based molecularly imprinted polymers for explosives detection" *Proc. SPIE* 7665

[29] Cormack P. A. G., Elorza A. Z. (2004) "Molecularly imprinted polymers: synthesis and characterization" *J. Chromatogr. B* 804:173-182

[30] Odian G. (2004) "Principles of polymerization" *Wiley*, IV edition

[31] Zimmerman S. C., Wendland M., Rakow N. A., Zharov I., Suslick K. S. (2002) "Synthetic hosts by monomolecular imprinting inside dendrimers" *Nature* 418:399-403

[32] Zimmerman S. C., Zharov I., Wendland M. S., Rakow N. A., Suslick K. S. (2003) "Molecular imprinting inside dendrimers" J. *Am. Chem. Soc*. 125:13504-13518

[33] Sherrington D. C. (1998) "Preparation, structure and morphology of polymer supports" *Chem. Commun*. 2275-2286

[34] Sergeyeva T. A. (2009) "Molecularly imprinted polymers as synthetic mimics of biorteceptors. 1. General principles of molecular imprinting" *Biopolym. Cell.* 25(4):253-265

[35] Haginaka J. (2009) "Molecularly imprinted polymers as affinity-based separation media for sample preparation" *J. Sep. Sci.* 32:1548-1565

[36] Mergola L., Scorrano S., Del Sole R., Lazzoi M. R., Vasapollo G. (2013) "Developments in the synthesis of a water compatible molecularly imprinted polymer as artificial receptor for detection of 3-nitro-L-tyrosine in neurological diseases" *Bios. Bioelectr.* 40:336-341

[37] Denderz N., Lehotay J., Čižmárik J., Cibulková Z., Šimon P.(2012) "Thermodynamic study of molecularly imprinted polymer used as the stationary phase in high performance liquid chromatography" *J. Chromatogr. A* 1235:77-83

[38] Tang Y., Fang G., Wang S., Li J. (2011) "Covalent imprinted polymer for selective and rapid enrichment of ractopamine by a noncovalent approach" *Anal. Bioanal. Chem* 401:2275-2282

[39] Toshifumi Takeuchi T, Haginaka J. (1999) "Separation and sensing based on molecular recognition using molecularly imprinted polymers" *J. Chromatogr. B* 728:1-20

[40] Benito-Peña E., Martins S., Orellana G., Moreno-Bondi M. C. (2009) "Water-compatible molecularly imprinted polymer for the selective recognition of fluoroquinolone antibiotics in biological samples" *Anal. Bioanal. Chem*. 393:235-245

[41] Pichon V., Kabi F. B. (2007) "Different approaches to synthesizing molecularly imprinted polymers for solid-phase extraction" LCGC Europe 20(7)

[42] Pasetto P., Maddock S. C., Resmini M. (2005) "Synthesis and characterization of molecularly imprinted catalytic microgels for carbonate hydrolysis" *Anal. Chim. Acta* 542:66-75

[43] Flavin K., Resmini M. (2009) "Imprinted nanomaterials: a new class of synthetic receptors" *Anal. Bioanal. Chem*. 393:437-444

[44] Pérez N., Whitcombe M. J., Vulfson E. N. (2000) "Molecularly imprinted nanoparticles prepared by core-shell emulsion polymerization*" J. Appl. Polym. Sci.* 77:1851-1859

[45] Pérez-Moral N., Mayes A. G. (2004) "Noncovalent imprinting in the shell of core-shell nanoparticles" *Langmuir* 20:3775-3779

[46] Carter S. R., Rimmer S. (2002) "Molecular recognition of caffeine by shell molecular imprinted core-shell polymer particles in aqueous media" *Adv. Mater*. 14(9):667-670

[47] Liu R., Guan G., Wang S., Zhang Z. (2011) "Core-shell nanostructured molecular imprinting fluorescent chemosensor for selective detection of atrazine herbicide" *Analyst* 136:184-190

[48] Xie C., Zhang Z., Wang D., Guan G., Gao G., Liu J. (2006) "Surface molecular self-assembly strategy for TNT imprinting of polymer nanowire/nanotube array" *Anal. Chem*. 78:8339-8346

[49] Wang H., Zhou W., Yin X., Zhuang Z., Yang H., Wang X. (2006) "Template synthesized molecularly imprinted polymer nanotube membranes for chemical separations" *J. Am. Chem. Soc*. 128:15954-15955

[50] Stephenson C. J., Shimizu K. (2007) "Colorimetric and fluorimetric molecularly imprinted polymer sensors and binding assay" *Polym. Internat.* 56:482-488

[51] Hedborg E., Winquist F., Lundstrom I., Andersson L. I., Mosbach K. (1993) "Some studies of molecularly-imprinted polymer membranes in combination with field-effect devices" *Sens. Act. A* 37-38:796-799

[52] Panasyuk T. L., Mirsky V. M., Piletsky S. A., Wolfbeis O. S. (1999) "Electropolymerized molecularly imprinted polymer as receptor layers in capacitivechemical sensor" *Anal. Chem* 71(20):4609-4613

[53] Piletsky S. A., Turner A. P. F. (2002) "Electrochemical sensors based on molecularly imprinted polymers" *Elecroanal.* 14(5):317-323

[54] Blanco-López M. C., Lobo-Castañón M. J., Miranda-Ordieres A. J., Tuñón-Blanco P. (2004) "Electrochemical sensors based on molecularly imprinted polymers" *Trends Anal. Chem.* 23(1):37-48

[55] Malitesta C., Losito I., Zambonin P. G. (1999) "molecularly imprinted electrosynthesized polymers: new materials for biomimetic sensors" *Anal. Chem*. 71:1366-1370

[56] Sergeyeva T. A., Piletsky S. A., Brovko A. A., Slinchenko E. A., Sergeeva L. M., El'skaya A. V. (1999) "Selective recognition of atrazine by molecularly imprinted polymer membranes. Development of conductometric sensor for herbicides detection" *Anal. Chim. Acta* 392:105-111

[57] Li X., He Y., Zhang W., Ye Z. (2015) "Molecularly imprinted polymer-based sensors for atrazine detection by electropolymerization of *o*-phenylenediamine" *RSC Adv*. 5:56534-56540

[58] Pernites R. B., Ponnapati R. R., Advincula R. C. (2010) "Surface Plasmon Resonance (SPR) detection of theophylline via electropolymerized molecularly imprinted polythiophenes" *Macromolecules* 43(23):9724-9735

[59] Xu X. Y., Tian X., Cai L. G., Xu Z. L., Lei H. T., Hong Wang H., Sun Y. M. (2014) "Molecularly imprinted polymer based surface plasmon resonance sensors for detection of Sudan dyes" *Anal. Methods* 6:3751-3757

[60] Bompart M., Gheber L. A., De Wilde Y., Haupt K. (2009) "Direct detection of analyte binding to single molecularly imprinted polymer particles by confocal Raman spectroscopy" *Bios. Bioelectr.* 25: 568-571

[61] Bompart M., De Wilde Y, Haupt K. (2010) "Chemical nanosensors based on composite molecularly imprinted polymer particles and Surface- Enhanced Raman Scattering" *Adv. Mater*. 22:2343-2348

[62] Xue J. Q, Li D. W., Qu L. L., Long Y. T. (2013) "Surface-imprinted core–shell Au nanoparticles for selective detection of bisphenol A based on surface-enhanced Raman scattering" *Anal. Chim. Acta* 777:57-62

[63] Moreno-Bondi M. C., Navarro-Villoslada F., Benito-Peña E., Urraca J. L. (2008) "Molecularly imprinted polymers as selective recognition elements in optical sensing" *Curr. Anal. Chem.* 4:316-340

[64] Turkewitsch P., Wandelt B., Darling G. D., Powell W. S.(1998) "Fluorescent functional recognition sites through molecular imprinting. A polymer-based fluorescent chemosensor for aqueous cAMP" *Anal. Chem*. 70:2025-2030

[65] Stringer R. C., Gangopadhyay S., Grant S. A. (2010) "Detection of nitroaromatic explosives using a fluorescent-labeled imprinted polymer" *Anal. Chem*. 82:4015-4019

[66] Kubo H., Yoshioka N., Takeuchi T. (2005) "Fluorescent imprinted polymers prepared with 2-acrylamidoquinoline as a signaling monomer" *Org. Lett*. 7(3):359-362

[67] Wang W., Gao S., Wang B. (1999) "Building fluorescent sensors by template polymerization: the preparation of a fluorescent sensor for D-Fructose" *Org. Lett*. 1(8):1209-1212

[68] Nguyen T. H., Hardwick S. A., Sun T., Grattan K. T. V. (2012) "Intrinsic fluorescence-based optical fiber sensor for cocaine using a molecularly imprinted polymer as the recognition element" *IEEE Sens. J.* 12(1):255-260

[69] Ton X. A., Bui B. T. S., Resmini M., Bonomi P., Dika I., Soppera O., Haupt K. (2013) "A versatile fiber-optic fluorescence sensor based on molecularly imprinted microstructures polymerized in situ" *Angew. Chem. Int. Ed.* 52:8317-8321

[70] Suárez-Rodrìguez J. L., Dìaz-Garcìa M. E. (2001) "Fluorescent competitive flow-through assay for chloramphenicol using molecularly imprinted polymers" *Biosens. Bioelectr.* 16:955-961

[71] Navarro-Villoslada F., Urraca J. L., Moreno-Bondi M. C., Orellana G. (2007) "Zearalenone sensing with molecularly imprinted polymers and tailored fluorescent probes" *Sens. Act. B* 121 67–73

[72] Urraca J. L., Moreno-Bondi M. C., Orellana G., Sellergren B., Hall A. J. (2007) "Molecularly imprinted polymers as antibody mimics in automated on-line fluorescent competitive assays" *Anal. Chem.* 79:4915-4923

[73] Levi R., McNiven S., Piletsky S. A., Cheong S. H., Yano K., Karube I. (1997) "Optical detection of chloramphenicol using molecularly imprinted polymers" *Anal. Chem*. 69:2017-2021

[74] Greene N. T., Shimizu K. D. (2005) "Colorimetric molecularly imprinted polymer sensor array using dye displacement" *J. Am. Chem. Soc*. 127:5695-5700

[75] Sànchez-Barragàn I., Karim K., Costa-Fernàndez J. M., Piletsky S. A., Sanz-Medel A. (2007) "A molecularly imprinted polymer for carbaryl determination in water" *Sens. Act. B* 123:798-804

[76] Suárez-Rodrìguez J. L., Dìaz-Garcìa M. E. (2000) "Flavonol fluorescent flow-through sensing based on a molecular imprinted polymer" *Anal. Chim. Acta* 405:67-76

[77] Rachkov A., McNiven S., El'skaya A., Yano K., Karube I. (2000) "Fluorescence detection of b-estradiol using a molecularly imprinted polymer" *Anal. Chim. Acta* 405:23-29

[78] Foguel M. V., Ton X. A., Zanoni M. V. B., Sotomayor M. D. P. T., Haupt K., Bui B. T. S. (2015) "A molecularly imprinted polymer-based evanescent wave fiber opticsensor for the detection of basic red 9 dye" *Sens. Act. B* 218:222-228

[79] Fan J. P., Xu X. K., Xu R., Zhang X. H., Zhu J. H. (2015) "Preparation and characterization of molecular imprinted polymer functionalized with core/shell magnetic particles (Fe3O4@SiO2@MIP) for the simultaneous recognition and enrichment of four taxoids in *Taxus x media*" *Chem. Eng. J.* 279:567-577

[80] Li J., Zheng Z., Fu S., Zhu J. (2012) "Preparation and characterization of paclitaxel imprinted silica nanoparticles" *Adv. Mat. Res.* 399-401:1894-1897

[81] Liu H., Hong Y., Chen L. (2015) "Molecularly imprinted polymers coated on carbon nanotubes for matrix solid phase dispersion extraction of camptothecin from Camptotheca acuminate" *Anal. Met.* DOI: 10.1039/c5ay01721a

[82] Roy B., Duy S. V., Puy J. Y., Martin C., Guitton J., Dumontet C., Périgaud C., Lefebvre-Tournier I. (2012) "Synthesis and Evaluation of a Molecularly Imprinted Polymer for Selective Solid-Phase Extraction of Irinotecan from Human Serum Samples" *J. Funct. Biomater*. 3:131-142

[83] Prasad B. B., Kumar D., Madhuri R., Tiwari M. P. (2012) "Nonhydrolytic sol–gel derived imprinted polymer–multiwalled carbon nanotubes composite fiber sensors for electrochemical sensing of uracil and 5-fluorouracil" *Electrochim. Acta* 71:106-115

[84] Prasad B. B., Srivastava S., Tiwari K., Sharma S. P. (2009) "Development of uracil and 5-Fluorouracil sensors based on molecularly imprinted polymer-modified hanging mercury drop electrode" *Sens. Mat.* 21(6):291-306

[85] Nezhadali A., Senobari S., Mojarrab M. (2016) "1,4-dihydroxyanthraquinone electrochemical sensor based on molecularly imprinted polymer using multi-walled carbon nanotubes and multivariate optimization method" *Talanta* 146:525-532

[86] Wei F., Wu Y., Xu G., Gao Y., Yang J., Liu L., Zhou P., Hu Q. (2014)"Molecularly imprinted polymer based on CdTe@SiO2 quantum dots as a fluorescent sensor for the recognition of norepinephrine" *Analyst* DOI: 10.1039/c4an00951g

[87] Carrasco S., Benito-Peña E., Walt D. R., Moreno-Bondi M. C. (2015) "Fiber-optic array using molecularly imprinted microspheres for antibiotic analysis" *Chem. Sci*. 6:3139-3147

2. Aim of the Project

In 2012, the Italian Association for Cancer Research (AIRC) granted a project on "*Application of Advanced Nanotechnology in the development of innovative cancer diagnostic tools"*. One of the aims of this very large project was the design and development of point of care devices for the therapeutic drug monitoring of anticancer drugs. The need for such fast methodologies has been outlined in the introduction of this thesis, it must be noted here that this target is very ambitious, as no point of care devices for the detection of drugs at the patient's bed are reported or commercialized. The device should be able to perform directly on small volumes of blood from finger pricks and not from phlebotomy, separate plasma from blood cells and measure directly the drug level in plasma with a cheap technique.

The Unit of the project at the Department of Chemical and Pharmaceutical Sciences of the University of Trieste has the task to investigate the potential of soluble imprinted polymeric nanoparticles as sensing elements for the direct detection of anticancer drugs in human plasma.

Plasma is a very complex matrix, containing thousands of different molecules and binding proteins as albumins and immunoglobulins.

Possible critical points on the feasibility of a MIP-based system for the detection in plasma include cross reactivity from the plasma pool of small molecules, competition for binding the target drugs from albumin, stability of the system with aggregation or precipitation of the polymer.

This thesis is the first approach to such problems, and deals with soluble MIPs for the detection of sunitinib, irinotecan, SN38 and paclitaxel in plasma. As the final device has to be as simplest and as cheaper as possible, we have considered the possibility of using the MIPs as the sensing units themselves, in optical devices with fluorimetric or colorimetric detection.

We have thus designed several examples of MIPs:

- Containing a fluorescent functional monomer that generates a signal to be quenched by the target
- Containing a quencher functional monomer that inhibits the emission of a fluorescent target
- Containing a fluorescent functional monomer that establishes a FRET pair with a labelled target
- Capable to recognize a colour dye that changes its colour upon displacement by the target

The aims were therefore the selection of functional monomers, optimization of the syntheses, physical characterization of the MIPs, evaluation of their binding ability and of their selectivity, evaluation of their optical properties and of their performance in human plasma.

Part of this work has been carried out at Queen Mary University of London and in cooperation with Cobik, a Slovenian centre of excellence in optical sensors.

3. Results and Discussion:

Fluorescent MIPs

In this PhD project different polymeric nanoparticles containing specific binding sites for the anticancer drugs sunitinib, paclitaxel, SN38 and its prodrug irinotecan were synthesized. The soluble binding materials were evaluated as sensing systems for the direct drug quantification in plasma (Scheme 3.1)

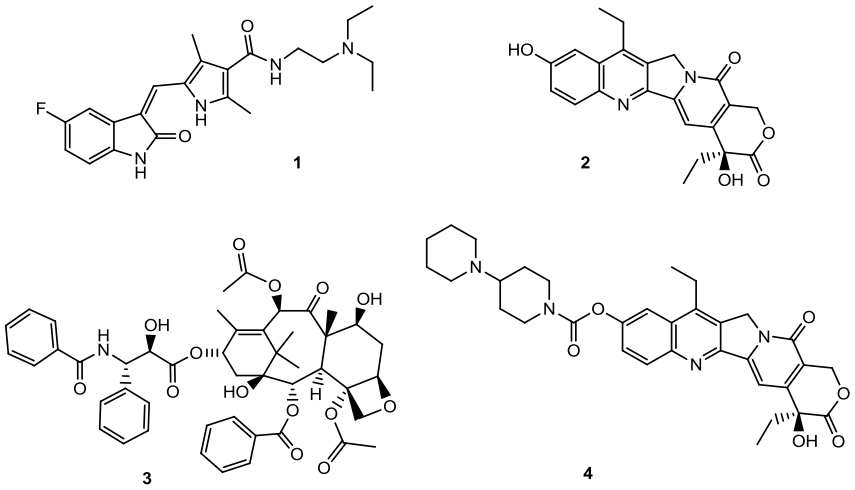

Scheme 3.1: chemical structures of sunitinib (1), SN38 (2), paclitaxel (3), irinotecan (4)

3.1 Synthesis of the Imprinted Polymers

Functional Monomers

In order to obtain specific polymers for anticancer drugs, is it necessary to select the best functional monomers able to interact with the target molecules. In this project the non-covalent imprinting process was only evaluated because it is an easy method that requires a low number of synthetic steps and it is applicable to a large variety of functional monomers and template molecules.[1]

This process consists of the instauration of non-covalent interactions between the functional monomers and the template before polymerization. Among the possible non-covalent interactions, it is possible to distinguish between weak interactions like π-staking, hydrogen bonding, hydrophobic interactions or van der Waals forces, and ion interactions that may be stronger depending on the environment and on the solvent polarity.

The first series of MIPs were synthesized planning only weak interactions during the imprinting process. Considering the aromatic structure and the presence of polar groups in the anticancer drugs studied in this project, four different functional monomers were evaluated as a first approach in the MIP synthesis:

- N-acryloyl-tyrosine methyl ester (**5b**) and N-acryloyl tryptophan methyl ester (**6b**) are modified amino acids that can mimic the interactions occurring between the drug and a protein in its binding site.[2] The presence of an aromatic structure can allow the formation of hydrophobic interactions with the target molecule, while hydrogen bonds can be created by the carbonyl and other polar groups of both the functional monomer and the template. Moreover, the tyrosine and tryptophan fluorescence properties could be exploited to investigate the polymer binding affinities at low drug concentrations.

- 7-acryloyloxycoumarin (**7b**) is a fluorescent molecule that could be used for the development of fluorescent sensors based on MIPs.[3,4] It could also interact with the anticancer drugs by its aromatic structure and its polar groups.

- 4-vinyl-piridine (**8**) is one of the most common functional monomers used for the MIP synthesis and it is cheap and commercially available.[5,6,7]

The presence of an acryloyl-group in the functional monomers structure is necessary to allow the incorporation of these molecules in the polymeric matrix of the molecularly imprinted polymers upon polymerization. N-acryloyl tryptophan methyl ester and N-acryloyl tyrosine methyl ester were synthesized from tyrosine methyl ester[8] (**5a**) and tryptophan methyl ester[9] (**6a**) by acylation on the amino group with acryloyl chloride in dichloromethane in the presence of triethylamine (Scheme 3.2). The same reagents were used to obtain 7-acryloyloxycoumarin, however in this case the acylation occurs on the hydroxyl group of 7-hydroxycoumarin (**7a**).[10]
During the synthesis of N-acryloyl-tyrosine methyl ester, the formation of a side-product was also observed. This side-product (**5c**) is generated by the acylation of both the phenolic chain of tyrosine methyl ester, and the amino group. The two products were separated by flash chromatography.

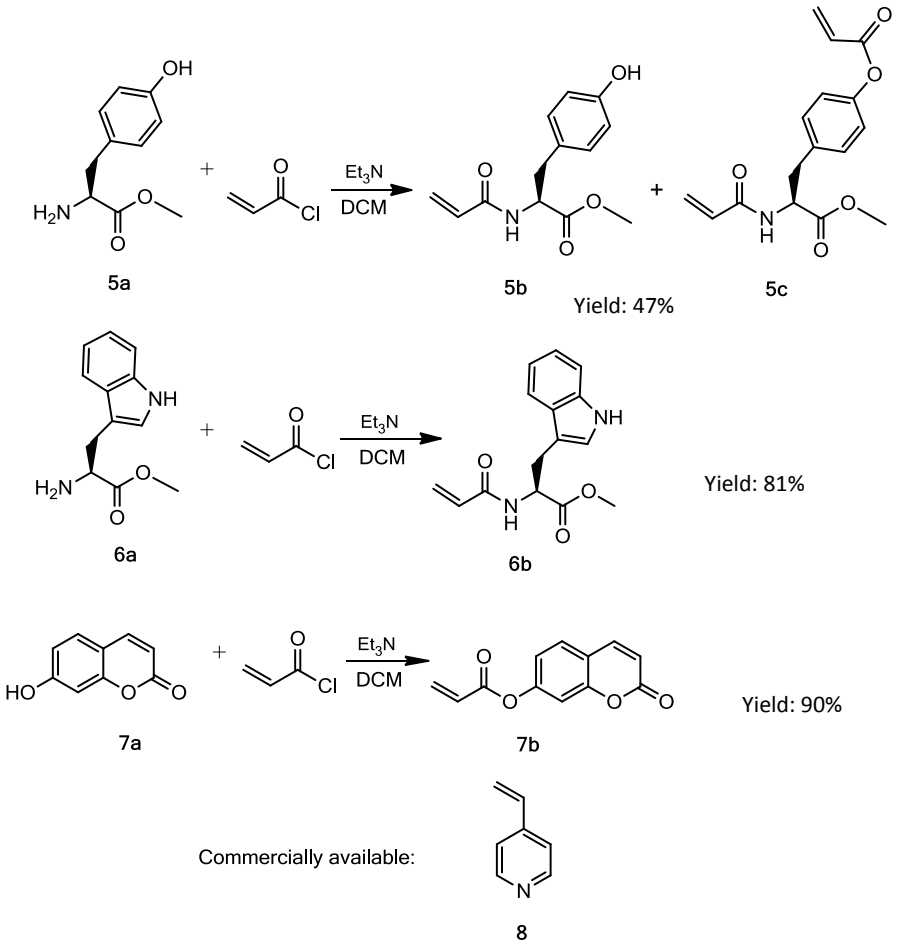

Scheme 3.2: synthesis of functional monomers

^{1}H NMR Titrations

^{1}HNMR titration experiments were exploited to investigate the nature and the strength of possible interactions involved in the functional monomer–template complex during the synthesis of molecularly imprinted polymers. Furthermore, NMR allows to identify the specific functionalities that are involved in the formation of the functional monomer-template complex before polymerization.[11]

In fact the complex formation (***LR***) between two molecules named ligand (***L***) and receptor (***R***) is a dynamic process where the free molecules are in equilibrium with the bond counterpart.

$$L + R \rightleftharpoons LR$$

In NMR the free receptor and the ligand-bond state have two different resonance frequencies, respectively ν_R and ν_{LR} , and the appearance of the characteristic signal of the two species depends on three main factors: the population of each state (P_R and P_{LR}), the chemical shift difference between the two frequencies ($\Delta\nu=|\nu_{LR}-\nu_R|$) and the relative values of the exchange rate: $k_{ex} = k_R + k_{RL}$. Therefore is possible to distinguish between three different situations during the complex formation, named *slow, intermediate and fast exchange regimen*, which lead to different NMR spectra (Figure 3.1).

In the *slow exchange regimen*, the ligand binding equilibrium has a very slow exchange rate compared to the NMR time scale ($k_{ex}<<|\Delta\nu|$), so there is not significant interconversion between the two states during the frequency detection period of NMR experiment. Therefore signals from both the free ligand and the bond-ligand are observed in the spectrum with different chemical shifts, also the intensity of each peak indicates the population of each species.

While if the *exchange regimen is fast*, the ligand binding equilibrium has a very fast exchange rate compared to the NMR time scale ($k_{ex}>>|\Delta\nu|$), so a very fast interconversion between **L** and **LR** occurs during the detection period of the NMR experiment leading to averaged peaks. Therefore only one signal is observed with a population-weighted chemical shift ($\delta_{obs}= P_R\delta_R+ P_{LR}\delta_{LR}$).

Finally, in the *intermediate exchange regimen*, or coalescence, intermediate situation of the two previously described occurs, so $k_{ex}\approx|\Delta\nu|$, and one signal is observed at a chemical shift between δ_R and δ_{LR} with a linewidth that is "exchange broadened" due to interference from the interconversion between **L** and **LR** during the detection period.[12, 13]

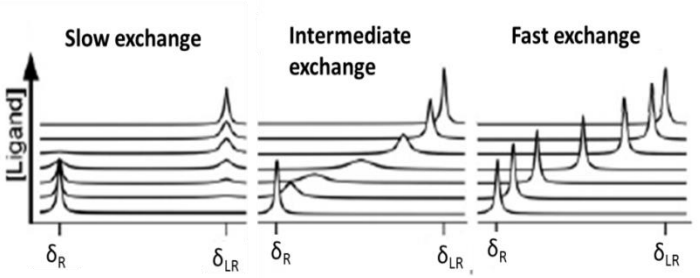

Figure 3.1: different situations that may occur during the ^{1}H-NMR titration (from ref[13])

The experiment consists of the addition of increasing equivalents of functional monomer (from 0.5 to 14 equivalents) to a fixed concentration of template molecule, which in this case is the drug. Since in this project the synthesis of molecularly imprinted polymers was performed in DMSO, also the interactions between the target molecule and the functional monomer were studied in deuterated DMSO.

In all the spectra obtained from the ^{1}H-NMR titrations only one set of signals is visible, indicating that the complexation equilibrium is close to a *fast exchange regimen*. In this context, the functional groups of both the target molecule and the functional monomer which are mainly involved in the complex are subjected to a large variation of their chemical shift that could be downfield or upfield with respect to the initial position of the signal.[14]

The variation of the proton chemical shift (δ_{final}-$\delta_{initial}$) of the target drug after addition of 14 equivalent of functional monomer is shown in Figure 3.2. In the same figure the functional monomers protons involved in the complex formation with the template are also indicated.

Comparing the shifts of both the template and the functional monomers it was possible to identify the interactions between the two molecules. Also the hydrogen bond formation between polar groups can be easily identified because it is usually associated to a strong downfield variation of chemical shift, as is possible to see in these titrations.[15]

Sunitinib, SN38, irinotecan and paclitaxel establish weak interactions with all the tested functional monomers.

In particular, the large changes in the shifts of indole proton 4 and of the methylidene proton of sunitinib, and the changes occurring in all the protons of the coumarin rings, indicate that the indole and methylidene systems of sunitinib are likely to make hydrophobic interactions with the aromatic system of 7-acryloyloxy-coumarin. The formation of hydrogen bonds between the indole NH of sunitinib and acceptors of N-acryloyl-tryptophan methyl ester and 4-vinyl pyridine is also observed. Furthermore the amide proton of sunitinib is involved in the interaction with N-acryloyl-tryptophan. The strength of N-acryloyl-tyrosine interactions is weaker than that of the other functional monomers; however a hydrogen bond with the amide group of sunitinib is observed (Figure 3.2a).

SN38 makes hydrogen bonds by its hydroxyl groups and π-stacking interactions by the aromatic rings, namely 4-vinyl pyridine molecules appear to interact with both the hydroxyls, while 7-acryloyloxy-coumarin and the amino-acids interact mainly with hydroxyl and other groups at the lactone side of the molecule (Figure 3.2b).

Finally, binding between paclitaxel and the functional monomers involves mainly its side chain, in fact the aromatic rings of the drug makes π-stacking interactions with 7-acryloyloxy-coumarin and N-acryloyl-tyrosine methyl ester leading to upfield variation of the chemical shift of aromatic protons. The hydroxyl and the amide group of paclitaxel establish hydrogen bonds with polar groups of the functional monomers (Figure 3.2c).

The interaction between irinotecan hydrochloride and functional monomers 5b, 6b and 7b seems to be stronger than that of other drugs, in particular on the piperidine moiety. A high variation of the piperidine protonated amino group signal, and low variations of the adjacent piperidine protons were observed. N-acryloyl-tryptophan

methyl ester interacts better than other functional monomers mainly by hydrogen bonds with the protonated piperidine group of irinotecan. Both hydrogen bonds with the NH of piperidine group and π-staking interactions with the aromatic rings are involved in the complex between irinotecan and 7-acryloxycoumarin. Even if the variation of drug NH chemical shift due to interaction with 7b is not stronger than that of 5b and 6b, its titration curve is the only one that reached a plateau after 14 equivalents added (Figure 3.2d).

3.2a

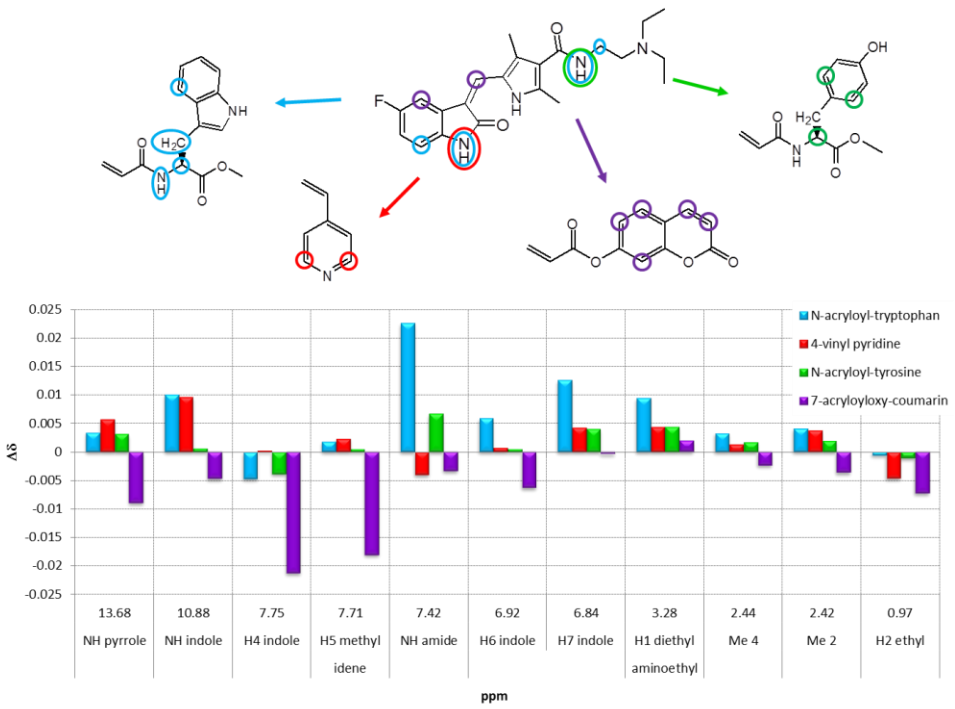

3.2b

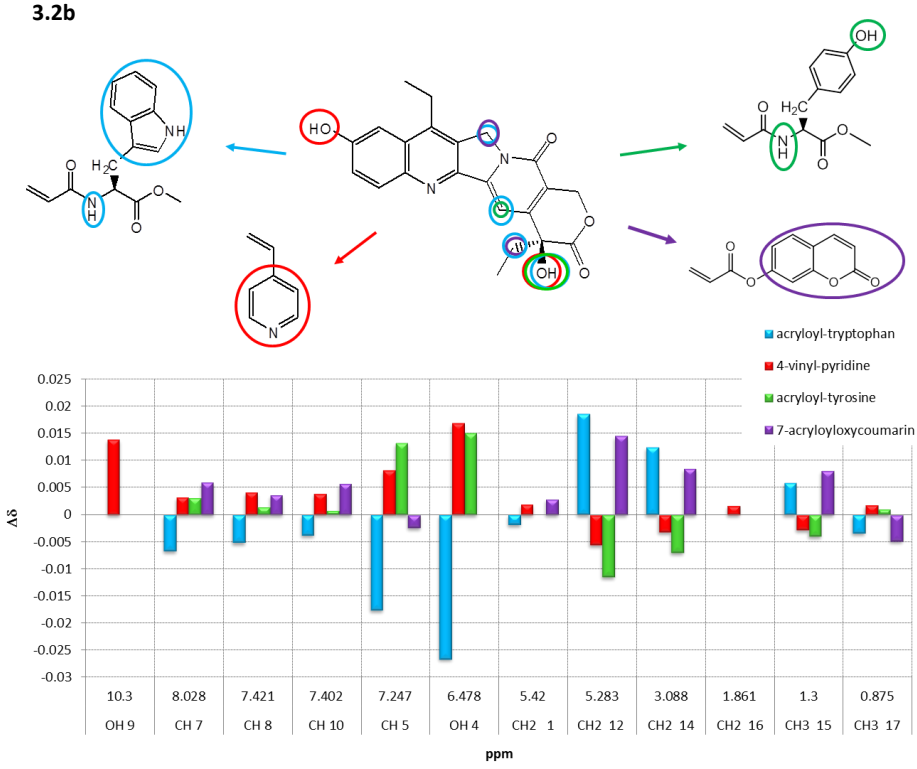
acryloyl-tryptophan
4-vinyl-pyridine
acryloyl-tyrosine
7-acryloyloxycoumarin
Δδ
0.025
0.02
0.015
0.01
0.005
0
-0.005
-0.01
-0.015
-0.02
-0.025
-0.03
10.3 OH 9
8.028 CH 7
7.421 CH 8
7.402 CH 10
7.247 CH 5
6.478 OH 4
5.42 CH2 1
5.283 CH2 12
3.088 CH2 14
1.861 CH2 16
1.3 CH3 15
0.875 CH3 17
ppm

3.2c

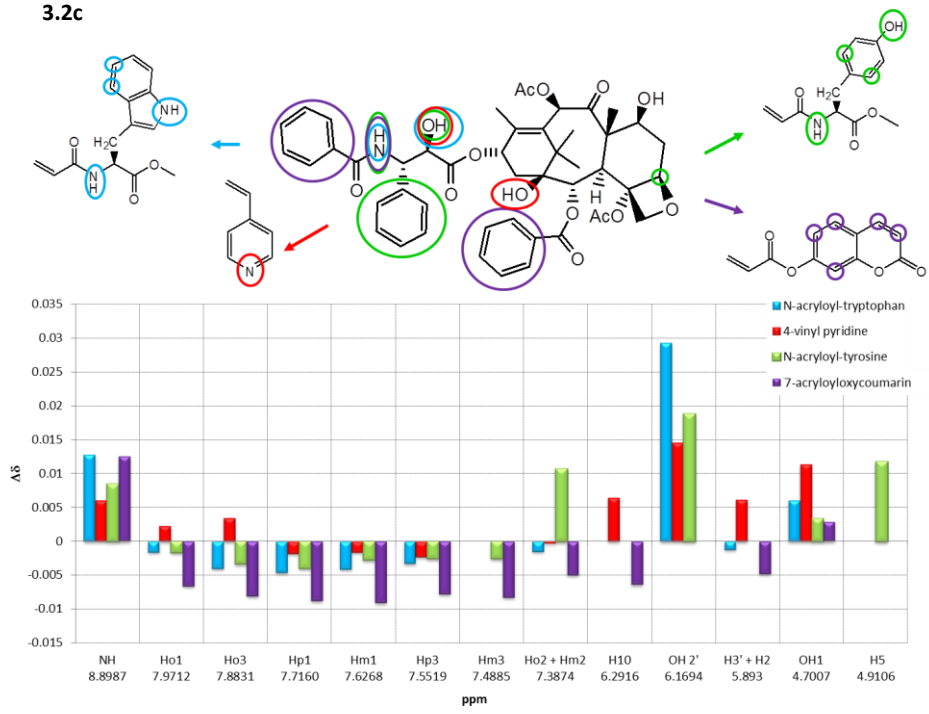
N-acryloyl-tryptophan
4-vinyl pyridine
N-acryloyl-tyrosine
7-acryloyloxycoumarin
Δδ
0.035
0.03
0.025
0.02
0.015
0.01
0.005
0
-0.005
-0.01
-0.015
NH 8.8987
Ho1 7.9712
Ho3 7.8831
Hp1 7.7160
Hm1 7.6268
Hp3 7.5519
Hm3 7.4885
Ho2 + Hm2 7.3874
H10 6.2916
OH 2' 6.1694
H3' + H2 5.893
OH1 4.7007
H5 4.9106
ppm

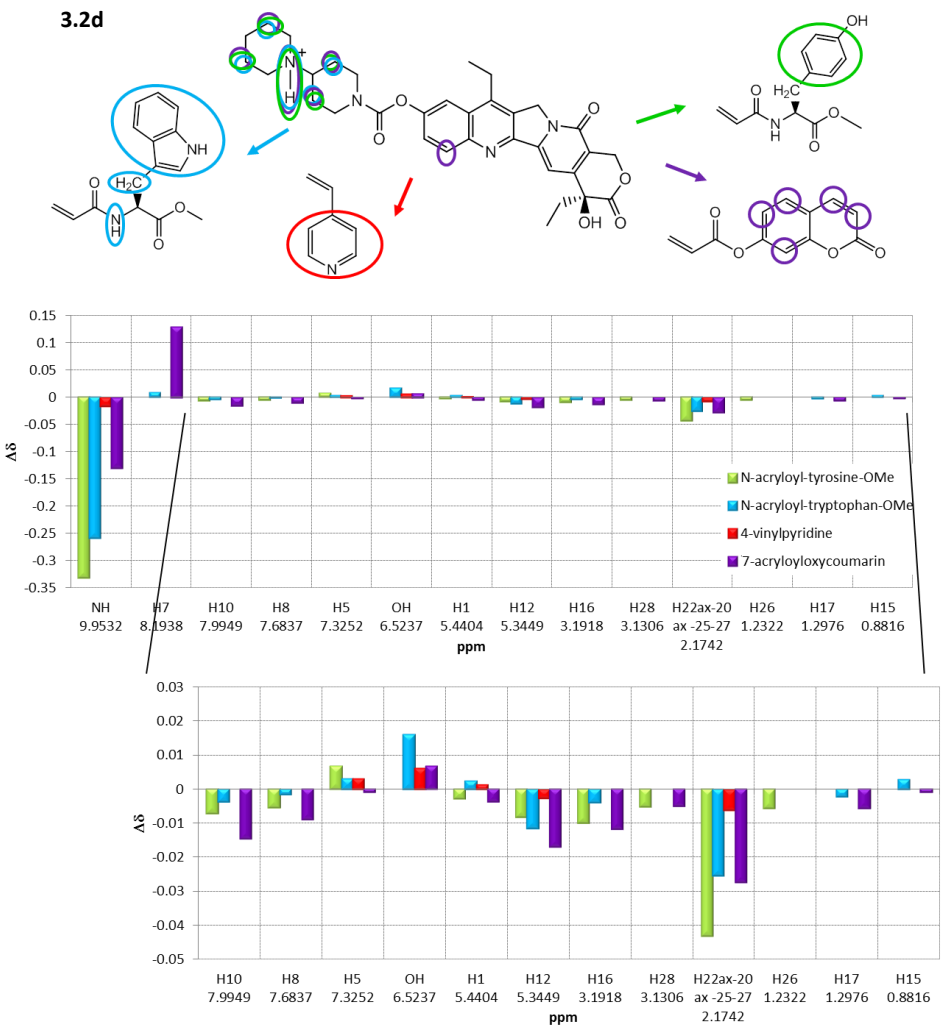

Figure 3.2: variation of proton chemical shift of sunitinib (3.2a), SN38 (3.2b), paclitaxel (3.2c), irinotecan (3.2d) upon addition of 14 equivalents of functional monomer. The protons of functional monomers that mainly interact with the drug giving an high variation of chemical shift are also indicated on the chemical structure of each functional monomer. Every colour corresponds to the interaction with a functional monomer: N-acryloyl-tryptophan-OMe (blue), 4-vinyl-piridine (red), N-acryloyl-tyrosine-OMe (green) and 7-acryloyloxy-coumarin (violet).

For each drug it is possible to identify some particular functional group that best interact with the functional monomers. Large variations of chemical shift were observed for polar groups, as the NH amide and the NH indole of sunitinib, the hydroxyl group of SN38 and the OH2' of paclitaxel, able to make hydrogen bonds with the functional monomers. However some large variation of chemical shift occurs also due to hydrophobic interactions that involve 7-acryloylxycoumarin monomer.

The variation of chemical shift of these groups after each addition of functional monomer was plotted in function of the equivalents of functional monomer added.
The titration curves of sunitinib amide group with N-acryloyl-tryptophan methyl ester and N acryloyl-tyrosine methyl ester and that of the sunitinib NH indole with 4-vinylpyridine and the H4 of sunitinib indole with 7-acryloxycoumarin showed mainly a linear behavior. Therefore the plateau is not reached after 14 equivalents added. The main variations of chemical shift were observed during the titration with N-acryloyl-tryptophan methyl ester and 7-acryloxycoumarin, suggesting a preference of sunitinib for these functional monomers. However while the interaction with N-acryloyl-tryptophan methyl ester occurs mainly by hydrogen bonds, that with 7-acryloxycoumarin is based on hydrophobic and π-stacking interactions (Figure 3.3).

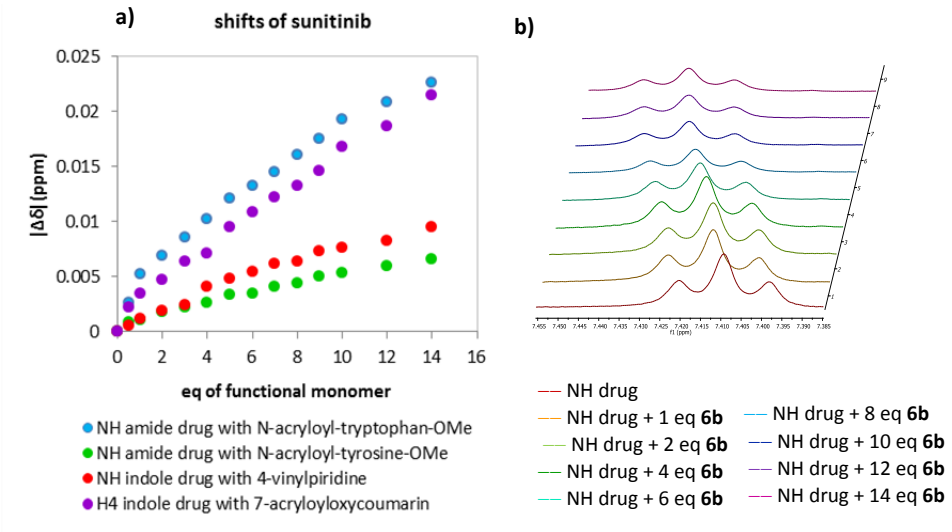

Figure 3.3: a) variation of amide and indole proton chemical shift of sunitinib upon interaction with the functional monomers; b): variation of amide chemical shift upon interaction with N-acryloyl-tryptophan methyl ester

The trend of the titration curves of OH2' and NH amide of paclitaxel is more variable among the different functional monomers. In fact the titration with N-acryloyl-tryptophan methyl ester leads to a plateau after six equivalents added, that corresponds to the saturation point.
In the titration curve with N-acryloyl-tyrosine methyl ester a first plateau is reached after 4 equivalents added, but increasing the functional monomer concentration, the variation of chemical shift further increased linearly and the second plateau is not even reached after 14 equivalents added. This behavior suggests a multiple interaction or weaker interaction with respect that with N-acryloyl-tryptophan methyl ester. The

complex between paclitaxel and 4-vinyl pyridine is even weaker, and in its titration curve the plateau is not reached.

The interaction with 7-acryloyloxycoumarin does not involves the hydroxyl 2' of paclitaxel but rather its amide group, giving a plateau in the titration curve after 12 equivalents added. So the complex between the drug and 7-acryloxycoumarin seems to be stronger than that with 4-vinyl pyridine but weaker than that with N-acryloyl-tryptophan methyl ester (Figure 3.4).

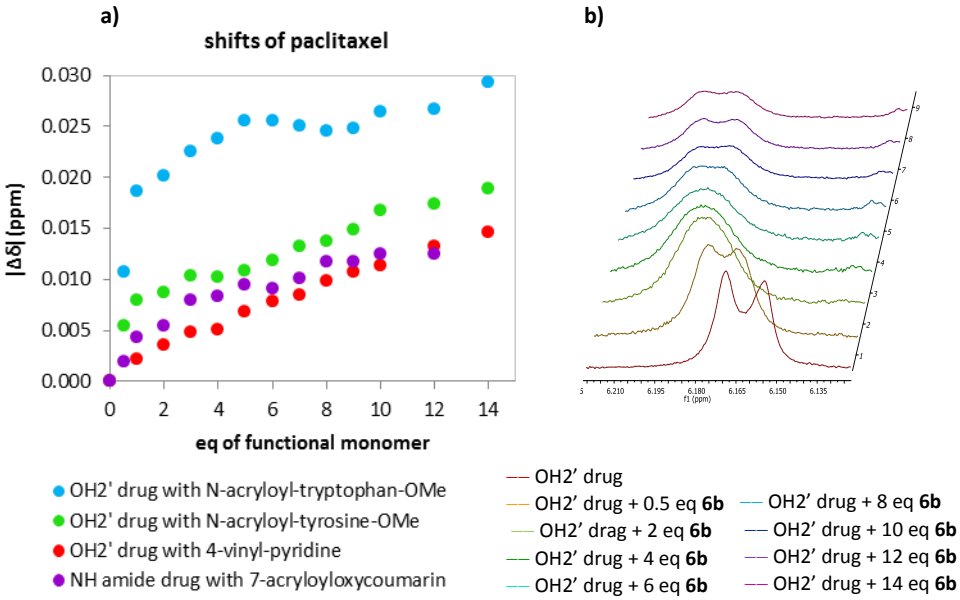

Figure 3.4: a) variation of the hydroxyl and amide protons of paclitaxel upon interaction of functional monomers; b) variation of OH2' of drug upon interaction with N-acryloyl-tryptophan methyl ester

Also for SN38 the largest variation of chemical shift was due to the interaction with N-acryloyl-tryptophan methyl ester by hydrogen bonding, which involves the hydroxyl at position 4 of the drug. However, for all the titrations of SN38 with the functional monomers the plateau was not reached after 14 equivalents added. Only the curve obtained by the titration with N-acryloyl-tyrosine-OMe decreases its slope after 10 equivalents. Instead, 7-acryloyloxycoumarin does not interact with the hydroxyl group in position 4, but mainly with the methylene group at position 12 by hydrophobic and π-staking interactions with the aromatic rings (Figure 3.5).

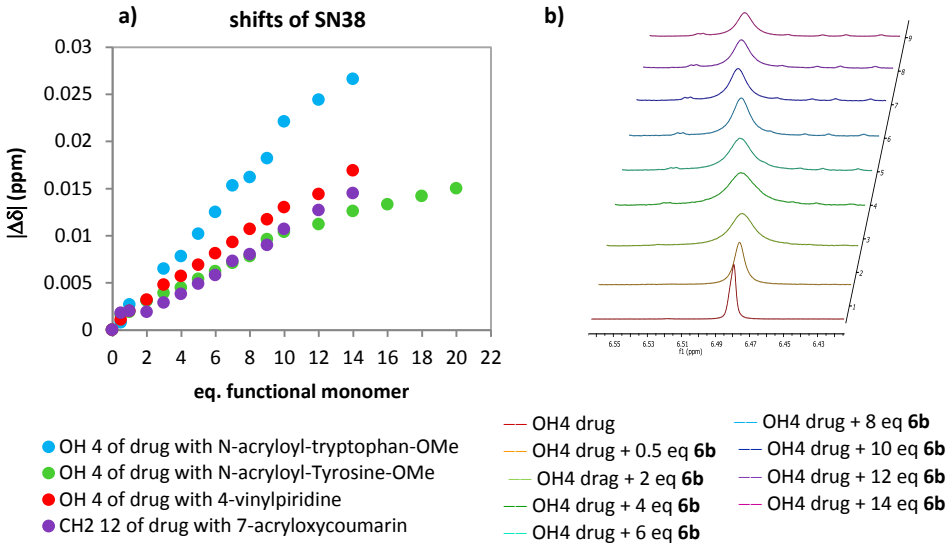

Figure 3.5: a) variation of the proton chemical shift of SN38 upon interaction with functional monomer; b) shift of OH-4 of SN38 upon interaction of N-acryloyl-tryptophan methyl ester

The main interaction with irinotecan occurs on its protonated piperidine group. The high field shift of this proton indicates a shield effect on the positive charged NH due to the interactions with functional monomers polar groups (Figure 3.6).

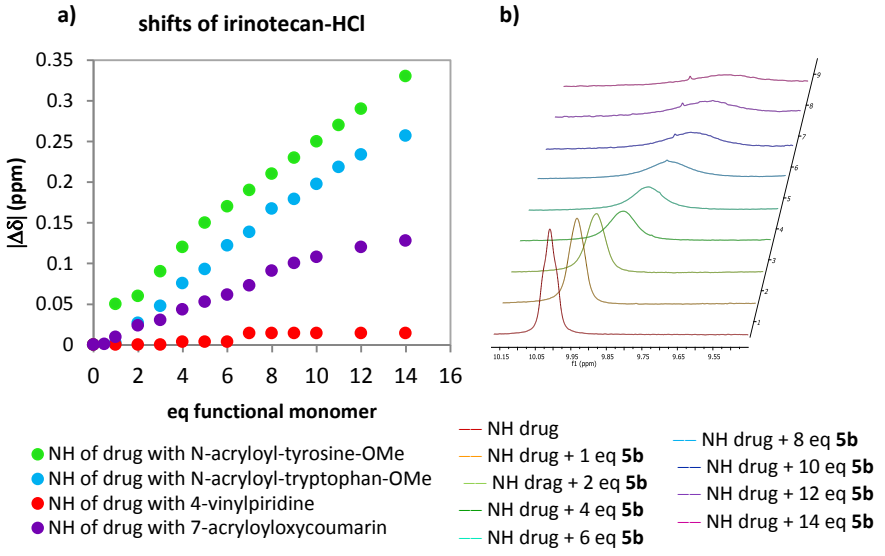

Figure 3.6: a) variation of proton chemical of irinotecan upon interaction with the functional monomers; b) shifts of NH group of irinotecan upon interaction with N-acryloyl-tyrosine methyl ester

Since all the investigated functional monomers showed the ability to interact relatively well with paclitaxel, sunitinib, SN38 and irinotecan, they were used in the synthesis of molecularly imprinted polymers.

Synthesis of Molecularly Imprinted Polymers

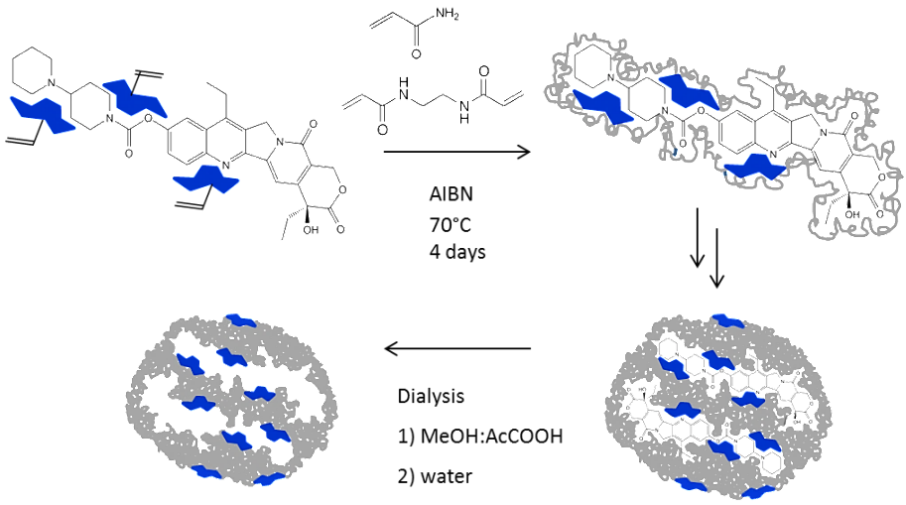

Figure 3.7: example of synthesis of a molecularly imprinted polymer for irinotecan

The nanogels were synthesized under high dilution radical polymerization conditions following a standard protocol developed in Prof. Resmini's research group at the Queen Mary University of London. This approach is characterized by two main parameters: the choice of solvent and the overall monomer concentration.[16,17]
During polymerization, unreacted double bonds on particle surface may induce inter-particles crosslinking leading to macrogelation. However, under diluted conditions with a "good" solvent, each polymeric particle is stabilized avoiding intermolecular crosslinking. In fact the solvating power of the solvent prevents macrogelation via osmotic repulsion forces and steric hindrance, without adding surfactants.[18] In this project DMSO was chosen as solvent for polymer synthesis since it allows dissolving well all the reagents involved in the polymerization. Furthermore, the choice of the concentration of all monomers in the pre-polymerization mixture is fundamental to obtain nanoparticles. It must be taken under a certain value obtained experimentally and called Critical Monomer Concentration (C_M). The C_M is the percentage by weight of all monomers used for the polymerization as compared to the percentage of the overall mass of monomers and solvent used for a polymer preparation.[19]

The amount of solvent necessary to obtain polymeric nanoparticles was calculated by the following equation:

$$m(S) = \frac{[m(fm) + m(bm) + m(cl)] \cdot \%\ solvent\ in\ mixture}{\%\ monomer\ in\ mixture\ (C_M)}$$

Where m*(fm)*, *m(bm)* and *m(cl)* are respectively the mass of the functional monomer, the co-monomer and the crosslinker.[20]

In this project acrylamide was chosen as co-monomer due to its high solubility in water.[21, 22] Also N,N'-ethylenebisacrylamide was chosen as crosslinker due to its water solubility and high compatibility between components. Finally, to obtain soluble nanoparticles, C_M was fixed at 1% w/w, since this value is below the gelation point, that corresponds to the limit at which the transition between macro- and microgelation occurs, calculated for a similar solvent and polymer composition of that used in this project.[20] Before synthesis, the formation of functional monomer-template complex was achieved leaving the functional monomers and the template to interact in DMSO for 1h. The ratio between functional monomer and template, that in this case is the drug, was fixed at 1:1.2. The little excess of template with respect the functional monomer was used in the attempt to obtain a high number of specific binding sites, assuming a 1:1 monomer:template interaction and taking advantage also of the presence of the comonomer and the crosslinker in the pre-polymerization mixture able to create a polymeric matrix around the template molecule. After this time, the comonomer acrylamide (15% in mol), the crosslinker N,N'-ethylene bisacrylamide (70% in mol) and the radical initiator AIBN were added to the solution.

The amount of radical initiator was fixed at 18% of the amount of the available double bonds in the pre-polymerization mixture, and was calculated from the following equation:

$$n(I) = [n(fm) + n(bn) + 2n(cl)] \cdot \%\ initiator$$

Where *n(I)*, *n(fm)*, *n(bm)* and *n(cl)* are respectively the number of mol of the initiator, the functional monomer, the co-monomer and the crosslinker.

This high amount of radical initiator is necessary to obtain a good yield of polymerization, in fact previous polymerization experiments performed with 1% AIBN showed a very low yield. The polymerization occurs on heating at 70°C for 4 days.

The use of a high percentage of crosslinker is fundamental to impart the necessary rigidity to preserve the cavities shape and to impart mechanical stability to the MIP. However a crosslinker content above 90% leads to too rigid and less flexible polymer

limiting its swelling and therefore its binding capability. On the other hand, a content of crosslinker lower than 70% leads to high flexible polymers decreasing their binding selectivity.[23]

After polymerization, a clear solution was obtained containing soluble nanoparticles in which the functional monomers are held in position by a highly crosslinked polymeric matrix. This method was applied for the synthesis of all MIPs for sunitinib, paclitaxel, SN38 and irinotecan with N-acryloyl tryptophan methyl ester, N-acryloyl-tyrosine methyl ester, 4-vinyl pyridine and 7-acryloyloxycoumarin (Table 3.1). For each functional monomer also a non-imprinted polymer (NIP) was synthesized as control polymer using the same polymerization procedure but without the presence of the template molecule. The yield of polymerization was calculated with the following equation:

$$\%\, yield = \frac{polymer\ weight}{\sum monomer\ weights}$$

Polymer	Drug	Functional monomer	Yield %
0.5	-	N-acryloyl-tyrosine-OMe	35
0.6	-	N-acryloyl-tryptophan-OMe	79
0.7	-	7-acryloyloxycoumarin	92
0.8	-	4-vinyl-pyridine	94
1.5	Sunitinib	N-acryloyl-tyrosine-OMe	63
1.6	Sunitinib	N-acryloyl-tryptophan-OMe	58
1.7	Sunitinib	7-acryloyloxycoumarin	86
1.8	Sunitinib	4-vinyl-pyridine	41
2.5	SN38	N-acryloyl-tyrosine-OMe	61
2.6	SN38	N-acryloyl-tryptophan-OMe	80
2.7	SN38	7-acryloyoxylcoumarin	90
2.8	SN38	4-vinyl-pyridine	27
3.5	Paclitaxel	N-acryloyl-tyrosine-OMe	41
3.6	Paclitaxel	N-acryloy-tryptophan-OMe	74
3.7	Paclitaxel	7-acryloyloxycoumarin	76
3.8	Paclitaxel	4-vinyl-pyridine	63
4.5	Irinotecan	N-acryloyl-tyrosine-OMe	68
4.6	Irinotecan	N-acryloy-tryptophan-OMe	77
4.7	Irinotecan	7-acryloyloxycoumarin	82
4.8	Irinotecan	4-vinyl-pyridine	45

Table 3.1: polymer composition and yield

Removal of the template occurs by dialyzing the polymers first in methanol and then in water.

The use of methanol increases the solubility of template molecules and leads to a polymer shrinkage that force the dissociation of the MIP-template complex. Finally, water allows to remove also unreacted functional monomers or by-products and to resume the better polymer conformation.[24]

The polymers synthesized with irinotecan as template undergo a further washing step by dialysis first in 7:3 methanol:acetic acid mixture and after in water because of the difficulty to remove completely the template from the polymeric matrix.[25]

^{1}H-NMR Characterization of MIPs

The success of polymerization was verified first by ^{1}H-NMR spectroscopy dissolving 2 mg of polymer in 800 μL of [D_6]DMSO. Examples of the resulting spectra are reported in figures 8 and 9. The spectra exhibit an envelope of signals at high fields corresponding to the aliphatic protons of the polymer, in particular the signals between 1 and 2.5 ppm are associated to α and β protons to amide group, while broad signals between 2.5 and 4 ppm are generated from the CH_2-N groups. The protons of amide groups of the polymeric matrix and the aromatic protons of pyridine incorporated into the polymer generated a broad signal between 6 and 7 ppm.[26]

The NMR signal of the drug are not present in the spectrum of MIP 1.8 (Figure 3.8), indicating that the template molecule was completely removed from the polymer binding sites.

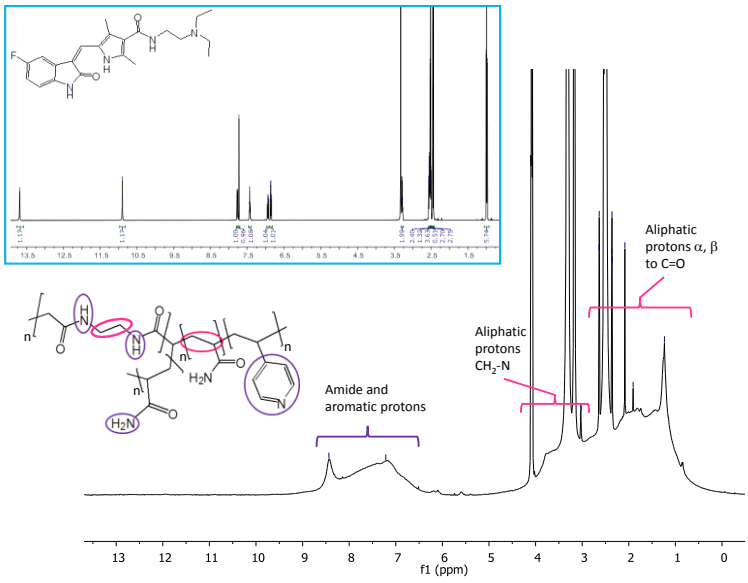

Figure 3.8: ^{1}H-NMR spectrum of MIP 1.8

A similar spectrum was also obtained for MIP 2.6 (Figure 3.9). The characteristic two broad signals between 1 and 4 ppm correspond to aliphatic protons and those between 7 and 8 ppm correspond to the amide groups of polymer; signals due to the aromatic protons of tryptophan are also observed. Both the MIP spectra showed a similar trend of signals because of the presence of an high percentage of the crosslinker (N,N'-ethylenebisacrylamide, 70%) and of the acrylamide functional monomer (15%) in the polymeric matrix with respect the amount of functional monomer (15%). Therefore the main visible signals are due to the acrylamide-based polymeric matrix.

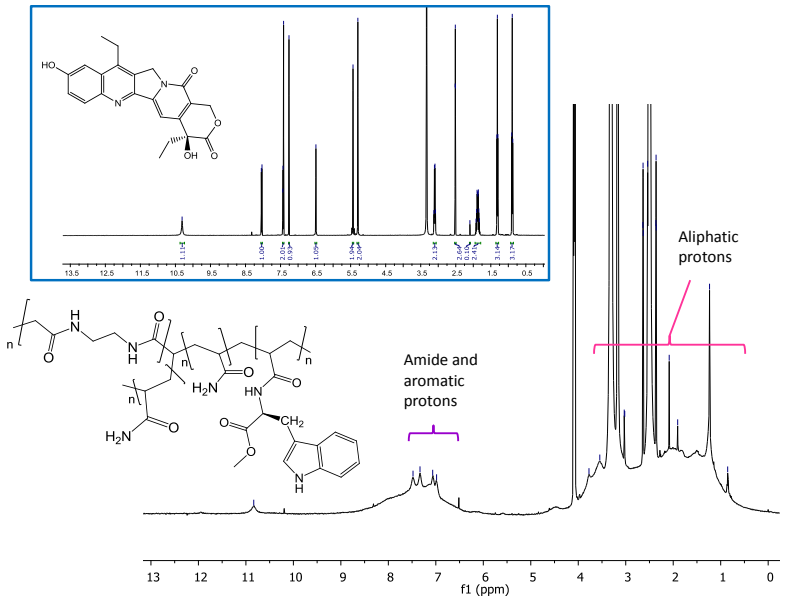

Figure3.9: ^{1}H-NMR spectrum of MIP 2.6

Determination of Particles Size

Analysis by NanoSight

Preliminary studies on particles size were performed by NanoSight LM10. This instrument utilizes the properties of both light scattering and brownian motion to obtain the size distribution and concentration measurement of particles in liquid suspension. A laser beam passes through the sample chamber leading to a light scattering due to the presence of the polymeric particles in suspension. The light scattered from each particle is easily visualized via a 20x magnification microscope onto which a camera is mounted. The camera captures a video file of the particles moving under brownian motion. This video is analyzed by a software that follows the movement of many particles individually calculating the mean squared displacement

for each particle for as long as it is visible in the video. From these values, the diffusion coefficient (D_t) and the hydrodynamic radius (r_h) were determined using the Stokes-Einstein equation:

$$D_t = \frac{K_B T}{6\pi\eta r_h}$$

Where the K_B is the Boltzmann's constant, T is the temperature and η is the viscosity.
Since each and every visible particle is separately tracked, it is possible to generate particle size distribution profiles that reflect the actual number of particles seen in the video.[27]
The particle sizes of water suspensions of MIPs and NIPs synthesized to capture sunitinib were first investigated using this technique. As shown in Figure 3.10a, all samples are characterized by a wide population of particles, with a fraction smaller than 100 nm and a major fraction of particles larger than 100 nm. However, after filtering the solution on 0.22 µm filter, only particles of about 100 nm size were visible (Figure 3.10b). While measuring the same sample after a long time, also the presence of particles of 300 nm and 490 nm was observed, suggesting the tendency of these particles to aggregate in water solution (Figure 3.10c).

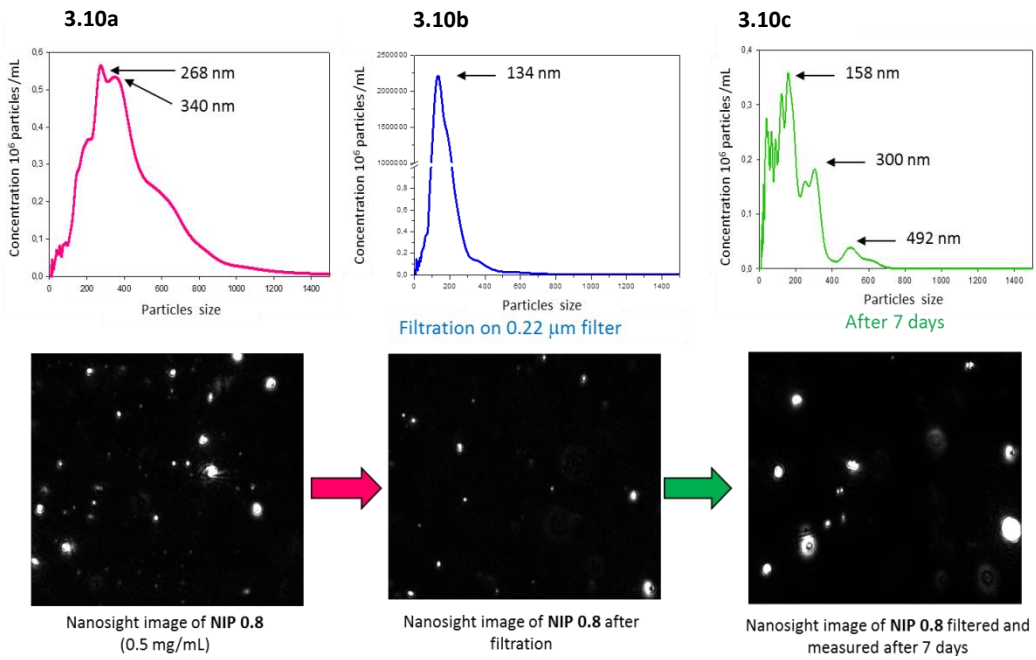

Figure 3.10: NanoSight measurements of NIP 0.8

Polymer	Concentration (mg/mL)	Particle size (nm) After filtration
1.6	0.125	105
0.6	0.5	103
1.8	2	100
0.8	0.5	134
1.5	0.125	155
0.5	0.125	149
1.7	1	89
0.7	0.5	127

Table 3.2: particle size of NIPs and MIPs for sunitinib, measured by NanoSight

However, this technique is based on the light scattering of particles, therefore the bigger particles are more visible than the smaller ones because the amount of light scattered by big particles is higher than that produced by a small particle.[28]
This reason, coupled with a low resolution of the instrument (10 nm), allows actually to detect only the presence of aggregates in the MIP samples. In fact probably these samples are characterized by a wide population of particles even lower than 100 nm size, but their scattering is not detectable due to the presence of larger aggregates.
Therefore all MIPs and NIPs were also analyzed by Dynamic Laser Light Scattering in DMSO.

Dynamic Laser Light Scattering (DLLS) Measurements

DLLS is an useful technique to measure the particle size from 0.3 nm to 10 micron diameter in a wide range of solvents.
The instrument uses a laser beam to illuminate a particles suspension and measure their size by analyzing the intensity fluctuations in the light scattered during their brownian motion.
If a small particle is illuminated by a light source such as a laser, the particle will scatter the light in all directions.
In a sample containing thousands of particles, the incident laser beam produces the light scattering of particles leading to a speckle pattern in the screen, similar to that shown in Figure 3.11. As all the particles suspended in a liquid move constantly due to brownian motion, the speckle will also appear to move. The speckle pattern shows some bright

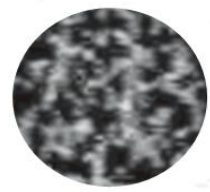

Figure 3.11: example of a speckle pattern produced by light scattering. (From ref. 32)

and dark areas that are created by the constructive or destructive interaction between different waves propagated from the particles.[29] If the waves arrive to the screen with the same phase, a constructive interference occurs and a bright patch is observed, while if the waves have different phases, a destructive interaction takes place giving dark areas in the speckle.

As the particles move around in the sample, the constructive and destructive phase addition of the scattered light will cause the bright and dark areas to grow and diminish in intensity leading to a fluctuating speckle. The instrument measures the rate of the intensity fluctuation and uses this to calculate the size of the particles. This could be done thanks to a digital correlator, able to measure the degree of similarity between two signals over a period of time that is usually very short, from 1 to 10 milliseconds. The intensity of the light scattered from different particles becomes even more different during the time, leading to an exponential decrease of the correlation in function of the time. A plot similar to Figure 3.12 can be obtained for each particle.[30]

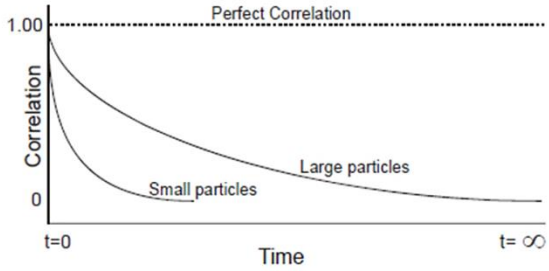

Figure 3.12: example of decay of correlation function of particles with different size.(From ref.32)

The brownian motion consists in the movement of particles due to the random collision with the molecules of the liquid that surrounds the particle. Therefore small particles move quickly, while large particles move slowly. This feature is very important for DLS measurements, in fact a small particle moving quickly will lead to a rapid fluctuation in the intensity of its speckle pattern and a rapid decreasing of its intensity correlation. Large particles moves slowly, and also the intensity fluctuation in the speckle and the rate of decay of the correlation function will be slow.

As the rate of decay of the correlation function is related to particle size, the instrument software uses algorithms to obtain a particle size distribution from the decay rates of the correlation function measured from the sample.

The size distribution by intensity shows the relative intensity of the scattered light in function of the particles size in nanometers. This size distribution by intensity could also be converted in distribution by volume using Mie theory. [31]

The particles size of all polymers synthesized in this project was measured by DLLS. Since previous experiments by NanoSight showed the tendency of these particles to

aggregate in water, the DLLS measurements were performed using 0.25 mg/mL particles suspensions in DMSO after sonication for 1h and filtration on 0.45 µm filter.

3.13a

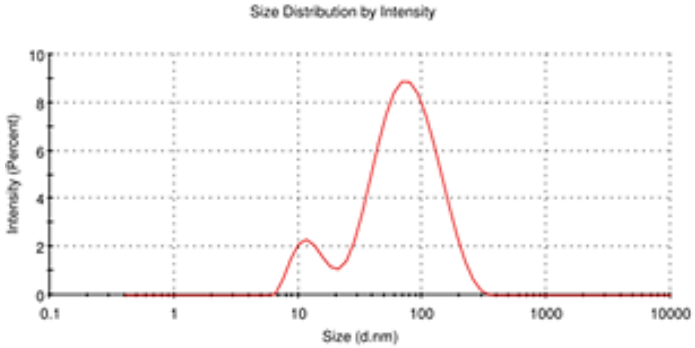

3.13b

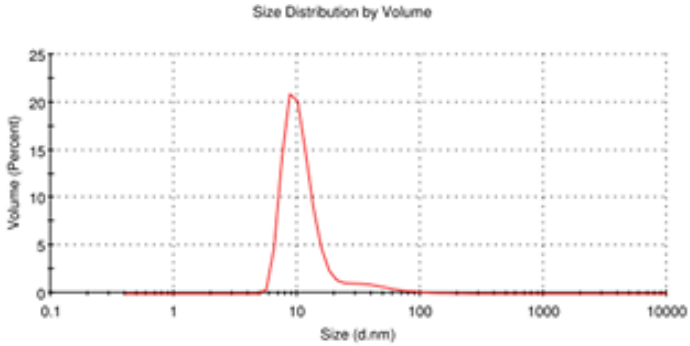

3.13c

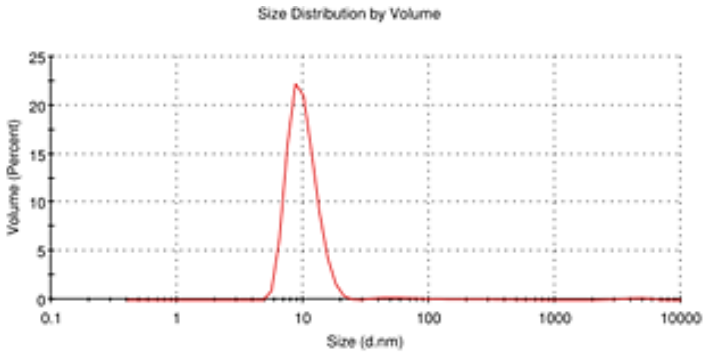

3.13d

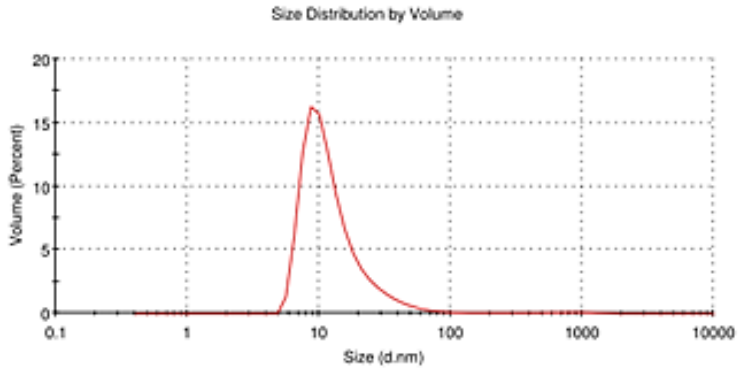

3.13e

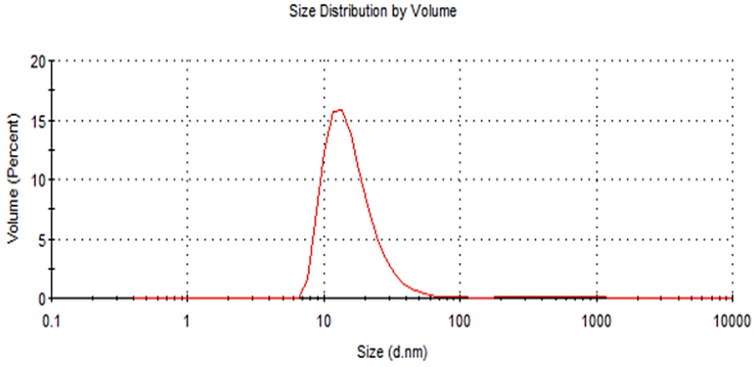

Figure 3.13: a) size distribution by intensity of MIP 3.6; b) size distribution by volume of MIP 3.6; c) size distribution by volume of MIP 1.7; d) size distribution by volume of MIP 2.6; e) size distribution by volume of MIP 4.5

The size distribution by intensity showed for all samples the presence of two populations of particles of 10 nm and 100 nm, while in the size distribution by volume only one peak corresponding to particles of 10 nm size is visible.

This behavior could be explained considering that large particles scattered the light more intensely than small particles, as explained by Rayleigh scattering equation where the intensity of a particle is related to the 6th power of the diameter:

$$I = I_0 \frac{1 + cos\vartheta}{2R^2}\left(\frac{2\pi}{\lambda}\right)^4 \left(\frac{n^2 - 1}{n^2 + 2}\right)^2 \left(\frac{d}{2}\right)^6$$

Where λ and I_0 are respectively the wavelength and the intensity of the beam of light, ϑ is the scattering angle, R is the distance between the particle and the detector, n is the refractive index of the particle and d is the diameter of the particle.[32]

Therefore in a sample containing an equal number of particles of 5 nm and 50 nm, the peak corresponding to 50 nm size population will be 10^6 higher than that of 5 nm size in the size distribution by intensity. In the size distribution by volume the peak corresponding to 50 nm size will be 10^3 higher than that of 5 nm size because the distribution by volume is obtained from the distribution by intensity considering the volume of sphere (*V*):

$$V = \frac{4}{3}\pi r^3$$

Were *r* is the radius of the sphere.

The results obtained by measurements on MIPs and NIPs indicate the presence of a large population of 10 nm size, because both the size distribution by intensity and by volume showed a peak at 10 nm size. The presence of an highly intense signal at 100 nm in the size distribution by intensity suggest the presence also of few particles of 100 nm size corresponding to aggregates, as observed by NanoSight measurements.

The polymer tendency to aggregate could be due to the presence of polar groups in the polymeric matrix that is basically made of ethylenebisacrylamide and acrylamide. The particle size for all MIPs and NIPs is shown in Table 3.3.

Polymer	Particle size (nm)	Polymer	Particle size (nm)
1.5	10.81	**3.7**	13.35
1.6	11.12	**3.8**	12.90
1.7	10.25	**4.5**	15.21
1.8	10.39	**4.6**	11.46
2.5	7.49	**4.7**	13.99
2.6	14.94	**4.8**	10.53
2.7	16.59	**0.5**	8.84
2.8	13.30	**0.6**	13.43
3.5	14.59	**0.7**	12.58
3.6	16.90	**0.8**	9.17

Table 3.3: particle size measured by DLLS

3.2 Recognition of the Targets

In the following table the amount of target molecule and other drugs captured by each polymer and measured as described below are shown.

Polymer	Target	Functional monomer	Rebinding (Q_{MIP}) [nmol mg^{-1}]	Cross rebinding [nmol mg^{-1}]			Imprinting factor
				Sunitinib	SN38	Paclitaxel	
1.5	1	5b	12	-	0	2	3
1.6	1	6b	25	-	0	0	3
1.7	1	7b	35	-	8	5	3
1.8	1	8	6	-	8	0	6
2.5	2	5b	46	22	-	4	1.7
2.6	2	6b	47	25	-	0	1.5
2.7	2	7b	45	38	-	0	2
2.8	2	8	45	16	-	3	2
3.5	3	5b	4	40	44	-	9
3.6	3	6b	3	40	5	-	6
3.7	3	7b	5	39	29	-	8
3.8	3	8	3	38	5	-	17
4.5	4	5b	10	11	44	2	7.1
4.6	4	6b	6	41	48	3	2.6
4.7	4	7b	15	39	48	0.9	0.7
4.8	4	8	7	42	47	0.9	8.6

Table 3.4: rebinding capabilities and selectivity of all MIPs synthesized for sunitinib, SN38 paclitaxel and irinotecan, measured after 1h of incubation. The imprinting factor was calculated at equilibrium.

Rebinding Tests

The molecularly imprinted polymers binding capability was investigated by rebinding tests. The test consists of the quantification during the time of the amount of free drug in a 1 mg/mL polymer water solution containing 50 μM initial drug concentration. After centrifugation to remove the polymeric nanoparticles, the unbonded drug concentration was quantified by an HPLC method. From the resulting data the polymer absorption capacity was calculated.[33]

The absorption capacity is the amount of drug captured by MIP or NIP per mg of polymer.
It is calculated by the following equation:

$$Q = \frac{(C_0 - C_s)V}{W}$$

Where *Q* is the absorption capacity in nmol of captured drug per mg of polymer, while C_0 and C_s are respectively the initial and the equilibrium concentrations of the target molecule in solution, *V* is the volume of the solution and *W* is the weight (mg) of the polymer.[34]
All the molecularly imprinted polymers templated with SN38 showed a good binding affinity for the target, in fact they bind about 45-47 nmol/mg of the drug after several minutes of incubation and they reach saturation within one hour. The majority of MIPs showed also a good stability, and they retain the captured drug also after 24 hours of incubation. Only the MIP containing 4-vinylpyridine tends to release the drug after 8 hours of incubation (Figure 3.14)).

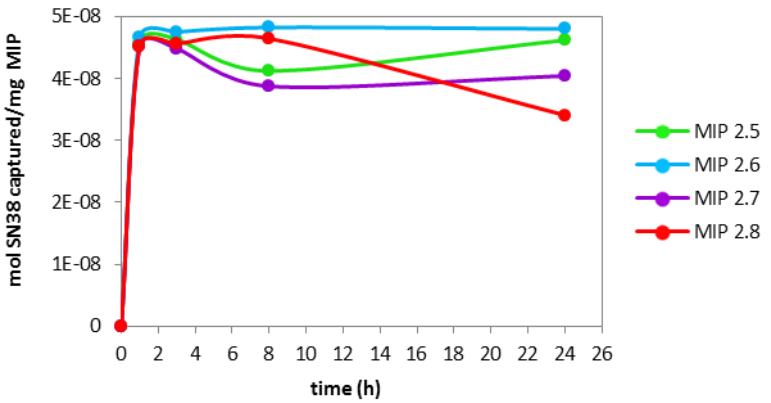

Figure 3.14: rebinding kinetics of SN38 with MIPs 2.5, 2.6, 2.7 and 2.8

The polymers synthesized to capture sunitinib showed a lower amount of drug captured with respect that for SN38. However, a good binding capability was observed for MIP 1.7 that could bind 35 nmol/mg of drug after several minutes and reaches saturation after 12 hours binding 42 nmol/mg drug. MIP 1.6 reaches saturation after 3 hours capturing 27 nmol/mg drug, but after long time it tends to release some of captured sunitinib. A similar value of bound sunitinib was also obtained using MIP 1.5 and MIP 1.8 that show a similar binding kinetics reaching the plateau after 3 hours of incubation (Figure 3.15).

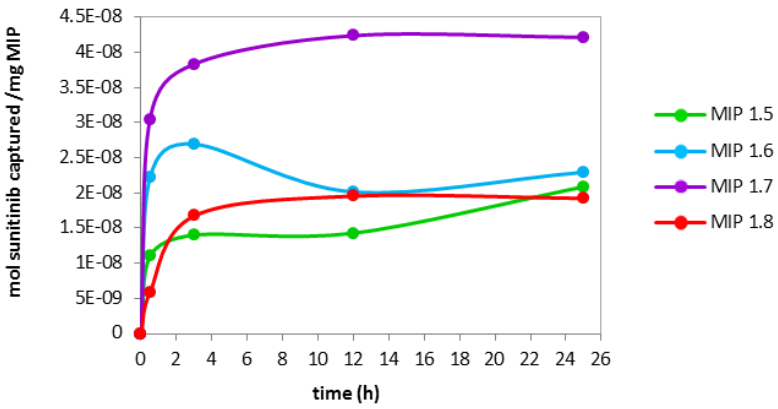

Figure 3.15: rebinding kinetics of sunitinib with MIPs 1.5, 1.6, 1.7, 1.8

Moreover, while the MIPs can bind and hold the drug for a long time, NIPs have a lower binding affinity and tend to release the drug after 3 hours probably due to aggregation phenomena between the nanoparticles which lead to the expulsion of surface-interacting molecules (Figure 3.16)

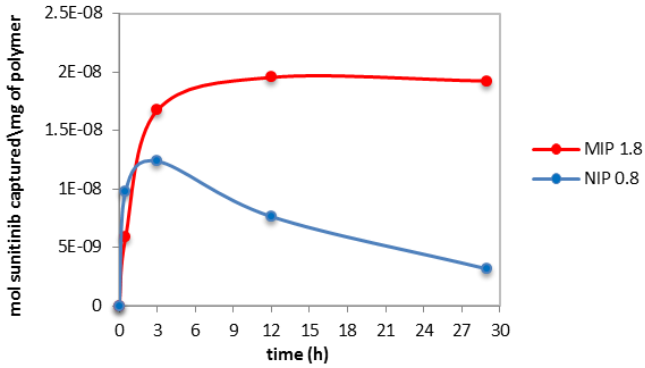

Figure 3.16: rebinding kinetic of sunitinib with MIP and NIP containing 4-vinyl piridine

All the MIPs imprinted with paclitaxel showed a lower binding capability and a lower stability at long times with respect the other polymers. In particular, the MIP containing 7-acryloyloxycoumarin and 4-vinylpyridine reached the maximum of captured drug within one hour, however after this time they tends to release the target molecule. This molecule is captured again after long times only by MIP 3.7. MIPs 3.6 and 3.5 show a slower binding kinetic reaching saturation after 2 hours and release the drug after long times. This behavior suggests that probably the majority of bound molecules are in proximity of the polymer surface and could be easily expelled due to aggregation

between polymer particles that could occur in water solutions. The amount of captured drug for these polymers never exceeded 10 nmol/mg (Figure 3.17).

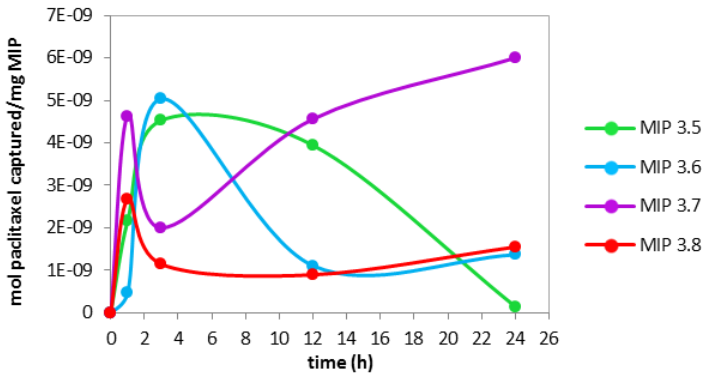

Figure 3.17: rebinding kinetics of paclitaxel with MIPs 3.5, 3.6, 3.7 and 3.8

Rebinding tests were also performed with the polymers synthesized to capture irinotecan. In this case all the imprinted polymers reached the saturation after 1 hour of incubation and hold the drug even after long times. The amount of irinotecan captured at saturation is between 10 nmol/mg and 5 nmol/mg. All the non-imprinted polymers showed a lower binding capability with respect the MIPs, suggesting a good efficiency of the imprinting process and a good specificity for the target drug. The best MIP in terms of binding affinity and specificity is the polymer containing N-acryloyl-tyrosine methyl ester as functional monomer (MIP 4.5) (Figure 3.18).

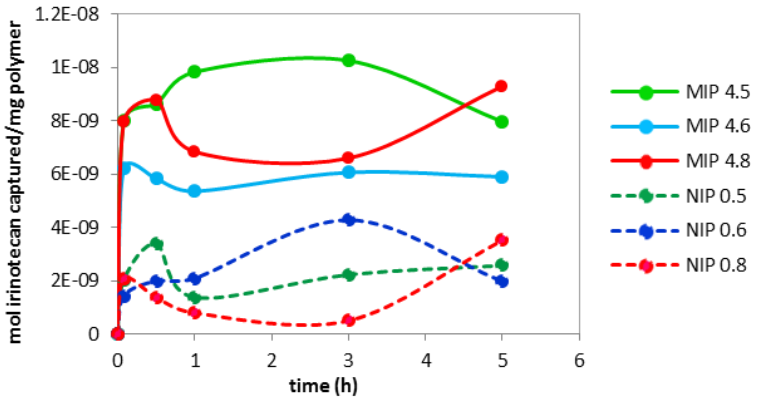

Figure 3.18: rebinding kinetics of irinotecan with MIPs 4.5, 4.6, 4.8 and the respective NIPs in water

The binding capability of these polymers was investigated also in citrate buffer at pH=3 because in these conditions all the irinotecan in solution is in its lactone form. The binding kinetics show that the binding affinity of MIP 4.6 is two times higher but the same amount of irinotecan was captured also by the non-imprinted polymer. Instead MIP 4.5 maintains its better performance over the NIP but its binding capability decreases in citrate buffer with respect to water (Figure 3.19).

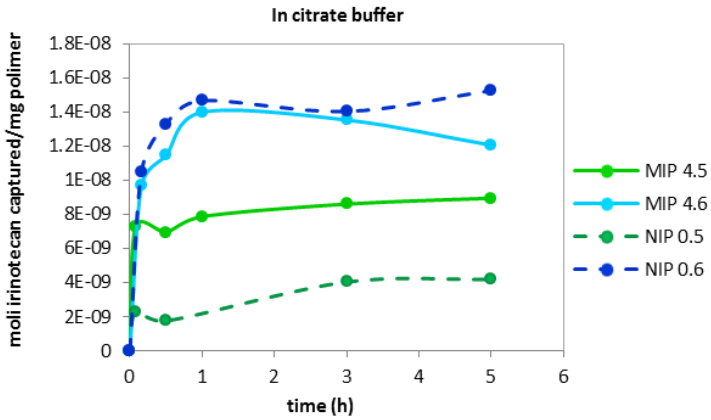

Figure 3.19: rebinding kinetics of irinotecan with MIP 4.5 and 4.6 and the corresponding NIPs in citrate buffer

Cross-reactivity

The selectivity of each MIP for its target molecule was also investigated by rebinding tests with other anticancer drugs. The tests were performed treating a 1 mg/mL water solution of MIP with a 50 μM drug and measuring, by HPLC, the remaining drug concentration in solution after different times.

All the MIPs synthesised to capture sunitinib, SN38 and irinotecan are unable to bind paclitaxel. Their highly crosslinked polymeric matrix having binding sites for fundamentally planar molecules as sunitinib, SN38 or irinotecan, probably could not allow the access of a complex and non planar molecule as paclitaxel inside the polymer. On the contrary the crossreactivity between sunitinib, SN38 or sunitinib is higher.

It is nevertheless possible to select several polymers having a good binding capability and a good selectivity. The best polymer for sunitinib is that containing coumarin as functional monomer (MIP 1.7), as it captures 35 nmol/mg of sunitinib after several minutes and its crossreactivity with SN38 and paclitaxel is 23% and 3% respectively (Figure 3.20).

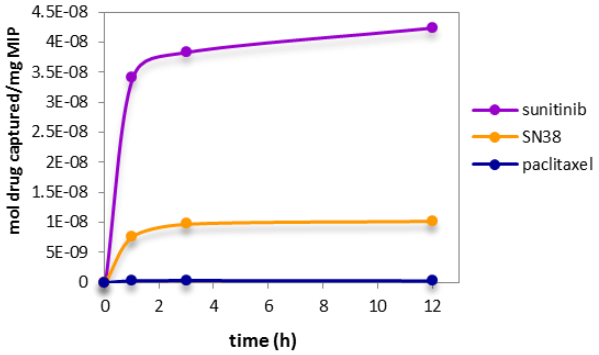

Figure 3.20: rebinding kinetics of sunitinib, SN38 and paclitaxel with MIP 1.7

MIP 2.5 and MIP 2.6 for SN38 show the best performance, they bind 46-47 nmol of target molecule per mg of polymer without any release after 24 hours. Also when tested with other drugs they could bind 22-25 nmol/mg of sunitinib after one hour of incubation and less than 5 nmol/mg of paclitaxel (Figure 3.21).

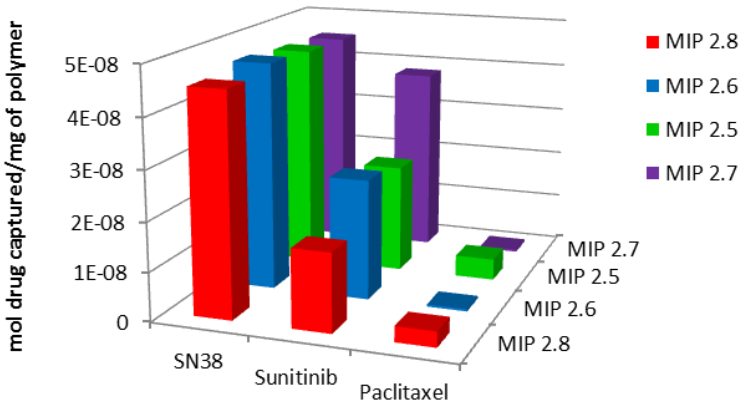

Figure 3.21: amount of SN38, sunitinib and paclitaxel bound by MIP 2.8, 2.6, 2.5 and 2.7 after 1 h of incubation

As to irinotecan, the MIP containing N-acryloyl-tyrosine methyl ester as functional monomer (MIP 4.5) shows the best performance, it captures 9.8 nmol/mg of irinotecan within one hour. However, its selectivity is lower, in fact it binds 2.9 nmol/mg of paclitaxel and 10.9 nmol/mg of sunitinib within one hour, but after this time both the drugs are released from the polymer reaching 7.8 nmol/mg for sunitinib and 0.9 nmol/mg for paclitaxel after 3 hours.

Imprinting Factor

The efficiency of the imprinting process was evaluated by measuring the imprinting factor obtained from the rebinding experiments of MIPs and NIPs.
The imprinting factor (*IF*) is calculated as the ratio of target drug amount bound to the imprinted polymer, to the amount of the same molecule captured by the non-imprinted polymer:

$$IF = \frac{Q_{MIP}}{Q_{NIP}}$$

Where Q_{MIP} and Q_{NIP} are respectively the absorption capability of the imprinted and the not-imprinted polymer having the same monomer formulation. This normalization method removes binding due to non-specific interactions.[35]
In this project the *IF* was preliminary calculated assuming that the number of functional monomers incorporated into the polymeric matrix of MIP and NIP is the same since the same polymer formulation was used with except for the presence of template molecule in MIP.
The imprinting factors calculated for many of polymers in Table 3.4 are between 1 and 3, this is consistent with the results of the NMR titrations with the monomers, where the scarce tendency to saturation indicates a relatively low affinity.[36] Only MIP 3.5, 3.7, 3.8, 4.5 and 4.8 showed higher values of *IF*. Therefore the imprinting process seems been more efficient with large template molecules, as irinotecan and paclitaxel, than with smaller molecules as sunitinib.

Coumarin Content

As the sunitinib MIPs containing coumarin resulted the most promising from the rebinding tests, we have further investigated their properties. The amount of coumarin incorporated into the polymeric matrix of MIP 1.7 and NIP 0.7 was quantified by UV-visible spectroscopy.
A calibration curve of 7-hydroxycoumarin in water was first obtained measuring the characteristic absorbance of coumarin at 324 nm (Figure 3.22).
The UV spectrum of 60 μM and 120 μM water polymers solutions was measured and the absorbance intensity at 430 nm, corresponding to the maximum of absorbance, was used to quantify the functional monomer covalently bonded into the polymer by the calibration curve of 7-hydroxycoumarin (Table 3.5).

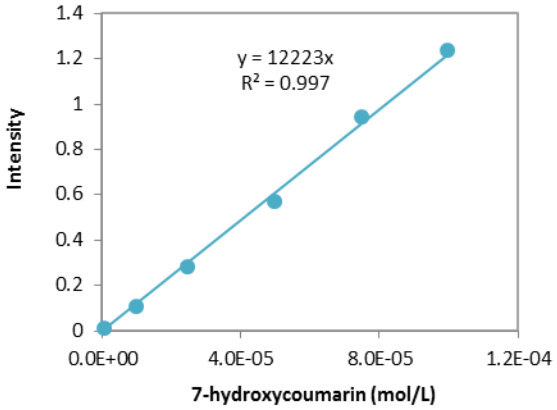

Figure 3.22: calibration curve of 7-hydroxycoumarin in water

Polymer (μg/mL)	Mean intensity	Coumarin (mol/L)
MIP 1.7 60	0.18	$1.44 \cdot 10^{-5}$
NIP 0.7 60	0.40	$3.30 \cdot 10^{-5}$
MIP 1.7 120	0.31	$2.56 \cdot 10^{-5}$
NIP 0.7 120	0.80	$6.54 \cdot 10^{-5}$

Table 3.5: amount of coumarin in the polymer

The amount of coumarin in the NIP is 548 pmol/μg, about twice the amount found in the MIP which contains 227 pmol/μg of functional monomer.
This difference could be explained considering that the main difference between the MIP and NIP polymerization, is the presence of the template molecule in the polymerization mixture of the imprinted polymer. The template molecule could interfere in the polymerization process, by steric hindrance or by side reactions with the monomers, reducing the rate of polymerization with respect that of the non-imprinted synthesis.
This finding allows to recalculate the imprinting factor for MIP 1.7 according to the actual amount of coumarin per mass of polymers. In this way the corrected imprinted factor is 6.

Fluorescence Properties of MIPs

Fluorescence spectroscopy is a highly sensitive and rapid technique widely applied to study the interaction between a fluorescent molecule, called fluorophore, and a quencher able to decrease the fluorophore fluorescence emission.
In the absence of quencher, the fluorescent molecule after excitation at certain radiation, tends to rapidly return to the ground state by emission of a photon. The emission occurs at higher wavelengths than the excitation one. The emission rates of fluorescence are typically in the order of 10^8 s^{-1}, so that a typical fluorescence lifetime is near 10 ns. The lifetime (τ_0) is the average time between excitation and return to the ground state.

The intensity of fluorescence emission could be decreased by a quenching mechanism that involves the interaction between the fluorophore and the quencher. Two different mechanisms could be distinguished: dynamic and static quenching.
Dynamic quenching, called also collisional quenching, occurs when a fluorophore in its excited state is deactivated upon contact with the quencher that diffuses in solution. The dynamic quenching is described by the Stern Volmer equation:

$$\frac{F_0}{F} = 1 + k_q \tau_0 [Q] = 1 + K_D [Q]$$

Where F_0 and F are the fluorescence emission intensities in absence and in presence of the quencher respectively, k_q is the bimolecular quenching constant, τ_0 is the lifetime of the fluorophore in the absence of quencher and $[Q]$ is the quencher concentration. If the quenching is dynamic the Stern Volmer constant is indicated ad K_D, and the values of bimolecular quenching constant are near $1 \cdot 10^{10} mol^{-1} L^{-1} s^{-1}$. Values of k_q larger than the diffusion-controlled limit suggest that a static quenching occurs. In this case the Stern Volmer constant is indicated as K_S.
Static quenching consist of the interaction between the fluorescent molecule and the quencher leading to a non-fluorescent ground state complex.[37] In static quenching the dependence of fluorescence intensity from the quencher concentration is derived considering the association constant of complex formation:

$$F + Q \rightleftharpoons FQ$$

$$K_S = \frac{[FQ]}{[F][Q]}$$

Where $[F]$ is the concentration of the free fluorophore, $[Q]$ is the concentration of free quencher and $[FQ]$ is the concentration of complex and K_S is the association constant. Since:

$$F_0 = [F] + [FQ]$$

$$K_S = \frac{[F_0] - [F]}{[F][Q]} = \frac{[F_0]}{[F][Q]} - \frac{1}{[Q]}$$

The Stern Volmer equation for static quenching becomes:

$$\frac{F_0}{F} = 1 + K_S [Q]$$

Where K_S is both the association and the Stern Volmer constant.[38]

The presence of tyrosine, tryptophan and coumarin in the polymeric matrix gives some fluorescent properties to the MIPs. Therefore the fluorescence technique was used to study the interaction of MIPs with their target molecules. The polymer binding ability at lower concentrations of drug was investigated by fluorescence titration of the polymer with increasing amounts of the drug. Fluorescence quenching was observed due to the interaction between the polymer and the drug. The quenching phenomenon was studied by the Stern-Volmer analysis, plotting the ratio of the fluorescence emission before and after addition of quencher, in function of the quencher concentration.

The Stern-Volmer plots obtained with all the fluorescent MIPs show a bimodal quenching behaviour, with a first, high slope, linear region occurring at low concentrations of drugs, and a further, low slope, linear region at higher drug concentrations. This behaviour suggests the presence of a non-homogeneous polymer containing binding sites with different affinity for the target molecule.[39]

Conversely, the Stern–Volmer plots reporting the fluorescence quenching of the free functional monomers upon titration with the drugs show a single linear behaviour with a slope similar to that found in the second region of the polymers (Figure 3.23).

3.23a

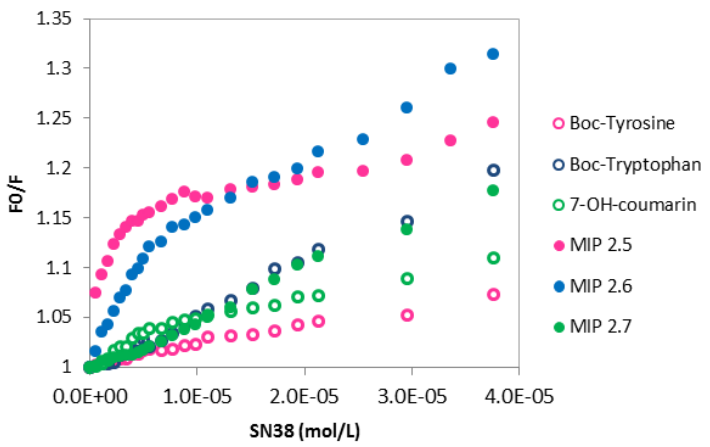

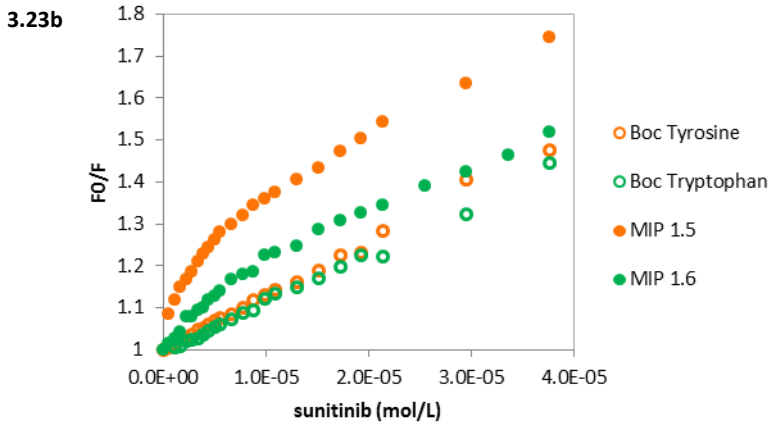

Figure 3.23: comparison between the Stern-Volmer plots of MIPs for SN38 and MIPs for sunitinib with analogues of the free functional monomers

The efficiency of the drugs in quenching the MIPs emission was investigated by the Stern-Volmer equation, as shown below, that was separately applied on the two linear regions of the Stern-Volmer plots.

$$\frac{F_0}{F} = K_{SV}^{app} \cdot [Q] + 1$$

Where F_0 is the initial fluorescence intensity of the polymer, F is the fluorescence intensity in the presence of the drug, $[Q]$ is the quencher concentration, and $K^{app}{}_{SV}$ is the apparent Stern-Volmer constant for the non-homogeneous MIP, that can be regarded as an apparent association constant between the population of fluorophores in the MIP and the quencher.[40]

The Stern–Volmer constants are reported in Table 6, with the bimolecular quenching constants $k_q{}^{app}$ calculated by the equation:

$$k_q^{app} = \frac{K_{SV}^{app}}{\tau_0}$$

where K_{SV} is the Stern-Volmer constant and τ_0 is the lifetimes of fluorophores, which were assumed to be $4.3 \cdot 10^{-9}$ s for coumarin,[41] $3.6 \cdot 10^{-9}$s for tyrosine and $3.1 \cdot 10^{-9}$ s for tryptophan.[42,43]

In any case, including the low slope regions of the plots, $k_q{}^{app}$ is larger than the value for the diffusion controlled quenching: $1 \cdot 10^{-10}$ $mol^{-1}L^{-1}s^{-1}$, therefore the fluorophore and

the quencher binds together leading to a static quenching. For this reason the observed quenching is to be considered as the consequence of a static interaction.
The high Stern-Volmer constants measured (Table 3.6) at drug concentrations lower than 5 μM for all polymers templated with sunitinib and for the polymers templated with SN38 and containing tyrosine and tryptophan, are most likely related to the presence of inner binding sites characterized by an higher apparent binding affinity. The amount of such sites appears as constant in the different MIPs, and probably related to the way chosen for their synthesis, namely to the molar ratio between the template, functional monomer, co-monomer and cross-linker. On the other side, lower affinity binding sites on the polymer surface may be associated to the behaviour of second region of the plot where the slope is similar to the Stern-Volmer constant obtained by the titration of the free functional monomers (Table 3.6). However, the increased slope of the Stern-Volmer plot of the polymer shows a good efficiency of the imprinting process that created binding sites complementary to the target molecule leading to an increased binding capability of the polymer than the corresponding functional monomer.

MIP	K_{SV}^{app} [$10^3 Lmol^{-1}$]	k_q^{app} [$10^{12} Lmol^{-1}s^{-1}$]		Molecule	K_{SV}^{app} [$10^3 Lmol^{-1}$]	k_q^{app} [$10^{12} Lmol^{-1}s^{-1}$]
1.5	37.6 (14.4)	10.4 (4)	with sunitinib	Boc-tyr	12.7	3.5
1.6	25.2 (10.7)	8.1 (3.4)		Boc-trp	12.2	3.9
1.7	61.0 (15.6)	14.2 (3.6)		7-OH-coum	18.5	4.3
2.5	26.1 (2.0)	7.2 (0.6)	with SN38	Boc-tyr	2.1	0.6
2.6	20.9 (6.1)	6.7 (1.9)		Boc-trp	5.6	1.8
2.7	5.7 (2.1)	1.3 (0.5)		7-OH-coum	7.9	1.8
3.5	4.3 (2.7)	1.2 (0.7)	with paclitaxel	Boc-tyr	3.7 (2.8)	1.0 (0.8)
3.6	110 (1.0)	35.5 (0.3)		Boc-trp	18.2 (1.7)	3.6 (0.3)
3.7	50.4 (2.5)	11.7 (0.6)		7-OH-coum	0.2	0.4

Table 3.6: Stern-Volmer and quenching constants of MIPs and free functional monomers analogues. The constants below and (over) 5 μM drug concentration were obtained from titrations performed in water with MIP from 1.5 to 2.7. Titrations of paclitaxel were performed in DMSO. For MIP 3.5 and 3.6 the constants refers to concentrations below and (over) 613 nM, while for the corresponding free molecules the values refers to concentrations below and (over) 9 μM. For MIP 3.7 the values refer to concentrations below and (over) 495 nM.

The behaviour of MIP 1.7**,** containing coumarin and capable of rebinding sunitinb, is particularly interesting due to its emission of visible light whose quenching can be appreciated also by the naked-eye (Figure 3.24). Moreover this polymer showed a binding affinity higher than other MIPs, as indicated also by the high value of its Stern-Volmer constant, and the presence of specific sites since the slope of the NIP 0.7 Stern-Volmer plot is lower than that of MIP 1.7.[44] Therefore MIP 1.7 was selected as a fluorescent sensor to set up a test in plasma.

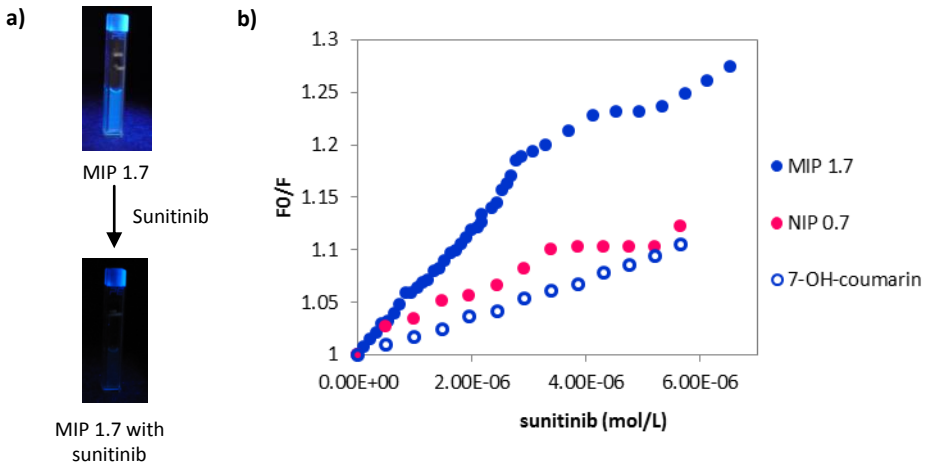

Figure 3.24: a) quenching of MIP 1.7 fluorescence upon addition of 50 μM sunitinib, b) Stern Volmer plot of MIP 1.7, NIP 0.7 and 7-hydroxycoumarin

All the titrations with paclitaxel were performed in DMSO due to the insolubility of this drug in water. MIP 3.7 containing coumarin showed a high binding affinity at drug concentrations lower than 495 nM, while increasing the concentration the affinity decreases drastically. These values indicate that MIP 3.7 has few inner highly specific binding sites that are occupied at low drug concentrations, while increasing the amount of drug added also the less specific and external binding sites are occupied. Since both the quenching constants for the highly and less specific sites are higher than 10^{10} $molL^{-1}s^{-1}$, static quenching occurs during all the titration. Finally, comparing the quenching and the SternVolmer constants of MIP 3.7 and those of free 7-hydroxycoumarin, it can be seen that the interaction with the free molecule is weak and occurs in part by a dynamic quenching. The incorporation of coumarin in the polymeric matrix increases drastically the quenching constant and the binding affinity due to the presence of specific binding sites in the MIP.

Finally, comparing the polymers synthesized to capture paclitaxel, MIP 3.6 showed the highest binding affinity at concentrations lower than 613 nM, and also a good specificity for paclitaxel since the slope of titration curves of both the non-imprinted

polymer and the free tryptophan is very low in comparison that of MIP 3.6. Therefore the imprinting process was very efficient for this polymer (Figure 3.25).

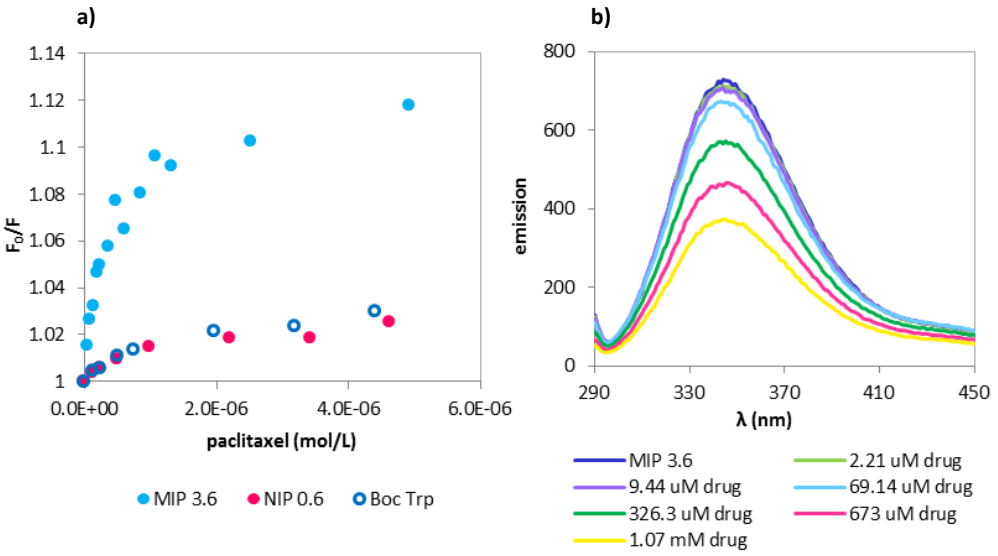

Figure 3.25: a) Stern Volmer plot of MIP 3.6, the respective NIP and the free functional monomer analogue; b) fluorescence quenching of MIP3.6 upon interaction with paclitaxel

Also the binding affinities of MIPs for irinotecan at low drug concentrations were first evaluated by the Stern Volmer analysis titrating MIPs 4.5 and 4.6 with increasing concentrations of irinotecan. As in the previous titrations, quenching of functional monomer fluorescence in the polymer was observed upon interaction with the drug. The calculated apparent Stern-Volmer and quenching constants indicate that for all polymers the interaction with the target leads to a static quenching. Moreover, the binding affinity of MIP 4.5 is twice that of the respective NIP 0.5 due to a good efficiency of the imprinting process (Figure 3.26a, Table 3.7).

The slopes of the Stern-Volmer plots of MIP 4.6 and NIP 0.6 corresponding to the apparent Stern-Volmer constant are conversely very similar, indicating that the number of specific binding sites in MIP 4.6 is very low (Figure 3.26b).

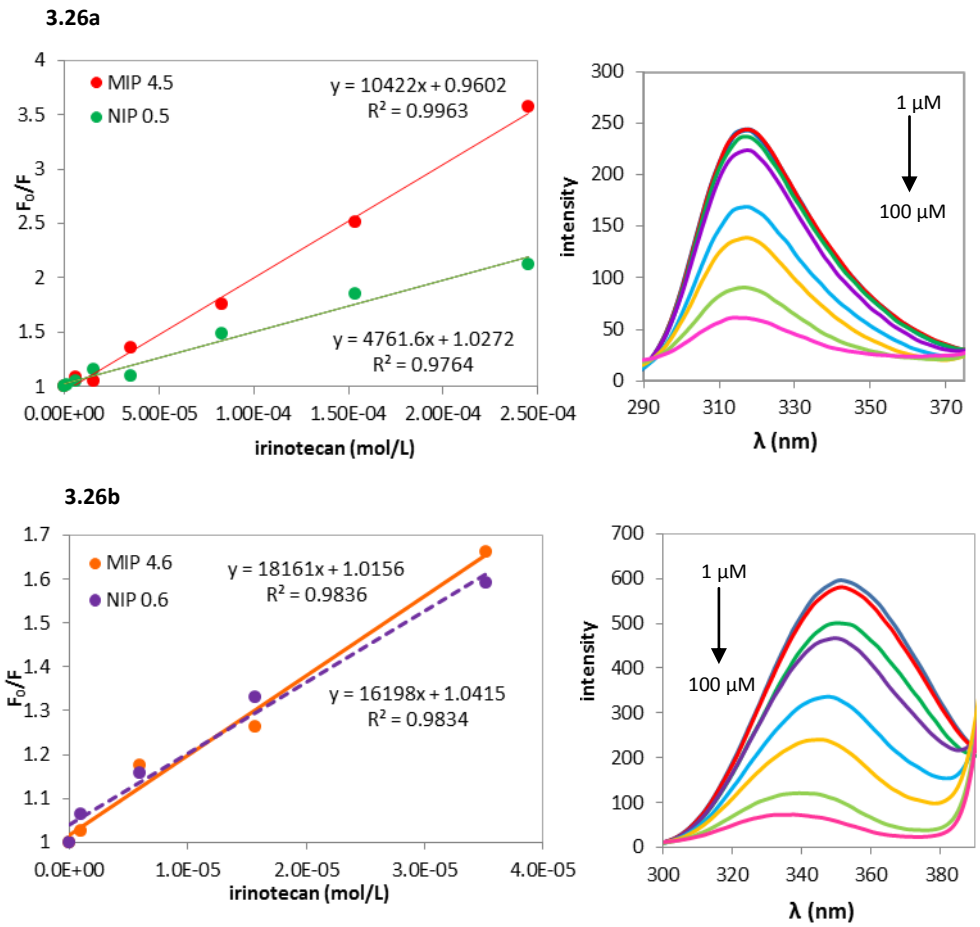

Figure 3.26: On the left: Stern-Volmer plots of MIP 4.5, 4.6 and the respecive NIPs. On the right: a) fluorescence quenching of MIP 4.5 upon addition of irinotecan; b) fluorescence quenching of MIP 4.6 upon addition of irinotecan

Polymer	K_{SV}^{app} [10^3Lmol^{-1}]	k_q^{app} [10^{12}Lmol^{-1}s^{-1}]
MIP 4.5	10.4	2.9
NIP 0.5	4.8	1.3
MIP 4.6	18.2	5.9
NIP 0.6	16.2	5.2

Table 3.7: apparent Stern-Volmer and quenching constants of MIP 4.5 and MIP 4.6 and the respective NIPs

The polymer containing coumarin was not analysed because the fluorescence emission band of coumarin is superimposed to that of irinotecan, therefore it is impossible to observe the quenching of coumarin fluorescence in the polymer during the titration with the drug.

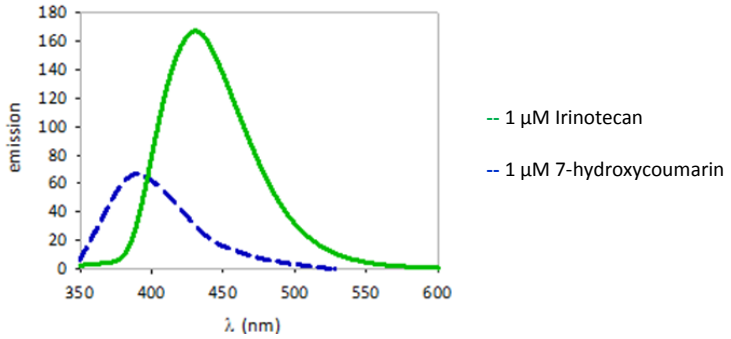

Figure 3.27: fluorescence emission spectra of irinotecan and 7-hydroxycoumarin

The fluorescence quenching of MIP 4.5 and 4.6 upon interaction with irinotecan is quite high within the range of drug concentrations commonly found in real samples. However, the measurement of the tyrosine or tryptophan fluorescence quenching in the polymer exciting at 230 nm or 280 nm, is not possible in blood or plasma samples containing irinotecan, due to the presence of proteins or peptides containing tyrosine or tryptophan that emit at the same wavelengths of the polymer interfering in the drug quantification.

3.3 Towards Fluorimetric Sensors: Two Proofs of Concept

Sunitinib: a Proof of Concept in Plasma

Since MIP 1.7 showed good binding capabilities and fluorescent properties, it was chosen as a potential fluorescent sensor to study its performance in quantifying sunitinib in plasma samples. We have therefore designed a possible test to be carried out by simply diluting the plasma sample in DMSO, adding the fluorescent MIP probe and reading the resulting MIP emission, compared with that of a reference sample of plasma without sunitinib. This choice was due to the fact that the polymer has been synthesized in DMSO, while it releases the target when washed in alcohols as methanol

or ethanol. Such solvents are the typical denaturising agents commonly used in the treatment of plasma samples, while DMSO is rarely reported. The action of alcohols on human plasma is very different from that of DMSO, as alcohols lead to the denaturation and precipitation of most of the serum albumin, while DMSO leads to unfolding without precipitation.[45,46] Serum albumin unfolding is nevertheless sufficient, in our hypothesis, to allow the release of the albumin-bound drugs.

In this view, a calibration curve was obtained first titrating 60 μg/mL MIP 1.7 with increasing amounts of sunitinib in a 4:1 DMSO : water mixture.

The titration was repeated in triplicate experiments carried out on different polymer preparations in 4:1 DMSO : water mixture and repeated in different days. From these titrations an average calibration curve was obtained and used to quantify sunitinib in spiked samples in both a serum albumin solution in buffer and real human plasma (Figure 3.28).

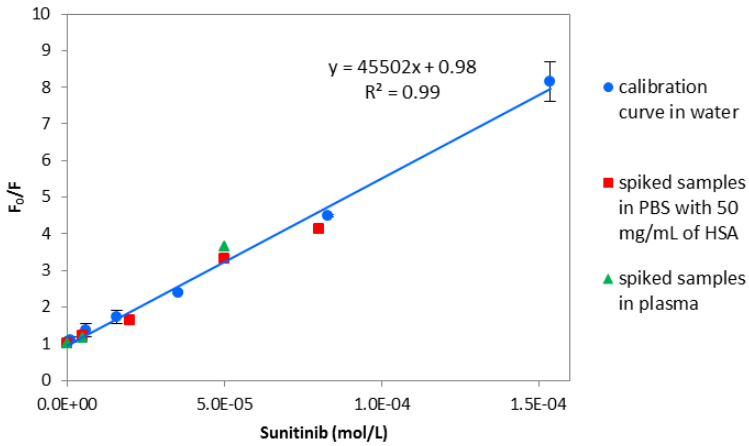

Figure 3.28: distribution of the spiked samples on the calibration curve

The precision of the calibration curve turned out to be very good, as the within-run variability (CV) is less than 9%, and the average within-day variability is less than 5%.

The lower limit of detection of sunitinib, defined as the lowest concentration of sunitinib leading to an emission of polymer fluorescence that can be statistically differentiated from the reference one (average emission under 3σ from the initial emission), can be placed at 400 nM, as a consequence of the apparent Stern-Volmer constant and of the observed variability.

Samples spiked with known quantities of sunitinib in both PBS and normal human plasma were treated with four volumes of DMSO to unfold proteins. Such treatment of the plasma sample lead to a slight white precipitate likely due to salts (as no absorbance at 280 nm was recorded after redissolving the precipitate in water). After

centrifugation, MIP1.7 was added from a mother solution in DMSO, its emission was compared with that obtained from a not spiked plasma sample, and the sunitinib concentration was calculated from the calibration curve made in 4:1 DMSO : water mixture. The recovered concentrations of the drug in the spiked samples are reported in Table 3.8.

Real sunitinib concentration ($mol \cdot L^{-1}$)	**Calculated sunitinib concentration ($mol \cdot L^{-1}$)**	
	In PBS with HSA 50 $mg \cdot mL^{-1}$	**In plasma**
$5 \cdot 10^{-6}$	$5.12 \cdot 10^{-6}$	$3.75 \cdot 10^{-6}$
$2 \cdot 10^{-5}$	$1.47 \cdot 10^{-5}$	-
$5 \cdot 10^{-5}$	$5.16 \cdot 10^{-5}$	$5.89 \cdot 10^{-5}$
$8 \cdot 10^{-5}$	$6.92 \cdot 10^{-5}$	-

Table 3.8: recovered sunitinib concentration in spiked samples

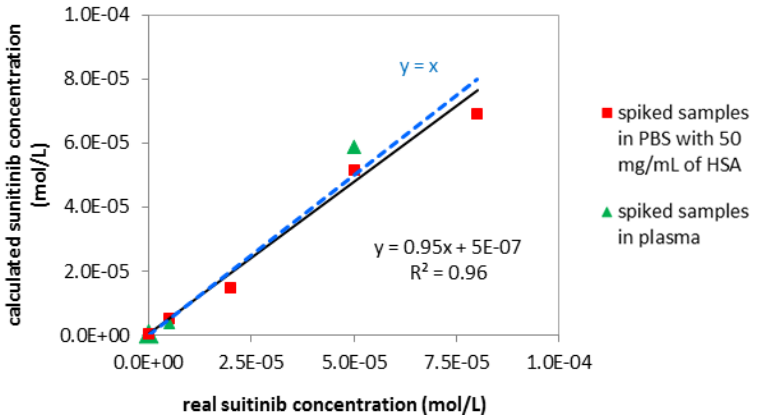

Figure 3.29: correlation between the calculated sunitinib concentration and the real drug concentration of spiked samples in PBS with 50 mg/mL HSA (red) and in plasma (green)

Despite the samples were quantified by a calibration curve performed in a different environment (DMSO : water mixture), the accuracy was encouraging, and the calculated concentrations correlate well with the theoretical ones in both PBS and plasma solutions. Therefore the robustness of the system upon changing the environment from DMSO : water to DMSO : PBS first, and then to DMSO : normal human plasma, is good.

The slope of the linear regression of such data is very close to the theoretical value of 1 for both the plasma samples and the buffer-albumin ones. The good results obtained

with this proof of concept on MIP 1.7 open the way to the possibility to use a fluorescent MIP as sensor for monitoring drug concentration directly in plasma without the need of any treatment except the addition of DMSO. However, the system would require a careful optimization of the MIP affinity in order to reach a better sensitivity, with a selection of other functional co-monomers. The sensitivity of this non optimized test could be enough for the expected plasma concentrations of other tyrosine kinase inhibitors as imatinib, but in the case of sunitinib the system could be useful only to detect plasma levels of sunitinib exceeding the therapeutic range, and preconcentration of the samples would be required if one would use the test to obtain the whole pharmacokinetic curve in a patient.

Signals from the Target: Irinotecan in Plasma

A fluorescence sensor could be obtained exploiting the variation of fluorescence properties of the recognition element upon binding of the target, or the intrinsic fluorescence of the target molecule.
Since irinotecan is a fluorescent molecule[47] giving a high emission at 430 nm when excited at 360 nm, the development of sensors based on MIPs able to quench the irinotecan fluorescence was evaluated as first approach. The functional monomers **5b**, **6b** and **7b** are characterized by a lower fluorescence emission than irinotecan but are able to make hydrogen bonds and π-staking interactions with the drug, as observed by ^{1}H-NMR titration experiments. As reported in section 3.2, it has been possible to detect the interaction of irinotecan with the tyrosine and tryptophan containing MIPs by titration of the monomer emission. Unfortunately this approach cannot be used in plasma samples, due to the presence of proteins and peptides themselves containing the same fluorophores. On the other side, coumarin emission is not useful with irinotecan, as it is a stronger emitter at close wavelengths.
We have therefore tested the possibility to exploit the tyrosine and tryptophan MIPs as quenchers of the irinotecan emission. The MIP containing tyrosine methyl ester was selected as best polymer able to capture irinotecan with high specificity, as shown by Stern Volmer analysis. Moreover, a preliminary fluorescence titration of the emission of 1 μM irinotecan with MIP 4.5 and MIP 4.6 in 3:1 DMSO:water mixture showed that MIP 4.5 is more efficient and gives the highest quenching of the irinotecan emission (Figure 3.30).

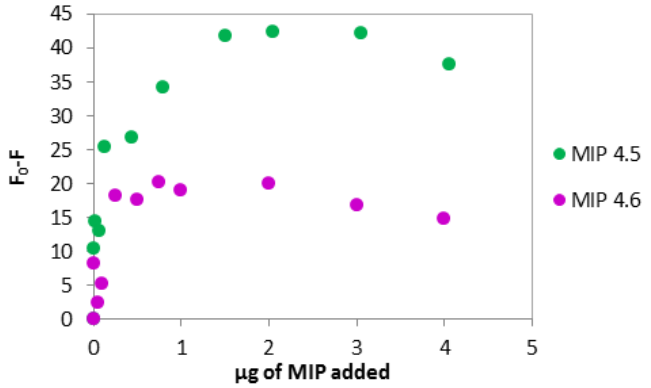

Figure 3.30: Fluorescence quenching of irinotecan upon addition of MIP 4.5 and MIP 4.6 in 3:1 DMSO:water mixture

Further fluorescence titrations of 1 µM irinotecan with increasing amounts of MIP 4.5 were performed in both 3:1 methanol:plasma and 3:1 DMSO:plasma mixtures. DMSO was used to increase the polymer binding capability since the polymerization was performed in this solvent. Methanol was used because it is the common solvent adopted by clinicians to treat plasma samples before drug quantification. Despite these different environments, MIP 4.5 showed the same behaviour during both the titrations and the ability to quench the drug reached a plateau after 2 µg of MIP added. The titration in methanol:plasma mixture was also repeated with different concentrations of irinotecan to investigate the dynamic range of the system. The variation of the quenching response in function of drug concentration was observed from 4.25 µM to 0.5 µM. The entity of quenching increases with the drug concentration because the binding equilibrium is shifted towards the complex formation increasing the concentration of target molecule in solution. At low concentrations binding to the polymer is more difficult and the plateau occurs before 2 µg of polymer added. Moreover, above 0.5 µM drug the titration curves are overlapped, indicating that the lower limit of detection was reached (Figure 3.31).

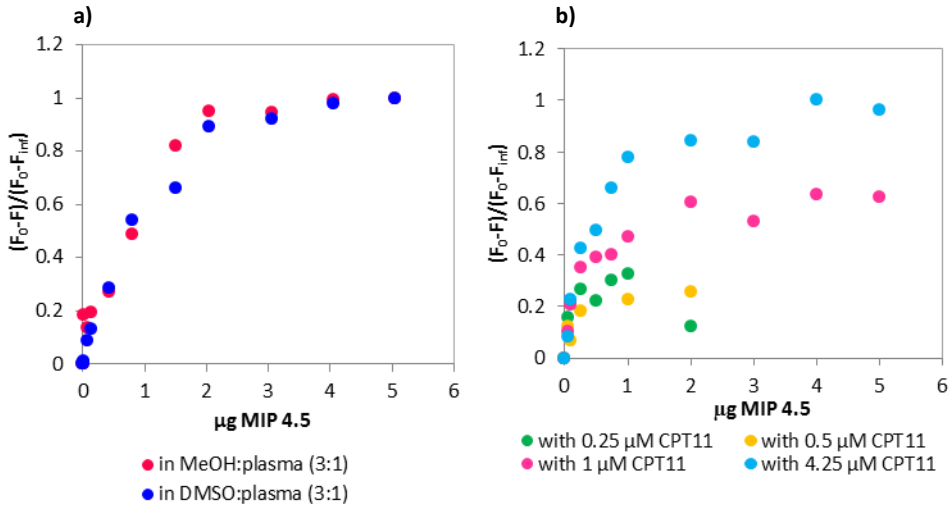

Figure 3.31: a) titration curve of irinotecan with MIP 4.5 in methanol:plasma and DMSO:plasma mixture; b) titration curves of different concentrations of irinotecan with MIP 4.5 in 3:1 methanol:plasma

Therefore a preliminary calibration curve was carry out treating, spiked samples containing different concentrations of irinotecan in 3:1 methanol:plasma mixture with 2 µg of MIP 4.5. The fluorescence emission before and after addition of the polymer was measured exciting at 360 nm and measuring at 430 nm. The amount of polymer added was chosen in base of the previous titration curves (Figure 3.32), where after 2 µg of MIP a plateau was reached.

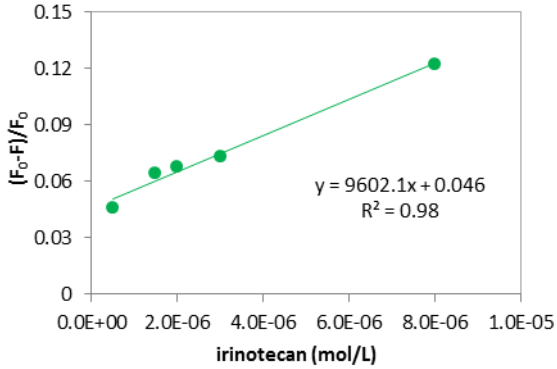

Figure 3.32: preliminary calibration curve of irinotecan with MIP 4.5 in 3:1 methanol:plasma

Even if the amount of quenching is not very high, a linear correlation was observed from 0.5 µM to 8 µM. Also this second proof of concept shows that MIPs are capable to work in plasma samples without significant decrease of their performance, even in the presence of methanol.

Signal from the Polymer: a Fluorescent MIP for Irinotecan

The second approach in sensor development for irinotecan consists of the synthesis of a molecularly imprinted polymer containing an highly fluorescent functional monomer whose fluorescence emission is quenched upon interaction with the drug.
To this aim we have identified a naftalimide-based functional monomer (**16c**) containing an amino group at the side chain able to make hydrogen bonds with irinotecan, and the aromatic system of naftalimide able to give an high emission fluorescence (Scheme 3.3). Analogues of this functional monomer are widely used in literature to obtain fluorescent polymers to be used in sensor development.[48] The synthesis was performed following the procedure of Konstantinova and co-workers.[49]

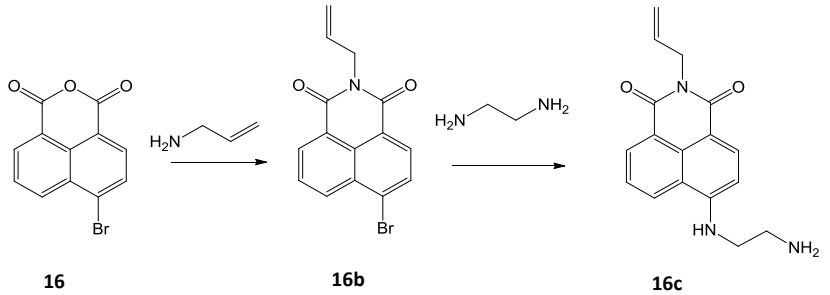

16 **16b** **16c**

Scheme 3.3: synthesis of the fluorescent functional monomer: 2-allyl-6-((3-aminoethyl)amino)-1H-benzo[de]isoquinoline-1,3(2H)-dione

The molecularly imprinted polymer was synthesized with 30% of functional monomer and 70% of ethylene glycol dimethacrylate (EGDMA). The choice of this crosslinker is due to the attempt to increase the polymer solubility and stability in water, since it is widely used in literature to obtain soluble molecularly imprinted polymers.[50, 51]
The fluorescent properties of this polymer were evaluated by fluorescence titration of 60 μg/mL polymer solution directly in 3:1 methanol:plasma mixture, with increasing amounts of irinotecan from 20 nM to 100 μM. The fluorescence emission of MIP was measured at 520 nm when excited at 448 nm. The Stren Volmer plot (Figure 3.33) corresponds to the mean of three independent titrations, the high variability of certain points is due to the low polymer stability and the tendency to aggregate in methanol:plasma mixture.
As shown in Figure 3.33 the quenching of fluorescence is not very high and a residual polymer fluorescence remains even after reaching the equilibrium state that corresponds to the plateau observed in the Stern Volmer plot. At the plateau all the accessible polymer binding sites are occupied and equilibrium between the free drug

and the bound drug is established. The polymer residual fluorescence could be due to the presence of some inner binding sites that are not accessible to the target molecule, or to the presence of an excess of functional monomer.

Despite these problems, the MIP fluorescence changed upon interaction of very low drug concentrations, showing a linear response between 20 nM and 100 nM.

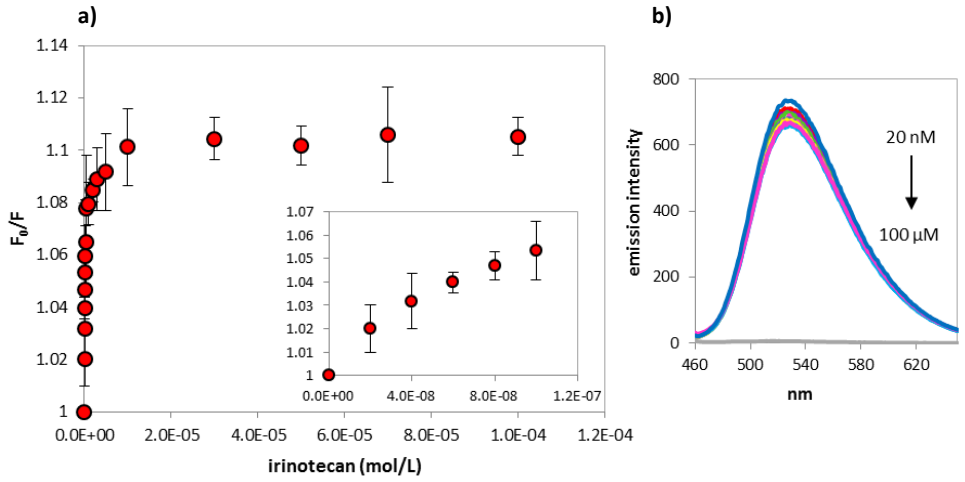

Figure 3.33: fluorescence titration of MIP with increasing concentrations of irinotecan in 3:1 methanol:plasma mixture. On the left: Stern Volmer Plot, on the right: quenching of polymer fluorescence emission upon addition of irinotecan.

The apparent Stern Volmer constant was calculated at low drug concentrations where the fluorescence quenching increase linearly with the amount of drug added. The obtained value is $406 \cdot 10^3$ $L \cdot mol^{-1}$, indicating a good binding affinity of this MIP for irinotecan. Also the apparent quenching constant was calculated, using the lifetime of 9-Butyl-4-butylamino-1,8-naphtalimide, an analogue molecule of the functional monomer used for MIP synthesis. The lifetime of this molecule in methanol is 8.3 ns,[52] therefore the obtained apparent quenching constant was $4.9 \cdot 10^{13}$, indicating that the quenching is static.

The obtained apparent Stern Volmer constant was very high with respect other MIPs previously synthesized. Moreover the fluorescence emission of naphtalimide occurs at higher wavelengths than both irinotecan and biomolecules that could be found in plasma, allowing the drug quantification in biological samples without any interference.

[1]Hu Y., Pan J., Zhang K., Lian H., Li G. (2013) "Novel applications of molecularly-imprinted polymers in sample preparation" *Trends Anal. Chem.* 43:37-52

[2] Roy S. G., De P. (2014) "pH Responsive polymers with aminoacids in the side chains and their potential applications" *J. Appl. Polym. Sci*. 41084:1-12

[3] Ayaz N., Bezgin F., Demirelli K. (2012) "Polymers based on methacrylate bearing coumarin side group: synthesis via free radical polymerization, monomer reactivity ratios, dielectric behavior, and thermal stabilities" *ISRN Polymer Science* ID 352759

[4] Nguyen t. H., Ansell R. J. (2009) "fluorescent imprinted polymer sensors for chiral amines" *Org. Biomol. Chem.* 7:1211-1220

[5] Scorrano S., Mergola L., Del Sole R., Vasapollo G. (2011) "Synthesis of molecularly imprinted polymers for amino acid derivates by using different functional monomers" *Int. J. Mol. Sci*. 12:1735-1743

[6] Puoci F., Gereffa C., Iemma F., Muzzalupo R., Spizzirri U. G., Picci N. "Molecularly imprinted solid phase extraction for detection of sudan I in food matrices" *Food Chem.* 93(2):349-353

[7] Caro e., Marcé R. M., Cormack P. A. G., Sherringhton D. C., Borrull F. (2003) "On-line solid-phase extraction with molecularly imprinted polymers to selectively extract substituted 4-chlorophenols and 4-nitrophenol from water" *J. Chromatogr. A* 995:233-238

[8] Bentolila A., Vlodavsky I., Ishai-Michaeli R., Kovalchuk O., Haloun C., Domb A. J. (2000) "Poly(N-acryl amino acids): a new class of biologically active polyanions" *J. Med. Chem.* 43: 2591-2600.

[9] Moore B.L., O'Reilly R. K. (2012) "Preparation of chiral amino acid materials and the study of their interactions with 1,1-Bi-2-naphthol" *J. Polym. Sci. A: polymer* 50: 3567–3574.

[10] Sinkel C., Greiner A., Agarwal S. (2010) "A polymeric drug depot based on 7-(2(-Methacryloyloxyethoxy)-4-methylcoumarin copolymers for photoinduced release of 5-Fluorouracil designed for the treatment of secondary cataracts" *Macromol. Chem. Phys*. 211: 1857–1867.

[11] Svenson J., Karlsson J. G., Nicholls I. A. (2004) "^{1}H Nuclear magnetic resonance study of the molecular imprinting of (-)-nicotine: template self-association, a molecular basis for cooperative ligand binding" *J. Chromatogr. A* 1024:39-44

[12] Hirose K. (2001) "A pratical guide for the determination of binding constants" *J. Incl. Phenom. Macroc. Chem.* 39:193-209

[13] Kleckner I. R., Foster M. P. (2011) "An introduction to NMR-based approaches for measuring protein dynamics" *Biochim. Biophys. Acta* 1814(8):942-968

[14] Athikomrattanakul U., Katterle M., Gajovic-Eichelmann N., Scheller F. W. (2009) "Development of molecularly imprinted polymers for the binding of nitrofurantoin" *Biosens. Bioelectron.* 25:82-87

[15] Quaglia M., Chenon K., Hall A. J., De Lorenzi E., Sellergren B. (2001) "Target analogue imprinted polymers with affinity for folic acid and related compounds" *J. Am. Chem. Soc.* 123:2146-2154

[16] Ye L., Mosbach K. (2001) "Molecularly imprinted microspheres as antibody binding mimics" *React. Funct. Polym.* 48:149-157

[17] Carboni D., Flavin K., Servant A., Gouverneur V., Resmini M. (2008) "The first example of molecularly imprinted nanogels with aldolase type I activity" *Chem. Eur. J.* 14(23):7059-7065

[18] Graham N. B., Cameron A. (1998) "Nanogels and microgels: The new polymeric materials playground" *Pure. App.l Chem.* 70(6):1271-1275

[19] Pasetto P., Maddock S. C., Resmini M. (2005) "Synthesis and characterisation of molecularly imprinted catalytic microgels for carbonate hydrolysis" *Anal. Chim. Acta.* 542:66-75

[20] Wulff G., Chong B. O., Kolb U. (2006) "Soluble single-molecule nanogels of controlled structure as a matrix for efficient artificial enzymes" *Angew. Chem. Int. Ed*. 45:2955- 2958

[21] Hernández-Barajas J., Hunkeler D. (1997) "Heterophase water-in-oil polymerization of acrylamide by a hybrid inverse-emulsion/inverse-microemulsion process" *Polymer* 38(22):5623-5641

[22] Wei S., Jakusch M., Mizaikoff B. (2006) "Capturing molecules with templated materials—Analysis and rational design of molecularly imprinted polymers" *Anal. Chim. Acta* 578 (2006) 50–58

[23] Yan H., Row K. H. (2006) "Characteristic and synthetic approach of molecularly imprinted polymer" *Int. J. Mol. Sci*. 7:155-178

[24] Lorenzo R. A., Carro A. M., Alvarez-Lorenzo C., Concheiro A. (2011) "To remove or not to remove? The challenge of extracting the template to make the cavities available in molecularly imprinted polymers (MIPs)" *Int. J. Mol. Sci*. 12:4327-4347

[25] Annamma K. M., Mathew B. (2011) "Design of 2,4-Dichlorophenoxyacetic Acid Imprinted Polymer with High Specificity and Selectivity" *Mater. Sci. Appl.* 2:131-140

[26]Liu Z., Cardosi M., Rodgers J., Lillie G., Simpson L. (2010) "Synthesis and study of copolymer of vinylferrocene, acrylamide and 2-(diethylamino)ethyl methacrylate as a polymeric mediator for electrochemical biosensors" *React. Funct. Polym.*70:715-725

[27] "NanoSight LM10 nanoparticle analysis system & NTA 1.5 analytical software – operating manual" (2008) *NanoSight Ltd* Doc No 001010151

[28] Filipe V., Hawe A., Jiskoot W. (2010) "Critical evaluation of nanoparticle tracking analysis (NTA) by NanoSight for the measurement of nanoparticles and protein aggregates" *Pharm. Res.* 27(5):796-810

[29] Mishchenko M. I., Travis L. D., Lacis A. A. (2002) "Scattering, absorption and emission of light by small particles"*Cambridge* ISBN 0 521 78252

[30] Long Y., Philip J. Y. N., Schllen K., Liu F., Ye L. (2010) "Insight into molecular imprinting in precipitation polymerization systems using solution NMR and dynamic light scattering" *J. Mol. Recognit*. 24:619-630

[31] "Zetasizer nano series-user manual" (2013) *Malvern* mano0485, issue 1.1

[32] Atkins P., De Paula J. (2014) "Physical Chemistry" *Oxford* ISBN 978 0 19 96740 3 p. 725

[33] Rostamizadeh K., Abdollahi H., Parsajoo C. (2013) "Synthesis, optimization, and characterization of molecularly imprinted nanoparticles" *Int. Nano Lett.* 3:20

[34] Jia X., Tan N., Cheng Y., Zhang W., Yan X., Li X. (2015) "Design, preparation, surface recognition properties, and characteristics of icariin molecularly imprinted polymers" *Cog. Chem.* 1: 1059597

[35] Cela-Pérez M.C., Lasagabáster-Latorre A., Abad-López M. J., López-Vilariño J. M., Gónzalez-Rodríguez M. V. (2013) "A study of competitive molecular interaction effects on imprinting of molecularly imprinted polymers" *Vibr. Spectrosc.* 65:74– 83

[36] Luliński P., Maciejewska D. (2009) "Examination of imprinting process with molsidomine as a template" *Molecules* 14:2212-2225

[37] Yu X., Yang Y., Lu S., Yao Q., Liu H., Li X., Yi P. (2011) "The fluorescence spectroscopic study on the interaction between imidazo[2,1-b]thiazole analogues and bovine serum albumin" *Spectrochim. Acta A* 83:322-328

[38] Lakowicz J. R. (2006) "Principles of Fluorescence Spectroscopy" *Springer*, Third Edition ISBN 978-0-387-46312-4

[39] Sarzehi S., Chamani J. (2010) "Investigation on the interaction between tamoxifen and human holo-transferrin: determination of the binding mechanism by fluorescence quenching, resonance light scattering and circular dichroism methods" *Int. J. Biol. Macromol.* 47:558–569

[40] Gao L., Li X., Zhang Q., Dai J., Wei X., Song Z.,Yan Y., Li C. (2014) "Molecularly imprinted polymer microspheres for optical measurement of ultra trace nonfluorescent cyhalothrin in honey" *Food Chem.* 156:1-6

[41] Boens N., Qin W., Basarić N., Hofkens J., Ameloot M., Pouget J., Lefèvre J. P., Valeur B., Gratton E., vande Ven M., Silva N. D. Jr, Engelborghs Y., Willaert K., Sillen A., Rumbles G., Phillips D., Visser A. J., van Hoek A., Lakowicz J. R., Malak H., Gryczynski I., Szabo A. G., Krajcarski D. T., Tamai N., Miura A. (2007) "Fluorescence lifetime standards for time and frequency domain fluorescence spectroscopy" *Anal. Chem*. 79(5):2137-2149

[42] Guzow K., Rzeska A., Mrozek J., Karolczak J., Majewski R., Szabelski M., Ossowski T., Wiczk W. (2005) "Photophysical properties of tyrosine and its simple derivatives in organic solvents studied by time-resolved fluorescence spectroscopy and global analysis" *Photochem. Photobiol.* 81(3):697-704

[43] Szabo A.G., Rayner D.M. (1980) "Fluorescence decay of tryptophan conformers in aqueous solution" *J. Am. Chem. Soc.* 102(2):554-563.

[44] Tommasini Martina (2013) "Sviluppo di polimeri ad imprinting molecolare per dispositivi di therapeutic drug monitoring" Masterly degree thesis, University of Trieste

[45] Sterling H. J., Prell J. S., Cassou C. A., Williams E. R. (2011) "Protein Conformation and Supercharging with DMSO from Aqueous Solution" *J. Am. Soc. Mass Spectrom*. 22:1178-1186

[46] Tjernberg A., Markova N., Griffiths W. J., Hallen D. (2006) "DMSO-related effects in protein characterization" *J. Biomol. Screen.* 11(2):131-137

[47] Cáceres M. I., Durán-Merás I., Soto N. E. O., López de Alba P. L., Martínez L-L. (2008) "Spectrofluorimetric determination of irinotecan in the presence of oxidant agents and metal ions" *Talanta* 74:1484-1491

[48] Syu M. J., Hsu T. J., Lin Z. K. (2010) "Synthesis of recognition matrix from 4-Methylamino-N-Allylnaphthal-Imide with fluorescent effect for the imprinting of creatinine" *Anal. Chem*. 82:8821–8829

[49] Konstantinova T. N., Miladinova P. M. (2008) "Synthesis and properties of some fluorescent 1,8-naphthalimide derivatives and their copolymers with methyl methacrylate" *J. Appli. Polym. Sci.* 111(4):1991-1998

[50] Wei S., Jakusch M., Mizaikoff B. (2006) "Capturing molecules with templated materials—Analysis and rational design of molecularly imprinted polymers" *Anal. Chim. Acta* 578:50–58

[51] Börje Sellergren (2000) "Imprinted Polymers with Memory for Small Molecules, Proteins, or Crystals" *Angew. Chem. Int*. Ed. 39(6):1031-1037

[52] May B., Poteau X., Yuan D., Brown R. G. (1999) "A study of a highly efficient resonance energy transfer between 7-N,N-diethylamino-4-methylcoumarin and 9-butyl-4-butylamino-1,8-naphthalimide" *Dyes Pigm.* 42:79-84

4. Results and Discussion:

A FRET-based MIP

4.1 Synthesis of a FRET-based MIP

Principles of FRET

In order to explore further possibilities to exploit MIP sensors, the Förster Resonance Energy Transfer (FRET) technique was employed to set up a competitive test for paclitaxel quantification. FRET is a photophysical phenomenon that involves the non-radiative transfer of excitation energy from an excited fluorophore called donor, after absorption of a higher–energy photon, to a ground state acceptor brought in close proximity. The energy transfer occurs through space by a dipole-dipole interaction without emission of photons. Moreover, in this process the donor and acceptor ground states are energetically coupled. After FRET the acceptor molecule is in an excited state, and it could undergo to different mechanisms depending on its nature. If the acceptor is a quencher, as DABCYL, the molecule returns in the ground state by a non-radioactive deactivation, resulting to a quenching of fluorescence. While if the acceptor is a fluorescent molecule, it returns to the ground state by fluorescence emission at a wavelength that is red shifted with respect that of the donor.[1]

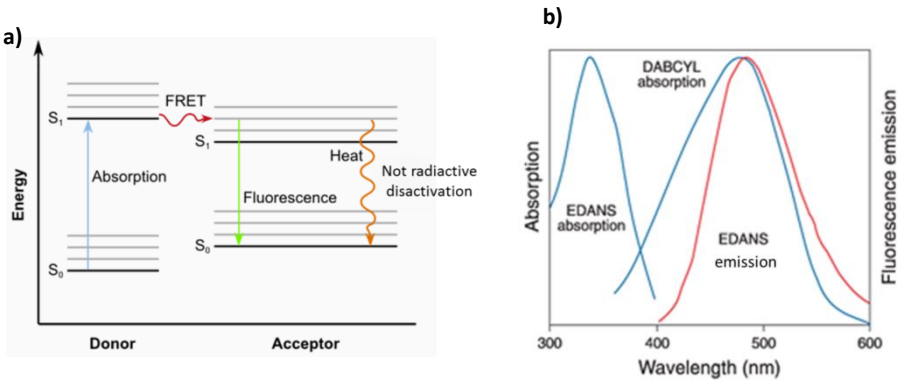

Figure 4.1: a) Jablonski diagram for FRET mechanism; b) absorption (blue) and emission (red) spectra of EDANS and DABCYL FRET pair[2]

The FRET efficiency depends on different factors:

- The spectral overlap integral (*I*) defined as a quantitative measure of the donor-acceptor spectral overlap over all wavelengths, as indicated by the following equation:

$$I = \int J(\lambda)d\lambda = \int PL_{D-corr}(\lambda) \cdot \lambda^4 \cdot \varepsilon_A(\lambda)d\lambda$$

Where $PL_{D\text{-}corr}$ is the normalized dimensionless spectrum of donor emission, ε_A is the acceptor absorption extinction coefficient and λ is the wavelength.
To have a high FRET efficiency, the donor emission spectrum must significantly overlap the absorption spectrum of the acceptor.

- The distance between FRET pairs, in fact the FRET efficiency (E) is inversely proportional to the sixth power of the distance between donor and acceptor molecules, as indicated by the following equation:

$$E = \frac{R_0^6}{R_0^6 + r^6}$$

Where r is the separation distance between donor and acceptor pair, while R_0 is the Förster distance corresponding to a rate of FRET (k_{DA}) equalling the rate of radiative decay ($k_{DA}=1/\tau_D$, where τ_D is the excited state radioactive lifetime of the donor). In fact:

$$k_{DA} = \left(\frac{1}{\tau_D}\right) \cdot \left(\frac{R_0}{r}\right)^6$$

And R_0 is calculated from the following equation:

$$R_0 = \left(\frac{9000(ln10)\kappa_p^2\, Q_D}{N_A 128\pi^5 n_D^4} I\right)^{1/6}$$

Where κ_p^2 depends on the relative orientation of the donor and acceptor dipoles, N_A is the Avogadro number, Q_D is the donor quantum yield and n_D is the relative index of the medium. Typically R_0 is between 20 and 100 Å. Therefore to have a FRET mechanism the distance between donor and acceptor must be between 1 nm and 10 nm.[3]

- Dipole-dipole interactions: the FRET efficiency depends also on the relative orientation of the donor and acceptor dipoles. In particular this efficiency is high when the donor emission dipole moment is parallel to the acceptor adsorption dipole moment.[4]

Synthesis of an EDANS Functional Monomer

5-((2-acryloylaminoethyl)amino)naphthalene-1-sulfonic acid (vinyl-EDANS, **10**) was selected as best functional monomer to obtain a fluorescent molecularly imprinted polymer whose fluorescence is quenched due to interaction with 4-([4-(Dimethylamino)phenyl]-azo)-benzoyl (DABCYL) by a Förster Resonance Energy Transfer (FRET) mechanism. Since DABCYL is also a red dye the obtained polymer will undergo to a change of both fluorescence intensity and color upon interaction with DABCYL.
The incorporation of EDANS into the polymeric matrix of the MIP requires the presence of an acryloyl-group in the molecule, able to polymerize with acrylamide and the crosslinker N,N'-ethylenebisacrylamide. Therefore vinyl-EDANS (**10**) was synthesized by coupling between EDANS and N-hydroxysuccinimidoyl acrylate (**9**) in water.[5] The reactant **9** was obtained by esterification of N-hydroxysuccinimmide with acryloyl chloride in dichloromethane with triethylamine.[6]

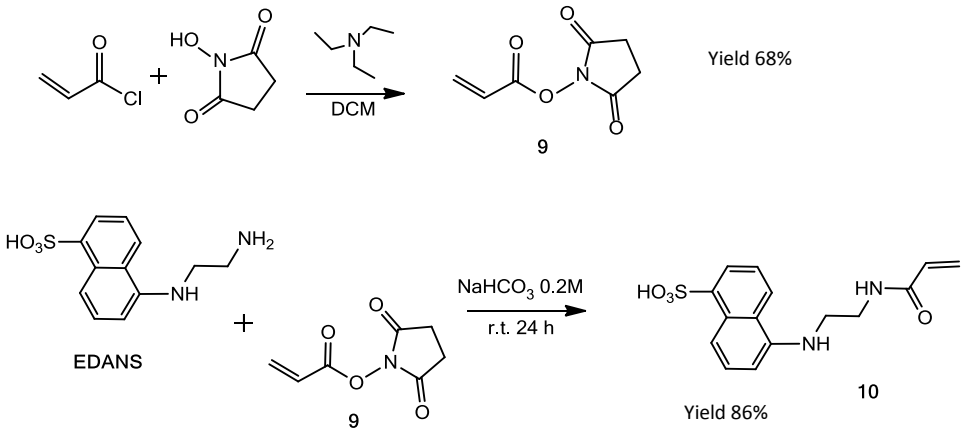

Scheme 4.1: synthesis of vinyl-EDANS

^{1}H-NMR Titration Study of Vinyl-EDANS with Paclitaxel

The study of interaction between the functional monomer and the drug was performed by ^{1}H-NMR titration of paclitaxel with increasing concentrations of vinyl-EDANS. As shown in Figure 4.2, the main variations of paclitaxel chemical sifts occurs due to hydrogen bonding with its amide group. Lower shifts were also observed on the adjacent CH2' and on protons of aromatic rings 2 and 3. Therefore the main interactions occur by both hydrogen bonds and π-staking involving the side chain of the

drug, probably because groups on the drug side chain are more accessible to vinyl-EDANS with respect the bacatinic nucleus of paclitaxel.

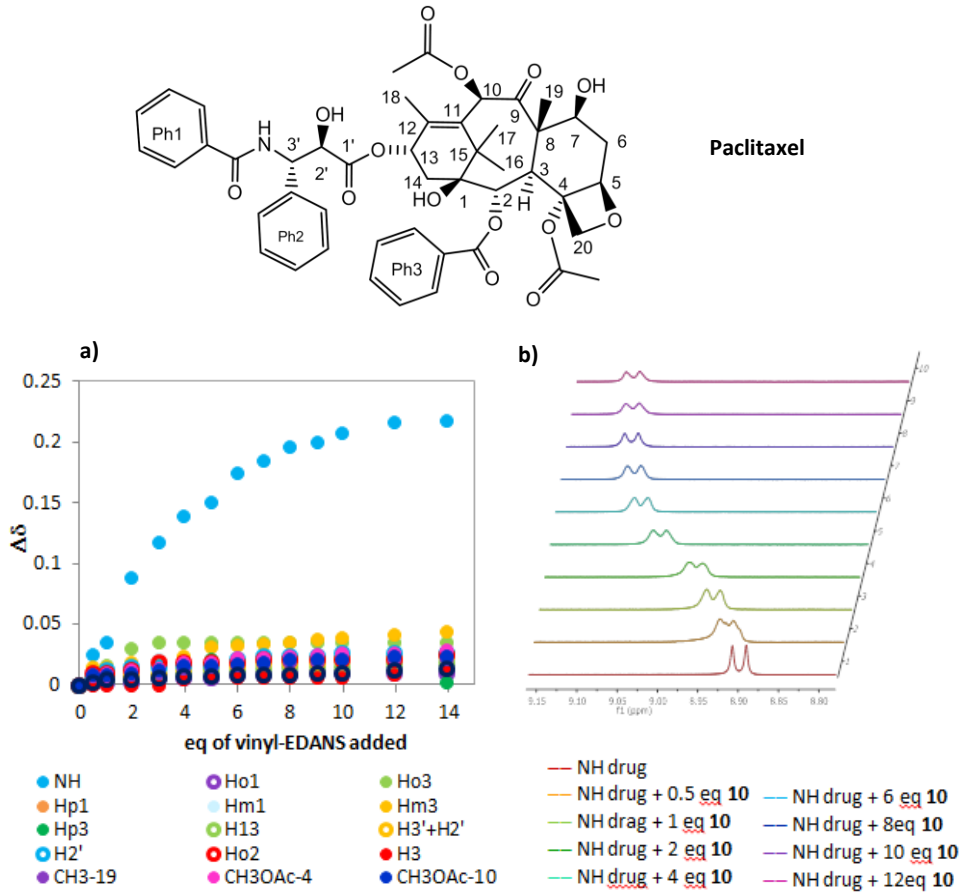

Figure 4.2: ^{1}H-NMR titration of paclitaxel with vinyl-EDANS: a) variation of protons chemical shifts; b) variation of the NH chemical shift

Synthesis of MIPs and NIPs Containing EDANS

Molecularly imprinted polymers containing EDANS (15% in mol) as functional monomer, acrylamide (15% in mol) as co-monomer and N,N'-ethylenebisacrylamide (70% in mol) were synthesized for paclitaxel and for irinotecan by high dilution radical polymerization in DMSO with the same procedure previously described for other MIPs synthesis. C_M was fixed at 1% w/w. The obtained yield is indicated in Table 4.1.

Polymer	Drug	Yield %
0.10	-	41%
3.10	Paclitaxel	59%
4.10	Irinotecan	48%

Table 4.1: yield of polymers containing EDANS

The size of the polymeric particles was analysed by Dynamic Laser Light Scattering. The analysis was performed in DMSO because it allows to solubilize these polymers, in fact it was also the porogen solvent used for their synthesis. The size distribution by volume of all MIPs and NIP shows particles of around 10 nm (Table 4.2), while the size distribution of intensity show also some particles of 100 nm even if the amount of these particles is very low since they are not visible in the size distribution by volume of NIP 0.10, while a small peak can be seen in the size distribution by volume of MIP 4.10 and MIP 3.10. As in the previous polymers the bigger particles are probably aggregates of nanoparticles.

Polymer	Size (nm)
0.10	11.32
3.10	13.39
4.10	12.35

Table 4.2: particles size measured in DMSO considering the size distribution by volume

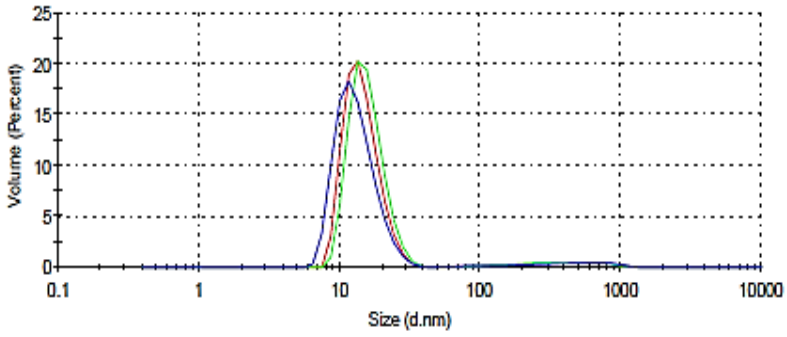

Figure 4.3: size distribution by volume of MIP 4.10. Three replicates

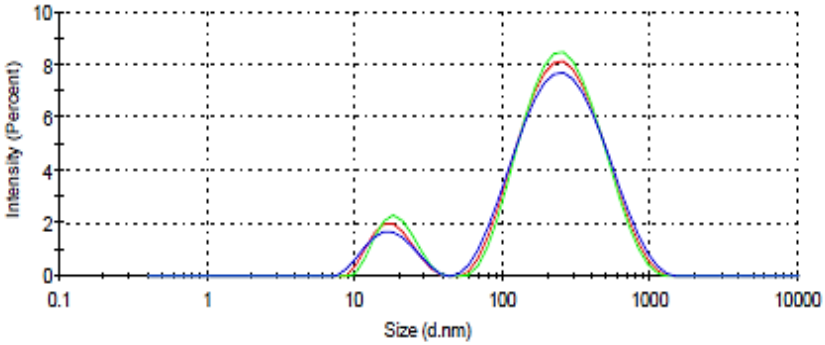

Figure **4.4**: size distribution by intensity of MIP 4.10. Three replicates

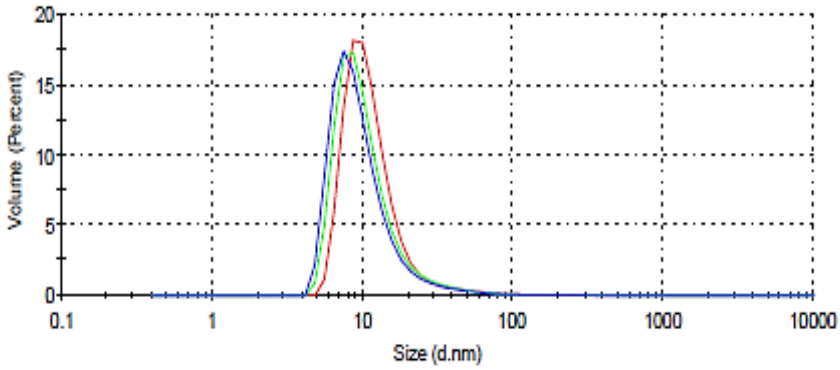

Figure 4.5: size distribution by volume of NIP 0.10. Three replicates

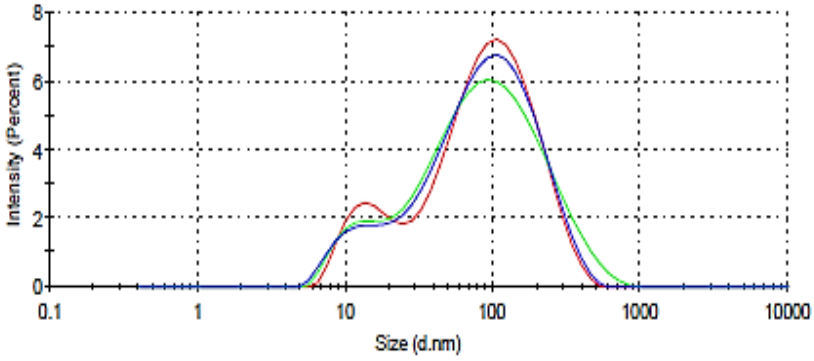

Figure 4.6: size distribution by intensity of NIP 0.10. Three replicates

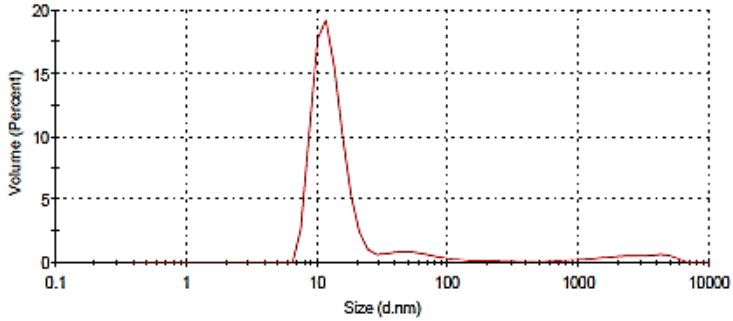

Figure 4.7: size distribution by volume of MIP 3.10

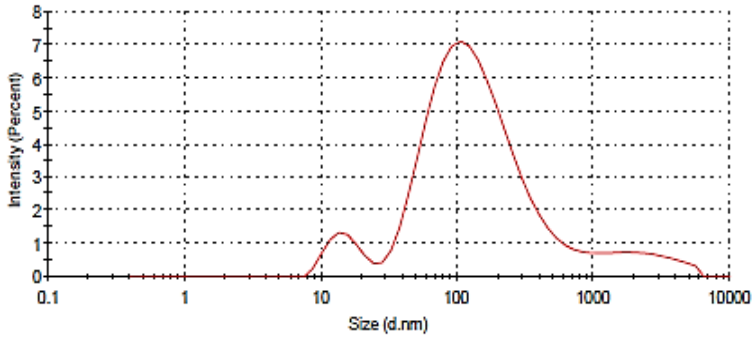

Figure 4.8: size distribution by intensity of MIP 3.10

The MIP particles are a slightly bigger than NIPs, probably because paclitaxel and irinotecan are relative large molecules, and during the imprinting process large cavities are likely created in the MIP leading to an increase of their size with respect to the non-imprinted polymer that contains only non-specific and superficial binding sites.

Quantification of EDANS into the Polymer

The amount of EDANS incorporated into the polymer was calculated by fluorescence spectroscopy. This is a useful technique because EDANS is the only fluorescent molecule in the polymer. Also since it is a high sensitive technique, it is possible to use low polymer concentrations and perform the test in PBS were the polymer is soluble only at low concentrations. A calibration curve of EDANS was obtained in PBS exciting at 335 nm end measuring the emission at 493 nm. Using this calibration curve, the amount of EDANS in 20 µg/mL, 40 µg/mL and 60 µg/mL MIP 3.10 and NIP 0.10 solutions in PBS (obtained from a batch solution in DMSO) was calculated. These polymers are in

fact soluble in PBS at low concentrations. This measurement was possible because EDANS is the only fluorescent molecule in the polymer.

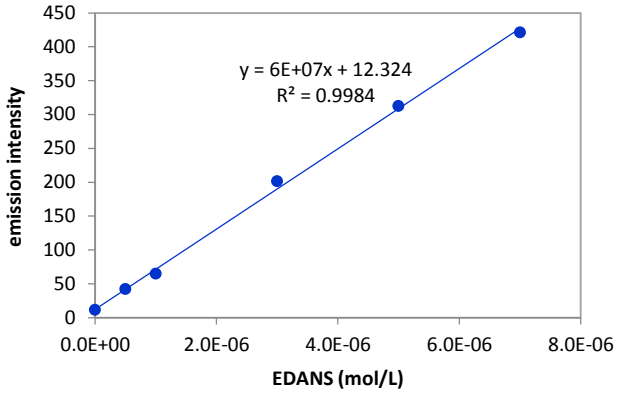

Figure 4.9: calibration curve of EDANS in PBS

Polymer	Polymer concentration (µg/mL)	Florescence intensity	Calculated EDANS concentration (mol/L)	Mean [EDANS] (mol/L) in 1 µg/mL of polymer	ng of EDANS in 1 µg of polymer
MIP 3.10	20	65.46	$8.96 \cdot 10^{-7}$	$4.51 \cdot 10^{-8}$	12.00
	40	110.61	$1.66 \cdot 10^{-6}$		
	60	186.25	$2.93 \cdot 10^{-6}$		
NIP 0.10	20	98.09	$1.45 \cdot 10^{-6}$	$7.45 \cdot 10^{-8}$	19.83
	40	180.33	$2.83 \cdot 10^{-6}$		
	60	297.5	$4.81 \cdot 10^{-6}$		

Table 4.3: amount of EDANS calculated into the MIP and NIP

The amount of EDANS found in MIP 3.10 is 60% than that in NIP. This result is also confirmed by UV measurements of MIP and NIP in DMSO: in fact in Figure 4.10 the absorbance of MIP 3.10 is higher than that of NIP 0.10.

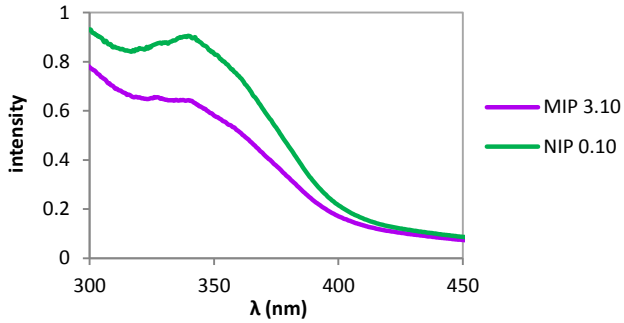

Figure 4.10: UV spectrum of 1 mg/mL MIP 3.10 and NIP 0.10 in DMSO

Rebinding Tests of Polymers Containing EDANS

The binding capability of MIP 3.10 and MIP 4.10 was investigated by rebinding tests and compared to the EDANS NIP. Tests with MIP 4.10 were performed in PBS to simulate pH and osmolality conditions similar to biological samples, and in citrate buffer to study the MIP binding capabilities when all irinotecan is in the closed lactone ring form.
Conversely, the rebinding test with MIP 3.10 was performed only in PBS with 8% of DMSO. The employment of DMSO allows to dissolve paclitaxel in aqueous solutions.
In Table 4.4 the amount of drug captured by polymers is reported taking into consideration that the MIPs have 40% of EDANS less than NIPs, as shown in the previous section.

Solvent	Polymer	Drug captured (nmol/mg of polymer)	Imprinting Factor
PBS	MIP 3.10	7.2	1.8
	MIP 4.10	6.0	1.1
Citrate buffer	MIP 4.10	3.5	2.2

Table 4.4: amount of target captured by MIP 3.10 and MIP 4.10 in different solvents, after 30 min of incubation, when the equilibrium was reached.

MIP 3.10 represents a good choice for the development of a FRET sensor, since it showed a higher binding capability than MIP 4.10 and also a good imprinting factor. Conversely the behaviour of MIP 4.10 is strongly dependent on the environment, in fact the polymer has a good binding specificity in acidic solutions but the number of captured molecules are half than that in PBS buffer.

4.2 Towards a FRET System

The MIPs containing EDANS can be used for the development of a fluorescence and colorimetric test based on the competition between the free drug and a labelled analogue of the drug covalently linked to DABCYL, for the binding into the polymer. Since DABCYL is a FRET quencher and a red dye, its interaction with EDANS will give both a quenching of polymer fluorescence and a red colour to the MIP. Therefore the drug concentration could be quantified by measuring variation of fluorescence and colour intensity of the polymer.

Synthesis of DABCYL-Paclitaxel

To develop a fluorescent and coloured test, the DABCYL dye was first covalently linked to paclitaxel to obtain a labelled drug.
The modification was done on the hydroxyl group at position 7 (Scheme 4.2) of paclitaxel since it is little involved in the interaction with the functional monomers, as observed by previous ^{1}H-NMR titrations. Moreover, a long spacer was added between paclitaxel and DABCYL to confer more flexibility to the labelled molecule and allow its binding inside the polymer. The spacer results from acylation of paclitaxel with succinic anhydride at hydroxyl 7, amidation of DABCYL at its carboxyl group, and convergent coupling of the two fragments. Several protection steps are required: paclitaxel contains three hydroxyl groups but only two are able to react with succinic anhydride, since hydroxyl 1 is a tertiary alcohol with high steric hindrance whose reactivity is very low. On the contrary, hydroxyl 2' is a secondary alcohol placed on the easily accessible side chain of the drug, therefore the reaction with succinic anhydride will be favoured. The group is also involved in the interactions with the functional monomers and it is important to maintain this functionality. To this aim the 2' hydroxyl was first protected with tert-butyl-dimethylsilyl chloride to avoid side reactions (yield 91%).[7] After this protection, the 2'-tert-butyl-dimethylsilyl-paclitaxel-7-hemisuccinate (**3c**) was obtained by esterification of hydroxyl 7 of paclitaxel with succinic anhydride in DMF in the presence of dimethylaminopiridine (DMAP) that acts as nucleophilic catalyst (yield 84%).[8] The ^{1}H-NMR spectrum of the resulting product **3c** showed the presence of aliphatic protons of the succinic linker at 2.61 ppm, the disappearance of the hydroxyl 7 proton signal at 2.45 ppm and the shift of proton 7 from 4.42 ppm to 5.62 ppm due to deshielding effect of the succinic ester.[9]

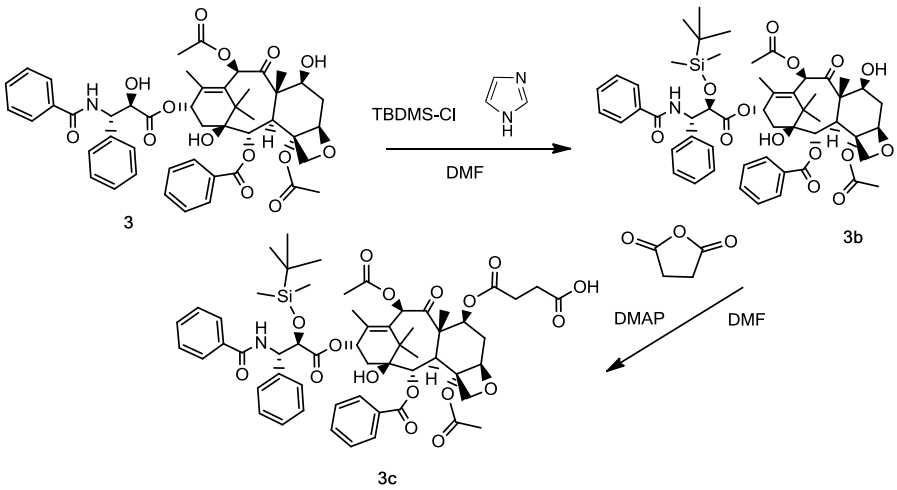

Scheme 4.2: synthesis of 2'-tert-Butyl-Dimethylsilyl-Paclitaxel-7-hemisuccinate (**3c**)

The product was then coupled with DABCYL-cadaverine (**12c**). The intermediate **12c** was obtained by a coupling reaction of hydroxysuccinimidyl-DABCYL (DABCYL-Osu) and Boc-cadaverine. The use of the commercially available reactant DABCYL-Osu allows to easily perform the coupling with Boc-cadaverine[10] in DMF and with the presence of N,N-diisopropyl-ethylamine (DIEA) base. The yield of the reaction was 90%. The following deprotection of Boc with TFA gives the intermediate **12c** (yield 93%).[11]

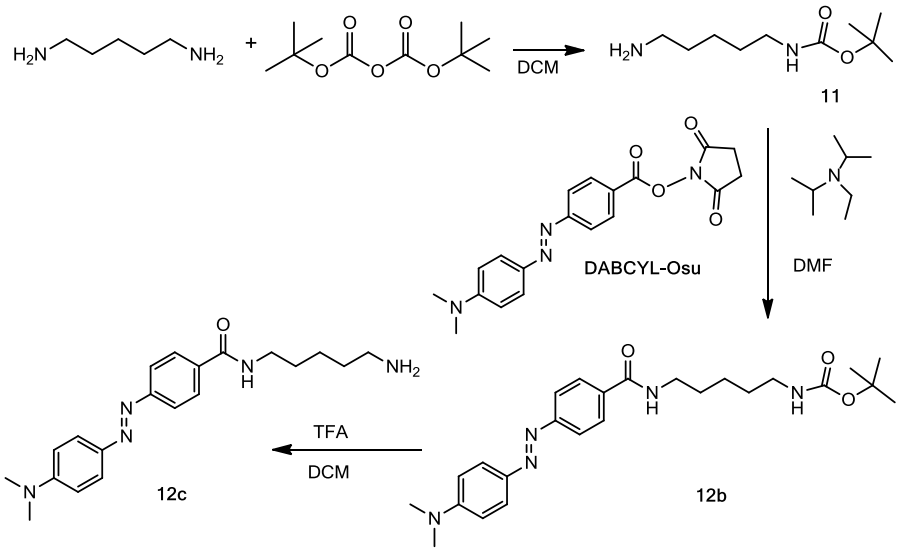

Scheme 4.3: synthesis of DABCYL-cadaverine (**12b**)

The coupling between **3c** and **12c** was obtained in anhydrous acetonitrile at 0°C with triethylamine after addition of HOBt and EDC-Cl (yield 65%). The resulting orange product (**3d**) was deprotected with HF/Py (30% pyridine in 70% HF) anhydrous solution at 0°C in pyridine leading to the final product **3e**[12] (yield 80%; total yield 40%)(Scheme 4.4).

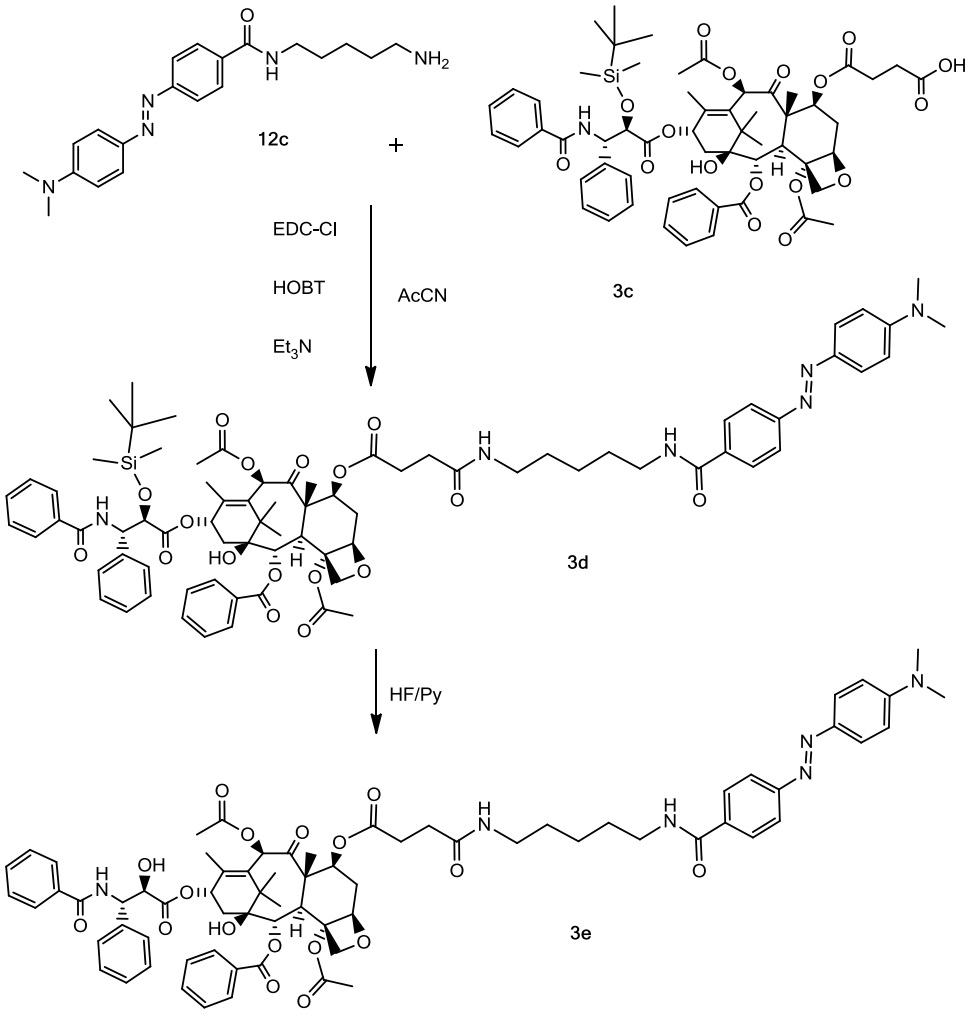

Scheme 4.4: coupling between **12c** and **3c** followed by removal of tert-butyldimethylsilyl group

Fluorescence Titrations of EDANS

The fluorescence properties of EDANS upon interaction with paclitaxel and the modified drug were first investigated by fluorescence titrations. This preliminary test was performed to verify the ability of DABCYL-paclitaxel (**3e**) at quenching EDANS and ensure that the EDANS fluorescence is not affected by paclitaxel interaction. A 3.9 µM EDANS solution in DMSO was titrated with increasing concentrations of paclitaxel or DABCYL-paclitaxel and the intensity at 455 nm, that corresponds to the maximum of emission peak, was measured after exciting at 335 nm. The EDANS molecule was used instead of vinyl-EDANS (**10**) because the vinyl-group could interfere on the fluorescence properties of EDANS.[13]

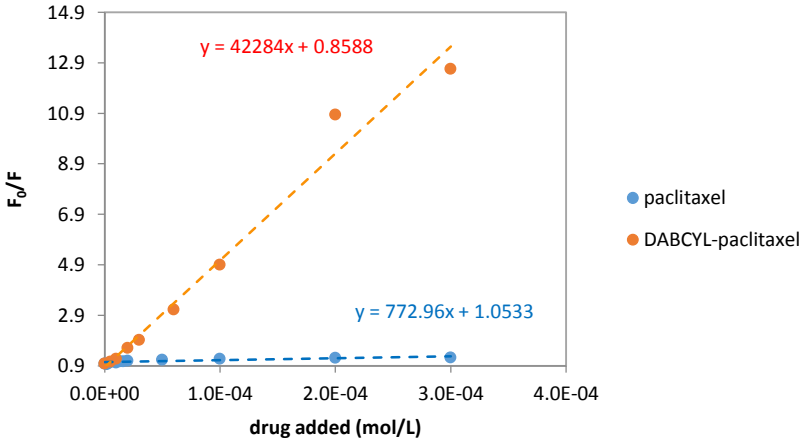

Figure 4.11: Stern Volmer plot obtained titrating EDANS with paclitaxel and with DABCYL-paclitaxel in DMSO

The Stern Volmer plots obtained by the titration with **3e** and with the free paclitaxel show a linear behavior in 2 µM - 300 µM range. As expected, the ratio F_0/F, that corresponds to EDANS quenching, increased rapidly upon interaction with **3e**, leading to a high slope in the plot. This behavior is due to FRET mechanism occurring between EDANS and DABCYL covalently linked to paclitaxel (**3e**). Conversely, a low quenching of EDANS was observed upon interaction with paclitaxel. Since a linear behaviour was observed within all the range of concentrations, it was possible to calculate the apparent Stern Volmer constants from the slope of Stern Volmer plot (Figure 20), while the apparent quenching constants were calculated by the obtained K_{SV} and the fluorescence lifetime of EDANS (12.7 ns)[14].

Molecule	K_{SV}^{app} [10^3 L·mol^{-1}]	k_q^{app} [10^{12} L·mol^{-1}·s^{-1}]
Paclitaxel	0.77	0.06
DABCYL-paclitaxel	42.28	3.33

Table 4.5: apparent Stern Volmer and quenching constants for paclitaxel and DABCYL-paclitaxel

The obtained values indicate also that a static quenching occurs with both paclitaxel and DABCYL-paclitaxel, in fact the quenching constants are higher than $1 \cdot 10^{10}$. The fluorescence quenching led to DABCY-paclitaxel interaction is largely higher than that of the free paclitaxel, indicating a correlation between the intensity of the quenching and the mechanism of interaction, since DABCYL is a FRET quencher of EDANS.

Fluorescence Titrations of Polymers

The ability of DABCYL-paclitaxel to quenching the EDANS fluorescence in the polymeric matrix by FRET mechanism was investigated with both MIP 3.10 and the non-imprinted EDANS polymer. The experiment was performed titrating the polymers with increasing amounts of DABCYL-paclitaxel in DMSO and measuring the polymer emission intensity at 455 nm after exciting at 335 nm. The emission was recorded after 30 min for each addition, to allow the diffusion of the modified-drug into the polymeric matrix.
As shown in the Stern Volmer plot of Figure 4.12 DABCY-paclitaxel was able to give a high quenching of MIP 3.10 fluorescence by a FRET mechanism, while the quenching with NIP 0.10 was considerably lower especially considering that the NIP has a higher number of EDANS molecules than MIP.

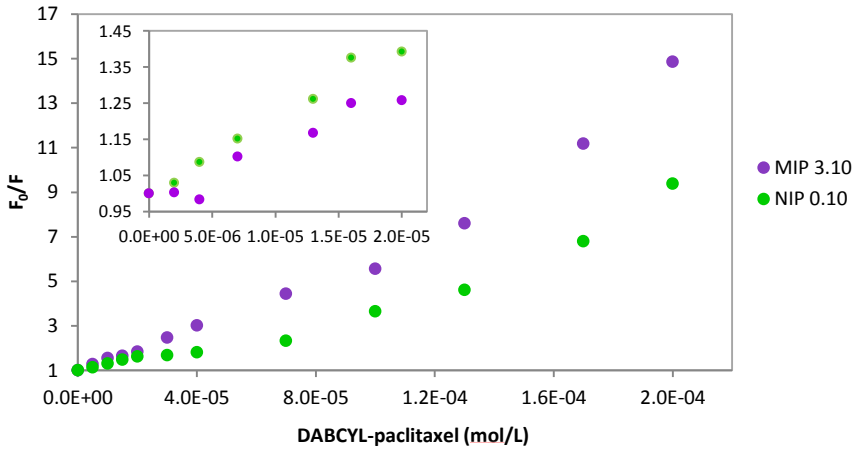

Figure 4.12: Stern Volmer plot of MIP and NIP emissions in DMSO with DABCYL-paclitaxel

The apparent polymer binding affinities were investigated by Stern Volmer analysis considering a range of concentrations similar to the paclitaxel values found in real samples of plasma. These values correspond to the low range of the Stern Volmer plot, between 2 µM and 20 µM. The calculated apparent Stern Volmer constants and quenching constants in this range are higher than that obtained titrating the free EDANS with DABCYL-paclitaxel, as expected in the presence of binding sites. The calculated apparent quenching constants reveal a static quenching for both MIP and NIP even if the binding affinity of NIP is half than that of MIP. This reveals a higher specificity of MIP with respect to NIP and a good efficiency of the imprinting process.

Polymer	K_{SV}^{app} $[10^3\ L \cdot mol^{-1}]$	k_q^{app} $[10^{12}\ L \cdot mol^{-1} \cdot s^{-1}]$
MIP 3.10	63.32	4.99
NIP 0.10	37.20	2.93

Table 4.6: apparent Stern Volmer and quenching constants of MIP and NIP

Competitive Test with MIP 3.10

The previous experiments showed a good capability of DABCYL-paclitaxel to quenching MIP 3.10 fluorescence and an increase quenching of MIP with respect NIP due to the imprinting process. Therefore the modified drug and MIP 3.10 can be used for the setup of a competitive test for paclitaxel quantification.

To this aim, the first approach consists in the evaluation of the ability of paclitaxel to displace the modified drug from the polymer binding sites, restoring the polymer fluorescence. MIP 3.10 was first saturated with DABCYL-paclitaxel leading to a fluorescence quenching. The addition of increasing amount of free paclitaxel should displace the DABCYL-paclitaxel from the binding sites leading to an increase of fluorescence. The test was performed using 30 µM concentration of DABCYL-paclitaxel to saturate 240 µg/mL MIP and, after 30 min necessary to allow the total incorporation of the dye into the polymer, increasing concentrations of paclitaxel were added. The intensity of fluorescence emission was measured after 30 min to allow the system to reach the equilibrium. In Figure 4.13 the drastic quenching of fluorescence measured after addition of 30 µM modified drug is shown. However the MIP fluorescence is not restored upon addition of free paclitaxel.

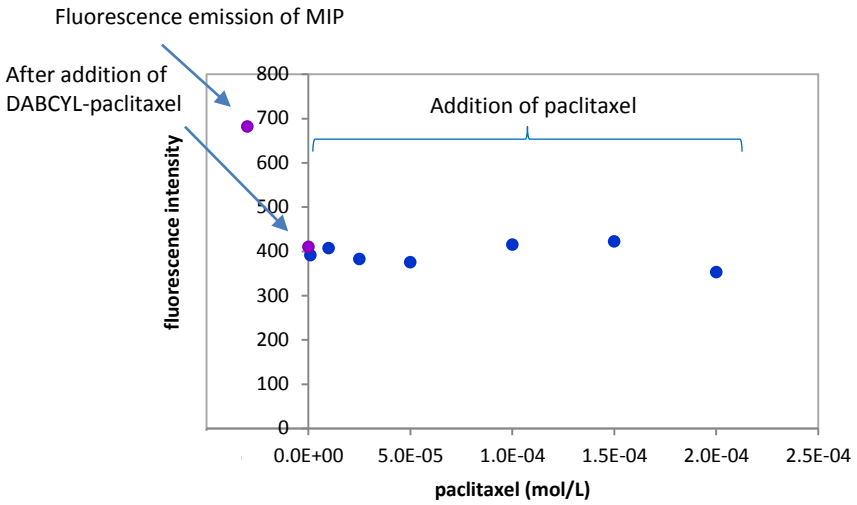

Figure 4.13: first attempt to set up a competitive test: DABCYL-paclitaxel (30μM) is not displaced by free paclitaxel

Probably this behaviour is due to the creation of a strong complex between the modified drug and EDANS into the polymer, preventing the dye displacement by free paclitaxel.

Reverse Competition Test with MIP 3.10

Considering the negative results of the previous experiment a second approach to develop the competitive test was followed. This approach consists of a reverse competition test. 240 μg/mL MIP in DMSO was first incubated with 50 μM paclitaxel for 30 min, and after titrated with increasing amounts of DABCYL-paclitaxel. The same experiment was repeated also in absence of free paclitaxel. Comparing the Stern Volmer plots of the two titrations, a decrease of the fluorescence quenching of MIP treated with paclitaxel was observed. Also the calculated apparent Stern Volmer and quenching constants indicated the tendency of MIP treated with paclitaxel to give a lower quenching of fluorescence upon addition of dye, with respect the untreated polymer (Table 4.7, Figure 4.14).

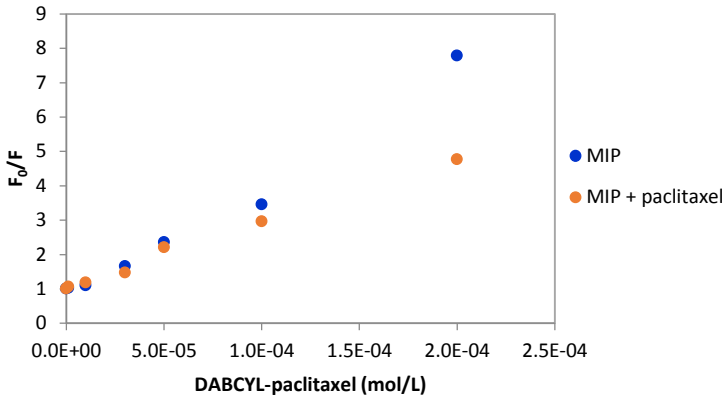

Figure 4.14: Stern Volmer plot obtained titrating MIP 3.10 with DABCYL-paclitaxel, before and after treatment with 50 µM paclitaxel.

Polymer	K_{SV}^{app} [10^3 L·mol^{-1}]	k_q^{app} [10^{12} L·mol^{-1}·s^{-1}]
MIP + paclitaxel	18.92	1.49
MIP	33.10	2.62

Table 4.7: apparent Stern Volmer and quenching constants obtained titrating MIP 3.10 with DABCYL-paclitaxel before and after treatment of 50 µM paclitaxel

A high difference of quenching between the MIP with and without paclitaxel was observed after 200 µM dye added, therefore this value was chosen to set up a calibration curve using the reverse competition test.

The calibration curve was obtained treating 240 µg/mL MIP solutions in DMSO with different concentrations of paclitaxel from 1 µM to 50 µM and adding 200 µM DABCYL-paclitaxel to each solution after 30 min. The fluorescence emission of MIP was measured before and after the dye addition. In Figure 4.15 the ratio between the fluorescence before addition of DABCYL-paclitaxel (F_0) and after addition of dye (F) is plotted in function of the paclitaxel concentration in the analysed samples.

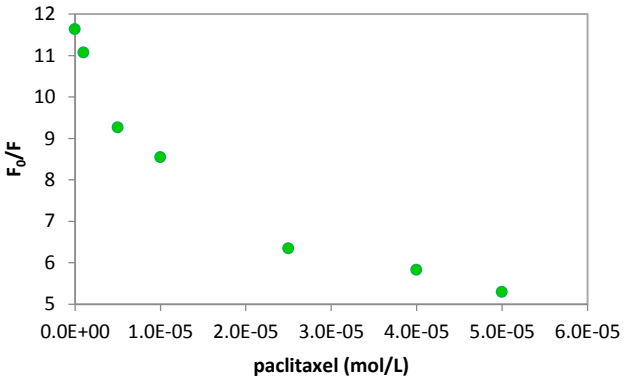

Figure 4.15: calibration curve of paclitaxel obtained by the reverse competitive test in DMSO

In the plot the fluorescence quenching of MIP decreases while increasing the paclitaxel concentration.

Moreover, the variation of quenching in this curve is quite high between 1 µM and 30 µM, and using this reverse competitive test it is possible to distinguish well between different paclitaxel concentrations within this range. The dynamic range of this curve is within the paclitaxel concentrations usually found in real samples, indicating that this reverse competitive test could be used to quantify paclitaxel in real plasma samples. However, this requires the capability of the system to perform also in plasma or methanol-plasma.

To investigate this possibility preliminary tests were performed titrating MIP 3.10 with increasing concentrations of DABCYL-paclitaxel in 3:1 methanol:plasma. The dye capability to quench the EDANS fluorescence in the polymer was maintained also in this solvent (Figure 4.16).

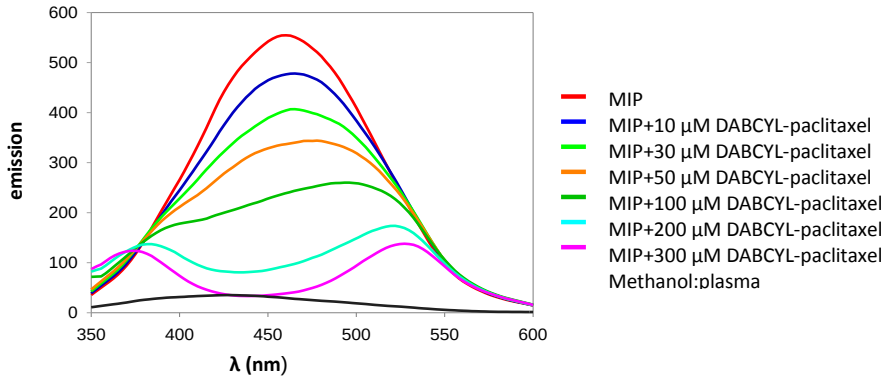

Figure 4.16: Fluorescence quenching of MIP 3.10 upon addition of DABCYL-paclitaxel in 3:1 methanol:plasma

The comparison of Stern Volmer plots corresponding to the MIP titrations with DABCYL-paclitaxel in DMSO and in 3.1 methanol:plasma mixture show in both cases a good fluorescence quenching. The FRET system with MIP 3.10 and DABCYL-paclitaxel represent a valid starting point for the development of a FRET sensor to rapidly quantify paclitaxel in plasma samples. Analysis of spiked plasma samples is currently being performed in order to setup an analytical methodology.

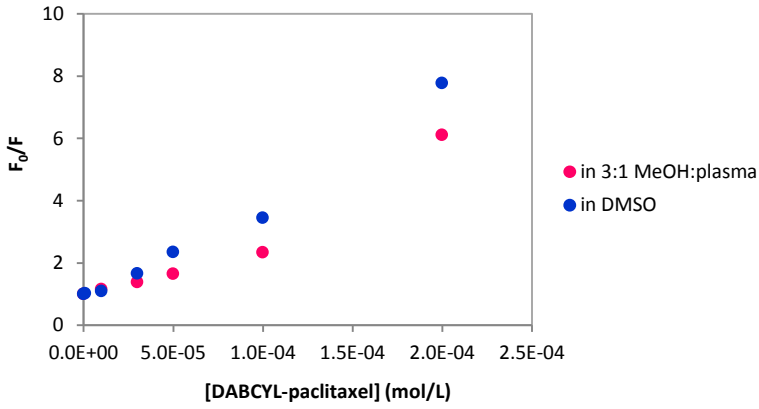

Figure 4.17: comparison of Stern Volmer plots corresponding to the MIP titrations with DABCYL-paclitaxel in DMSO and in 3.1 methanol:plasma mixture

[1] Reppy M. A. (2010) "Structure, emissive properties, and reporting abilities of conjugated polymers" Chapter of Advanced fluorescence reporters in chemistry and biology II *, Springer* Series on fluorescence vol. 9, pp 357-388

[2] Guo J., Xu C., Li X., Chen S. (2014) "A simple, rapid and sensitive FRET assay for botulinum neurotoxin serotype B detection" *Plos One* 9(12):1-15

[3] Clapp A. R., Medintz I. L., Mattoussi H. (2006) "Förster resonance energy transfer investigations using quantum-dot fluorophores" *Chem. Phys. Chem*. 7: 47–57

[4] Sahoo H. (2011) "Förster resonance energy transfer–a spectroscopic nanoruler: principle and applications" *J. Photochem. Photobiol. C:* 12:20–30

[5] Miyata T. (2010) "Stimulus-responsive gel with optical characteristic molecule introduced therein, external stimulus measuring apparatus making use of the same, and method of measuring external stimulus" *Patent* US20100063771 A1

[6] Allen A. L., Tan K. J., Fu H., Batteas J. D., Bergbreitter D. E. (2012) "Solute and temperature-responsive "smart" grafts and supported membranes formed by covalent layer-by-layer assembly" *Langmuir* 28(11):5237-42

[7] Gibson J. D., Khanal B. P., Zubarev E. R., (2007) "Paclitaxel-functionalized gold nanoparticles" *J. Am. Chem. Soc.* 129(37):11653-61

[8] Chmurny N., Hilton B. D., Brobst S., Look S. A., Witherup K. M., Beutler J. A. (1992) "^{1}H- and ^{13}C-NMR assignments for taxol, 7-epi-Taxol, and Cephalomannine Gwendolyn" *J. Nat. Prod*. 55 (4):414–423

[9] Belfiore Nicole (2013) "Sviluppo di polimeri ad imprinting molecolare per il therapeutic drug monitoring del tassolo" Masterly degree thesis, University of Trieste

[10] Fontanive G. (2010) "Libraries of short receptor peptides and antibodies for the recognition of small organic molecules" www.openstarts.units.it/dspace/handle/10077/3612

[11] Hu M., Li L., Wu H., Su Y., Yang P. Y., Uttamchandani M., Xu Q. H., Yao S. Q. (2011) "One- and two-photon imaging of enzymatic activities in live cells with fluorescently quenched activity-based probes (qABPs)" *J. Am. Chem. Soc*. 133 (31):12009–12020

[12] Rice A., Liu Y., Michaelis M. L., Himes R. H., Georg G. I., Audus K. L. (2005) "Chemical modification of paclitaxel (Taxol) reduces P-glycoprotein interactions and increases permeation across the blood-brain barrier in vitro and in situ" *J. Med. Chem*. 48(3):832-8

[13] Cespugli Marco (2014) "Polimeri ad imprinting molecolare per il rilevamento di antitumorali mediante tecniche fluorimetriche e spettrometria di massa" Masterly degree thesis, University of Trieste

[14] Peterson K. J., Peterson K. C., Muretta J. M., Higgins S. E., Gillispie G. D., Thomas D. D. (2014) "Fluorescence lifetime plate reader: Resolution and precision meet high-throughput" *Rev. Sci. Instrum.* 85:113101

5. Results and Discussion:

A Colorimetric System

Part of this PhD project was focused on the development of a colorimetric sensor able to easily quantify irinotecan from plasma samples. This project was developed at Queen Mary University of London, in the research group of Prof. Marina Resmini during a six months secondment. In order to obtain a colorimetric sensor based on molecularly imprinted polymers, two different approaches can be followed if the target is not a strongly coloured molecule. The first approach consists of the employment of a coloured functional monomer in order to obtain a coloured polymer that has to change its colour upon interaction with the target. However, since the majority of dyes changes colour upon their protonation or de-protonation, the target molecule must be a strong acid or base. Otherwise, it is possible to develop a colorimetric test by a dye displacement technique, which is based on the competition between the drug and the dye for binding inside the polymer. This approach does not require a particularly property of the target, but only a higher affinity of the imprinted polymer for the analyte than for the dye. Colorimetric tests for analyte quantification based on a dye-displacement technique have been already developed using molecularly imprinted polymers.[1]

Since irinotecan is not a strongly coloured molecule, the dye displacement technique represents the easiest method to obtain a colorimetric test for the quantification of this drug.

5.1 Finding the Best Functional Monomer: ^{1}H-NMR Titrations

The development of a dye displacement test requires first the synthesis of a highly specific molecularly imprinted polymer for irinotecan. To this aim, different functional monomers were evaluated according to the interactions that they could make with the target molecule. 2-acrylamido-2-metylpropane sulfonic acid (AMPS, **17**) (scheme 5.1) was chosen since it is a strong acid able to protonate free base irinotecan giving an ion pair, and also to make hydrogen bonds with the drug. Furthermore this functional monomer has been widely used to obtain highly soluble molecularly imprinted polymers exploited for the quantification of serotonin,[2] biotin[3] and D-phenylalanine.[4]

The binding affinity of AMPS for irinotecan was also compared to that of 4-vinyl benzene sulfonate (4-VBS, **18**) and of acrylic acid (**19**) for the same drug. Acrylic acid is a common functional monomer used for the synthesis of imprinted polymers and is able to make both hydrogen bonds and ion interactions with the target molecule, 4-vinyl benzene sulfonate can make ion interactions with the protonated piperidine moiety of protonated irinotecan and π-staking interactions with the drug aromatic rings. 4-vinyl benzene sulfonate has been widely used for the synthesis of ion exchange membranes[5] or nanoparticles[6].

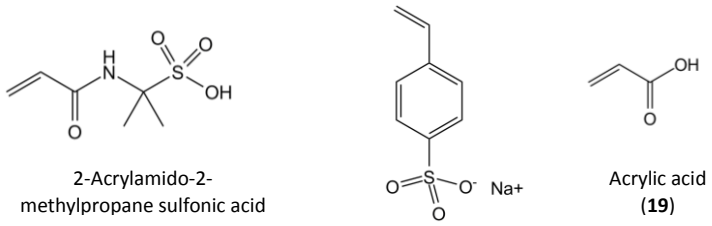

Scheme 5.1: functional monomers

In order to find the functional monomer able to best interact with irinotecan, ^{1}H-NMR titrations of protonated drug with increasing amounts of functional monomers were performed in different solvents. The force of interactions, in fact, could be dependent on the solvent in which the titration is performed.

In Table 5.1 the variations of chemical shift of each proton of protonated irinotecan that best interact with the functional monomers are reported. As expected, 4-VBS makes π-staking interactions with the aromatic rings of irinotecan, protons 7, 8 and 10, giving a small variation of chemical shift, larger shifts were observed due the interaction with the piperidine group of the drug, mostly with the NH and the adjacent protons 20 and 22. Conversely, acrylic acid made only hydrogen bonds with the irinotecan NH group and protons 24, 28 of the piperidine group.

The variation of chemical shifts due to the creation of hydrogen bonds between the two molecules is also favoured in non-polar solvents, like deuterated acetone, DMF and chloroform, as observed from the entity of shifts obtained from the titrations with 4-VBS and with acrylic acid in different solvents.

The interaction of irinotecan with AMPS was stronger than with other functional monomers. In fact a high variation of chemical shift was observed for protons of the piperidine group and the NH group, and also for protons 8 and 10 probably due to hydrophobic interactions or hydrogen bonds with the near carbamate group of the drug.

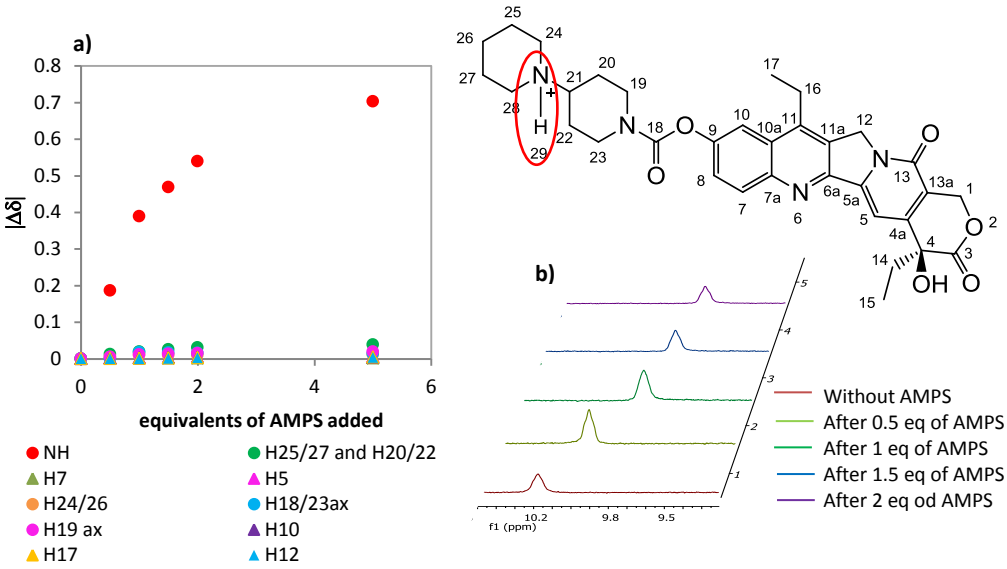

Figure 5.1: a) variation of protons chemical shifts of irinotecan-HCl upon interaction with AMPS; b) shifts of NH of irinotecan in DMSO-d_6

Functional monomer	Solvent	Δδ H of di-piperidine group after 5eq of functional monomer added				Δδ H of aromatic rings after 5eq of functional monomer added		
		H 24/26	H20/22	H23/19	NH	H8	7	H10
4-VBS	DMSO-d6	0	0.0336	0	0.3017	0.00165	0.00345	0.00055
	MeOD	0	0	0.03785		0.0105	0.03015	0.0136
	Acetone+ 40% DMF-d7	0.0453	0.0242				0.0142	
	D2O	0	0	0		0.0236	0.0172	
	DMF-d7	0	0.0434	0	0	0.0028	0.0028	0.0028
acrylic acid	DMSO-d6	0	0	0	0	0	0	0
	MeOD	0.0059	0	0		0.0008	0.0013	0.00085
	CDCl3 + 6% AcCN-d3	0.0177	0	0	0.2146		0.01025	
AMPS	DMSO-d6	0.0114	0.03885	0.0191	0.7032	0	0.0017	0.0037

Table 5.1: variation of proton chemical shifts of irinotecan due to the addition of 5 equivalents of AMPS in different solvents

To further improve the interactions between the functional monomers and the drug, the titrations were repeated also with free base irinotecan. Irinotecan hydrochloride was first neutralized by NaOH and extracted in DCM to obtain free base irinotecan with a good yield (91%). The product was titrated with increasing amounts of acrylic acid and of AMPSA. In both the titrations the variation of protons chemical shifts of the piperidine group became larger with respect than with protonated irinotecan.
Moreover, the titration curves obtained from the shifts of these protons upon addition of AMPS, reach the plateau after only 1 equivalent added, indicating that a strong interaction occurs. This interaction consists of the proton transfer from the sulfonic acid group of AMPS to the piperidine group of free base irinotecan, in fact the appearance of the NH signal of irinotecan salt was also observed during the titration.

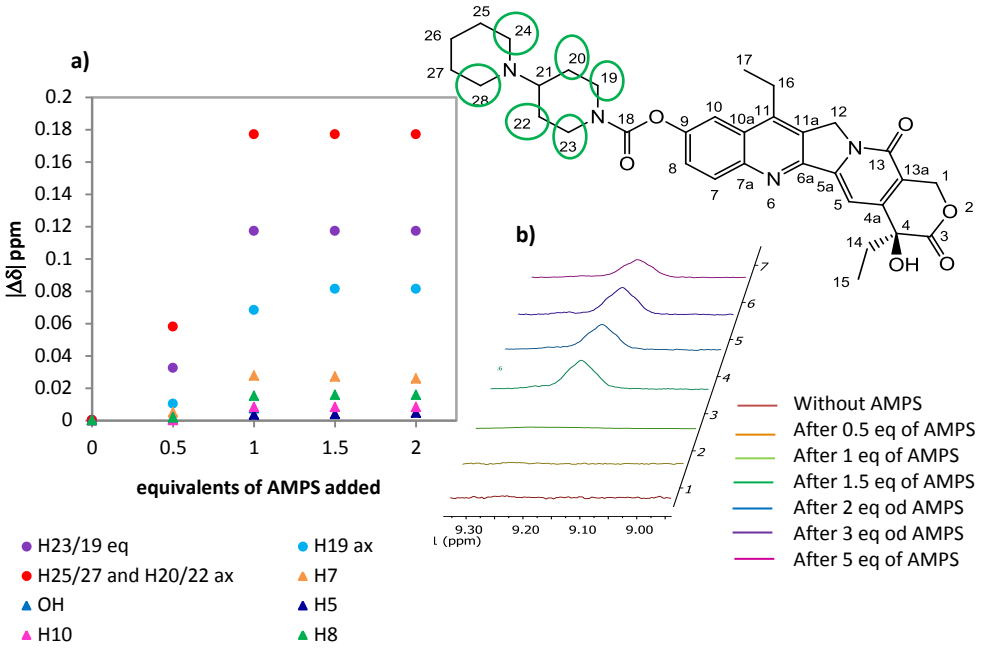

Figure 5.2:a) variation of proton chemical shift of free base irinotecan upon interaction with AMPS;
b) appearance of NH peak upon addition of AMPS

Functional monomer	Solvent	Δδ H of di-piperidine group after 5eq of functional monomer added			Δδ H of aromatic rings after 5eq of functional monomer added		
		H 24/26	H20/22	H23/19	H8	H7	H10
acrylic acid	$CDCl_3$	0.5367	0.23685	0.0542	0.0085	0.0164	0.0083
	CD_2Cl_2	0.5758	0.3333	0.108		0.0239	0.0105
AMPS	DMSO-d6		0.1768	0.11055	0.01565	0.0214	0.0084

Table 5.2: variation of proton chemical shifts of free base irinotecan upon interaction with 5 equivalents of AMPS

Therefore AMPS was chosen to obtain a highly selective molecularly imprinted polymer for irinotecan. Moreover, since AMPS is a strong acid with a pKa of 1.9,[7,8] it could protonate the aniline yellow dye (pKa of 2.28)[9] giving a change of colour from yellow to red. The interaction between aniline yellow and sulfonate salts is already reported in literature.[10] So a molecularly imprinted polymer containing AMPS and the aniline yellow dye could be used to set up a colorimetric test where the amount of drug captured by the polymer is quantified observing the colour of the sample.

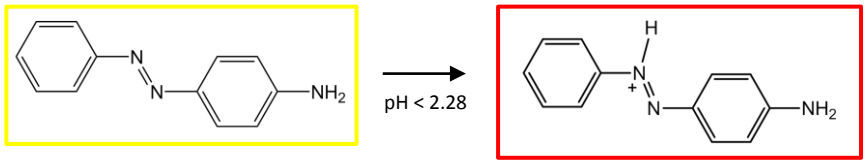

4-aminoazobenzene (Aniline yellow) pKa = 2.28

Scheme 5.2: aniline yellow dye: change of colour from yellow to red in acidic conditions

5.2 Synthesis of Molecularly Imprinted Polymers for Irinotecan

Molecularly imprinted polymers containing different amounts of AMPS, acrylamide or N-isopropylacrylamide as co-monomer and N,N'-methylenebisacrylamide as crosslinker were synthesized in DMSO. The use of N-isopropylacrylamide allows to increase the polymer solubility in water[11, 12] even if it is already improved with respect the previous polymers thanks to AMPS functional monomer. The choice of the amount of AIBN was

fundamental to obtain a good yield of polymerization. As first approach polymers were synthesized using only 1% of radical initiator, however very low yields were observed in particular for the imprinted polymers. Therefore the amount of AIBN was increased to 5% leading to a good yield of polymerization for both MIPs and NIPs. Finally the C_M was fixed at 0.5% in weight respect to the weight of DMSO to obtain soluble nanoparticles and avoid aggregation.
In table 5.3 the composition and yield of MIPs and NIPs containing AMPS is shown.

Polymer	Irinotecan [mg]	Functional monomer	Co-monomer	Cross-linker	AIBN	Solvent of dialysis	Yield
0.0	-	-	Acrylamide 30%	MBA 70%	1%	H_2O+HCl pH=2	95%
0.15a	-	AMPS 10%	Acrylamide 20%	MBA 70%	1%	1) MeOH: AcCOOH 2) H_2O	43%
0.15b	-	AMPS 5%	Acrylamide 25%	MBA 70%	1%	1) MeOH: AcCOOH 2) H_2O	95%
0.15c	-	AMPS 10%	Acrylamide 20%	MBA 70%	5%	1) MeOH AcCOOH 2) H_2O+HCl pH=2	88%
0.15d	-	AMPS 5%	Acrylamide 25%	MBA 70%	5%	1) MeOH AcCOOH 2) H_2O+HCl pH=2	61%
0.15e	-	AMPS 10%	NIPAM 20%	MBA 70%	5%	1) MeOH AcCOOH 2) H_2O+HCl pH=2	91%
4.15a	16.2	AMPS 10%	Acrylamide 20%	MBA 70%	1%	1) MeOH: AcCOOH 2) H_2O	18%
4.15b	7.4	AMPS 5%	Acrylamide 25%	MBA 70%	1%	1) MeOH:AcCOOH 2) H_2O	1%
4.15c	15.0	AMPS 10%	Acrylamide 20%	MBA 70%	5%	1) MeOH AcCOOH 2) H_2O+HCl pH=2	75%
4.15d	13.2	AMPS 5%	Acrylamide 25%	MBA 70%	5%	1) MeOH AcCOOH 2) H_2O+HCl pH=2	50%
4.15e	15.0	AMPS 10%	NIPAM 20%	MBA 70%	5%	1) MeOH AcCOOH 2) H_2O+HCl pH=2	89%

Table 5.3: polymer composition and yield

After synthesis, the polymerization mixture was dialyzed to remove both side products and the template molecule. First polymers were dialyzed in methanol:acetic acid mixture that is necessary to remove irinotecan from the polymeric matrix, and then in water. However the sulfonic acid group dissociates at neutral pH in water. Therefore, since the retention of the acidic functionality in the polymer is necessary to perform the colorimetric test, the polymer was further dialyzed in acidic water. The pH of water was kept at 2 because this is the lower pH supported by the dialysis membrane; at this pH the sulfonate groups of the polymer are protonated, since their pKa increases with respect the free functional monomer.[13] In fact the polymeric matrix around the sulfonic groups decreases the polarity of their environment leading to an increase of the sulfonic acid pKa.

The removal of irinotecan from the polymeric matrix was difficult since highly specific binding sites were created. First attempts were performed dialyzing only with methanol and after in water but the majority of template remained inside the polymer. Therefore different mixtures of methanol:acetic acid or methanol:TFA were tested on MIP 4.15a. After synthesis, 2.3 mL of the polymerization mixture in DMSO were dialyzed only in water as reference, the remaining solution was divided in four samples. The first one was 50% diluted with a 7:3 methanol:acetic acid mixture, stirred overnight and then dialyzed in water with 10% of 7:3 methanol:acetic acid mixture (washing n°1). The second sample was directly dialyzed in 7:3 methanol:acetic acid mixture changing the mixture twice (washing n°2). The third sample was dialyzed in 7:3 methanol:TFA mixture (washing n°3) and finally the last one was dialyzed in 6:4 methanol:acetic acid mixture changing the mixture twice (washing n°4). After each washing step, all samples were dialyzed in water and freeze-dried. The obtained MIPs were analysed by UV-visible spectroscopy and compared to the MIP dialyzed only in water. The UV absorbance of MIP solutions in DMSO was measured at 363 nm, the irinotecan characteristic absorption. The amount of drug still inside the polymer was calculated from the measured absorption using a calibration curve of irinotecan in DMSO.

As shown in Figure 5.3 the best removal of template was achieved with 6:4 methanol:acetic acid mixture. Therefore this mixture was used to wash all imprinted polymers until complete removal of the drug.

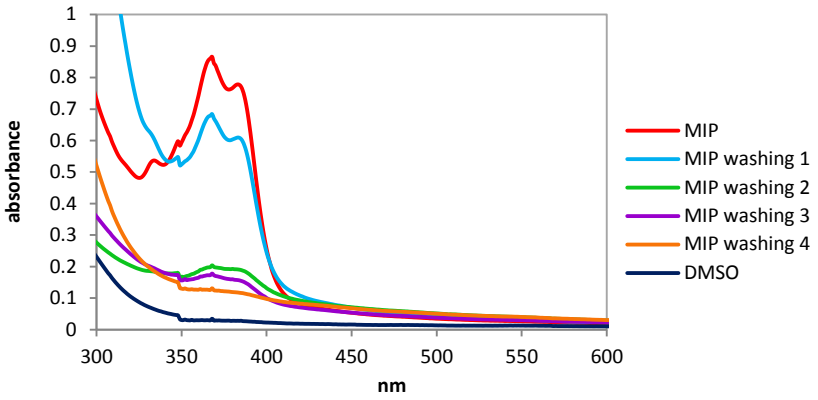

Figure 5.3: comparison between the UV spectra of 0.125 mg/mL MIP 4.15a solutions in DMSO after different washing steps.

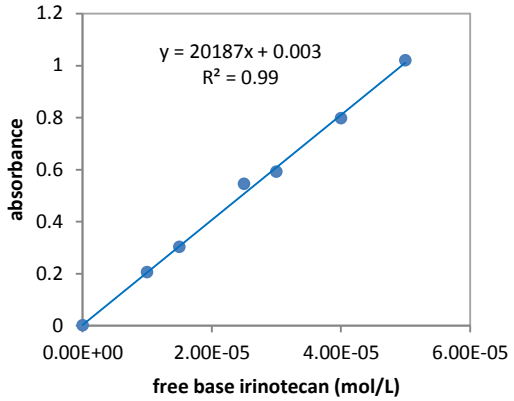

Figure 5.4: calibration curve of free base irinotecan in DMSO

n° washing	nmol irinotecan/mg MIP
0	345
1	242
2	63
3	50
4	35

Table 5.4: amount of irinotecan in the MIP, calculated by the calibration curve

5.3 MIP Characterization

Dynamic Laser Light Scattering

The particle size of the polymers dissolved in water solutions were measured by DLLS. All the solutions showed the presence of a majority of particles of about 10 nm size, and a low number of bigger particles that probably corresponds to aggregates of nanoparticles. The polymer solubility was increased with respect the polymers previously synthesized, thanks to the use of AMPS functional monomer, nevertheless the tendency to aggregate occurs also in these polymers.
Some measurements were also performed with polymers in DMSO in the attempt to decrease the number of aggregates. However, also in this case some aggregates were

observed while the dimensions of the majority of particles were around 10 nm as observed in water.

Finally, the presence of irinotecan in the polymerization mixture of MIP affects also the particle size, in fact the majority of imprinted polymers are smaller than the respective non imprinted polymer.

5.5a

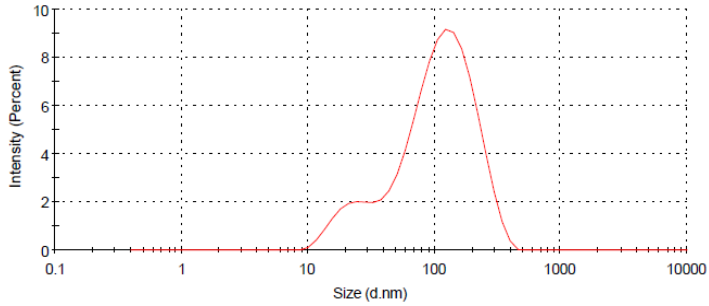

5.5b

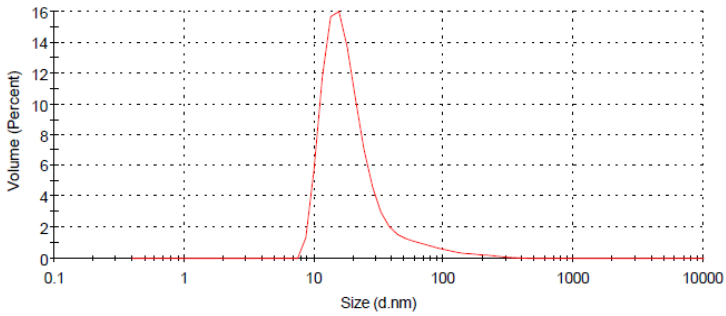

5.5c

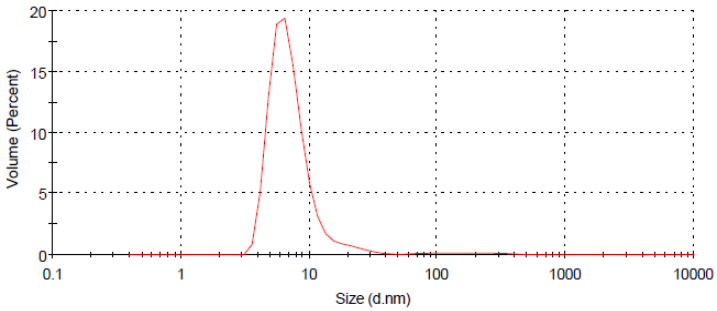

5.5d

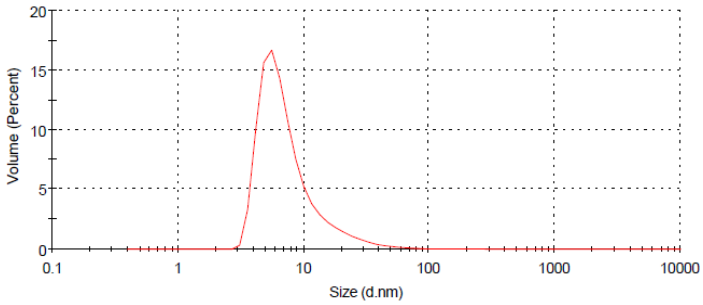

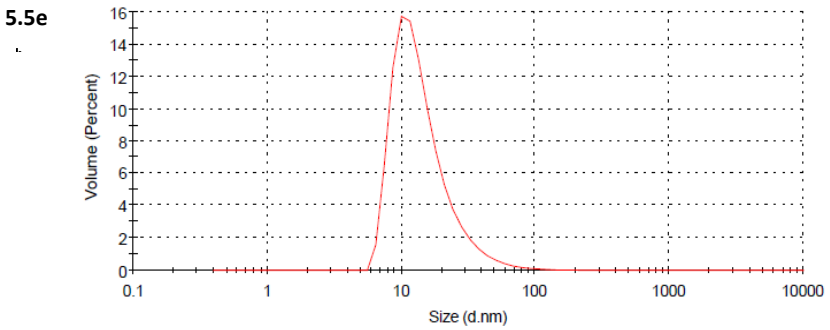

Figure 5.5: measurements by DLLS: a) size distribution by intensity of NIP 0.15c, b) size distribution by volume of NIP 0.15c, c) size distribution by volume of MIP 4.15c, d) size distribution by volume of MIP 4.15e, e) size distribution by volume of NIP 0.15e

Solvent	Polymer	Size (nm)
water	4.15d	10.19
	0.15d	15.57
	4.15c	7.53
	0.15c	15.14
	4.15e	6.21
	0.15e	12.84
DMSO	0.15c	14.48
	4.15e	10.21
	0.15e	12.10

Table 5.5:polymer size obtained from the size distribution by volume, in water and in DMSO

Z-potential

The zeta potential of nanoparticles was measured to verify the incorporation of the sulfonic acid groups inside the polymeric matrix. In fact these groups dissociate in water giving negative charges in the polymer.

When a charged particle moves in solution there is a thin layer of counter ions, called Stern layer,[14] that is close to the particle and moves with it, while increasing the distance from the particle, the charges are less firmly attached to the surface and does not move with the particle, leading to a diffuse layer. The zeta potential is the potential measured at the boundary between the Stern layer and the diffuse layer.[15] This boundary is called slipping plane. In practice, the zeta potential is calculated form the

Henry equation after measuring the electrophoretic motility that corresponds to the measure of particles velocity during their movement towards the electrode of opposite charge. This velocity was obtained measuring the fluctuating intensity of light scattered by the particles during their movement to the electrode of opposite charge. The rate of the fluctuations is proportional to the particles velocity. The Henry equation is:

$$U_E = \frac{2\varepsilon z f(K_a)}{3\eta}$$

Where *z* is zeta potential, U_E is the electrophoretic motility, ε is the dielectric constant and η is the viscosity and $f(K_a)$ is the Henry function.[16]

The zeta potential is usually measured to verify also the stability of particles suspension, in fact values more positive than +30 mV or more negative than -30 mV are associated to stable suspensions. If the particles have intermediate values between -30 mV and +30 mV of zeta potential, there is no enough force to allow the repulsion of particles having the same charge, therefore they tend to aggregate.[17]

The zeta potential of all MIPs and NIPs synthesized is negative and the values between -24 mV and -17 mV indicate that the polymer suspensions are not highly stables. This result is consistent with the presence of aggregates observed by DLLS measurements.

Polymer	mV
4.15d	-21.40
0.15d	-20.85
4.15c	-19.97
0.15c	-24.45
4.15e	-17.35
0.15e	-17.4

Table 5.6: zeta potential of polymers in water

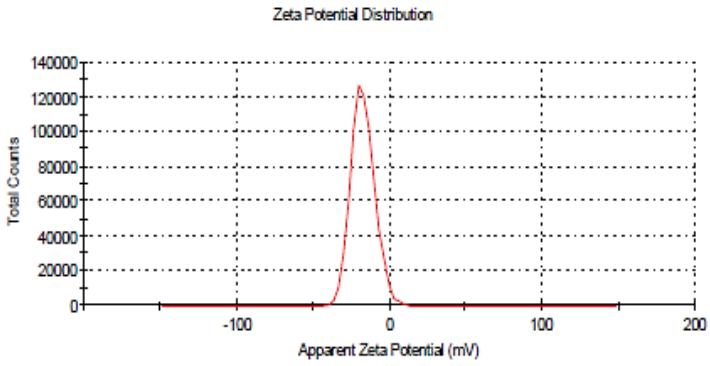

Figure5.6: zeta potential of NIP 0.15e in water

IR Spectroscopy of Polymers

The incorporation of AMPS in the polymeric matrix was also evaluated by IR spectroscopy, and the characteristic bands corresponding to the asymmetric stretching of S=O bond between 1180 cm^{-1} and 1200 cm^{-1} and the band at 1038 cm^{-1} of symmetric stretching of S=O was observed in all polymers. [18, 19, 20]

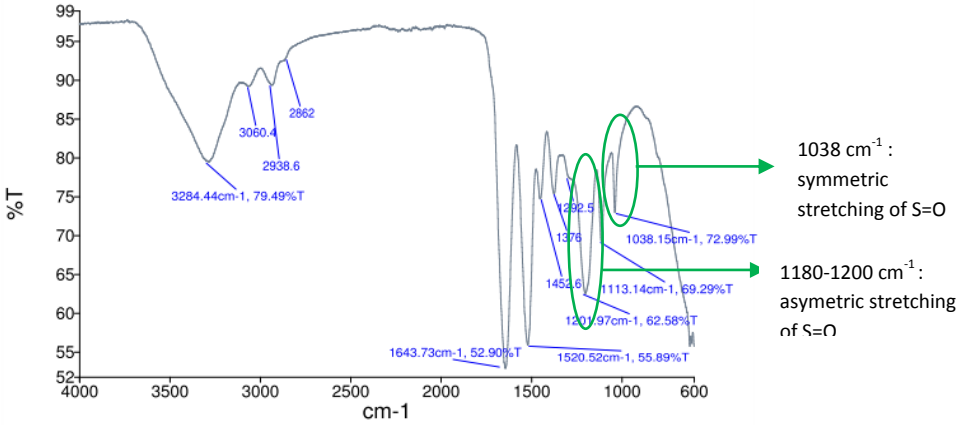

Figure 5.7: IR spectrum of NIP 0.15c

5.4 Recognition of Irinotecan

The polymer binding capability was investigated by rebinding tests with MIP 4.15e and NIP 0.15e in different solvents. In particular the MIP performance was first evaluated in water since we aimed to use this polymer for irinotecan quantification in plasma.
1.5 mL of 50 µM irinotecan solution were treated with 1.5 mg of MIP and after different times the amount of captured drug was measured by a HPLC method. Since at neutral pH the sulfonic acid groups in the polymer are in their anion form and irinotecan hydrochloride is used in this test to allow drug solubility, a ion pair can be created inside the polymer binding site. As shown in Figure 5.8, MIP 4.15e reaches the equilibrium within one hour capturing 8 nmol/mg of irinotecan and is able to hold the drug during the time. The amount of drug captured by NIP 0.15e is near to zero, therefore an imprinting factor of 22 was calculated, assuming that the number of binding sites of the MIP is the same of NIP. This value is higher than that obtained from MIPs previously synthesized and suggest a good efficiency of the imprinting process.

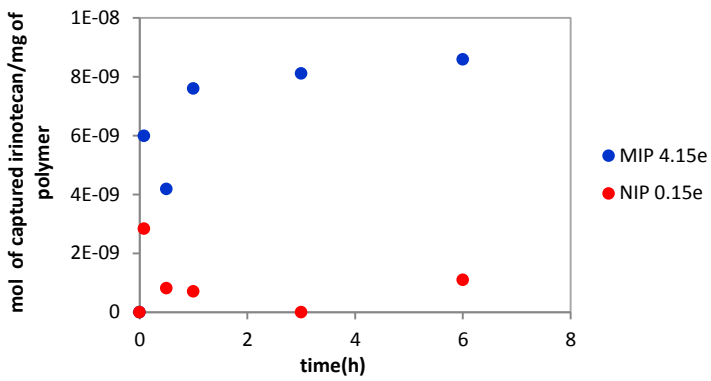

Figure 5.8: rebinding kinetics of protonated irinotecan with MIP 4.15e and NIP 0.15e in water

The rebinding test was also performed in citrate buffer at pH=3 to study the polymer binding capability when all irinotecan is in the protonated form with the closed lactone ring. The amount of drug captured by both MIP 4.15e and NIP 4.15e in this solvent is very low and near to zero.

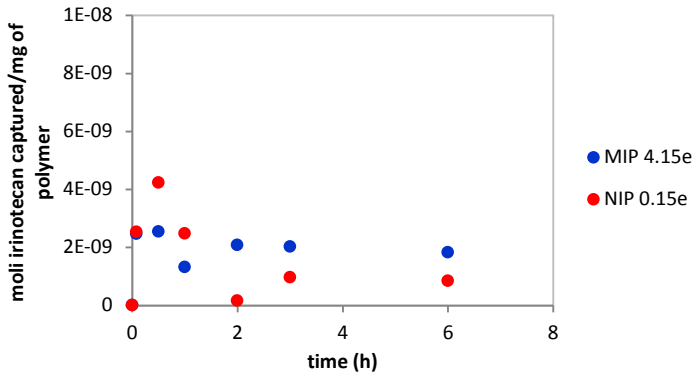

Figure 5.9: rebinding kinetics of protonated irinotecan with MIP 4.15e and NIP 0.15e in citrate buffer

These results were also compared to the recovery of irinotecan free base in acetonitrile, using the same polymer and irinotecan concentrations of previous tests. The binding kinetics of MIP 4.15e is similar to that of NIP 0.15e capturing 30 nmol per mg of polymer after 5 h when the equilibrium is reached. The rebinding capability in acetonitrile is over 3 times higher than in water, in fact MIP 4.15e was synthesized using irinotecan free base as template molecule. Also in these conditions the sulfonic acid group of AMPS in the polymer can protonate irinotecan free base giving a strong interaction. The similar behavior observed for both MIP and NIP may be due to the MIP tendency to aggregate in acetonitrile, decreasing the number of accessible binding sites

to irinotecan. To verify this hypothesis the test was repeated decreasing the polymer concentration at 0.5 mg/mL to avoid aggregation and increasing the drug concentration to 100 µM to facilitate the rebinding process. In these conditions the imprinted polymer reaches the plateau after 3h and captures 100 nmol of drug per mg of polymer, NIP 0.15e captures only 40 nmol after 3h, so the imprinting factor is greatly increased. Since a high irinotecan rebinding and a good selectivity was guaranteed using these polymer and drug concentrations, they could be taken in consideration for the development of a preliminary colorimetric test in acetonitrile.

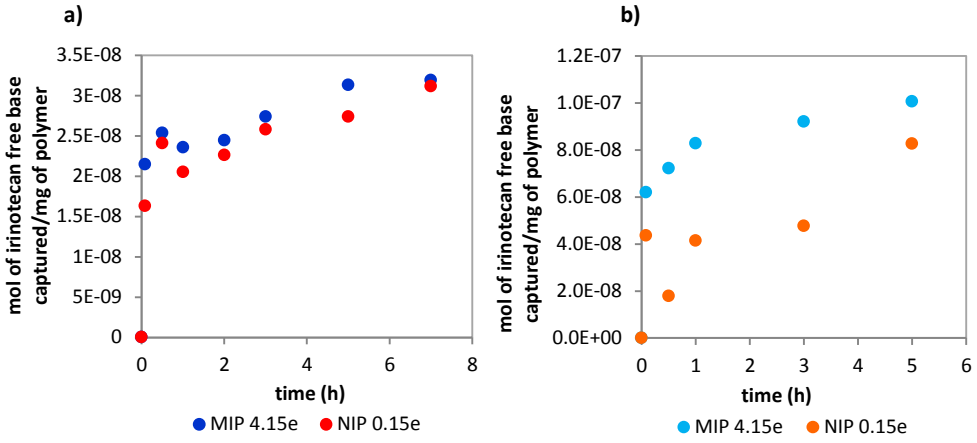

Figure 5.10: a) rebinding kinetics of irinotecan free base in acetonitrile with 1 mg/mL MIP 4.15e and NIP 0.15e and 50 µM drug; b) rebinding kinetics of irinotecan free base in acetonitrile with 0.5 mg/mL MIP 4.15e and NIP 0.15e and 100 µM drug

Cross Reactivity Tests

Since MIP 4.15e showed a high specificity in water, cross reactivity tests were also performed in this solvent. The tests consist in the quantification of the drug captured by 1.5 mg of MIP 4.15e suspended in 1.5 mL of 50 µM water solution of sunitinib or paclitaxel.

As shown in Figure 5.11, MIP 4.15e has a good selectivity, since the amount drug captured is very low with respect to the amount of protonated irinotecan captured.

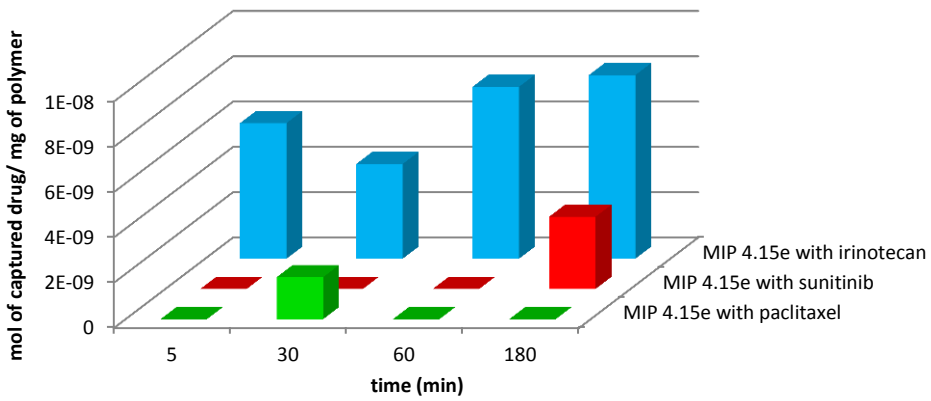

Figure 5.11: selectivity test of MIP 4.15e with paclitaxel and sunitinib in water

The good binding specificity and selectivity of MIP 4.15e observed in water make this polymer potentially useful for the drug quantification in plasma samples.

5.5 Towards a Colorimetric Test

Choice of the Best Solvent

In order to develop the colorimetric test for irinotecan quantification, the interaction between the aniline yellow dye and AMPS functional monomer was first investigated in different solvents. Aniline yellow dye (20 µM) was titrated with increasing amounts of AMPS in different solvents to find the solvent in which the proton transfer from the sulfonic acid to the dye is best visible, giving a change of colour. In fact the neutral form of this dye is yellow, its protonated form is red.[21, 22]

As shown in Figure 5.12, the change of colour of aniline yellow dye from yellow to red corresponds to the decrease of intensity of its absorption peak at 370 nm and the simultaneous appearance of the peak at 500 nm. However, this change occurs only in non-polar solvents as DCM and acetonitrile, while in all polar solvents like water, methanol and DMSO the dye remains yellow even after 10 equivalent of acid added. This behaviour could be explained considering that the pKa of aniline yellow is 2.8, therefore the dye is protonated by AMPS but the protonated aniline yellow immediately transfers its proton to water. Therefore the resulting colour of the solution is yellow. Probably the proton exchange from aniline yellow to solvents molecules occurs also in other polar solvents like methanol and DMSO where a low amount of

water is usually present. Conversely, in acetonitrile and in DCM the proton transfer occurs only between the sulfonic acid group and the dye, giving an immediate response.

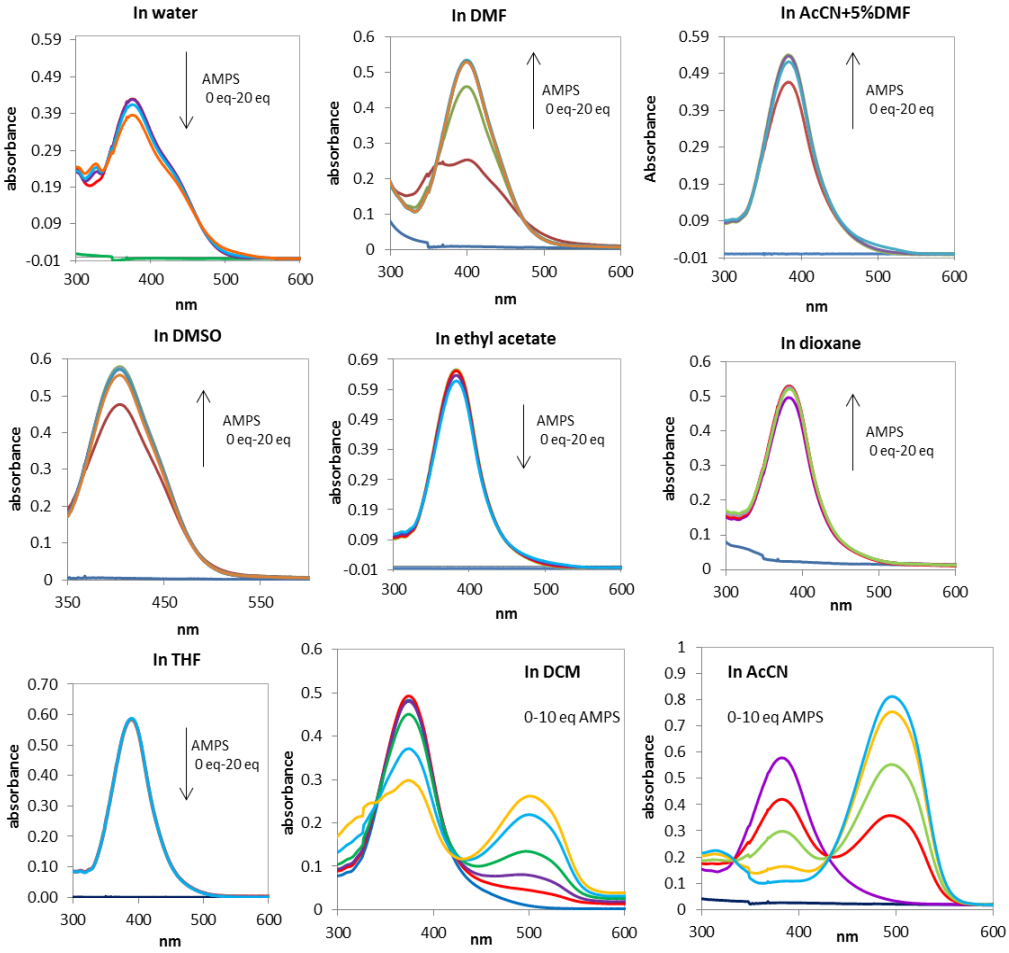

Figure 5.12: Titrations of 20 µM aniline yellow with AMPS from 0.5 to 10 or 20 eq in different solvents.

The best colour variation was observed in acetonitrile where all the dye was protonated after 10 equivalents of AMPS added. Moreover, the extinction coefficient of both neutral and protonated form of dye is higher in acetonitrile than in other solvents, allowing to work with low concentrations, in fact the change of colour is well visible both by UV-vis spectroscopy and by the necked eye with 10 µM dye (Figure 5.13).Therefore acetonitrile was chosen as the best solvent to set up the colorimetric systems.

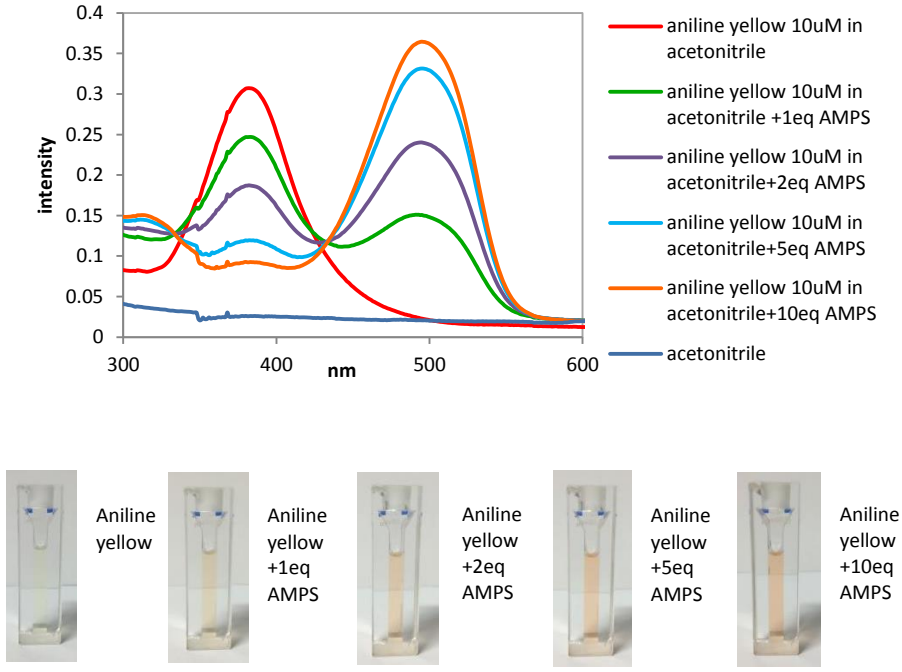

Figure 5.13: top: UV-visible titration of aniline yellow 10 µM in AcCN with increasing concentrations of AMPS from 0.5 eq to 10 eq; bottom: pictures of the obtained solutions.

Since the final aim is the irinotecan quantification in plasma samples, but is impossible to perform the colorimetric test in water environment, we exploited also the possibility to perform the test diluting plasma or aqueous irinotecan samples in acetonitrile. This approach requires first to find of the maximum quantity of water that the test could support when performed in acetonitrile.

To this aim 20 µM aniline yellow solution in acetonitrile was first titrated with increasing concentrations of AMPS until the complete saturation of dye. The titration was followed by UV visible spectroscopy. After 24 equivalents of AMPS added, only the red peak is visible. Starting from this condition, small amounts of water were added, from 0.5% to 10% volume.

The UV spectrum showed a large decrease of the peak at 500 nm and an increase of the peak at 400 nm after 2% of water added.

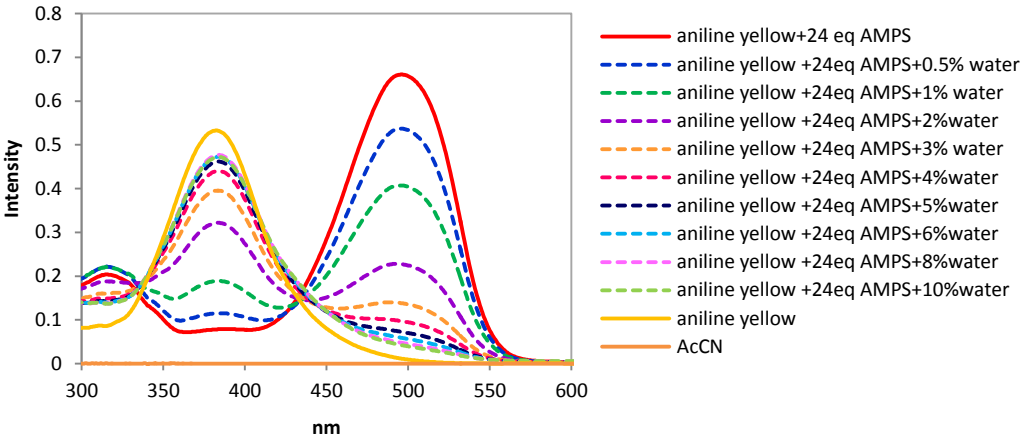

Figure 5.14: titration with water of 20 μM aniline yellow solution containing 24 equivalents of AMPS in acetonitrile

This experiment proved that the colorimetric test does not support the presence of water even in minimum quantities. Therefore a new strategy is necessary to quantify irinotecan from plasma samples using the colorimetric test in acetonitrile. A possible solution may be the addition of a sample treatment step before performing the colorimetric test. The step consists of drying small amounts of blood or plasma samples at room temperature and recover irinotecan in. To this aim cartridges able to treat and dry small amounts of patients' blood or plasma are already commercialized.[23,24,25]

Treatment of Plasma Samples

To evaluate this sample treatment step aimed to recover irinotecan in acetonitrile, a first attempt was preformed drying 5 μL of plasma spiked with different concentrations of irinotecan in the 250 nM – 750 μM range (corresponding to the expected amounts in real samples), and recovering the drug in 1 mL of acetonitrile, after sonication. However the amount of drug captured was very low maybe because the majority of irinotecan is still bounded to plasma proteins. Therefore the experiment was repeated treating with methanol plasma samples containing irinotecan, in order to unfold and remove proteins. The resulting 3:1 methanol:plasma solution was dried at room temperature and dissolved in the same volume of acetonitrile. After sonication, the amount of irinotecan recovered from dried plasma was quantified by HPLC.

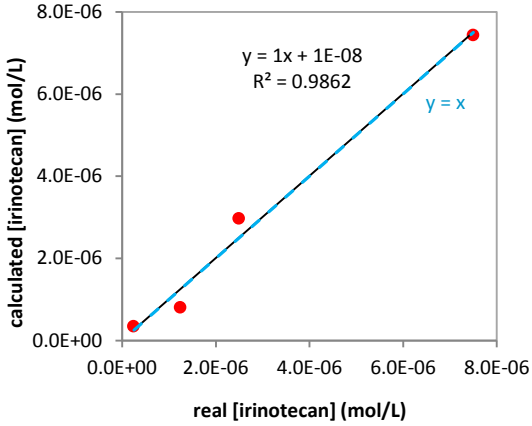

Figure 5.15: recovery of irinotecan from dried plasma after treatment with methanol

Real [irinotecan] (mol/L)	Calculated [irinotecan] (mol/L)
$2.50 \cdot 10^{-7}$	$3.41 \cdot 10^{-7}$
$1.25 \cdot 10^{-6}$	$8.03 \cdot 10^{-7}$
$2.50 \cdot 10^{-6}$	$2.97 \cdot 10^{-6}$
$7.50 \cdot 10^{-6}$	$7.43 \cdot 10^{-6}$

Table 5.7: real and recovered irinotecan concentrations from spiked samples in plasma

Even if this is a very preliminary experiment, its result is encouraging and a reasonable trend in recovery accuracy is observed. Further work aimed at optimizing the system and coupling the sample preparation with the colorimetric test is currently going on in cooperation with the industrial partner.

The colorimetric test that we aimed to set up can be based on two different approaches. The first consists of the drug quantification by measuring the dye displacement from the polymer binding sites upon interaction with irinotecan. This approach exploits the increased binding affinity of MIP for irinotecan than that for the dye. The second approach consists first of the treatment of the sample containing irinotecan with a polymer suspension in acetonitrile and after of the measurement of the sample colour due to addition of aniline yellow dye. In this way the dye colour in the sample is dependent on the amount of drug captured by the polymer. In the absence of drug all the polymer binding sites, containing AMPS, are able to protonate aniline yellow leading to a red colour. If the entire polymer is saturated with irinotecan, all the sulfonic acid groups will interacts with the drug, therefore aniline yellow will be not protonated.

UV-titration of MIP 4.15c

Following the first approach the irinotecan ability to displace the dye from the polymer binding sites was evaluated by UV-visible titration. The experiment was performed treating MIP 4.15c with 40 µM aniline yellow and measuring the UV spectrum before and after addition of increasing concentrations of irinotecan free base in acetonitrile.

In this case an intense red colour is observed at the starting point due to the interaction between MIP and aniline yellow, the colour intensity decreases increasing the drug concentration. In Figure 5.16 the absorbance intensity of the sample at 500 nm is plotted in function of the drug concentration added to the sample. The obtained curve is linear in the 100 µM- 600 µM range.

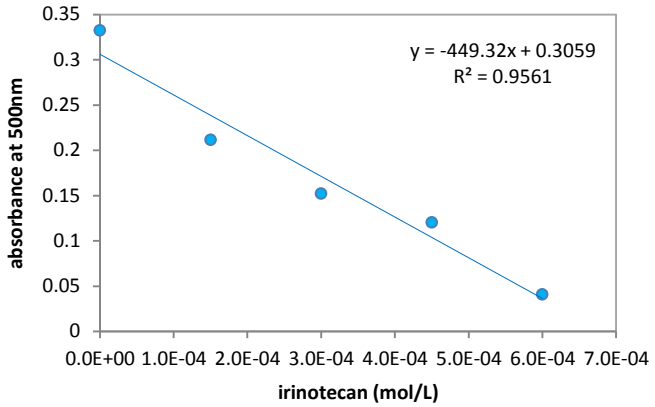

Figure 5.16: titration of MIP 4.15c treated with aniline yellow, with increasing amounts of irinotecan free base in acetonitrile

The observed decrease in the absorbance intensity of peak at 500 nm and consequent change of colour from red to yellow is due to the displacement of the dye from the polymer binding sites due to the binding of irinotecan. The test also verified a good affinity of MIP 4.15c for irinotecan.

Qualitative Colorimetric Test with MIP 4.15d

In order to set up the colorimetric test also the second approach was evaluated. To this aim a first qualitative experiment was performed treating 1 mL of 400 µM free base irinotecan solution in acetonitrile with 2 mg of MIP 4.15d and adding , after 10 min, aniline yellow to a 40 µM final concentration. The colour of the sample was compared to that of a polymer solution containing the same concentrations of MIP and aniline yellow but without the drug. As shown in Figure 5.17 the sample containing irinotecan remained yellow since all the polymer binding sites are occupied by the drug, while the sample untreated with the drug, has a more red colour. This colour increases its intensity during the time, since MIP 4.15d is composed only by 5% of AMPS and it is not completely soluble in acetonitrile, therefore the accessibility of the dye inside the binding sites can be difficult leading to a low kinetic. However, after overnight incubation, the colour of the sample without irinotecan is completely red, and that of the sample saturated with the drug is still yellow.

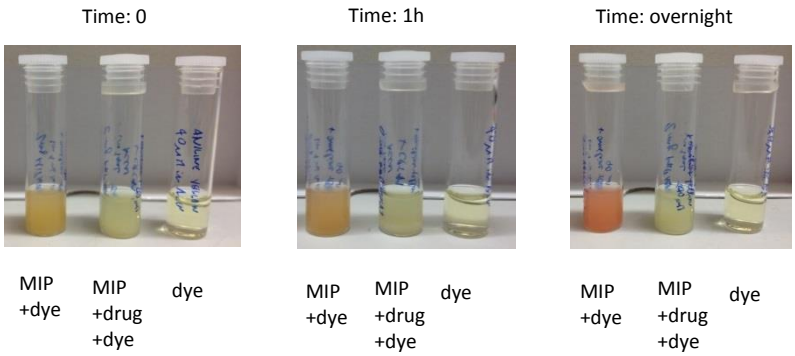

Figure 5.17: first colorimetric test in acetonitrile using 2 mg/mL MIP 4.15d, 400 μM free base irinotecan and 40 μM aniline yellow

Encouraged by these positive results we focused on the development of a quantitative test by UV-visible spectroscopy.

Choice of Aniline Yellow Concentration

In order to set up a quantitative test, MIP 4.15e (0.25 mg/mL in acetonitrile) was first titrated with different concentrations of aniline yellow dye to find the dye concentration necessary to saturate all the polymer binding sites. MIP 4.15e was chosen aiming at increasing and speed up the colorimetric response, since this polymer is synthesized with a double amount of AMPS with respect to MIP 4.15d, and with N-isopropyl acrylamide as co-monomer.

During the titration, the intensity of the peak at 500 nm increases since, increasing the dye concentration, aniline yellow is forced to bind inside the polymer. However, at high dye concentrations the absorbance peak at 400 nm produced by the unreacted molecules becomes large and partially superimpose the peak at 500 nm. Therefore a correction was made subtracting the absorbance intensity of different concentrations of aniline yellow without polymer measured at 500 nm, to the values obtained during the titration. The resulting curve reached the plateau after 200 μM dye.

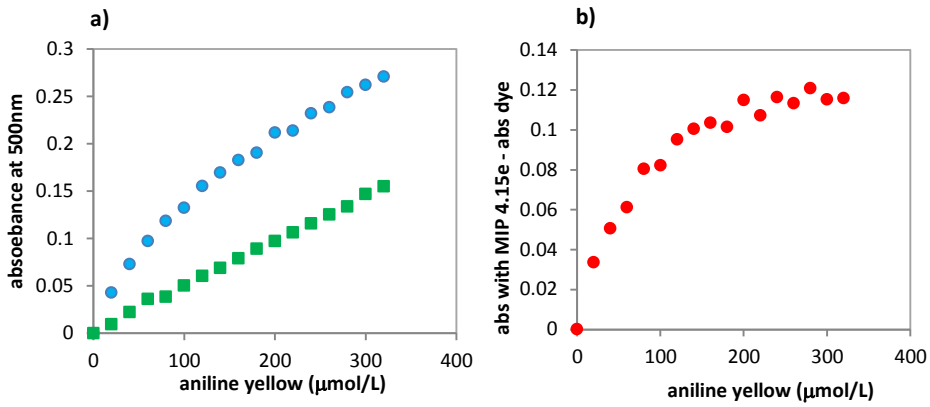

Figure 5.18: a) titration curve of the polymer with aniline yellow and reference curve of the dye; b) subtraction of the reference curve.

5.6 Colorimetric Test

With 0.25 mg/mL MIP 4.15e

The first colorimetric test was performed adding to a 0.25 mg/mL of polymer suspension in acetonitrile different concentrations of free base irinotecan. After 5 min, 200 µM aniline yellow was added. After recording the UV spectrum, the absorbance intensity at 520 nm was corrected subtracting the residual absorbance of the free dye, and plotted in function of the irinotecan concentration in the sample. The resulting curve showed a linear response from 2 µM to 20 µM drug.

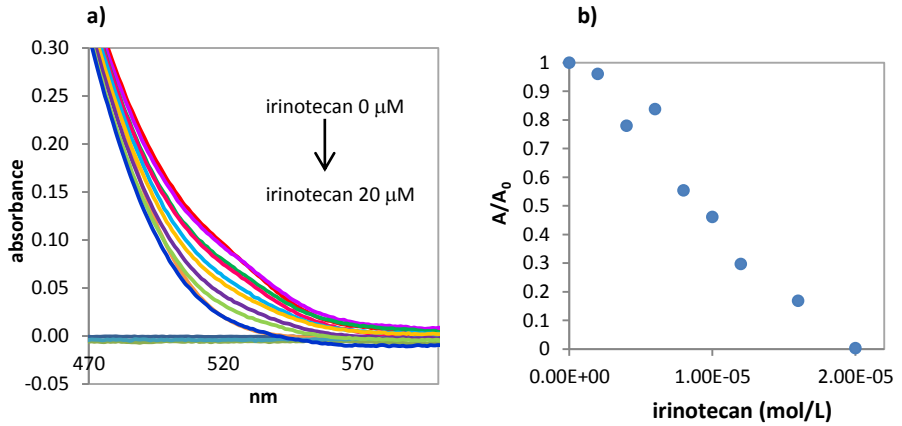

Figure 5.19: a) colorimetric test with 0.25 mg/mL MIP 4.15e; b) calibration curve obtained from the test

In order to increase the intensity of the signal at the starting point and increase the sensitivity, the polymer concentration was increased first to 0.4 mg/mL and after to 0.5 mg/mL. The colorimetric test performed with 0.5 mg/mL polymer suspension and 400 µM aniline yellow showed a visible change of color from red to yellow increasing the irinotecan concentration from 3.6 µM to 112 µM. Moreover, a calibration curve was obtained plotting the absorbance at 520 nm of the sample, normalized with the absorbance at 520 nm of the sample without irinotecan, in function of the drug concentration. The dynamic range of this curve is 3.6 µM-75 µM

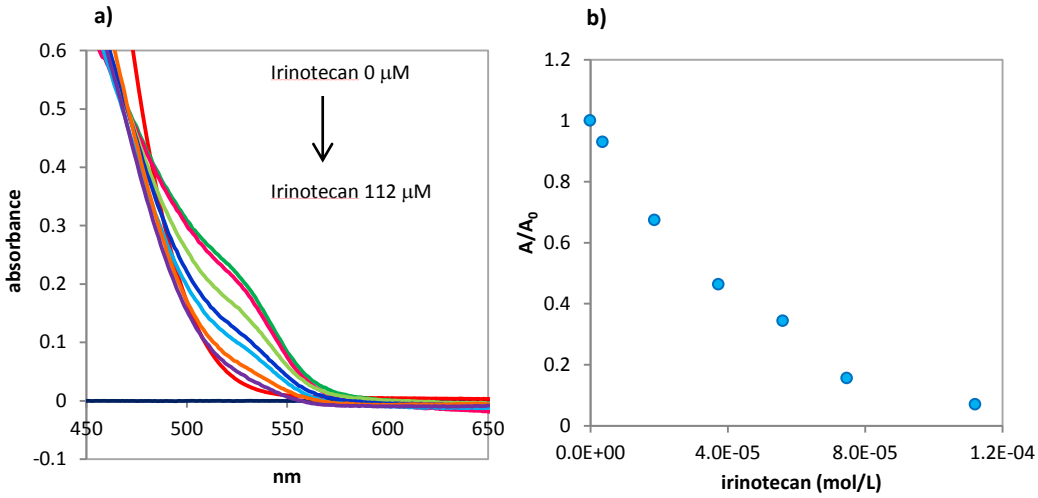

Figure 5.20 : a) colorimetric test with 0.5 mg/mL MIP 4.15e; b) calibration curve obtained from the test

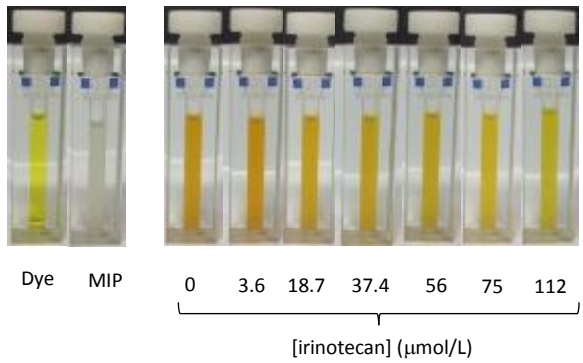

Figure 5.21: colorimetric test: color variation of samples containing different concentrations of irinotecan

This colorimetric test with 0.5 mg/mL MIP 4.15e represent a potentially good system to quantify irinotecan in real samples, since the drug concentrations usually found in patient samples are within the dynamic range of this curve. Therefore this test could be used for the development of a point of care device similar to that used for glycaemia analysis[26,27] or pregnancy test[28], to be used directly by patients for a rapid and easy irinotecan quantification.
From the engineering point of view this requires the development of a portable device able to measure the UV absorbance of the sample at 520 nm. To this aim, collaboration with the Center of Excellence for Biosensors, Instrumentation and Process Control (COBIK) is still in progress.

[1] McNiven S., Kato M., Levi R., Yano K., Karube I. (1998) "Chloramphenicol sensor based on an in situ imprinted polymer" *Anal. Chim. Acta* 365:69-74

[2] Okutucu B., Telefoncu A. (2008) "Optimization of serotonin imprinted polymers and recognition study from platelet rich plasma" *Talanta* 76:1153-1158

[3] Piletska E., Piletsky S., Karim K, Terpetsching E., Turner A. (2004) "Biotin-specific synthetic receptors prepared using molecular imprinting" *Anal. Chim. Acta* 504:179-183

[4] Piletsky S., Andersson H. S., Nicholls I. (1998) "The rational use of hydrophobic effect-based recognition in molecularly imprinted polymers" *J. Mol. Recognit.* 11:94-97

[5] Hickner M. A., Ghassemi H., Kim Y. S., Einsla B. R., McGrath J. (2004) "Alternative polymer systems for proton exchange membranes (PEMs)" *Chem. Rev*. 104:4587-4612

[6] Pitia E., Shaw M. T., Weiss R. A. (2011) "Synthesis of high proton conducting nanoparticles by emulsion polymerization" *Polymer* 52:297-306

[7] Travas-Sejdic J., Easteal A. (1997)"Swelling equilibria and volume phase transition of polyelectrolyte gel with strongly dissociated groups" *Polym. Gel. Netw.* 5:481-502

[8] Hazer O., Soykan C., Kartal Ş. (2008) "Synthesis and swelling behavior analysis of poly(acrylamidoxime-co-2-acrylamido-2-methylpropane sulfonic acid) hydrogels" *J. Macrom. Sci., A* 45, 45–51

[9] Sawicki e., Gerber D. S. (1956) "The physical properties of aminoazobenzene dyes. II. Further studies of the basicity" *J. Org. Chem*. 21(4):410-412

[10] Smith G., Wermuth U. D., Young D. J., White J. M. (2009) "Proton-transfer versus nontransfer in compounds of the diazo-dye precursor 4-(phenyldiazenyl) aniline (aniline yellow) with strong organic acids: the 5-sulfosalicylate and the dichroic benzenesulfonate salts, and the 1:2 adduct with 3,5-dinitrobenzoic" *Acta Crystallographi. C* 65(10):o543-o548

[11] Kuckling D., Adler H. J. P., arndt K. F., Ling L., Habicher W. D. (200) "Temperature and pH dependent solubility of novel poly(N-isopropylacrylamide) copolymers" *Macromol. Chem. Phys*. 201:273-280

[12] Schild H. G. (1992) "Poly(N-isopropylacrylamide): experiment, theory and application" *Prog. Polym. Sci.* 17:163-249

[13] Yoo J. E., Lee K. S., Garcia A., Tarver J., Gomez J. T., Baldwin K., Sun Y., Meng H., Nguyen T. Q., Loo Y. L. (2010) "Directly patternable, highly conducting polymers for broad applications in organic electronics" *PNAS* 107(13):5712-5717

[14] Mangelsdorf C., White L. R. (1998) "The dynamic double layer-Part 1: Theory of a mobile Stern layer" *J. Chem. Soc., Faraday Trans*. 94(16):2441-2452

[15] Glawdel T., Ren C. (2008) "Zeta potential measurement" Enciclopedia of Microfluidics and Nanofluidics pp 2199-2207

[16] Clogston J. D., Patri A. K. (2010) "Zeta potential measurement" Book: Characterization of nanoparticles intended for drug delivery, *Meth. Mol. Biol.* 697:63-70

[17] Zetasizer nano series, user manual (2013) *mano485 issue 11*

[18] Çavuş S. (2010) "Poly(methacrylamide-co-2-acrylamido-2-methyl-1-propanesulfonic acid) hydrogels: investigation of pH- and temperature-dependent swelling characteristics and their characterization" *J. Polym. Sci. B* 48:249-2508

[19] Atta A. M., Al-Shafey H. (2013) "Synthesis and surface activity of amphiphilic 2-acylamido-2-methylpropane sulfonic acid - co-N-isopropyl acylamide nanoparticles in aqueous media" *Int. J. Electrochem. Sci.* 8:4970-4985

[20] Durmaz S., Okay O. (200) "Acrylamide/2-acrylamido-2-methylpropane sulfonic acid sodium salt-based hydrogels: synthesis and characterization" *Polymer* 41:3693-3704

[21] Prabhu A. A. M., Venkatesh G., Sankaranarayanan R. K., Siva S., Rajendiran N. (2010)"Azonium-ammonium tautomerism and inclusion complexation of 4-amino-2'-3-dimethylazobenzene" *Indian J. Chem.* 49A:407-417

[22] Zakerhamidi M. S., Ghanadzadeh A., Moghadam M. (2012) "Solvent effects on the UV/ visible absorption spectra of some aminoazobenzene dyes" *Chem. Sci. Trans.* 1(1):1-8

[23] "Noviplex card plasma separator technology" *Shimadzu*- www.DriedPlasmaSpots.com

[24] "HemaSpot^{TM} blood collection device" *Spot*On Sciences* MKT-002 Rev A - www.SpotOnSciences.com

[25] Manicke N. E., Abu-Rabie P., Spooner N., Ouyang Z., Cooks R. G.(2011) "Quantitative analysis of therapeutic drugs in dried blood spot samples by paper spray mass spectrometry: an avenue to therapeutic drug monitoring" *J. Am. Soc. Mass Spectrom*. 22:1501Y1507

[26] Bronzino J. D. (2006) "Medical devices and systems" *The Biomedical Engineering Handbook* Third Edition 66-2 - 66-9

[27] Ramana V. V., Yamuna K. R., Jaunakais I. (2003) "Colorimetric test strips" *Patent: US6541269 B1*

[28] Maddison S. D. (2010) "Pregnancy testing method" *Patent: US20100129935 A1*

6. Experimental Section

6.1 Instrumentation

Thin layer chromatographies (TLC) were conducted on *Merck* plastic sheets pre-coated with 0.25 mm silica gel 60F-254. TLC plates were examined under UV light or were stained with aqueous permanganate solution or iodine vapors.
Flash chromatography purifications were carry out with *Merck* silica gel 60 (230-240 Mesh).
Melting points were measured on a *Büchi SMP-20* apparatus.
Nuclear magnetic resonance (NMR): 500 MHz ^{1}H-NMR and 125 MHz ^{13}C-NMR spectra were obtained on a *Varian 500* spectrometer. All the ^{1}H-NMR titrations were performed with the *Varian 500* spectrometer except for that with AMPS, acrylic acid and 4-vinylbenzenesulfonate that were recorded with a *Bruker 400 MHz* spectrometer. The characterization of neutral irinotecan was obtained with a *Bruker AV600* spectrometer.
Mass spectrometry measurements (MS): electrospray ionization (ESI) spectra were collected on a *Esquire 400 (Bruker Daltonics)* spectrometer.
Infrared spectra (IR) were recorded on a Perkin-Elmer *Avatar 320 FT-IR* spectrometer on thin films samples over sodium chloride, while IR spectra of polymers were performed with a *Perkin Elmer Spectrum 65 FT-IR* spectrometer.
High performance liquid chromatography (HPLC) analysis were run on an *Agilent series 1100* liquid chromatograph equipped with *Agilent 1100* series variable wavelength detector and a Phenomenex reverse phase *Luna C18* column.
Fluorescence measurements were performed with a *CARY Eclipse (Varian)* spectrometer.
UV-visible spectra were recorded on a *UV-1800 spectrometer (Shimadzu)* and on a *CARY-100 UV-visible spectrometer (Varian).*
Particles size were measured first by a *NanoSight Ltd LM10* instruments, and after by Dynamic Laser Light Scattering (DLLS) on *Zetasizer nano-S (Malvern)* instrument that was used also to measure the z-potential.

6.2 Materials

Chemicals and solvents were purchased from Sigma Aldrich, deuterated solvents from Aldrich and Cambridge Isotope Laboratories. Anhydrous dichloromethane was obtained drying the solvent over $CaCl_2$ overnight and distillation, while anhydrous pyridine and THF were purchased by Sigma Aldrich. When anhydrous conditions were required, reaction flasks were flame-dried and placed under a flux of argon.
Crimp cap Weaton vials used for the polymer synthesis were purchased from Sigma Aldrich.
Spectra/Por3 dialysis membrane MWCO 3500 Da was purchased from Spectrumlabs.

Pure drugs: Iriontecan-HCl, Paclitaxel, Sunitinib and SN38 were purchased from Bepharm.
The citrate buffer pH=3 used for the rebinding tests was obtained by addition of 18 mL of 0.1 M trisodium citrate to 82 mL of 0.1 M citric acid.

6.3 Fluorescent MIPs: n. 1.5 - 4.8

Synthesis of Functional Monomers

Methyl 2-acrylamido-3-(4'-hydroxyphenyl)propanoate
(*N*-acryloyl L-tyrosine methyl ester; **5b**)

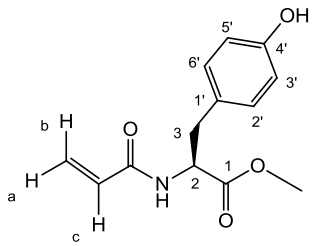

2.0 g (10.2 mmol) of L-tyrosine methyl ester were dissolved in 150 mL of anhydrous DCM and 4.5 mL (32.4 mmol) of triethylamine. After cooling at 0°C, a solution of acryloyl chloride (1 mL, 12.3 mmol, 1.2) in 50 mL of DCM was added dropwise and the reaction mixture was stirred overnight under anhydrous atmosphere. The solvent was removed in vacuum and the crude product was purified by silica gel column chromatography (elution with DCM:ethyl acetate from 1:1 to 2.5:7.5) leading to white crystals of the product (1.2 g, yield 47%).
MS-ESI (m/z): 272.0 $[M+Na]^+$
^{1}H NMR (500 MHz, $CDCl_3$, 25 °C, ppm) δ = 3.05 (dd, ^{2}J = 14 Hz, ^{3}J = 9 Hz, 1H, CH_2-**3 pro-R**), 3.12 (dd, ^2J = 14 Hz, ^3J = 6 Hz, 1H, CH_2-**3 pro-S**), 3.75 (s, 3H, COO-C**H**$_3$), 4.94 (m, 1H, CH-**2**), 4.68 (dd, $^3J_{trans}$ = 10 Hz, $^3J_{cis}$ = 1.2 Hz, 1H, CH-**c**), 5.93 (s, 1H, N**H**), 6.10 (bb, O**H**), 6.09 (dd, ^2J = 17 Hz, $^3J_{trans}$ = 10 Hz, 1H, CH_2-**b**), 6.29 (dd, $^2J_{trans}$ = 17 Hz, $^3J_{cis}$ = 1.2 Hz, 1H, CH_2-**a**), 6.73 (d, ^3J = 8.5 Hz, 2H, CH-**2'**, **6'**), 6.94 (d, ^3J = 8.5 Hz, 2H, CH-**3'**, **5'**).
^{13}C NMR (500 MHz, $CDCl_3$, 25 °C, ppm) δ = 37.27 (1C, CH_2-**3**), 52.62 (1C, COO-C**H**$_3$), 53.49 (1C, CH-**2**), 115.69 (2C, CH-**2'**, **6'**), 127.41 (1C, CH-**c**), 127.70 (1C, CH_2-**a**, **b**), 130.30 (1C, C-**4'**), 130.51 (2C, CH-**3'**, **5'**), 152.32 (C, C-**1'**), 165.30 (1C, **C**O-NH), 172.27 (1C, **C**OO-CH_3).
IR (cm^{-1}): 1662 (C=O), 1721 (C=O), 3318 (N-H).
mp: 125.6 – 129°C.

(S)-methyl 2-acrylamido-3-(1'H-indol-3'-yl)propanoate

(*N*-acryloyl L-tryptophan methyl ester **6b**)

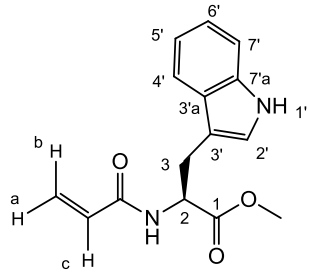

0.5 g (1.96 mmol) of L-tryptophan methyl ester were dissolved in 10 mL of anhydrous DCM and 0.67 mL (4.8 mmol) of triethylamine. After cooling at 0 °C, a solution of acryloyl chloride (0.2 mL, 2.3 mmol) in 5 mL of DCM was added dropwise and the reaction mixture was stirred overnight under anhydrous atmosphere. The solvent was removed in vacuum and the crude product was purified by silica gel column chromatography (elution with DCM:ethyl acetate from 8:2 to 5:5) leading to white crystals of the product (0.4 g, yield 81%).

MS-ESI (m/z*)*: 295 $[M+Na]^+$

^{1}H-NMR (500 MHz, $[D_6]$DMSO, 25 °C, ppm) δ = 3.07 (dd, ^2J = 14.6 Hz, ^3J = 8.5 Hz, 1H, CH_2-**3 pro-R**), 3.18 (dd, ^2J = 14.6 Hz, ^3J = 5 Hz, 1H, CH_2-**3 pro-S**), 3.59 (s, 3H, COO-C**H**$_3$), 4.60 (m, 1H, CH-**2**), 5.60 (dd, $^3J_{cis}$ = 2 Hz, $^3J_{trans}$ = 10 Hz, 1H, CH-**c**), 6.07 (dd, ^2J = 17.11 Hz, $^3J_{cis}$ = 2 Hz, 1H, CH-**a**), 6.29 (dd, ^2J = 17.11 Hz, $^3J_{trans}$ = 10 Hz, 1H, CH-**b**), 6.98 (td, $^3J_{ortho}$ = 8 Hz, $^4J_{meta}$ = 1 Hz, 1H, CH-**6'**), 7.06 (td, $^4J_{meta}$ = 1 Hz, $^3J_{ortho}$ = 4 Hz, 1H, CH-**4'**), 7.13 (d, ^3J = 2 Hz, 1H, CH-**2'**), 7.33 (d, $^3J_{ortho}$ = 8 Hz, 1H, CH-**5'**), 7.49 (d, $^3J_{ortho}$ = 8 Hz, 1H, CH-**7'**), 8.54 (d, ^3J = 8 Hz, 1H, N**H** amide), 10.85 (s, 1H, N**H** indole).

^{13}C-NMR (500 MHz, $[D_6]$DMSO, 25 °C, ppm) δ = 27.79 (1C, CH_2-**3**), 52.55 (1C, COO-**C**H$_3$), 53.21 (1C, CH-**2**), 110.14 (1C, C-**3'**), 111.41 (1C, CH-**5'**), 118.76 (1C, CH-**7'**), 119.89 (1C, CH-**4'**), 122.41 (1C, CH-**2'**), 122.90 (1C, CH-**6'**), 127.29 (1C, CH_2-**a,b**), 127.82 (1C, C-**3'a**), 130.56 (1C, CH-**c**), 136.33 (1C, C-**7a**), 165.13 (1C, **C**O-NH), 172.38 (1C, **C**OO-CH_3).

IR (cm^{-1}): 1662 (C=O amide), 1737 (C=O ester), 3296 (N-H).

mp: 49-49.5 °C.

2-oxo-2H-chromen-7-yl acrylate

(7-acryloyloxycoumarin; **7b**)

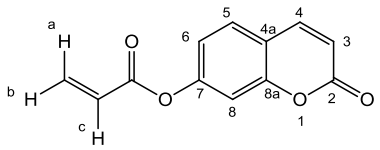

0.5 g (3.1 mmol) of 7-hydroxy-coumarin were dissolved in 10 mL of anhydrous DCM and 1.26 mL (9.1 mmol) of triethylamine. After cooling at 0 °C, a solution of acryloyl chloride (0.4 mL, 4.6 mmol) in 7 mL of DCM was added dropwise and the reaction mixture was stirred overnight under anhydrous atmosphere. After addition of a saturated solution of sodium chloride, a red precipitate was removed by filtration and the remaining solution was washed 3 times with a saturated solution of sodium chloride. The organic phase was evaporated in vacuum leading to an orange product that was purified by silica column chromatography (elution with DCM:petroleum ether:ethyl acetate 2:1:1) to yield the pure product as white crystals (0.6 g, yield 90%).

MS-ESI (m/z*)*: 238.9 $[M+Na]^+$

^{1}H-NMR (500 MHz, $CDCl_3$, 25 °C, ppm) δ = 6.08 (dd, $^3J_{trans}$ = 10.5 Hz, $^3J_{cis}$ = 1 Hz, 1H, CH-**c**), 6.33 (dd, ^2J= 17 Hz, $^3J_{trans}$ = 10.5 Hz, 1H, CH_2-**b**), 6.40 (d, $^3J_{ortho}$ = 9.6 Hz, 1H, CH-**4**), 6.65 (dd, ^2J = 17 Hz, $^3J_{cis}$ = 1 Hz, 1H, CH_2-**a**), 7.10 (dd, $^3J_{ortho}$ = 8.4 Hz, $^4J_{meta}$ = 2 Hz, 1H, CH-**6**), 7.17 (d, $^4J_{meta}$ = 2 Hz, 1H, CH-**8**), 7.50 (d, $^3J_{ortho}$ = 8.4 Hz, 1H, CH-**5**), 7.70 (d, $^3J_{ortho}$ = 9.6 Hz, 1H, CH-**3**).

^{13}C-NMR (500 MHz, $CDCl_3$, 25 °C, ppm) δ = 110.57 (1C, CH-**8**), 116.27 (1C, CH-**4**), 116.86 (1C, C-**4a**), 118.49 (1C, CH-**6**), 127.44 (1C, CH-**c**), 128.70 (1C, CH-**5**), 133.82 (1C, CH_2-**a**, **b**), 142.96 (1C, CH-**3**), 153.23 (1C, C-**7**), 154.85 (1C, C-**8a**), 160.45 (**C**=O), 163.90 (**C**=O).

IR (cm^{-1}) : 1734 (2 C=O).

mp: 136.9-137.5 °C.

^{1}H NMR Titrations

The interaction between the functional monomers and the template molecule were investigated by titrating the drug with the functional monomers **5b**, **6b**, **7b** and 4-vinyl pyridine (**8**). In particular, a 7 mM solution of SN38 in $[D_6]$DMSO was titrated with increasing amounts of the functional monomer to obtain final concentrations ranging from 3.5 mM to 98 mM. A 5 mM solution of paclitaxel in $[D_6]$DMSO was titrated with increasing amounts of functional monomers to obtain final concentrations ranging from 2.5 mM to 70 mM, and a 6.7 mM sunitinib solution in $[D_6]$DMSO was titrated with the functional monomers from 3.35 mM to 93.7 mM. Finally, irinotecan-HCl 5.3 mM (3.0 mg, 4.4 µmol in 840 µL) in $[D_6]$DMSO was titrated with increasing concentrations of

functional monomer from 2.6 mM to 74.2 mM. The ^{1}H NMR spectrum was recorded after every addition.

Recrystallization of AIBN

2.0 g of AIBN were placed in a round-bottomed flask equipped with a stirring bar and a condenser. The vacuum and a flow of argon was alternated in the system for 10 times, to avoid any trace of oxygen. AIBN was dissolved in 5mL of ethanol and the temperature was increased slowly to 50-55 °C. At this temperature 2 mL of ethanol were added to solubilize the product. The flask was then left to reach room temperature to allow the crystallization.

Synthesis of Molecularly Imprinted Polymers 1.5 – 4.8

1 eq of functional monomer and 1.2 eq of the drug were dissolved in a total amount of DMSO corresponding to the 99% in weight of total functional monomers and crosslinker. After stirring in anhydrous conditions for 40 minutes, the solution was transferred in a crimp cap Wheaton vial and 70% (in mol) of *N,N'*-ethylenebisacrylamide, 18% (in mol, calculated on the amount of the available double bonds) of recrystallized AIBN and 15% (in mol, 1eq) of acrylamide were added. The vial was left first under vacuum and then was flushed with argon (3 times for 10 minutes). Radical polymerization was achieved heating the vial up to 70°C for 4 days. Each polymer was synthesised either in presence of the template molecule, leading to MIP particles, or without the template, leading to NIP. The resulting clear solutions were dialyzed against methanol for 2 days and against water for other 2 days, changing the solvent 3 times a day. Finally the solution was freeze-dried leading to a fluffy polymer.
Since a low amount of drug remains entrapped in certain MIPs, they were further washed by suspending 2 mg of polymer in 1 mL of methanol; after shaking for 5 min, the mixture was centrifuged at 13000 rpm for 10 min. After removal of the supernatant, the MIP was resuspended in methanol and the washing step was repeated again until the drug was no longer detected in the supernatant. Finally the MIP was dissolved in water and freeze-dried.
The composition of the polymerization mixtures for each polymer is reported in the following table.

Polymer	Drug [mg]	Functional monomer [mg]	Co-monomer [mg]	*N,N*-ethylene Bisacrylamide [mg]	AIBN [mg]	DMSO [mL]	Yield %
0.5	-	N-acryloyl-tyrosine-OMe 12	Acrylamide 3.4	37.7	16.1	4.8	35
0.6	-	N-acryloyl-tryptophan-OMe 13.1	Acrylamide 3.4	37.7	16.1	4.9	79
0.7	-	7-acryloyloxycoumarin 10.4	Acrylamide 3.4	37.7	16.1	4.6	92
0.8	-	4-vinyl-pyridine 3.5	Acrylamide 2.4	26	11.1	2.9	94
1.5	Sunitinib 23	N-acryloyl-tyrosine-OMe 12	Acrylamide 3.4	37.7	16.1	4.8	63
1.6	Sunitinib 23	N-acryloyl-tryptophan-OMe 13.1	Acrylamide 3.4	37.7	16.1	4.9	58
1.7	Sunitinib 23	7-acryloyloxycoumarin 10.4	Acrylamide 3.4	37.7	16.1	4.6	86
1.8	Sunitinib 23	4-vinyl-pyridine 5.0	Acrylamide 3.4	37.7	16.1	4.1	41
2.5	SN38 23	N-acryloyl-tyrosine-OMe 12.2	Acrylamide 3.5	38.3	16.3	4.8	61
2.6	SN38 23	N-acryloyl-tryptophan-OMe 13.3	Acrylamide 3.5	38.3	16.3	4.9	80
2.7	SN38 23	7-acryloyoxylcoumarin 10.6	Acrylamide 3.5	38.3	16.3	4.7	90
2.8	SN38 23	4-vinyl-pyridine 5.1	Acrylamide 3.5	38.3	16.3	4.2	27
3.5	Paclitaxel 32.9	N-acryloyl-tyrosine-OMe 8.0	Acrylamide 2.3	25.2	10.7	3.2	41
3.6	Paclitaxel 37.6	N-acryloy-tryptophan-OMe 10.0	Acrylamide 2.6	28.8	12.3	3.7	74
3.7	Paclitaxel 23.5	7-acryloyloxycoumarin 5.0	Acrylamide 1.6	9	4.5	1	76
3.8	Paclitaxel 34.1	4-vinyl-pyridine 3.5	Acrylamide 2.4	26	11.1	2.9	63
4.5	Irinotecan 40.6	N-acryloyl-tyrosine-OMe 12.5	Acrylamide 3.5	39.2	16.7	5.78	68
4.6	Irinotecan 40.6	N-acryloy-tryptophan-OMe 13.6	Acrylamide 3.5	39.2	16.7	5.07	77

4.7	Irinotecan 40.6	7-acryloyloxycoumarin 10.8	Acrylamide 3.5	39.2	16.7	4.8	82
4.8	Irinotecan 40.6	4-vinyl-pyridine 5.3	Acrylamide 3.5	39.2	16.7	4.3	45

Washing of MIPs 4.5 – 4.8

10 mg of MIP 4.5, 4.6, 4.7 and 4.8 were dissolved in 4 mL of a 7:3 methanol:acetic acid mixture and dialyzed first against the same mixture (2 changes), then against methanol only (3 changes) and finally against water (5 changes). After freeze-drying, clean fluffy MIPs were obtained.

Nanosight

The non-imprinted polymers 0.5 – 0.8 and the molecularly imprinted 1.5 -1.8 synthesized for sunitinib were dissolved in water at concentrations ranging from 2 $mg \cdot mL^{-1}$ to 0.125 $mg \cdot mL^{-1}$ and filtered on 0.22 μm filter before the analysis.

Dynamic Laser Light Scattering

All MIPs and NIPs were dissolved in DMSO to obtain a 0.25 $mg \cdot mL^{-1}$ concentration and the solution was placed into an ultrasonic bath for 1 h. After filtration on 0.45 μm filter, the size distribution by intensity and by volume was recorded in triplicate on a Malvern Zetasizer instrument using a 1 mL quartz cuvette with light path of 1 cm.

Coumarin Content in MIP 1.7 and NIP 0.7

The concentration of coumarin in its polymers was calculated by UV-visible spectroscopy.
The absorbance intensity at 324 nm in the UV-visible spectrum of 60 μg/mL and 120 μg/mL polymer water solution, after sonication for 20 min, was measured for the MIP synthesized for sunitinib and for the respective NIP (350 μL in a quartz cuvette of 1 mL). The obtained values were used to calculate the coumarin concentration from a calibration curve of coumarin in water. In order to create such curve, the absorbance intensity at 324 nm of increasing solutions of 7-hydroxycoumarin from 1 μM to 100 μM in water, was recorded.

Rebinding Tests

The rebinding kinetics of the drugs to MIPs were investigated dissolving 1.5 mg of the polymer in 1.5 mL of a 50 μM drug solution in water. The mixtures were incubated at 25°C under continuous stirring and 200 μL aliquots of the solution were taken after different times (from 10 min to 12 h) and enriched with 5 μL of a 1 mM quinolinone or caffeic acid solution as external standard. This new solution was centrifuged (10000 rpm for 6 min) to remove the polymer, and the supernatant, containing an unknown amount of the drug and 25 μM external standard, was analysed by HPLC to quantify the drug concentration. The ratio between the area of the drug peak and the reference peak in the chromatogram of the sample treated with the polymer was compared with that of a reference sample containing only the drug, untreated with the polymer, to calculate the amount of drug captured by the polymer.[1]

Cross-reactivity Studies

The polymer selectivity was investigated by the same rebinding test by HPLC, however in this case the MIPs templated with sunitinib were treated with a 50 μM solution of SN38 or paclitaxel, while the MIPs for SN38 were treated with 50 μM sunitinib or paclitaxel, moreover the MIPs synthesised to capture paclitaxel, were treated with SN38 or sunitinib. Finally the MIPs synthesized to capture irinotecan were treated with 50 μM sunitinib or paclitaxel or SN38.

Fluorescence Titration of MIPs 1.5 – 4.8

The binding capability of MIPs were also analysed by fluorescence titration of a 60 μg/mL solution of the polymer in water with a small amount of DMSO as shown below, with increasing concentrations of the drug. The fluorescence emission of the polymers containing tyrosine was analysed at 303 nm, when they are excited at 274 nm, while all polymers containing tryptophan were excited at 280 nm and the emission at 340 nm was observed. Finally the fluorescence emission of all polymers containing coumarin were analysed at 456 nm when the polymer is excited at 327 nm with exception of the polymer templated with paclitaxel whose fluorescence emission of coumarin was at 393 nm because of the change of solvent (DMSO). All the polymers templated with sunitinib were dissolved in water with 3% of DMSO and titrated with the drug from 0.5 μM to 88.8 μM. Also the polymers templated with SN38 were dissolved in water with 3% of DMSO with the exception of the polymer containing tryptophan that was dissolved in water with 15% of DMSO because of its low solubility. During the titration, increasing concentrations of SN38 were added from 0.5 μM to 165 μM. Finally, all the

polymers templated with paclitaxel were dissolved in DMSO and titrated with increasing amounts of paclitaxel from 0.1 μM to 1 mM in DMSO because of the insolubility of paclitaxel in water.
During all the titrations the excitation and emission slits were set to 10 nm, and the emission was averaged over 1s, with the exception of the polymer 2.6 that was analysed with 5 nm excitation slit; while the polymers 1.7 and 2.7 were analysed with both the slits at 5 nm.
The presence of low amounts of DMSO as co-solvent during the titrations was also evaluated measuring the polymer emission after increasing additions of DMSO. The fluorescence emission is not affected by DMSO.

Fluorescence Titration of Fluorophores

Titration of Boc-tyrosine

The fluorescence of *Boc*-tyrosine was measured at an excitation wavelength of 274 nm and emission wavelength of 303 nm, slit set at 10 nm, average time of 1s. About the titration with SN38, to a 2.1 μM solution of Boc-tyrosine in water with 3% of DMSO, different amounts of SN38 from 0.5 μM to 165 μM were added. While for the titration with sunitinib, increasing amounts of the drug, from 0.5 μM to 88 μM, were added to a 3.2 μM solution of *Boc*-tyrosine in water with 3% of DMSO.
Finally the titration with paclitaxel was performed in DMSO by the addition of the drug from 0.1 μM to 1 mM, to a 25.5 μM solution of Boc-tyrosine in DMSO. In this case the fluorescence emission at 303 nm was observed with the emission slit set at 5 nm.

Titration of Boc-tryptophan

in all the titrations of *Boc*-tryptophan the fluorescence was measured at an excitation wavelength of 280 nm and at an emission wavelength of 340 nm. The titration with sunitinib (from 0.5 μM to 88 μM) was performed with a 510 nM solution of *Boc*-tryptophan in water with 3% of DMSO. The fluorescence was measured with slits set at 10 nm, average time of 1s. In the titration with SN38 (from 0.5 μM to 165 μM), a 1.5 μM solution of *Boc*-tryptophan in water with 15% of DMSO was used and the fluorescence was measured with excitation slit set at 5 nm and average time of 1s. Finally a 3 μM solution of *Boc*-tryptophan in DMSO was also titrated with paclitaxel (from 0.1 μM to 1 mM) with excitation slit set at 5 nm, average time of 1s.

Titration of 7-hydroxy-coumarin

Sunitinib: to 400 μL of a of 5 μM aqueous solution 7-hydroxy-coumarin, increasing amounts of sunitinib were added (from 0.5 μM to 73 μM) and the quenching of fluorescence was measured at an excitation wavelength of 327 nm, emission at 456 nm, excitation slit 2.5 nm, average time of 1s. SN38: 350 μL of a 1 μM solution of 7-hydroxy-cumarin in water with 3% of DMSO were titrated with SN38 from 0.5 μM to 212 μM. The solution was excited at 327 nm and the fluorescence emission at 456 nm was observed with slits set at 5 nm, average time of 1s. Paclitaxel: 400 μL of 1 μM 7-hydroxy-coumarin in DMSO was titrated with paclitaxel (from 0.1 μM to 1 mM) and the fluorescence quenching was measured at 393 nm exciting at 327 nm with silts of 10 nm.

Fluorescence Properties of MIP 4.7

The fluorescence properties of MIP 4.7 and of the corresponding NIP were investigated by fluorescence spectroscopy exciting the polymer at 327 nm and measuring the emission from 350 nm to 600 nm with excitation and emission slits of 5 nm. Using these conditions fluorescence spectra were recorded for 60 μg/mL MIP and NIP solutions in 4:1DMSO:water, obtained by dilution of the 1 mg/mL in DMSO. The emission spectra of the polymers were compared to that of 1 μM 7-hydroxycoumarin solutions in DMSO, in water and in 4:1DMSO:water, obtained by dilution from the 7.4 mM mother solution in DMSO (1.2 mg, 7.4 μmol in 1 mL), and to that of 1 μM irinotecan solution in DMSO (batch solution: 4 mM, 1.7 mg, 2.5 μmol in 625 μL of DMSO).

Fluorescence Titrations of MIPs 4.5 and 4.6

The quenching of fluorescence of the MIPs and NIPs synthesized to capture irinotecan and containing tyrosine-OMe and tryptophan-OMe was investigated by fluorescence titrations with the drug.

1 mg of polymer was dissolved in 1 mL of DMSO. After sonication for 30 min, a 60 μg/mL polymer solution was obtained in 4:1 DMSO:water by dilution from the 1 mg/mL mother solution. The solution was titrated with increasing amounts of irinotecan from 1 μM to 100 μM using a 4 mM (1.7 mg, 2.5 μmol, in 625 μL of DMSO:water 4:1) irinotecan batch solution.

In the titration of the polymers containing tyrosine-OMe, the emission intensity at 318 nm when the polymer was excited at 274 nm was measured setting the excitation and emission slits respectively at 10 and 20 nm. The fluorescence emission of the polymers containing tryptophan-OMe was measured at 350 nm exciting at 280 nm with excitation and emission slits of 10 nm.

The polymers containing tryptophan-OMe were also titrated in citrate buffer at pH=3. In this case the 1 mg/mL polymer solution in DMSO was diluted to the 60 µg/mL in citrate buffer and increasing amounts of irinotecan from 1 µM to 100 µM were added in the cuvette from the 4 mM drug solution in citrate buffer (1.7 mg, 2.5 µmol, in 625 µL of citrate buffer). The titration was performed exciting at 280 nm and measuring the emission at 357 nm with excitation and emission slits set respectively at 15 nm and 20 nm.

Fluorescence Titration of Irinotecan with MIPs

400 µL of 1 µM irinotecan in 3:1 DMSO:water (obtained by dilution from the 400 µM mother solution in DMSO) were titrated with MIP 4.6 and with MIP 4.5 from 0 µg to 4 µg final amount in the cuvette using the 10 µg/mL, 50 µg/mL, 250 µg/mL MIP solutions in 3:1 DMSO:water and 1 mg/mL polymer solutions in DMSO. The fluorescence emission of irinotecan at 430 nm exciting at 360 nm was measured before and after the addition of polymer using excitation and emission slits of 5 nm.
The 10 µg/mL, 50 µg/mL, 250 µg/mL MIP 4.5 solutions in 3:1 DMSO:water and 1 mg/mL polymer solutions in DMSO were also used to titrate 400 µL of 0.25 µM, 0.5 µM, 1 µM and 4.25 µM irinotecan in treated 3:1 methanol:plasma. The methanol:plasma solutions were obtained by addition of three volumes of methanol to one volume of plasma, and 3 centrifugation runs for 10 min at 13000 rpm at 4 °C. The 0.25 µM, 0.5 µM, 1 µM and 4.25 µM irinotecan solutions were obtained by dilution in treated 3:1 methanol:plasma of the 2.95 mM mother drug solution (2 mg of irinotecan, 2.95 µmol in 1 mL of water). The excitation and emission wavelength were respectively 360 nm and 430 nm while the excitation and emission slits were 5 nm for the 0.5 µM and 1 µM irinotecan titrations, 5 nm and 10 nm for the 0.25 µM drug titration and 5 nm and 2.5 nm for the 4.25 µM irinotecan titration.

Calibration Curve with MIP 4.5

MIP 4.5 was used to create a calibration curve by fluorescence spectroscopy to quantify irinotecan from samples of plasma after treatment with three volumes of methanol and centrifugation at 13000 rpm for 10 min at 4 °C to remove proteins. 2 µg of MIP **4.5** (obtained from a 1 mg/mL batch polymer solution in 3:1 DMSO:water) were added to samples containing different concentrations of irinotecan from 0.5 µM to 8 µM in 3:1 methanol:plasma (irinotecan batch solution 3.1 mM in water: 2.1 mg, 3.1 µmol in 1 mL). The fluorescence emission of irinotecan was measured at 430 nm before and 30 min after the addition of polymer, exciting at 360 nm with excitation and emission slits of 5 nm for 0.5 µM, 1 µM, 2 µM and 1.5 µM drug, while excitation slit of 5 nm and emission slit of 2.5 nm were used for 3 µM, 4 µM and 8 µM drug concentrations. Fluorescence emission spectra were also recorded between 370 nm and 600 nm.

Validation Test of MIP 1.7

1 mg/mL solution of MIP **1.7** in DMSO was diluted to a final 60 μg/mL concentration in 4:1 DMSO:water. In order to obtain the calibration curve, 400 μL of the 60 μg/mL MIP solution were titrated with increasing amounts of sunitinib (from 1 μM to 154 μM) with a 4 mM and a 400 μM sunitinib mother solution in 4:1 DMSO:water.
The spiked samples at 5 μM, 50 μM and 80 μM sunitinib were made diluting the 4 mM or the 400 μM sunitinib solution in PBS with 50 mg/mL HSA or in plasma. After the addition of 4 volumes of DMSO and the MIP (the final polymer concentration was 60 μg/mL), the fluorescence emission was measured at 456 nm after excitation at 327 nm with excitation and emission slits of 5 nm.

A fluorescent Polymer for Irinotecan

Synthesis of *2-allyl-6-bromo-1H-benzo[de]isoquinoline-1,3(2H)-dione* (16b)

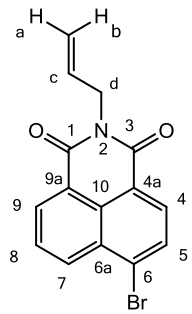

312 mg (1.13 mmol, 1 eq) of 6-bromobenzo[de]isochromene-1,3-dione (**16**) were dissolved in 7 mL of ethanol and the resulting solution was heated up to 55 °C under continuous stirring; at this temperature 89 μL of allyl amine (68 mg, 1.19 mmol, 1 eq) were added. The mixture was refluxed for four hours and the reaction was monitored by TLC using a 1:1 dichloromethane:ethyl acetate mixture as mobile phase. After cooling at room temperature, the solid was filtered, washed with ethanol and dried under vacuum. 239 mg (yield 67%) of light brown powder were obtained.
ESI-MS (m/z): 338.4 and 340.3 $[M+Na]^+$, 355.2 and 357.2 $[M+K]^+$
^{1}H-NMR (δ, ppm, 500 MHz, $CDCl_3$): 4.79 (d, ^{3}J= 6 Hz, 2H, CH_2-**d**), 5.21 (dd, $^3J_{cis}$= 10.2 Hz, 1H, ^{4}J= 1.2 Hz, CH_2-**1b**), 5.32 (dd, ^{4}J= 1.4 Hz, 1H, $^3J_{trans}$= 17.2 Hz, CH_2-**1a**), 5.98 (m, 1H, CH-**c**), 7.85 (t, $^3J_{orto}$= 7.4 Hz, $^3J_{orto}$= 7.4 Hz, 1H, CH-**8**), 8.04 (d, 1H, $^3J_{orto}$= 8 Hz, CH-**5**), 8.42 (d, $^3J_{orto}$= 8 Hz, 1H, CH-**4**), 8.57 (d, $^3J_{orto}$= 8.5 Hz, 1H, CH-**7**), 8.66 (d, $^3J_{orto}$ = 7.3 Hz, 1H, CH-**9**)

^{13}C-NMR (δ, ppm, 500 MHz, $CDCl_3$): 42.68 (1C, CH_2-**d**), 117.97 (1C, CH_2-**ab**), 122.30 e 123.17 (2C, C-**6a**, **10**), 128.25 (1C, CH-**8**), 129.21, 130.55 (2C, C-**4a**, **9a**), 130.83 (1C, C-**6**), 131.28 (1C, CH-**4**), 131.50 (1C, CH-**5**), 132.07 (1C, CH-**c**), 132.32 (1C, CH-**9**), 133.54 (1C, CH-**7**), 163.47, 163.49 (2C, C-**1**, **3**)

Synthesis of *2-allyl-6-((3-aminoethyl)amino)-1H-benzo[de]isoquinoline-1,3(2H)-dione* (16c)

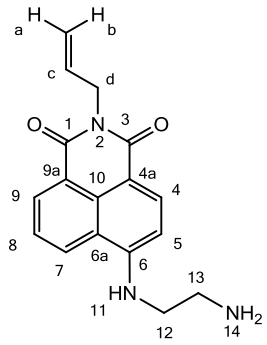

A mixture of 645 mg of (**16b**) (2.04 mmol, 1 eq), 1.63 mL of ethylene diamine (1.47 g, d=0.90 g/mL, 24.5 mmol, 12 eq) and 40 mL of ethanol was heated under reflux. The reaction was monitored by TLC using a 1:1 dichloromethane:ethyl acetate mixture as mobile phase. After 20, 23, 42 and 46 hours, further three equivalents of ethylene diamine were added. 66 hours were required to fully complete the reaction. After this time the solvent was removed under reduced pressure to obtain a red oil. 60 mL of water were added to the oil and the mixture was cooled overnight at 4 °C. The resulting solid was filtered, washed with cool water and dried at 60 °C for two days. 553 mg of pure **16c** were obtained as red solid (yield 92%).

ESI-MS (m/z): 296.4 $[M+H]^+$

^{1}H-NMR (δ, ppm, 500 MHz, $CDCl_3$): 3.18 (s, 2H, CH_2-**13**), 3.41 (d, ^{3}J= 4 Hz, 2H, CH_2-**12**), 4.79 (d, ^{3}J= 4Hz, 2H, CH_2-**d**), 5.18 (d, $^3J_{cis}$= 10 Hz, 1H, CH_2-**b**), 5.29 (d, $^3J_{trans}$= 17 Hz, 1H, CH2-**a**), 6.00 (m, 1H, CH-**c**), 6.19 (bbd, 1H, NH-**11**), 6.705 (d, ^{3}Jorto= 8.4 Hz, 1H, CH-**5**), 7.62 (t, $^3J_{orto}$= 7.6 Hz, 1H, CH-**8**), 8.18 (d, $^3J_{orto}$= 8.3 Hz, 1H, CH-**7**), 8.46 (d, $^3J_{orto}$= 8.2 Hz, 1H, CH-**4**), 8.59 (d, 1H, 3Jorto= 7.1 Hz, CH-**9**)

^{13}C-NMR (δ, ppm, 500 MHz, $CDCl_3$): 40.30 (1C, CH_2-**13**), 42.31 (1C, CH_2-**d**), 44.99 (1C, CH_2-**12**), 104.62 (1C, CH-**5**), 110.29 (1C, C-**6a**), 117.12 (1C, CH_2-**ab**), 120.65 (1C, C-**10**), 123.16 (1C, C-**4a/9a**), 124.85 (1C, CH-**8**), 126.49 (1C, CH-**7**), 130.06 (1C, C-**4a/9a**), 131.42 (1C, CH-**9**), 132.87 (1C, CH-**c**), 134.81 (1C, CH-**4**), 149.93 (1C, C-**6**), 164.03, 164.61 (2C, C-**1**, **3**)

Synthesis of MIP

30 mg of functional monomer **16c** (100 μmol, 30% in mol) were dissolved in 6.9 mL of DMSO with 41 mg of irinotecan hydrochloride (60 μmol) and stirred for 40 min. After this time, ethylene glycol dimethacrylate (EGDMA) (44 μL, 233 μmol, 70% in mol) and AIBN (17 mg, 102 μmol) were added. The monomer concentration C_M was fixed at 1% in weight respect to the weight of DMSO. The mixture was transferred in a crimp cap Wheaton vial that was first left under vacuum and after flushed with argon alternatively for 4 times. The polymerization occurs heating at 70°C for 4 days. The resulting clear solution was dialyzed fist in 7:3 methanol:acetic acid mixture and after in water milliQ. After freeze-drying a yellow fluffy polymer was obtained (58.3 mg, yield 77%)(MIP 4.16). A non imprinted polymer was synthesized having the same composition but synthesised in the absence of irinotecan in the polymerization mixture (32.2 mg, yield 42%).

Fluorescence Titration of MIP 4.16

1 mg of MIP 4.16 was dissolved in 1 mL of DMSO and the resulting solution was diluted in 3:1 methanol:plasma to the 60 μg/mL solution. 400 μL of the 60 μg/mL MIP solution were titrated with increasing concentrations of irinotecan from 20 nM to 100 μM, using a mother irinotecan solution in 3:1 methanol:water mixture (3.2 mg, 4.7 μmol in 1.2 mL). The emission intensity of polymer at 525 nm was measured when excited at 448 nm, using excitation slit of 10 nm and emission slit of 5 nm.

6.4 A FRET-based MIP

Synthesis of the Functional Monomer

2,5-dioxopyrrolidin-1-yl acrylate
(N-acryloxysuccinimide; **9**)

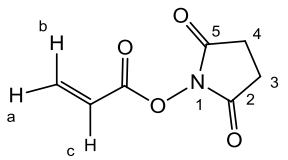

1.0 g (8.7 mmol) of N-hydroxysuccinimide was dissolved in 13 mL of DCM and 1.2 mL (9.0 mmol) of triethylamine. After cooling at 0 °C, 0.75 mL (9.2 mmol) of acryloyl chloride were added dropwise into the solution. The mixture was stirred for 20 min at 0

°C and for 1 h at room temperature. The salt created during the reaction as side product was removed by filtration, while the solution was washed twice with 8 mL of cold water and 8 mL of cold brine. The organic phase was dried with anhydrous sodium sulphate and concentrated by vacuum to a 1 mL volume. The concentrated solution was cooled at 0 °C, diluted with 2.5 mL of 6:1 hexane:ethyl acetate mixture and stirred for 20 min. The white precipitate was collected by filtration and dried under vacuum (0.95 g, yield 68 %).

MS-ESI (m/z): 192 $[M+Na]^+$

^{1}H-NMR (500 MHz, $CDCl_3$, 25 °C, ppm) δ = 2.85 (s, 4H, CH_2-**3**, **4**), 6.17 (d, ^{3}J=11 Hz, 1H, CH-**a**), 6.32 (dd, 1H, ^{3}J=11 Hz, ^{3}J=18 Hz, CH-**c**), 6.70 (d, ^{3}J=18 Hz, 1H, CH-**b**).

^{13}C-NMR (500 MHz, $CDCl_3$, 25 °C, ppm) δ = 25.83 (2C, CH_2-**3**, **4**), 122.94 (1C, CH-**c**), 136.11 (1C, CH_2-**a, b**), 160.96 (2C, C-**2**, **5**), 168.87 (1C, CH_2=CH-**C**=O-N).

5-((2-acryloylaminoethyl)amino)naphthalene-1-sulfonic acid

(vinyl-EDANS; **10**)

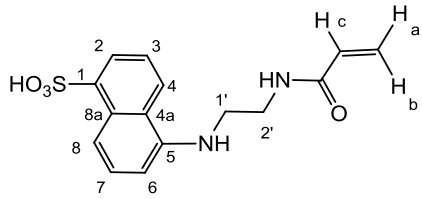

EDANS (50 mg, 0.18 mmol), sodium hydrogen carbonate (420 mg, 5.0 mmol) and N-hydroxy succinimidoyl acrylate (38 mg, 0.22 mmol) were dissolved in 25 mL of water. The mixture was left at room temperature under stirring for 24 h. After this time 25 mL of acetone were added, the resulting precipitates were removed by filtration and the solvents were removed under vacuum. The resulting crude was purified by flash chromatography (6:4 DCM:methanol) to obtain 52 mg of a dark yellow solid (yield 86 %).

MS-ESI (m/z): 319 $[M-H]^-$

^{1}H-NMR (500 MHz, $[D_6]$DMSO, 25 °C, ppm) δ = 3.22 (t, ^{3}J=6 Hz, 2H, CH_2-**1'**), 3.49 (t, ^{3}J=6 Hz, 2H, CH_2-**2'**), 5.60 (dd, $^3J_{cis}$=10 Hz, ^{2}J=2 Hz, 1H, CH_2-**a**), 5.75 (s, 1H, SO_3**H**), 6.13 (dd, $^3J_{trans}$=17 Hz, ^{2}J=2 Hz, 1H, CH_2-**b**), 6.20 (t, ^{3}J=5 Hz, 1H, Ar-N**H**), 6.25 (dd, $^3J_{trans}$=17 Hz, $^3J_{cis}$=10 Hz, CH-**c**), 6.56 (d, ^{3}J=8 Hz, 1H, CH-**2**), 7.25 (dd, ^{3}J=8 Hz, 1H, CH-**3**), 7.31 (dd, ^{3}J=7 Hz, ^{3}J=8 Hz, 1H, CH-**7**), 7.91 (d, ^{3}J=6 Hz, 1H, CH-**6**), 8.09 (d, 1H, ^{3}J=8 Hz, CH-**4**), 8.10 (d, 1H, ^{3}J=8 Hz, CH-**8**), 8.45 (t, ^{3}J=5 Hz, 1H, N**H**-CO).

^{13}C-NMR (500 MHz, $[D_6]$DMSO, 25 °C, ppm) δ = 38.12 (1C, CH_2-**2'**), 43.51 (1C, CH_2-**1'**), 102.40 (1C, CH-**2**), 115.66 (1C, CH-**8**), 122.10 (1C, CH-**7**), 122.60 (1C, CH-**4**), 124.14 (1C,

CH-**6**), 125.18 (1C, CH_2-**a**, **b**), 126.03 (1C, CH-**3**), 129.41 (C, C-**4a**), 131.6 (1C, CH-**c**), 131.76 (1C, C-**5**), 135.09 (1C, C-**8a**), 164.79 (1C, **C**=O).
IR (cm^{-1}): 1620 (N-H), 1654 (C=O), 2916.4 (C-H).

Paclitaxel Modification with the DABCYL dye

Tert-butyl 5-aminopentylcarbamate
(Boc-cadaverine; **11**)

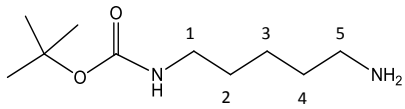

3.0 g (5.3 eq, 29.4 mmol) of 1,5-diaminopentane were dissolved in 40 mL of DCM. Maintaining the temperature at 0°C, a solution of di-tert-butyl dicarbonate in dichloromethane (1eq, 5.5 mmol, 1.2 g in 20 mL) was added drop by drop. The solution was stirred for 1 h at 0°C and for 1 h at room temperature. The byproduct generated during the reaction in the form of a yellow powder was removed by filtration, while the remaining solution was evaporated under reduced pressure to obtain a yellow oil. The product was dissolved in 20 mL of ethyl acetate and washed with saturated sodium bicarbonate and brine. After drying on anhydrous sodium sulphate, the filtered solution was dried under reduced pressure to obtain a yellow oil (1.04 g, yield 94%).
MS-ESI (m/z): 203.1 $[M+H]^+$
^{1}H-NMR (500 MHz, $CDCl_3$, 25 °C, ppm): δ= 1.30-1.36 (m, 2H, CH_2- **3**), 1.44 (s, 11H, N**H**$_2$ and OC(C**H**$_3$)$_3$), 1.46-1.49 (m, 2H, CH_2- **4**), 1.49-1.56 (m, 2H, CH_2- **2**), 2.68 (t, J^3=7 Hz, 2H, CH_2-**5**), 3.10 (m, 2H, CH_2- **1**), 4.56 (s, 1H, N**H**).
^{13}C-NMR (500 MHz, $CDCl_3$, 25 °C, ppm): δ= 24.20 (1C, CH_2- **3**), 28.56 (3C, CH_3, OC(**C**H_3)$_3$), 30.07 (1C, CH_2- **2**), 33.42 (1C, CH_2- **4**), 40.54 (1C, CH_2- **1**), 42.16 (1C, CH_2-**5**), 79.18 (1C, O**C**$(CH_3)_3$), 156.16 (1C, **C**=O).
IR (cm^{-1}): 3335 (N-H), 1697 (C=O).

(E)-tert-butyl (5-(4-((4-(dimethylamino)phenyl)diazenyl)benzamido)pentyl)carbamate
(DABCYL-Boc-cadaverine; **12b**)

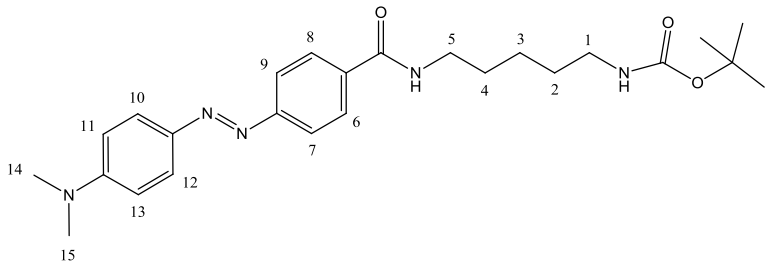

To 50 mg (1 eq, 0.14 mmol) of DABCYL-Osu dissolved in 3.2 mL of DMF, a solution of 33 mg (1.2 eq, 0.2 mmol) of tert-butyl 5-aminopentylcarbamate in 500 µL of DMF was added. After addition of 28.2 µL (1.2 eq, 0.2 mmol) of DIEA the solution was kept overnight at room temperature. The progress of the reaction was followed by TLC using 8:2 DCM:MeOH as mobile phase. After this time DCM was added and the organic phase was washed with water and with brine. The organic layer was dried and evaporated to obtain the product as a red solid (yield 90%).
MS-ESI (m/z): 476 $[M+Na]^+$
^{1}H-NMR (500 MHz, $CDCl_3$, 25 °C, ppm): δ= 1.42 (s, 9H, OC(C**H**$_3$)$_3$), 1.43 (m, 2H, CH_2- **3**), 1.54 (m, 2H,CH_2-**2**), 1.66 (m, 2H, CH_2-**4**), 3.11 (s, 6H, N(C**H**$_3$)$_2$), 3.13 (m, 2H, CH_2-**1**), 3.47 (t, ^{3}J=6 Hz, 2H, CH_2-**5**), 4.59 (s, 1H, N**H**COOC(CH$_3$)$_3$), 6.28 (s, 1H, NHCOAr), 6.77 (d, ^{3}J=9 Hz, 2H, CH-**11**, **13**), 7.85 (m, 4H, CH-**6**, **7**, **8**, **9**), 7.91 (d, ^{3}J=9 Hz, 2H, CH-**10**, **12**).
^{13}C-NMR (500 MHz, $CDCl_3$, 25 °C, ppm): δ=23.72 (1C, CH_2-**3**), 28.49 (3C, C(**C**H$_3$)$_3$), 29.05 (1C, CH_2-**4**), 29.56 (1C, CH_2- **2**), 40.03 (1C, CH_2-**5**), 40.21 (1C, CH_2-**1**), 40.5 (2C, CH_3, N(**C**H$_3$)$_2$), 111.58 (2C, CH-**11**, **13**), 122.07 (2C, CH-**10**, **12**), 127.84 (4C, CH-**6**,**7**,**8**,**9**).
IR (cm^{-1})= 1629.3 (C=O), 1686.7 (C=O), 2931 (C-H), 3315.9 (N-H amides).

(E)-N-(5-aminopentyl)-4-((4-(dimethylamino)phenyl)diazenyl)benzamide
(DABCYL-cadaverine; **12c**)

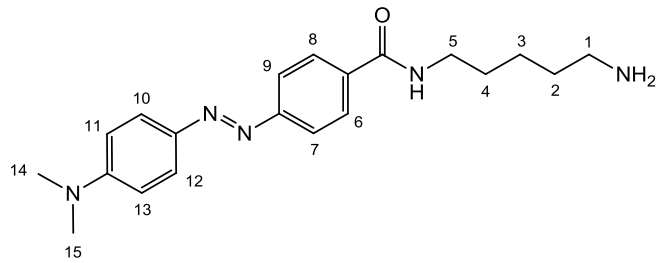

20 mg of compound **12b** were dissolved in 5 mL of a 20% solution of TFA in DCM and the mixture was kept at room temperature overnight. After removal of the solvent, the resulting crude was dissolved in DCM and washed with saturated sodium hydrogen carbonate and dried with Na_2SO_4 anhydrous. Finally, the solvent was removed to give the compound **12c** as an orange solid (93%).

MS-ESI (m/z): 354 $[M+H]^+$

^{1}H-NMR (500 MHz, CD_3OD, 25°C, ppm): δ= 1.49 (m, 2H, CH_2-**3**), 1.72 (m, 4H, CH_2-**2**, **4**), 2.94 (t, ^{3}J=7 Hz, 2H, CH_2-**1**), 3.12 (s, 6H, CH_3-**14**, **15**), 3.43 (t, ^{3}J=7 Hz, 2H, CH_2-**5**), 6.86 (d, ^{3}J=9, 2H, CH-**11**, **13**), 7.88 (m, 6H, CH-**6**, **7**, **8**, **9**, **10**, **12**).

^{13}C-NMR (500 MHz, CD_3OD, 25°C, ppm): δ= 23.74 (1C, CH_2-**3**), 28.53 (1C, CH_2-**4**), 28.94 (1C, CH_2-**2**), 38.89 (2C, CH_3-**14**, **15**), 39.37 (1C, CH_2-**5**), 40.23 (1C, CH_2-**1**), 111.32 (2C, CH-**11**, **13**), 121.61 (2C, CH-**7**, **9**), 125.18 (2C, CH-**10**, **12**), 128.02 (2C, CH-**6**, **8**), 135.2 (1C, **C**-C=O), 141.07 (1C, $N(CH_3)_2$-Ar-**C**-N=N), 145.23 (1C, $N(CH_3)_2$-**C**-Ar), 155.57 (1C, N=N-**C**-Ar-C=O), 168.74 (1C, **C**=O).

IR (cm^{-1})= 1626.7 (C=O), 2920.5 (C-H), 3416.2 (N-H).

2'-tert-Butyl-Dimethylsilyl-Paclitaxel (**3b**)

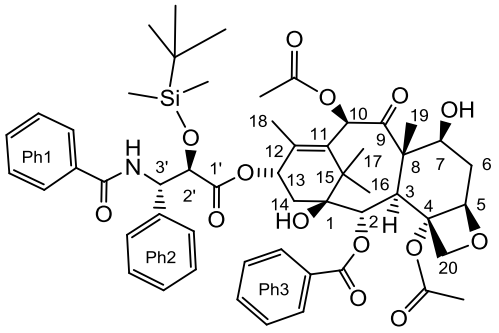

570 mg (3.8 mmol) of tert-Butyl-dimethylsilyl chloride and 520 mg (7.6 mmol) of imidazole were dissolved in 1 mL of anhydrous DMF. 500 µL of the resulting light blue solution were added to 100 mg (0.1 mmol) of paclitaxel. The pale yellow solution was stirred under a flux of argon for 1h. The reaction was followed by TLC with 1:1 ethyl acetate:hexane as mobile phase. Finally 2 mL of DCM were added to the solution and the organic phase was washed with brine and dried. The solvent was removed under reduced pressure to obtain 106 mg of a white powder (yield 91%).

MS-ESI (m/z): 990 $[M+Na]^+$

^{1}H-NMR (500 MHz, $CDCl_3$, 25 °C, ppm): δ= -0.29 (s, 3H, C**H**$_3$Si), -0.01 (s, 3H, C**H**$_3$Si), 0.8 (s, 9H, (C**H**$_3$)$_3$CSi), 1.13 (s, 3H, CH_3-**16**), 1.24 (s, 3H, CH_3-**17**), 1.61 (s, O**H**-C1), 1.69 (s, 3H, CH_3-**19**), 1.88 (m, 1H, CH-**6$_b$**), 1.90 (s, 3H, CH_3-**18**), 2.13 (m, 1H, CH-**14$_a$**), 2.23 (s, 3H,

C**H**$_3$(CO)C-10), 2.40 (m, 1H, CH-**14$_b$**), 2.57 (m, 1H, CH-**6$_a$**), 2.63 (s, 3H, C**H**$_3$(CO)C-4), 3.82 (d, ^{3}J=7 Hz, 1H, CH-**3**), 4.22 (d, ^{2}J=9 Hz, 1H, CH-**20$_a$**), 4.33 (d, ^{2}J=9 Hz, 1H, CH-**20$_b$**), 4.44 (dd, ^{3}J=10 Hz, ^{4}J=7 Hz, 1H, CH-**7**), 4.66 (d, ^{4}J=2 Hz, 1H, CH-**2'**), 4.98 (dd, ^{3}J=10 Hz, ^{4}J= 2 Hz, 1H, CH-**5**), 5.71 (m, 2H, CH-**3'**, CH-**2**), 6.29 (m, 2H, CH-**10**, CH-**13**), 7.04 (d, ^{3}J=9 Hz, 1H, N**H**), 7.30 (m, 1H, C**H**$_p$-Ph2), 7.32 (m, 2H, C**H**$_m$-Ph3), 7.40 (m, 4H, C**H**$_m$-Ph2, C**H**$_m$-Ph1), 7.5 (m, 1H, C**H**$_p$-Ph3), 7.52 (m, 2H, C**H**$_o$-Ph2), 7.60 m, 1H, C**H**$_p$-Ph1), 7.74 (m, 2H, C**H**$_o$-Ph3), 8.14 (m, 2H, C**H**$_o$-Ph1)

^{13}C-NMR (500 MHz, CDCl$_3$, 25 °C, ppm): δ= -5.12 (1C, C**H**$_3$Si), -5.90 (1C, C**H**$_3$Si), 9.73 (1C, CH$_3$-**19**), 15.18 (1C, CH$_3$-**18**), 20.68 (1C, **C**H$_3$(CO)C-10), 22.42 (1C, CH$_3$-**16**), 23.22 (1C, **C**H$_3$(CO)C-4), 25.69 (3C, (**C**H$_3$)$_3$CSi), 26.89 (1C, CH$_3$-**17**), 35.75 (1C, CH$_2$-**14**), 35.92 (1C, CH$_2$-**6**), 45.65 (1C, CH-**3**), 55.71 (1C, CH-**3'**), 71.38 (1C, CH-**13**), 72.16 (1C, CH-**7**), 75.05 (1C, CH-**2**), 75.49 (1C, CH-**2'**), 75.78 (1C, CH-**10**), 76.70 (1C, CH-**20**), 84.58 (1C, CH-**5**), 126.60 (2C, **C**H$_m$-Ph3), 127.09 (2C, **C**H$_o$-Ph3), 128.19 (1C, **C**H$_p$-Ph2), 128.89 (2C, **C**H$_m$-Ph2), 128.91 (2C, **C**H$_m$-Ph1), 130.40 (2C, **C**H$_o$-Ph1), 131.87 (1C, **C**H$_p$-Ph3), 133.76 (1C, **C**H$_p$-Ph1).

IR (cm^{-1}): 1243.2 (C-O), 1653 (C=O), 1724.4 (C=O), 2955.7 (C-H), 2977.6 (C-H), 3442.6 (O-H), 3501 (O-H).

2'-tert-Butyl-Dimethylsilyl-Paclitaxel-7-hemisuccinate (**3c**)

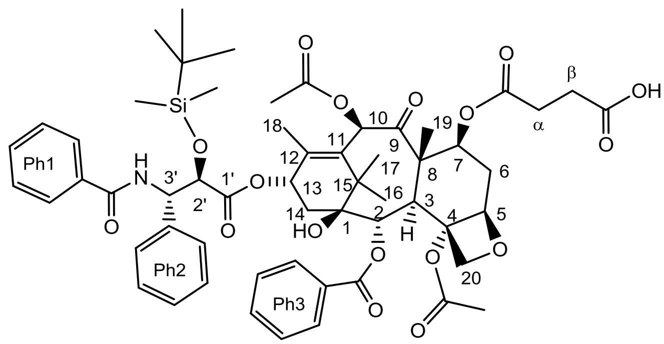

13 mg (1.23 eq, 0.127 mmol) of succinic anhydride, 100 mg (1eq, 0.103 mmol) of 2'-tertbuthyl-dimethylsilyl-paclitaxel and 126 mg (10 eq, 1.032 mmol) of DMAP were dissolved in 4 mL of anhydrous toluene under an argon atmosphere. The mixture was kept at 90°C for two days.

The reaction was followed by TLC using a 9:1 DCM:MeOH mixture.

After cooling to room temperature, 10 mL of 0.2% hydrochloric acid were added. The solution was extracted with DCM, the organic phase was dried and evaporated to give 93 mg of pure product (yield 84%).

MS-ESI (m/z): 1090 [M+Na]$^+$

^{1}H-NMR (500 MHz, $CDCl_3$, 25 °C, ppm): δ= -0.30 (s, 3H, C**H**$_3$Si), -0.03 (s, 3H, C**H**$_3$Si), 0.80 (s, 9H, (C**H**$_3$)$_3$CSi), 1.16 (s, 3H, CH$_3$-**16**), 1.24 (s, 3H, CH$_3$-**17**), 1.76 (br, 1H, O**H**-C1), 1.82 (s, 3H, CH$_3$-**19**), 1.85 (m, 1H, CH-**6$_b$**), 1.97 (s, 3H, CH$_3$-**18**), 2.15 (s, 3H, C**H**$_3$(COO)C-10), 2.18 (m, 1H, CH-**14$_b$**), 2.41 (m, 1H,CH-**14$_a$**), 2.57 (s, 3H, C**H**$_3$(COO)C-4), 2.62 (m, 4H, CH$_2$-**α, β**), 2.67 (m, 1H, CH-**6$_a$**), 3.96 (d, ^{3}J=7 Hz, 1H, CH-**3**), 4.21 (d, ^{2}J=9 Hz, 1H, CH-**20$_a$**), 4.34 (d, ^{2}J=9 Hz, 1H, CH-**20$_b$**), 4.67 (d, ^{4}J=2 Hz, 1H, CH-**2'**), 4.98 (d, ^{3}J=9 Hz, 1H, CH-**5**), 5.62 (dd, ^{3}J=10 Hz, ^{4}J=7 Hz, 1H, CH-**7**), 5.69 (d, ^{3}J=6 Hz, 1H, CH-**2**), 5.72 (dd,^{3}J=8 Hz, ^{4}J=2 Hz, 1H, CH-**3'**), 6.27 (m, 2H, CH-**10**,**13**), 7.32 (m, 1H, C**H**$_p$-Ph2), 7.43 (m, 4H, C**H**$_m$-Ph2, C**H**$_m$-Ph3), 7.54 (m, 5H, C**H**$_m$-Ph1, C**H**$_o$-Ph2, C**H**$_p$-Ph3), 7.60 (m, 1H, C**H**$_p$-Ph1), 7.75 (m, 2H, C**H**$_o$-Ph3), 8.14 (m, 2H, C**H**$_o$-Ph1)

^{13}C-NMR (500 MHz, $CDCl_3$, 25 °C, ppm): δ= -5.87 (1C, **C**H$_3$Si), 10.69 (1C, CH$_3$-**19**), 14.80 (1C, CH$_3$-**18**), 20.82 (1C, **C**H$_3$(COO)C-10), 21.27 (1C, CH$_3$-**16**), 23.10 (1C, **C**H$_3$(COO)C-4), 25.48 (3C, (**C**H$_3$)$_3$CSi), 26.39 (1C, CH$_3$-**17**), 29.01 (1C, CH$_2$-**α**), 29.69 (1C, CH$_2$- **β**), 33.12 (1C, CH$_2$-**6**), 35.52 (1C, CH$_2$-**14**), 46.78 (1C, CH-**3**), 55.68 (1C, CH-**3'**), 71.21 (1C, CH-**13**), 71.56 (1C, CH-**7**), 74.43 (1C, CH-**2**), 74.96 (1C, CH-**2'**), 75.33 (1C, CH-**10**), 76.29 81C, CH-**20**), 84.08 (1C, CH-**5**), 126.32 (2C, **C**H$_m$-Ph3), 127.15 (2C, **C**H$_o$-Ph3), 128.11 (1C, **C**H$_p$-Ph2), 128.90 (6C, **C**H$_o$-Ph2, **C**H$_m$-Ph2, **C**H$_m$-Ph1), 130.36 (2C, **C**H$_o$-Ph1), 131.96 (1C, **C**H$_p$-Ph3), 133.87 (1C, **C**H$_p$-Ph1).

IR (cm^{-1}): 1242.3 (C-O), 1653.2 (C=O), 1734 (C=O), 2951.5 (C-H), 3447.1 (O-H).

2'-tert-Butyl-Dimethylsilyl-Paclitaxel-7-[3-(5-(4-(4 (dimethylamino) styryl) benzamido) pentylcarbamoyl)] propanoate (**3d**)

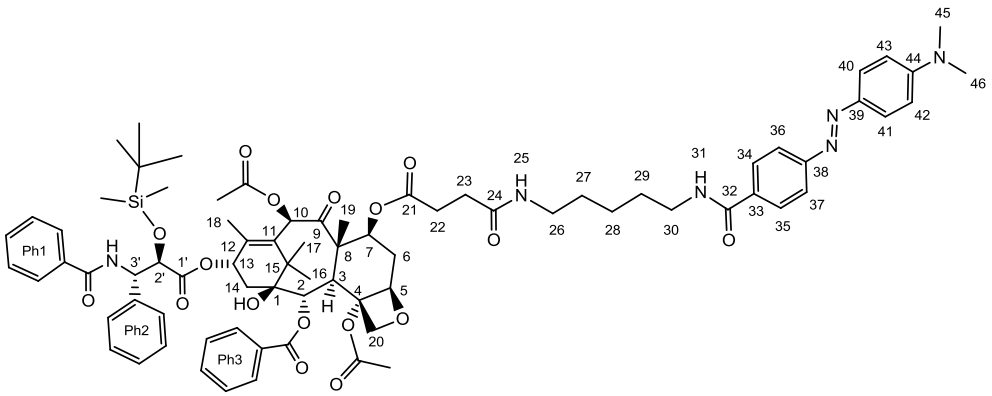

20 mg (1 eq, 18.7 µmol) of compound **3c** were dissolved in 1.5 mL of anhydrous acetonitrile and 0.5 mL of triethylamine were added. After cooling at 0°C, 3.8 mg (1.5 eq, 28.1 µmol) of HOBt and 8.0 mg (2.7 eq, 51.5 µmol) of EDC-Cl were added and the solution was stirred at 0°C for 30 min.

After this time, 9 mg (1.4 eq, 26.2 µmol) of compound **12c** in 4 mL of acetonitrile were added and the mixture was stirred for 30 min at 0°C and for 4 days at room temperature.

5 mL of DCM were added and the organic phase was washed first with 5 mL of 0.1% sodium hydroxide and then twice with 5 mL of brine. Evaporation of the solvent gave an orange oil. The crude was purified by flash-chromatography with a 9:1 DCM – methanol mobile phase on silica. 17 mg of compound **3d** (65%) were obtained.

MS-ESI (m/z): 1426 $[M+Na]^+$

^{1}H-NMR (500 MHz, $CDCl_3$, 25 °C, ppm): δ= -0.3 (s, 3H, C**H**$_3$Si), 0.02 (s, 3H, C**H**$_3$Si), 0.80 (s, 9H, (C**H**$_3$)$_3$CSi), 1.16 (s, 3H, CH_3-**16**), 1.25 (s, 3H, CH_3-**17**), 1.43 (m, 2H, CH_2-**28**), 1.56 (m, 2H, CH_2-**27**), 1.66 (m, 2H, CH_2-**29**), 1.67 (s, 3H, CH_3-**19**), 1.81 (s, 3H, CH_3-**18**), 1.88 (m, 1H, CH_2-**6a/b**), 2.42 (m, 2H, CH_2-**14**), 2.56 (m, 3H, C**H**$_3$(COO)C-4), 2.62 (m, 1H, CH_2-**6a/b**), 2.66 (m, 4H, CH_2-**22**, **23**), 3.10 (s, 6H, N(C**H**$_3$)$_2$), 3.31 (m, 2H, CH_2-**26**), 3.48 (m, 2H, CH_2-**30**), 3.96 (m, 1H, CH-**3**), 4.20 (d, ^{2}J=9 Hz, 1H, CH_2-**20$_b$**), 4.33 (d, ^{2}J=9 Hz, 1H, CH_2-**20$_a$**), 4.69 (d, ^{4}J=2 Hz, 1H, CH-**2'**), 4.96 (t, ^{3}J=9 Hz, 1H, CH-**5**), 5.61 (m, 1H, CH-**7**), 5.70 (m, 2H, CH-**3'**, CH-**2**), 5.91 (t, ^{3}J=6 Hz, 1H, NH-**25**), 6.25 (m, 2H, CH-**10**, CH-**13**), 6.43 (m, 1H, NH-**31**), 6.74 (m, 2H, CH- **42**, **43**), 7.07 (d, ^{3}J=8 Hz, N**H**-CO-Ph1), 7.32 (m, 2H, C**H**$_p$-Ph2), 7.41 (m, 4H, C**H**$_m$-Ph2, C**H**$_m$-Ph3), 7.51 (m, 5H, C**H**$_p$-Ph3, C**H**$_o$-Ph2, C**H**$_m$-Ph1), 7.61 (m, 1H, C**H**$_p$-Ph1), 7.75 (m, 2H, C**H**$_o$-Ph3), 7.87 (m, 6H, CH-**34**, **35**, **36**, **37**, **40**, **41**), 8.11 (m, 2H, C**H**$_o$-Ph1).

^{13}C-NMR (500 MHz, $CDCl_3$, 25 °C, ppm): δ= -5.67 (1C, **C**H$_3$Si), -5.087 (1C, **C**H$_3$Si), 11.06 (1C, CH_3-**18**), 21.64 (1C, CH_3-**16**), 23.06 (1C, **C**H$_3$(COO)C-4), 23.57 (1C, CH_3-**19**), 24.07 (1C, CH_2-**28**), 25.68 (3C, (**C**H$_3$)$_3$CSi), 28.09 (1C, CH-**6a/b**), 29.26 (1C, CH_2-**29**),29.57 (1C, CH_3-**17**), 29.90 (1C, CH_2-**27**), 30.03 (1C, CH_2-**22**, **23**), 31.19 (1C, CH_2-**14**), 33.46 (1C, CH-**6a/b**), 39.27 (1C, CH_2-**26**), 40.13 (1C, CH_2-**30**), 40.49 (3C, N(**C**H$_3$)$_2$), 43.52 (1C, C-**15**), 47.21 (1C, CH-**3**), 55.91 (1C, CH-**3'**), 71.5 (1C, CH-**10**), 71.98 (1C, CH-**7**), 74.9 (1C, CH-**2**), 75.44 (1C, CH-**2'**), 75.62 (1C, CH-**13**), 76.69 (1C, CH_2-**20**), 84.24 (1C, CH-**5**), 111.95 (1C, CH-**42**, **43**), 122.5 (2C, CH-**36**, **37**), 123.1 (3C, **C**H$_p$-Ph3, **C**H$_o$-Ph2), 125.67 (2C, CH-**40**, **41**), 126.72 (1C, **C**H$_p$-Ph2), 127.3 (1C, **C**H$_o$-Ph3), 128.11 (2C, CH-**34**, 35), 129.06 (4C, **C**H$_m$-Ph2, **C**H$_m$-Ph3), 129.30 (1C, **C**H$_m$-Ph1), 130.57 (2C, **C**H$_o$-Ph1), 132.69 (1C, C-**11**), 133.9 (1C, **C**H$_p$-Ph1), 134.31 (1C, **C**-Ph3), 134.81 (1C, **C**-Ph2), 134.95 (1C, **C**-Ph1), 135.37 (1C, C-**33**), 138.51 (1C, CH-**12**), 152.86 (1C, C-**44**), 155.28 (1C, C-**38**), 167.1 (1C, **C**=O-Ph3), 167.25 (1C, **C**=O-Ph1), 167.6 (1C, C-**32**), 170.04 (1C, **C**OO-C-10), 170.49 (**C**OO-C-4), 172.11 (1C, C-**21**), 172.23 (1C, C-**24**), 172.34 (1C, C-**1'**), 203.9 (1C, C-**9**).

IR (cm^{-1}): 1621.2 (C=O), 1725.7 (C=O), 2924.9 (C-H), 2956.2 (C-H), 3347.4 (O-H, N-H).

Paclitaxel-7-[3-(5-(4-(4(dimethylamino)styryl)benzamido)pentylcarbamoyl)] propanoate

(DABCYL-paclitaxel; **3e**)

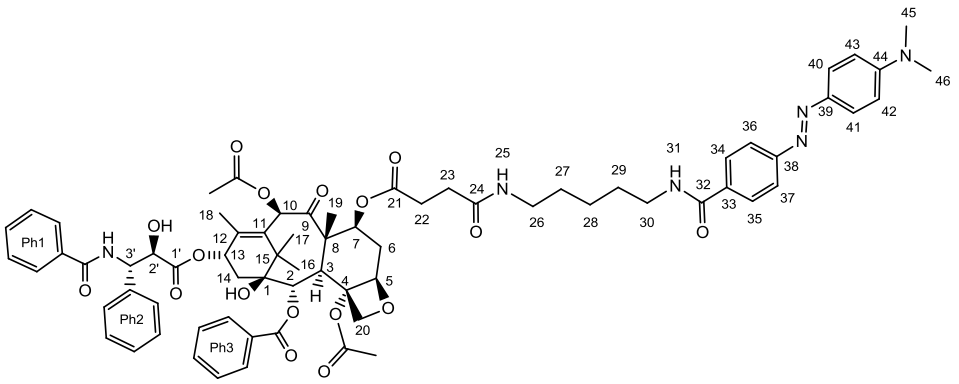

10 mg (7.12 µmol) of compound **3d** were dissolved in 2 mL of anhydrous pyridine. After cooling at 0°C, 12 drops of HF/Py were added and the mixture was stirred for 15 min at 0°C and for 22 h at room temperature. 10 mL of DCM were added in solution and the organic phase was washed twice with 2% HCl and dried with $MgSO_4$. After filtration, the solvent was evaporated to obtain 7 mg of a dark red solid (yield 80%).

MS-ESI (m/z): 1311 $[M+Na]^+$, 1323 $[M+Cl]^-$

^{1}H-NMR (500 MHz, $[D_6]$DMSO, 25 °C, ppm): δ= 0.98 (s, 3H, CH_3-**17**), 1.04 (s, 3H, CH_3-**16**), 1.41 (m, 1H, CH_2-**6b**), 1.46 (m, 2H, CH_2-**28**), 1.51 (m, 4H, CH_2-**27**, **29**), 1.65 (s, 3H CH_3-**19**), 1.74 (s, 3H, CH_3-**18**), 1.77 (m, 1H, CH_2-**14b**), 1.88 (m, 1H, CH_2-**14a**), 2.11 (s, 3H, C**H**$_3$(COO)C-10), 2.23 (s, 3H, C**H**$_3$(COO)C-4), 2.3 (m, 1H, CH_2-**6a**), 2.38 (m, 4H, CH_2-**22**, **23**), 3.07 (s, 6H, CH_3-**45**, **46**), 3.49 (m, 4H, CH_2-**26**, **30**), 3.70 (d, ^{2}J=7 Hz, 1H, CH-**3**), 4.04 (s, 2H, CH_2-**20**), 4.59 (d, ^{3}J=8 Hz, 1H, CH-**2'**), 4.70 (s, 1H, O**H**), 4.96 (d, ^{3}J=9 Hz, CH-**5**), 5.41 (m, 3H, CH-**3'**, CH-**2**, CH-**7**), 5.89 (t, ^{3}J=9 Hz, 1H, CH-**13**), 6.04 (s, 1H, CH-**10**), 6.84 (m, 2H, CH-**42**, **43**), 7.22 (m, 1H, C**H**$_p$-Ph2), 7.40 (m, 4H, C**H**$_m$-Ph2, C**H**$_o$-Ph2), 7.49 (m, 2H, C**H**$_m$-Ph3), 7.55 (m, 1H, C**H**$_p$-Ph3), 7.63 (m, 2H, C**H**$_m$-Ph1), 7.71 (m, 1H, C**H**$_p$-Ph1), 7.80 (m, 4H, CH-**36**, **37**, **40**, **41**), 7.86 (m, 2H, C**H**$_o$-Ph3), 7.96 (m, 4H, C**H**$_o$-Ph1, CH-**34**, **35**), 8.52 (m, 1H, NH-**25**), 8.93 (d, ^{3}J=9 Hz, 1H, NH-**31**).

^{13}C-NMR (500 MHz, $[D_6]$DMSO, 25 °C, ppm): δ= 10.11 (1C, CH_3-**19**), 12.76 (1C, CH_3-**17**), 13.39 (1C, CH_3-**18**), 20.16 (1C, C**H**$_3$(COO)C-10), 22.32 (1C, C**H**$_3$(COO)C-4), 24.03 (1C, CH_2-**27**), 25.78 (1C, CH_3-**16**), 28.32 (1C, CH_2-**29**), 28.44 (1C, CH_2-**28**), 29.15 (1C, CH_2-**6**), 28.77 (2C, CH_2-**22**, **23**), 32.80 (2C, CH_2-**30**), 39.53 (2C, CH_3-**45**, **46**), 45.57 (1C, CH-**3**), 55.96 (1C, CH-**7**), 69.11 (1C, CH-**13**), 70.48 (1C, CH-**2**), 73.27 (1C, CH-**2'**), 73.68 (1C, CH-**3'**), 74.37 (1C, CH-**10**), 74.68 (1C, CH_2-**20**), 82.37 (1C, CH-**5**), 111.11 (2C, CH-**42**, **43**), 121.22 (2C, CH-**41**, **42**), 124.75 (2C, CH-**36**, **37**), 126.04 (2C, C**H**$_o$-Ph3), 127.54 (4C, C**H**$_m$-Ph2, CHo-Ph2), 127.92 (2C, C**H**$_m$-Ph3), 128.04 (2C, CH-**34**, **35**), 128.29 (1C, C**H**$_p$-Ph1), 128.42 (2C, C**H**$_m$-Ph1), 128.70 (1C, C**H**$_p$-Ph2), 129.20 (2C, C**H**$_o$-Ph1), 131.08 (1C, C**H**$_p$-Ph3), 132.69 (1C, C-**11**), 134.31 (1C, **C**-Ph3), 134.81 (1C, **C**-Ph2), 134.95 (1C, **C**-Ph1), 135.37 (1C, C-**33**),

138.51 (1C, CH-**12**), 152.86 (1C, C-**44**), 155.28 (1C, C-**38**), 167.1 (1C, **C**=O-Ph3), 167.25 (1C, **C**=O-Ph1), 167.6 (1C, C-**32**), 170.04 (1C, **C**OO-C-10), 170.49 (**C**OO-C-4), 172.11 (1C, C-**21**), 172.23 (1C, C-**24**), 172.34 (1C, C-**1'**), 203.9 (1C, C-**9**).
IR (cm^{-1}): 1620.9 (C=O), 1735.7 (C=O), 2924 (C-H), 2956 (C-H), 3347.8 (O-H, N-H).

^{1}H-NMR Titration

The interactions between vinyl-EDANS and the template molecule (paclitaxel or irinotecan), were investigated by ^{1}H-NMR titrations of the drug with increasing amounts of functional monomer.
Paclitaxel (4 mg, 4.69 µmol) was dissolved in 840 µL of [D_6]DMSO to obtain a final 5.58 mM concentration. To the solution different concentrations of vinyl-EDANS were added from 2.79 mM to 78.12 mM and the ^{1}H-NMR spectrum was recorded before and after every addition.
The same experiment was performed with 7 mM irinotecan (4 mg, 5.90 µmol in 840 µL of [D_6]DMSO) and increasing amounts of vinyl-EDANS from 3.5 mM to 98 mM.

Synthesis of MIPs and NIP 3.10 – 4.10

1 equivalent of vinyl-EDANS was dissolved in a total amount of DMSO equal to the 99% in weight of total functional monomers and crosslinker with 1.2 eq of drug. After stirring in anhydrous conditions for 40 minutes, the solution was transferred in a crimp cap Wheaton vial and 70% (in mol) of *N,N'*-ethylenebisacrylamide, 15% (in mol, 1eq) of acrylamide and 18% (in mol, calculated on the amount of the available double bonds) of recrystallized AIBN and were added. The vial was left first under vacuum and then was flushed with argon (3 times for 10 minutes). After heating at 70°C for 4 days, the resulting clear solution was dialyzed against methanol for 2 days and against water for other 2 days, changing the solvent 3 times a day. As reference also a non-imprinted polymer was synthesized. This polymer has the same composition of MIPs but was synthesized without the template molecule.
After dialysis the polymer solutions were freeze-dried and the MIPs were further washed shaking them in methanol and removing the supernatant by centrifugation (13000 rpm for 10 min). Polymers were finally dissolved in water and freeze-dried. The composition of the polymerization mixtures for each polymer is reported in the following table:

Polymer	Drug [mg]	Functional monomer [mg]	Co-monomer [mg]	*N,N*-ethylene Bisacrylamide [mg]	AIBN [mg]	DMSO [mL]	Yield [mg] %
0.10	-	EDANS 12.5	Acrylamide 2.8	30.6	13.1	4.1	41%
3.10	paclitaxel 40	EDANS 12.5	Acrylamide 2.8	30.6	13.1	4.1	59%
4.10	Irinotecan 40	EDANS 15.7	Acrylamide 3.5	38.6	16.5	5.2	48%

DLLS

1 mg of polymer was dissolved in 4 mL of DMSO and the mixture was left into an ultrasonic bath for 1 h. The resulting solution was filtered on 0.45 µm filter and used for DLLS analysis.

Rebinding Tests

1.5 mg of polymer was suspended in 1.5 mL of PBS or citrate buffer at pH=3 with 50 µM drug. After different times between 5 min and 5 hours, 200 µL of the supernatant were collected and the solution was centrifuged at 13000 rpm for 10 min to completely remove the polymer. The obtained supernatant was analyzed by HPLC as reported in ref[1]. The same HPLC methods were applied to create calibration curves of paclitaxel and of irinotecan from 0 µM to 100 µM in PBS where each drug concentration was measured in 5 replicates. From the obtained calibration curves the the amount of drug captured by the polymer was quantified.

Quantification of EDANS into the Polymer

1 mg of MIP **3.10** and NIP **0.10** were dissolved in 1 mL of DMSO and the solution was diluted to 20 µg/mL, 40 µg/mL and 60 µg/mL in PBS. The fluorescence emission of the resulting solutions was measured at 493 nm with an excitation wavelength of 335 nm and both excitation and emission slits of 5 nm.
The EDANS concentration in the polymer solutions was obtained from a calibration curve of EDANS from 0 µM to 7 µM in PBS (all concentrations were made in triplicates), using excitation and emission wavelengths of 335 nm and 493 nm and slits of 5 nm.
Moreover, the absorbance of EDANS into the imprinted and non-imprinted polymer was compared by UV-visible spectroscopy using 1 mg/mL polymer solutions in DMSO.

Fluorescence Titrations of EDANS

3.9 µM EDANS obtained by dilution from the 3.7 mM mother solution (1 mg of EDANS, 3.7 µmol, in 1 mL of DMSO) was titrated by addition of increasing concentrations of paclitaxel from 0 µM to 300 µM using the 5 mM, 400 µM and 100 µM paclitaxel solutions in DMSO.
The titration of 3.9 µM EDANS was also performed with DABCYL-paclitaxel (from 0 to 300 µM) in DMSO using a 500 µM and a 4 mM (1.7 mg, 1.32 µmol in 329.5 µL of DMSO) batch solution of modified drug. For both the titrations the emission intensity at 455 nm was measured when EDANS was excited at 335 nm using excitation and emission slits respectively of 5 nm and 10 nm.

Fluorescence Titration of MIP 3.10 and NIP 0.10

1 mg of polymer was dissolved in 1 mL of DMSO and diluted with the same solvent to a final 240 µg/mL concentration. This solution was titrated with increasing concentrations of DABCYL-paclitaxel from 0 µM to 200 µM using a 1 mM and 500 µM modified drug solution in DMSO obtained by dilution of the 4 mM (1.7 mg, 1.3 µmol in 329.5 µL of DMSO). The emission intensity was measured after 30 min from every addition of DABCYL-paclitaxel to promote the interaction between the polymer and the modified drug.
The polymer emission was recorded at 455 nm exciting at 335 nm with excitation and emission slits of 5 nm and 10 nm. The titration was performed with both the imprinted and the non-imprinted polymer.

Competition Test with MIP 3.10

MIP **3.10** was used to set up a competition test between the free paclitaxel and DABCYL-paclitaxel for the binding with the polymer. The MIP saturation step was performed by the addition of 3 µL of a 4 mM DABCYL-paclitaxel mother solution in DMSO to 400 µL of a 240 µg/mL MIP solution in DMSO (obtained by dilution of the 1 mg/mL batch solution in DMSO) to obtain a polymer solution containing 30 µM modified drug. The fluorescence emission of EDANS was measured at 455 nm exciting at 335 nm with excitation slit of 5 nm and emission slit of 10 nm, before and after the addition of DABCYL-paclitaxel and after waiting for 30 min.
After saturation, increasing concentrations of free paclitaxel from 0 µM to 500 µM were added using a 1 mM (obtained diluting the 4 mM) and 4 mM (1.71 mg, 2 µmol in 500 µL of DMSO) drug solutions. The titration was performed exciting at 335 nm and measuring the emission at 455 nm with excitation and emission slits respectively of 5 nm and 10 nm, after waiting for 30 min.

Reverse Competition Test with MIP 3.10

Investigating the Best DABCYL-paclitaxel Concentration

1 mg of MIP was dissolved in 1 mL of DMSO. Two samples containing 240 µg/mL MIP in DMSO were obtained from this solution by dilution. One of these samples was used as the reference of the test, while 42.7 µL of 1.17 µM paclitaxel in DMSO were added to the second sample to obtain a 50 µM drug concentration.
The fluorescence emission of these samples with and without the addition of DABCYL-paclitaxel from 0 µM to 200 µM (using 1 mM and 4 mM DABCYL-paclitaxel solutions in DMSO) was measured after 30 min of interaction, exciting at 335 nm and measuring at 455 nm with excitation slit of 5 nm and emission slit of 7 nm.

Creation of a Calibration Curve

Different samples containing 240 µg/mL MIP and increasing concentrations of free paclitaxel from 0 µM to 50 µM were prepared in DMSO. After measuring its fluorescence intensity at 455 nm exciting at 335 nm with excitation and emission slits respectively of 5 nm and 7 nm, 200 µM DABCYL-paclitaxel was added to these samples and their fluorescence emission was measured again after 30 min.

6.5 A Colorimetric System

^{1}H-NMR Titrations

Irinotecan-HCl

3 mg (4.43 µmol) of irinotecan-HCl were dissolved in 750 µL of deuterated solvent, and different equivalents of functional monomer, from 0.5 eq to 5 eq were added. The ^{1}H-NMR spectrum of the drug was compared to that recorded after each addition of functional monomer.
The drug was titrated with sodium 4-vinylbenzenesulfonate in [D_6]DMSO, CD_3OD, $(CD_3)_2CO$ with 40% DMF-d_7, D_2O and DMF-d_7, while with acrylic acid in [D_6]DMSO, CD_3OD and in $CDCl_3$ with 6% AcCN-d_3. Finally the titration was performed also with 2-acrylamido-2-ethyl-1-propane sulfonic acid (AMPS) in [D_6]DMSO.
The 400 MHz spectrometer was used for all the titrations.

Free Base Irinotecan

(S)-4,11-diethyl-4-hydroxy-3,14-dioxo-3,4,12,14-tetrahydro-1H-pyrano[3',4':6,7]indolizino[1,2-b]quinolin-9-yl [1,4'-bipiperidine]-1'-carboxylate irinotecan free base, **4a**)

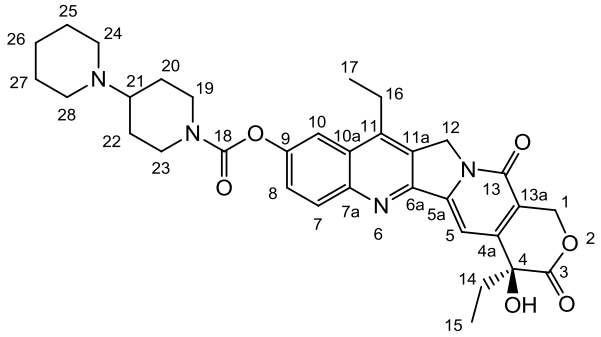

40 mg (1 eq, 59 µmol) of irinotecan hydrochloride were dissolved in 8 mL of water. After addition of 48.4 µL of 1.28 M NaOH (1.05 eq, 61.9 µmol), the irinotecan free base was extracted with DCM. Anhydrous sodium sulfate was added to the organic phase and after filtration, the solvent was removed under reduced pressure to obtain a yellow solid (31.4 mg, 91%).

^{1}H-NMR (600 MHz, $CDCl_3$, 25 °C, ppm): δ= 1.03 (t, ^{3}J=7, 3H, CH_3-**15**), 1.40 (t, ^{3}J= 8 Hz, 3H, CH_3-**17**), 1.48 (m, 2H, CH_2-**26**), 1.64 (m, 6H, CH_2-25, 27; CH_2-**20$_{ax}$**, **22$_{ax}$**), 1.87 (m, 2H, CH_2-**14**), 1.96 (m, 2H, CH_2-**20$_{eq}$**, **22$_{eq}$**), 2.59 (m, 5H, CH_2-**24**, **28**; CH-**21**), 2.90 (t, ^{3}J= 12 Hz, 1H, CH_2-**19$_{ax}$**), 3.07 (t, ^{3}J= 12 Hz, 1H, CH_2-**23$_{ax}$**), 3.15 (q, ^{3}J= 7 Hz, 2H, CH_2-**16**), 3.79 (s, 1H, O**H**), 4.34 (d, ^{3}J= 12 Hz, 1H, CH_2-**19$_{eq}$**), 4.44 (d, ^{3}J= 12, 1H, CH_2-**23$_{eq}$**), 5.25 (s, 2H, CH_2-**12**), 5.30 (d, ^{2}J= 15 Hz, 1H, CH_2-**1$_a$**), 5.75 (d, ^{2}J= 15 Hz, 1H, CH_2-**1$_b$**), 7.58 (dd, ^{3}J= 9 Hz, ^{2}J= 3 Hz, 1H, CH-**8**), 7.63 (s, 2H, CH-**5**), 7.83 (d, ^{4}J= 2 Hz, 1H, CH-**10**), 8.21 (d, ^{3}J= 9 Hz, 1H, CH-**7**).

^{13}C-NMR (600 MHz, $CDCl_3$, 25 °C, ppm): δ=7.89 (1C, CH_3-**15**), 14.11 (1C, CH_3-**17**), 24.92 (1C, CH_2-**26**), 26.25 (4C, CH_2-**25**, **27**; CH_2-**20**, **22**), 31.34 (1C, CH_2-**14**), 50.27 (3C, CH_2-**24**, **28**), 62.36 (1C, CH-**21**), 44.09 (1C, CH_2-**19**), 44.43 (1C, CH_2-**23**), 22.90 (1C, CH_2-**16**), 49.51 (1C, CH_2-**12**), 66.11 (1C, CH_2-**1**), 125.76 (CH-**8**), 97.56 (1C, CH-**5**), 114.50 (1C, CH-**10**), 132.44 (1C, CH-**7**), 118.53 (1C, C-**13a**), 127.31 (1C, C-**10a**), 127.7 (1C, **11a**), 145.26 (1C, **5a**), 147.15 (1C, C-**11**), 147.34 (1C, C-**7a**), 150.34 (1C, C-**4a**), 150.54 (1C, C-**6a**), 151.66 (1C, C-**9**), 153.26 (1C, C-**18**), 157.75 (1C, C-**13**), 174.08 (1C, C-**3**).

IR (cm^{-1}): 1594.6 (C-C aromatics), 1653.2 (C=C), 1717.4 (C=O), 2932.3 (C-H), 3388.4 (O-H).

^{1}H-NMR Titration of Irinotecan Free Base

3 mg (5.1 µmol) of irinotecan free base were dissolved in 600 µL of deuterated solvent. The ^{1}H-NMR spectrum was recorded before and after the addition of increasing amounts of functional monomer. The titration was performed in $CDCl_3$ and in CD_2Cl_2 with acrylic acid and in [D_6]DMSO with 2-acrylamido-2-ethyl-1-propane sulfonic acid.

Synthesis of MIP 4.15

1 eq of irinotecan free base and 1 eq (10% or 5% in mol) of AMPS were dissolved in 2 mL of DMSO and stirred for 1 h to allow the interaction between the template and the functional monomer. After this time, the solution was placed in a crimp cap Weathon vial and the co-monomer acrylamide or N-isopropyl acrylamide (NIPAM) (20% or 25% in mol), the crosslinker methylene-bisacrylamide (MBA) (70% in mol), and the radical initiator AIBN (5% in mol calculated on the amount of available double bonds) dissolved in DMSO were added in solution. The monomer concentration C_M was fixed at 0.5% in weight respect to the weight of DMSO. After flushing the mixture with argon and making vacuum alternatively for 4 times to remove oxygen, the polymerization was achieved by heating at 70°C for 4 days.

A non imprinted polymer was synthesized having the same composition of MIP but synthesized in the absence of irinotecan in the polymerization mixture.

The resulting clear solutions were dialyzed first against 6:4 methanol: acetic acid (three changes for two days) and after against milliQ water containing HCl (final pH=2) for three days changing the solvent twice a day. The dialyzed solutions were freeze-dried to obtain a white fluffy polymer.

The composition of each polymer is reported in the following table:

Polymer	Irinotecan [mg]	Functional monomer [mg]	Co-monomer [mg]	Cross-linker [mg]	AIBN [mg]	DMSO [mL]	Solvent of dialysis	Yield [mg]
0.0	-	-	Acrylamide 30% 5	MBA 70% 25.3	1% 0.6	5.5	H_2O+HCl pH=2	28.8 (95%)
0.15a	-	AMPS 10% 5.7	Acrylamide 20% 3.9	MBA 70% 29.8	1% 0.8	7.1	1) MeOH: AcCOOH 2) H_2O	16.8 (43%)
0.15b	-	AMPS 5% 2.6	Acrylamide 25% 4.5	MBA 70% 27.8	1% 0.8	6.2	1) MeOH: AcCOOH 2) H_2O	32.7 (95%)

0.15c	-	AMPS 10% 5.3	Acrylamide 20% 3.6	MBA 70% 27.5	5% 3.6	6.6	1) MeOH: AcCOOH 2) H_2O +HCl pH=2	32.1 (88%)
0.15d	-	AMPS 5% 4.7	Acrylamide 25% 8	MBA 70% 48.6	5% 6.4	11.1	1) MeOH: AcCOOH 2) H_2O+HCl pH=2	37.4 (61%)
0.15e	-	AMPS 10% 5.3	NIPAM 20% 5.8	MBA 70% 27.5	5% 3.5	7.0	1) MeOH: AcCOOH 2) H_2O+HCl pH=2	35.2 (91%)
4.15a	16.2	AMPS 10% 5.7	Acrylamid e 20% 3.9	MBA 70% 29.8	1% 0.8	7.1	1) MeOH: AcCOOH 2) H_2O	7.0 (18%)
4.15b	7.4	AMPS 5% 2.6	Acrylamid e 25% 4.5	MBA 70% 27.8	1% 0.8	6.2	1) MeOH:AcCOOH 2) H_2O	0.4 (1%)
4.15c	15.0	AMPS 10% 5.3	Acrylamid e 20% 3.6	MBA 70% 27.5	5% 3.6	6.6	1) MeOH AcCOOH 2) H_2O+HCl pH=2	27.1 (75%)
4.15d	13.2	AMPS 5% 4.7	Acrylamid e 25% 8.0	MBA 70% 48.6	5% 6.4	11.1	1) MeOH AcCOOH 2) H_2O+HCl pH=2	31.0 (50%)
4.15e	15.0	AMPS 10% 5.3	NIPAM 20% 5.8	MBA 70% 27.5	5% 3.5	7.0	1) MeOH AcCOOH 2) H_2O+HCl pH=2	34.2 (89%)

Template Removal

After polymerization of MIP 4.15a, 2.3 mL of the MIP solution in DMSO were dialyzed against water only, while to the remaining MIP solution (4.8 mL) the same volume of 7:3 MeOH:acetic acid was added and the resulting mixture was stirred overnight. The polymer was dialyzed first against water with 10% of 7:3 methanol:acetic acid and then against Millipore water only.

The polymer was further dialyzed in different mixtures of 7:3 or 6:4 methanol:acetic acid or in 7:3 methanol:TFA, and finally dialyzed against MilliQ water.

After each washing process the polymer was freeze-dried and the amount of irinotecan entrapped in the polymer was quantified from a calibration curve of irinotecan free base. The calibration curve was obtained measuring the UV-visible absorbance of different concentrations of drug in DMSO, from 10 µM to 50 µM, starting from the 1.9 mM irinotecan free base batch solution in DMSO. The intensity of the characteristic peak of irinotecan at 363 nm was plotted in function of drug concentration.

1 mg of the washed MIP was dissolved in 1 mL of DMSO to obtain the 1 mg/mL batch solution that was further diluted to the 0.125 mg/mL and the 0.612 mg/mL solutions in DMSO that were measured by UV-visible spectroscopy.

DLLS

The particle size of NIPs and MIPs were measured by Dynamic Laser Light Scattering using a Malvern Zetasizer instrument. 0.5 mg of polymer were dissolved in 2 mL of water and left into an ultrasonic bath for 1 h. The solution was filtered on a 0.45 µm filter, placed in a 1 mL plastic cuvette with a 1 cm optical path and analyzed in triplicate. The size distributions by intensity and by volume were recorded.
Some polymers were also measured in a DMSO solution after sonication and filtration. In this case a 1 mL quartz cuvette of was used with a 1 cm optical path .

Z-potential

All the MIPs and NIPs containing AMPS as functional monomer were analyzed by z-potential to verify the presence of charges on the polymer surface. 0.5 mg of polymer was dissolved in 2 mL of water and the solution was placed into an ultrasonic bath for 1 h. After filtration on 0.45 µm filter, the solution was analyzed in triplicate.

Solid State IR

NIPs 0.15c, 0.15d and 0.15e were analyzed by IR-spectroscopy to verify the presence of the sulfonic acid incorporated into the polymeric matrix. The IR spectrum of NIP containing AMPS was compared with the spectrum of a control NIP **0.0** containing only acrylamide and MBA .
IR of NIP 0.15c: 3283 cm^{-1}: stretching NH of acrylamide and of AMPS, stretching OH of SO_3H; 1648 cm^{-1}: stretching of C=O of acrylamide and of amide group of AMPS; 1528 cm^{-1}: bending of NH of amide groups; 1449 cm^{-1}: bending of C-N bond of amide groups; 1115 cm^{-1} and 1205 cm^{-1}: C-C stretching of polymer, 1021 cm^{-1}: symmetric stretching of S=O group
IR of NIP 0.15d: 3284 cm^{-1}: stretching NH of acrylamide and of AMPSA, stretching OH of SO_3H; 1643.7 cm^{-1}: stretching of C=O of acrylamide and of amide group of AMPS; 1520 cm^{-1}: bending of NH of amide groups; 1452 cm^{-1}: bending of C-N bond of amide groups; 1201.9 cm^{-1}: asymmetric stretching of S=O and C-C stretching of polymer; 1113 cm^{-1}: C-C stretching of polymer; 1038 cm^{-1}: symmetric stretching of S=O group.
IR of NIP 0.15e: 3288 cm^{-1}: stretching NH of acrylamide and of AMPSA, stretching OH of SO_3H; 1643 cm^{-1}: stretching of C=O of acrylamide and of amide group of AMPS; 1522 cm^{-1}: bending of NH of amide groups; 1456 cm^{-1}: bending of C-N bond of amide groups;

1203 cm^{-1}: asymmetric stretching of S=O and C-C stretching of polymer; 1111.6 cm^{-1}: C-C stretching of polymer; 1038 cm^{-1}: symmetric stretching of S=O group.
IR of NIP 0.0: 3283 cm^{-1}: stretching NH of acrylamide; 1641.8 cm^{-1}: stretching of C=O of acrylamide; 1521.9 cm^{-1}: bending of NH of amide groups; 1449 cm^{-1}: bending of C-N bond of amide groups; 1205 cm^{-1} and 1111.6 cm^{-1}: C-C stretching of polymer.

Rebinding Test with MIP 4.15e and NIP 0.15e

Rebinding of Irinotecan Free Base in Acetonitrile

1.5 mg of MIP 4.15e or NIP 0.15e were suspended in 1.5 mL of a 50 µM solution of irinotecan free base in acetonitrile, obtained by dilution of the 1.7 mM mother solution (1 mg, 1.7 µmol in 1 mL of AcCN). After different times from 5 min to 7 h, 200 µL of the supernatant were collected and centrifuged at 13000 rpm for 10 min. 50 µL of the resulting solution were injected into the HPLC for the drug quantification.[1]

Rebinding of Protonated Irinotecan in Citrate Buffer

1.5 mg of MIP 4.15e or NIP 0.15e were dissolved in 1.5 mL of a 50 µM irinotecan solution in citrate buffer at pH=3 obtained by dilution of the 1.5 mM mother solution (1 mg, 1.47 µmol in 1 mL of citrate buffer). After different times from 5 min to 12 h, 200 µL of the polymer mixture were centrifuged at 13000 rpm for 10 min and 50 µL of the obtained supernatant were analyzed by HPLC.[1]

Rebinding of Protonated Irinotecan in Water

1.5 mg of MIP 4.15e or NIP 0.15e were dissolved in 1.5 mL of a 50 µM irinotecan solution in water, obtained diluting the 4 mM mother solution (2.7 mg, 4 µmol in 1 mL of water). After different times from 5 min to 12 h, 200 µL of the polymer mixture were centrifuged at 13000 rpm for 10 min and 50 µL of the obtained supernatant were analyzed by HPLC[1].

Cross Reactivity Tests of MIP 4.15e and NIP 0.15e

1.5 mg of polymer were suspended in 1.5 mL of 50 µM acqueous solutions of paclitaxel, sunitinib of SN38. After different times 200 µL of the supernatant were collected and 5 µL of internal standard (1 mM quinolinone in AcCN for SN38 and paclitaxel, and 1 mM caffeic acid in 1:1 water:acetonitrile for sunitinib) were added. After centrifugation at 13000 rpm for 10 min, 50 µL of the supernatant were analyzed by HPLC[1].

Choice of the Best Solvent for the Colorimetric Test

1 mg of aniline yellow was dissolved in 1 mL of the following solvents: water, DMSO, DMF, dioxane, ethyl acetate, THF, acetonitrile and methanol to obtain the 5.1 mM batch solutions. These solutions were diluted to 20 µM aniline yellow in the different solvents. The 20 µM solution in DCM was obtained from the 5.1 mM dye solution in methanol. The diluted solutions were titrated by the addition of increasing amounts of AMPS from 1 eq to 10 eq. Since AMPS is not soluble in ethyl acetate, dioxane and DCM, the titrations in these solvents were performed with the AMPS batch solution respectively in 1:1 DMF:ethyl acetate, in 1:1 DMF:dioxane and 1:1 MeOH:DCM.
The UV-visible spectrum from 300 nm to 600 nm was recorded without AMPS and after each addition of functional monomer. The titration in acetonitrile was repeated also with 10 µM dye.
In order to find the maximum quantity of water that the system can support, 20 µM protonated aniline yellow in acetonitrile was titrated with increasing concentrations of water from 0.5% to 10%. Protonated aniline yellow was obtained adding AMPS in acetonitrile until complete protonation. The UV spectrum was recorded from 280 nm to 600 nm after every addition.

Recover of Irinotecan from Dried Plasma

5 µL of plasma containing irinotecan from 3.7 µM to 15 µM were dried in a glass vial and acetonitrile was added to recover irinotecan. The UV spectrum of the obtained mixture was recorded before and after sonication. The drug concentration in solution was quantified by a calibration curve of irinotecan from 0 to 15 µM (irinotecan batch solution 2.36 mM in AcCN). However the amounts of drug recovered from dried samples were very low, so an additional step was added to the test. In particular irinotecan solutions in plasma from 1 µM to 30 µM were obtained by dilution with plasma of the 2.07 mM (1.4 mg, 2.07 µmol in 1 mL) drug in water. 600 µL of methanol were added to 200 µL of irinotecan solutions in plasma, a white solid precipitated and the mixture was centrifuged at 13000 rpm for 10 min at 4 °C. After collecting the supernatant, the centrifugation and removal of the white solid was repeated twice to obtain a clear solution of treated plasma containing irinotecan. 200 µL of drug solutions in 3:1 methanol:plasma were spotted on the bottom of a glass vial and the solution was dried at room temperature under flux of air. After drying, 200 µL of acetonitrile were added and the mixture was left into an ultrasonic bath for 45 min. 50 µL of the solution were injected into an HPLC to quantify irinotecan.

First Qualitative Colorimetric Test with MIP 4.15d

2 mg of MIP **4.15d** containing 5% of AMPS were suspended in 1 mL of AcCN in a vial and irinotecan free base was added to obtain a 400 µM drug concentration in the vial. After 10 min, 40 µM (7.8 µL of 5.1 mM in AcCN) aniline yellow was added to the mixture. As reference 2 mg of the same polymer were suspended in 1 mL of AcCN and treated with 40 µM aniline yellow without drug.
Pictures of both the samples were taken immediately before the addition of dye, after 1 h and after 12 h.

UV-titration of MIP 4.15c

1 mg of MIP **4.15c** was suspended in 1 mL of AcCN and the mixture was left in an ultrasonic bath for 15 min. After the addition of 40 µM aniline yellow (7.8 µL of 5.1 mM in AcCN), increasing amounts of irinotecan free base were added from 150 µM to 600 µM (36.1 µL of 4.16 mM irinotecan in AcCN for each addition). UV-visible spectra were recorded at each step.

Titration of MIP 4.15e

2 mg of polymer were suspended in 8 mL of AcCN and left into an ultrasonic bath for 90 min. 1 mL of the suspension was placed in both the reference and the sample cuvette to record the baseline correction. Aniline yellow was added to the sample cuvette, from a 5.63 mM batch solution in acetonitrile to reach final concentrations from 20 µM to 320 µM with 20 µM increments . The UV spectrum was recorded after each addition.

Colorimetric Test with MIP 4.15e

The colorimetric test was performed at different polymer concentrations: 0.25 mg/mL (4.0 mg of MIP 4.15e in 16 mL of acetonitrile), 0.4 mg/mL (4.0 mg of MIP 4.15e in 10 mL of acetonitrile) and 0.5 mg/mL (5.0 mg of MIP 4.15e in 10 mL of acetonitrile). Each polymer suspension was placed into an ultrasonic bath for 90 min and the baseline correction was made with both the reference and the sample cuvette filled with 1 mL of the polymer suspension.
The samples containing 0.25 mg/mL MIP were treated with different amounts of a freshly prepared 2.6 mM solution of irinotecan free base in acetonitrile with 28.6% of dichloromethane, in order to obtain final drug concentrations from 2 µM to 20 µM. After 5 min, 35.5 µL of a freshly prepared 5.63 mM solution of aniline yellow, were added to obtain a 200 µM dye concentration. The UV spectrum was recorded from 200 nm to 800 nm. The samples containing 0.4 mg/mL MIP were treated with irinotecan

free base from 4 µM to 80 µM using a 2.6 mM batch solution of drug in acetonitrile with 28.6% of dichloromethane. After 5 min aniline yellow was added to the sample and the UV spectrum was measured from 200 nm to 800 nm. The final dye concentration in cuvette was 320 µM (56.9 µL of 5.63 mM batch solution in acetonitrile).

Finally, to 1 mL of 0.5 mg/mL polymer suspension different concentration of irinotecan free base, from 4 µM to 120 µM were added using a 2.6 mM batch solution of irinotecan free base in acetonitrile with 28.6% of dichloromethane. After 5 min, 71.1 µL of aniline yellow 5.63 mM were added to obtain a 400 µM solution of dye in cuvette. The UV spectrum of each sample was recorded from 200 nm to 800 nm maintaining the 0.5 mg/mL suspension of MIP **4.15e** in acetonitrile in the reference cuvette. The peak corresponding to the protonated dye is visible at 520 nm.

6.6 Characterization of Drugs

(Z)-N-(2-(diethylamino)ethyl)-5-((5'-fluoro-2'-oxoindolin-3'-ylidene)methyl)-2,4-dimethyl-1H-pyrrole-3-carboxamide (Sunitinib, **1**)

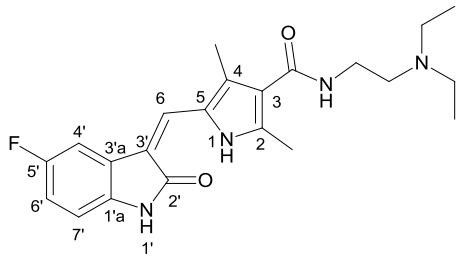

^{1}H-NMR (500 MHz, [D_6]DMSO, 25°C, ppm) δ= 0.99 (t, ^{3}J = 7 Hz, 6H, N(CH_2C**H**$_3$)$_2$), 2.44 (s, 3H, C**H**$_3$C-4), 2.46 (s, 3H, C**H**$_3$C-2), 2.50-2.57 (m, 6H, C**H**$_2$N(C**H**$_2$$CH_3$)$_2$), 3.27 (q, ^{3}J = 7 Hz, 2H, C**H**$_2$$CH_2$N($CH_2$$CH_3$)$_2$), 6.85 (dd, ^{3}J = 8 Hz, ^{4}J = 4 Hz, 1H, CH-7'), 6.93 (dt, ^{3}J = 9 Hz, ^{4}J = 3 Hz, 1H, CH-4'), 7.43 (t, ^{3}J = 6 Hz, 1H, CO-N**H**- $CH_2CH_2N(CH_2CH_3)_2$), 7.71 (s, 1H, CH-6), 7.76 (dd, ^{3}J = 9 Hz, ^{4}J = 2 Hz, 1H, CH-6'), 10.89 (s, 1H, NH-1'), 13.69 (s, 1H, NH-1).

^{13}C-NMR (500 MHz, [D_6]DMSO, 25°C, ppm) δ= 10.48 (1C, C**H**$_3$C-4), 11.81 (2C, N(CH_2C**H**$_3$)$_2$), 13.32 (1C, C**H**$_3$C-2), 46.45 (2C, N(**C**H$_2$$CH_3$)$_2$), 51.75 (1C, **C**H$_2$N($CH_2$$CH_3$)$_2$), 36.78 (1C, **C**H$_2$$CH_2$N($CH_2$$CH_3$)$_2$), 109.58 (1C, CH-**7'**), 124.78 (1C, CH-**6**), 105.47 (1C, CH-**6'**), 112.11 (1C, CH-**4'**), 120.64 (1C, C-**3**), 124.3 (1C, C-**3'a**), 125.81 (1C, C-**5**), 127.54 (1C, C-**3'**), 130.09 (1C, C-**4**), 136.58 (1C, C-**1'a**), 134.37 (1C, C-**2**), 164.46 (1C, NH**C**OC-3), 169.63 (1C, C-**2'**), 159.59 (1C, C-**5'**).

IR (cm^{-1}): 1650 (C=O), 1674.1 (C=O), 2966 (C-H), 3289.9 (N-H).

(S)-4,11-diethyl-4,9-dihydroxy-1H-pyrano[3',4':6,7]indolizino[1,2-b]quinoline-3,14(4H,12H)-dione (SN-38, **2**)

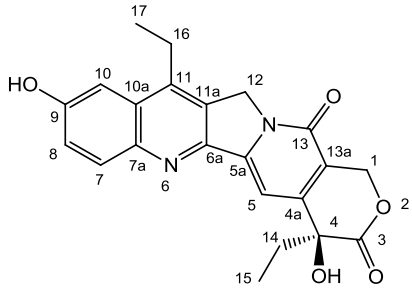

^{1}H-NMR (500 MHz, [D_6]DMSO, 25°C, ppm) δ= 0.89 (t, ^{3}J= 7 Hz, 3H, CH_3-**15**), 1.31 (t, ^{3}J= 7 Hz, 3H, CH_3-**17**), 1.88 (m, 2H, CH_2-**14**), 3.10 (q, ^{3}J= 7 Hz, 2H, CH_2-**16**), 5.29 (s, 2H, CH_2-**12**), 5.43 (s, 2H, CH_2-**1**), 6.49 (s, 1H, O**H**-C4), 7.26 (s, 1H, CH-**5**), 7.41 (s, 1H, CH-**10**), 7.43 (m, 1H, CH-**8**), 8.04 (dd, ^{3}J= 8 Hz, ^{4}J= 2 Hz, 1H, CH-**7**), 10.31 (s, 1H, O**H**-C9).

^{13}C-NMR (500 MHz, [D_6]DMSO, 25°C, ppm) δ= 7.72 (1C, CH_3-**15**), 13.4 (1C, CH_3-**17**), 22.3 (1C, CH_2-**16**), 30.11 (1C, CH_2-**14**), 49.32 (1C, CH_2-**12**), 65.09 (1C, CH_2-**1**), 72.28 (1C, C-**4**), 95.6 (1C, CH-**5**), 104.45 (1C, CH-**10**), 117.96 (1C, C-**13a**), 122.42 (1C, CH-**8**), 128.06 (1C, C-**10a**), 128.23 (1C, C-**11a**), 131.47 (1C, CH-**7**), 140.8 (1C, C-**11**), 142.68 (1C, C-**7a**), 143.55, 146,38 (1C, C-**5a**), 149.97 (1C, C-**4a**), 150.05 (1C, C-**9**), 156.82 (1C, C-**13**), 172.47 (1C, C-**3**).

IR (cm^{-1}): 1583.9 (C-C aromatics), 1653.02 (C=O), 1732.4 (C=O), 2918.1 (C-H), 3350 (O-H).

(2aR,4S,4aS,6R,9S,11S,12S,12aR,12bS)-9-(((2R,3S)-3-benzamido-2-hydroxy-3-phenylpropanoyl)oxy)-12-(benzoyloxy)-4,11-dihydroxy-4a,8,13,13-tetramethyl-5-oxo-2a,3,4,4a,5,6,9,10,11,12,12a,12b-dodecahydro-1H-7,11-methanocyclodeca[3,4]benzo[1,2-b]oxete-6,12b-diyl diacetate
(Paclitaxel, **3**)

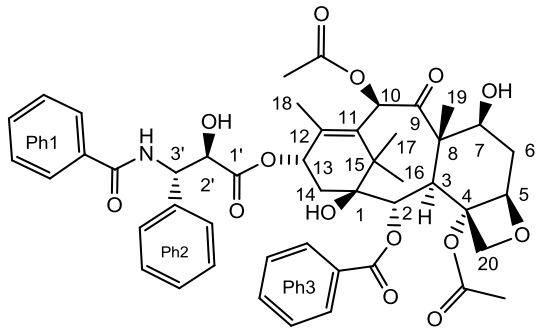

^{1}H-NMR (500 MHz, [D_6]DMSO, 25°C, ppm) δ= 1.15 (s, 3H, CH_3-**16**), 1.27 (s, 3H, CH_3-**17**), 1.69 (s, 3H, CH_3-**19**), 1.80 (s, 3H, CH_3-**18**), 2.25 (s, 3H, C**H**$_3$COOC-10), 2.33 (m, 2H, CH_2-**14**), 2.40 (s, 3H, C**H**$_3$COOC-4), 2.45 (s, 1H, O**H**), 2.56 (m, 2H, CH_2-**6**), 3.53 (d, ^{3}J = 4 Hz, 1H, N**H**), 3.81 (d, ^{3}J = 7 Hz, 1H, CH-**3**), 4.20 (d, ^{2}J = 9 Hz, 1H, CH_2-**20a**), 4.30 (d, ^{2}J = 9 Hz, 1H, CH_2-**20b**), 4.41 (dd, 1H, ^{3}J = 8 Hz, ^{3}J =11 Hz, CH-**7**), 4.80 (m, 1H, CH-**2'**), 4.96 (dd, ^{3}J = 10 Hz, ^{4}J = 1 Hz, 1H, CH-**5**), 5.68 (d, ^{3}J = 7 Hz, 1H, CH-**2**), 5.80 (dd, ^{3}J = 9 Hz, ^{3}J = 2 Hz, 1H, CH-**3'**), 6.24 (t, ^{3}J = 9 Hz, 1H, CH-**13**), 6.28 (s, 1H, CH-**10**), 6.98 (d, ^{3}J = 9 Hz, 1H, N**H**), 7.36 (dt, ^{3}J = 8 Hz, ^{4}J =2 Hz, 1H, C**H**$_p$-Ph2), 7.40 (m, 2H, C**H**$_m$-Ph1), 7.42 (m, 2H, C**H**$_m$-Ph2), 7.46 (m, 2H, C**H**$_o$-Ph2), 7.50 (m, 1H, C**H**$_p$-Ph1), 7.51 (m, 2H, C**H**$_m$-Ph3), 7.60 (dt, ^{3}J = 8 Hz, ^{4}J =2 Hz, 1H, C**H**$_p$-Ph3), 7.74 (dd, ^{3}J =8 Hz, ^{4}J =2 Hz, 2H, C**H**$_o$-Ph1), 8.13 (dd, ^{3}J = 8, ^{4}J =2 Hz, 2H, C**H**$_o$-Ph3).

^{13}C-NMR (500 MHz, [D_6]DMSO, 25°C, ppm) δ= 9.48 (1C, CH_3-**19**), 14.72 (1C, CH_3-**18**), 20.44 (1C, **C**H$_3$COOC-10), 21.85 (1C, CH_3-**16**), 22.27 (1C, **C**H$_3$COOC-4), 26.92 (1C, CH_3-**17**), 35.58 (1C, CH_2-**14**), 42.42 (1C, C-**15**), 45.26 (1C, CH-**3**), 55.01 (1C, CH-**3'**), 58.64 (1C, C-**8**), 72.06 (1C, CH-**7**), 72.26 (1C, CH-**13**), 73.18 (1C, CH-**2'**), 74.99 (1C, CH-**2**), 75.47 (1C, CH-**10**), 76.35 (1C, CH_2-**20**), 79.05 (1C, C-**1**), 81.15 (1C, C-**4**), 84.3 (1C, CH-**5**), 126.95 (2C, **C**H$_o$-Ph1),127.03 (2C, **C**H$_o$-Ph2),128.43 (1C, **C**H$_p$-Ph2), 128.58 (2C, **C**H$_m$-Ph3), 128.81 (2C, **C**H$_m$-Ph1), 128.95 (2C, **C**H$_m$-Ph2), 130.1 (1C, **C**-Ph3), 130.20 (2C, **C**H$_o$-Ph3), 131.90 (1C, **C**H$_p$-Ph1), 133.5 (1C, **C**-Ph2), 133.68 (1C, **C**H$_p$-Ph3), 134.1 (1C, **C**-Ph1), 134.3 (1C, C-**11**), 140.1 (1C, C-**12**), 166.2 (1C, **C**OOC-2), 167.31 (1C, **C**ONH), 171.07 (1C, **C**OO), 170.37 (1C, **C**OO), 180.39 (1C, C-**1'**), 201.85 (1C, C-**9**).

IR (cm^{-1}): 1250 (C-O), 1660 (C=C), 1730 (C=O), 2943 (C-H), 3433.1 (O-H).

(S)-1-(1-(((4,11-diethyl-4-hydroxy-3,14-dioxo-3,4,12,14-tetrahydro-1H-pyrano[3',4':6,7]indolizino[1,2-b]quinolin-9-yl)oxy)carbonyl)piperidin-4-yl)piperidin-1-ium (protonated irinotecan, **4**)

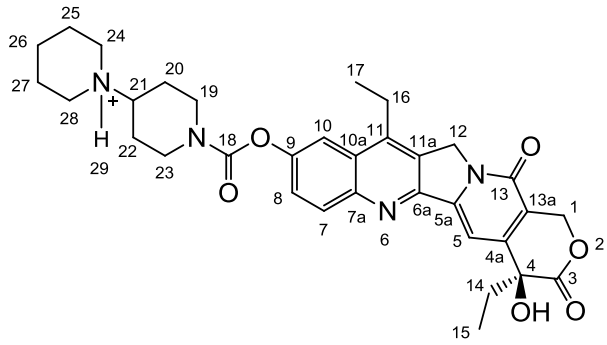

^{1}H-NMR (500 MHz, $CDCl_3$, 25 °C, ppm): δ= 1.04 (t, ^{3}J= 7 Hz, 3H, CH_3-**15**), 1.41 (t, ^{3}J= 7 Hz, 3H, CH_3-**17**), 1.46 (m, 1H, CH_2-**26$_{ax}$**), 1.88 (q, ^{3}J= 7 Hz, 2H, CH_2-**14**), 1.92 (m, 2H, CH_2-**20$_{ax}$**, **22$_{ax}$**), 1.95 (m, 1H, CH_2-**26$_{eq}$**), 2.24 (m, 4H, CH_2-**25**, **27**), 2.39 (d, ^{3}J= 9 Hz, 2H, CH_2-**20$_{eq}$**, **22$_{eq}$**), 2.78 (m, 2H, CH_2-**24$_{ax}$**, **28$_{ax}$**), 2.96 (t, ^{2}J= 12 Hz, 1H, CH_2-**19$_{ax}$**), 3.13 (m, 1H, CH_2-**23$_{ax}$**), 3.15 (q, ^{3}J= 7 Hz, 2H, CH_2-**16**), 3.42 (t, ^{3}J=11 Hz, 1H, CH-**21**), 3.59 (d, ^{2}J= 10 Hz, 2H, CH_2-**24$_{eq}$**, **28$_{eq}$**), 3.83 (s, 1H, O**H**), 4.52 (d, ^{2}J= 12 Hz, 1H, CH_2-**19$_{eq}$**), 4.59 (d, ^{2}J= 12 Hz, 1H, CH_2-**23$_{eq}$**), 5.26 (s, 2H, CH_2-**12**), 5.31 (d, ^{2}J= 17 Hz, 1H, CH_2-**1$_a$**), 5.74 (d, ^{2}J= 17 Hz, 1H, CH_2-**1$_b$**), 7.56 (dd, ^{3}J= 9 Hz, ^{4}J=2 Hz, 1H, CH-**8**), 7.65 (s, 1H, CH-**5**), 7.84 (d, ^{4}J= 2 Hz, 1H, CH-**10**), 8.21 (d, ^{3}J= 9 Hz, CH-**7**), 12.02 (br, 1H, N**H**).

^{13}C-NMR (500 MHz, $CDCl_3$, 25 °C, ppm): δ= 7.80 (1C, CH_3-**17**), 13.97 (2C, CH_3-**15**), 22.35 (1C, CH_2-**26**), 22.83 (2C, CH_2-**25**, **27**), 23.12 (1C, CH_2-**14**), 26.35 (2C, CH_2-**20**, **22**), 31.58 (1C, CH_2-**16**), 42.66 (2C, CH_2-**19**, **23**), 49.24 (1C, CH_2-**12**), 49.27 (2C, CH_2-**24**, **28**), 63.39 (1C, CH-**21**), 66.18 (1C, CH_2-**1**), 72.65 (1C, C-**4**), 98.12 (1C, CH-**5**), 114.53 (1C, CH-**10**), 118.36 (1C, C-**13a**), 125.34 (1C, CH-**7**), 127.18 (1C, C-**10a**), 127.21 (1C, C-**11a**), 131.60 (1C, CH-**8**), 145.36 (1C, C-**11**), 145.94 (1C, **7a**), 147.6 (1C, C-**5a**), 150.05 (1C, C-**9**), 151.44 (1C, C-**6a**), 156.99 (1C, C-**18**), 157.47 (1C, C-**13**), 173.72 (1C, C-**3**).

IR (cm^{-1}): 1654 (C=O), 1718.9 (C=O), 1745.4 (C=O), 2927.5 (C-H), 3389 (O-H).

[1] For rebinding test of SN38, the 50 μM solution was obtained by dilution in water of the 2.55 mM mother solution (1 mg of SN38, 2.55 μmol, in 1 mL of DMSO). The reference used was 1 mM quinolinone in acetonitrile. Samples were analysed by HPLC with a 78:22 water:acetonitrile mobile phase with 0.05% of TFA. The UV-visible detector was set to 208 nm wavelength and the flux was fixed at 1 mL/min. For the

rebinding test of sunitinib, the 50 μM solution of the drug was made by dilution in water of a 2.51 mM mother solution (1 mg of sunitinib, 2.51 μmol dissolved in 1 mL of 1:1 water:acetonitrile). The reference used was 1 mM caffeic acid in water, obtained by dilution of a 15 mM mother solution (2.7 mg, 15 μmol in 1 mL of 1:1 water:acetonitrile mixture). For each HPLC run, 50 μL of the supernatant were injected (mobile phase: 75:25 water:acetonitrile with 0.05% of TFA, UV wavelength: 265 nm). For rebinding tests of paclitaxel, the 50 μM solution of the drug was made by dilution in water of a 10.5 mM mother solution (4.5 mg of paclitaxel, 5.27 μmol in 500 μL of acetonitrile), while the reference was 1 mM quinolinone in acetonitrile. For HPLC analysis a 55:45 water:acetonitrile mobile phase was used with 0.05% of TFA, UV-visible wavelength 230 nm. Finally, for the rebinding test of irinotecan, the 50 μM drug solution was obtained diluting in water the 1.48 mM mother solution (1 mg of irinotecan, 1.48 μmol in 1 mL of water). 50 μL of the supernatant was centrifuged before injection into the HPLC. The amount of irinotecan captured by the polymer was calculated from a calibration curve from 0 μM to 100 μM drug in water. These drug solutions were obtained by dilution in water of a 2.95 mM irinotecan mother solution (2 mg, 2.95 μmol in 1 mL). The HPLC method used for both the experiment and the calibration curve consists on a mobile phase of 75:25 water:acetonitrile with 0.05% of TFA and UV detection at 363 nm. The rebinding test for the MIPs 4.5 and 4.6 were also performed in citrate buffer (pH=3). In this case the 50 μM drug solution was obtained diluting in citrate buffer the 3.4 mM mother solution (2.3 mg of irinotecan, 3.4 μmol, in 1 mL of citrate buffer). The mobile phase was 75:25 water:acetonitrile with 0.05% of TFA, UV wavelength: 363 nm.

The retention times of quinolinone and SN38 in 78:22 water:acetonitrile were 7.01 min and 12.56 min respectively. The retention times of caffeic acid and sunitinib in 75:25 water:acetonitrile were 2.70 min and 12.67 min. The retention times of quinolinone and paclitaxel in 55:45 water:acetonitrile were 2.61 min and 13.64 min respectively. Finally the retention time of irinotecan in 75:25 water:acetonitrile was 4.56 min.

7. Conclusions

In this thesis, about 30 MIPs have been studied.

Among fluorescent polymers, the most promising result has been obtained with coumarin as sensing monomer, namely on the recognition of sunitinib. The performance of the MIPs as binders resulted from moderately good to very good, and their selectivity against other anticancer drugs was satisfactory in particular against large molecules as paclitaxel. MIPs showed also a satisfactory stability in methanol : plasma mixture without need to further optimization of MIP structure. The fluorimetric system based on coumarin was tested in plasma samples treated with four volumes of DMSO and turned out to be robust, satisfactory as to its precision and accuracy. It was possible to demonstrate its ability to recover sunitinib from spiked plasma samples and to quantify the drug within 5 $\mu mol \cdot L^{-1}$ - 100 $\mu mol \cdot L^{-1}$ range with a LOD of 400 $nmol \cdot L^{-1}$, using a calibration curve obtained in 4:1 DMSO : water mixture. These results are currently under submission and are similar to that obtained by Zhang and co-workers with a bulk MIP containing 7-acryloyloxy-4-methylcoumarin as fluorescent functional monomer, ethylene glycol dimethacrylate as crosslinker and methacrylic acid as co-monomer. Measuring the quenching of MIP fluorescence, the sulfadiazine antibiotic was quantified within 1 $\mu mol \cdot L^{-1}$ and 40 $\mu mol \cdot L^{-1}$ range with a LOD of 0.48 $\mu mol \cdot L^{-1}$ in both acetonitrile and milk.[1] The results can be also compared to that of Li and co-workers for the alachlor herbicide quantification by a fluorescent sensor based on bulk MIP. The MIP fluorescence decreases linearly upon binding the target in the 1 $\mu mol \cdot L^{-1}$ – 150 $\mu mol \cdot L^{-1}$ range with a LOD of 0.5 $\mu mol \cdot L^{-1}$.[2]

Two different fluorescence tests for irinotecan quantification in 3:1 methanol:plasma mixture were developed as proof on concept of fluorimetric sensors. The first test employed a MIP containing tyrosine methyl ester to quenching the intrinsic fluorescence of irinotecan. The test turned out to be robust, since the same performance was obtained in 3:1 DMSO:plasma mixture and the obtained calibration curve showed a linear response between 0.5 $\mu mol \cdot L^{-1}$ to 8 $\mu mol \cdot L^{-1}$ drug. Conversely the second fluorimetric system is based on a fluorescent MIP containing a naphthalimide-based functional monomer as fluorescent label, whose fluorescence is quenched upon binding of irinotecan. Using this system the sensitivity has been greatly increased than other fluorescent MIPs, showing a linear response between 20 $nmol \cdot L^{-1}$ and 100 $nmol \cdot L^{-1}$. Moreover these results are better than that obtained by Syu and co-workers for a MIP film imprinted for creatinine detection, having a similar composition and a similar functional monomer than ours. In fact the linear range of their calibration curve was within 177 $\mu mol \cdot L^{-1}$ and 885 $\mu mol \cdot L^{-1}$ with an LOD of 56 $\mu mol \cdot L^{-1}$.[3] While synthesizing a core shell MIP on the extremity of an optical fiber, Ton and co-workers obtained a more sensitive fluorescent sensor able to quantify the 2,4-dichlorophenoxyacetic acid herbicide in nM concentrations in water, with a LOD of 2.5 nM. The polymer had a core of poly-pentaerythritol triacrylate (PETIA) and a shell of MIP containing 4-vinyl pyridine, EGDMA as crosslinker and a fluorescent piperazinyl

naphtalimide monomer whose fluorescence is enhanced upon interaction with the target molecule.[4]

The FRET-based MIP specific for paclitaxel has been exploited to setup a competitive test in DMSO. The resulting calibration curve has a linear behavior from 1 $\mu mol \cdot L^{-1}$ and 30 $\mu mol \cdot L^{-1}$ and represents a valid starting point for the development of a FRET sensor for paclitaxel quantification in patients samples. This preliminary test is similar but less sensitive than that obtained by Carrasco and coworkers for enrofloxacin quantification by a fiber-optic sensor based on a dye displacement technique where the linear range was between 0.29 $\mu mol \cdot L^{-1}$ and 21.5 $\mu mol \cdot L^{-1}$. [5] However our test is enough sensitive to quantify the higher paclitaxel concentrations found in real samples and it is not optimized on a sensor device.

In principle, it is possible to setup also a colorimetric test for irinotecan quantification in real samples. The dye displacement technique has been employed to develop a test based on a MIP containing 2-acrylamido-2-methylpropane sulfonic acid functional monomer able to interact with aniline yellow leading to a change of colour. The colour intensity is proportional to the amount of drug captured. The resulting calibration curve in acetonitrile showed a linear response between 3.6 $\mu mol \cdot L^{-1}$ and 75 $\mu mol \cdot L^{-1}$. Since the irinotecan concentrations usually found in patients samples are within the dynamic range of this curve, this colorimetric test represent a potentially good system for the drug quantification in real samples. Moreover, it has been verified the possibility to dry small amounts of treated plasma samples and recover the drug in acetonitrile, necessary to perform the colorimetric test. The colorimetric system showed a higher sensitivity and a similar dynamic range than that obtained by McNiven and co-workers for a colorimetric competitive test based on MIP for chloramphenicol quantification. In fact they obtained a linear range between 12 $\mu mol \cdot L^{-1}$ and 93 $\mu mol \cdot L^{-1}$ with a LOD of 9.3 $\mu mol \cdot L^{-1}$.[6]

As future perspective, in collaboration with Center of Excellence for Biosensors, Instrumentation and process Control (COBIK), the most promising fluorescent MIPs will be immobilized or deposited on glass wells to be used for the setup of a point of care system using the fluorimetric devices developed by COBIK.

[1] Zheng Z., Li M., Shen F., Ren X. (2015) "Direct fluorescence quantification of sulfadiazine from quenching of novel functional monomer based molecularly imprinted polymers" *Anal. Methods* DOI: 10.1039/c5ay01023c

[2] Li M., Shen F., Zhang Z., Ren X. (2016) "A novel 2-acrylamide-6-methoxybenzothiazole fabricated molecularly imprinted polymers for direct fluorescent sensing of alachlor" *Chromatrgr.* 79:71-78

[3] Syu M. J., Hsu T. J., Lin Z. K. (2010) "Synthesis of recognition matrix from 4-methylamino-N-allylnaphtal-imide with fluorescent effect for the imprinting of creatinine" *Anal. Chem*. 82:8821-8829

[4] Ton X. A., Bui B. T. S., Resmini M., Bonomi P., Dika I., Soppera O., Haupt K. (2013) "A versatile fiber-optic fluorescence sensor based on molecularly imprinted microstructures polymerized in situ" Angew. Chem. Int. Ed. 52:8317-8321

[5] Carrasco S., Benito-Peña E., Walt D. R., Moreno-Bondi M. C. (2015) "Fiber-optic array using molecularly imprinted microspheres for antibiotic analysis" *Chem. Sci*. 6:3139-3147

[6] McNiven S., Kato M., Yano K., Karube I. (1998) "Chloramphenicol sensor based on an in situ imprinted polymer" *Anal. Chimica. Acta* 365:69-74

Acknowledgements

Special thanks to:

The research group of Dr. Giuseppe Toffoli at CRO of Aviano to have financed this project

Prof. Marina Resmini (School of Biological and Chemical Sciences at Queen Mary University of London) for the possibility to join her group and work on the colorimetric test with imprinted polymers

Prof. Fabio Benedetti head of our research group and Dr. Federico Berti for the precious advices

Martina Tommasini, Nicole Belfiore, Marco Cespugli for their contributions to this thesis

All the friends, members and ex-members of our research group, who helped me during these years in the laboratories 330-333 and all the friends in the department of Chemical and Pharmaceutical Science.

Finally my family and Patrick